Université de Montréal

Nanostructure des particules polymériques : aspects physiques, chimiques et biologiques

par
Jean-Michel Rabanel

Université de Montréal
Faculté de pharmacie

Thèse présentée à la Faculté de pharmacie
en vue de l'obtention du grade de PhD en Sciences Pharmaceutiques,
Option technologie pharmaceutique

avril 2015

Université de Montréal
Faculté des Études Supérieures et Postdoctorales

Cette thèse intitulée :

Nanostructure des particules polymériques : aspects physiques, chimiques et biologiques

Présentée par
Jean-Michel Rabanel

Université de Montréal, Faculté de pharmacie

a été évaluée par un jury composé des personnes suivantes :

Président-Rapporteur : Pr François-Xavier Lacasse
Examinateur externe : Pr Michel Chérel
Membre du jury : Dr Sophie-Dorothée Clas
Directeur de recherche : Pr Patrice Hildgen
Co-directeur de recherche : Pr Xavier Banquy
Représentant du doyen de la FESP : Pr Christian Pellerin

Résumé

Les nanotechnologies appliquées aux sciences pharmaceutiques ont pour but d'améliorer l'administration de molécules actives par l'intermédiaire de transporteurs nanométriques. Parmi les différents types de véhicules proposés pour atteindre ce but, on retrouve les nanoparticules polymériques (NP) constituées de copolymères "en bloc". Ces copolymères permettent à la fois l'encapsulation de molécules actives et confèrent à la particule certaines propriétés de surface (dont l'hydrophilicité) nécessaires à ses interactions avec les milieux biologiques. L'architecture retenue pour ces copolymères est une structure constituée le plus fréquemment de blocs hydrophiles de poly(éthylène glycol) (PEG) associés de façon linéaire à des blocs hydrophobes de type polyesters. Le PEG est le polymère de choix pour conférer une couronne hydrophile aux NPs et son l'efficacité est directement liée à son organisation et sa densité de surface. Néanmoins, malgré les succès limités en clinique de ces copolymères linéaires, peu de travaux se sont attardés à explorer les effets sur la structure des NPs d'architectures alternatives, tels que les copolymères en peigne ou en brosse.

Durant ce travail, plusieurs stratégies ont été mises au point pour la synthèse de copolymères en peigne, possédant un squelette polymérique polyesters-co-éther et des chaines de PEG liées sur les groupes pendants disponibles (groupement hydroxyle ou alcyne). Dans la première partie de ce travail, des réactions d'estérification par acylation et de couplage sur des groupes pendants alcool ont permis le greffage de chaîne de PEG. Cette méthode génère des copolymères en peigne (PEG-g-PLA) possédant de 5 à 50% en poids de PEG, en faisant varier le nombre de chaînes branchées sur un squelette de poly(lactique) (PLA). Les propriétés structurales des NPs produites ont été étudiées par DLS, mesure de charge et MET. Une transition critique se situant autour de 15% de PEG (poids/poids) est observée avec un changement de morphologie, d'une particule solide à une particule molle ("nanoagrégat polymére"). La méthode de greffage ainsi que l'addition probable de chaine de PEG en bout de chaîne principale semblent également avoir un rôle dans les changements observés. L'organisation des chaînes de PEG-g-PLA à la surface a été étudiée par RMN et XPS, méthodes permettant de quantifier la densité de surface en chaînes de PEG. Ainsi deux propriétés clés que sont la résistance à l'agrégation en conditions saline ainsi que la résistance

à la liaison aux protéines (étudiée par isothermes d'adsorption et microcalorimétrie) ont été reliées à la densité de surface de PEG et à l'architecture des polymères.

Dans une seconde partie de ce travail, le greffage des chaînes de PEG a été réalisé de façon directe par cyclo-adition catalysée par le cuivre de mPEG-N3 sur les groupes pendants alcyne. Cette nouvelle stratégie a été pensée dans le but de comprendre la contribution possible des chaines de PEG greffées à l'extrémité de la chaine de PLA. Cette librairie de PEG-g-PLA, en plus d'être composée de PEG-g-PLA avec différentes densités de greffage, comporte des PEG-g-PLA avec des PEG de différent poids moléculaire (750, 2000 et 5000). Les chaines de PEG sont seulement greffées sur les groupes pendants. Les NPs ont été produites par différentes méthodes de nanoprécipitation, incluant la nanoprécipitation « flash » et une méthode en microfluidique. Plusieurs variables de formulation telles que la concentration du polymère et la vitesse de mélange ont été étudiées afin d'observer leur effet sur les caractéristiques structurales et de surface des NPs. Les tailles et les potentiels de charges sont peu affectés par le contenu en PEG (% poids/poids) et la longueur des chaînes de PEG. Les images de MET montrent des objets sphériques solides et l'on n'observe pas d'objets de type agrégat polymériques, malgré des contenus en PEG comparable à la première bibliothèque de polymère. Une explication possible est l'absence sur ces copolymères en peigne de chaine de PEG greffée en bout de la chaîne principale. Comme attendu, les tailles diminuent avec la concentration du polymère dans la phase organique et avec la diminution du temps de mélange des deux phases, pour les différentes méthodes de préparation. Finalement, la densité de surface des chaînes de PEG a été quantifiée par RMN du proton et XPS et ne dépendent pas de la méthode de préparation.

Dans la troisième partie de ce travail, nous avons étudié le rôle de l'architecture du polymère sur les propriétés d'encapsulation et de libération de la curcumine. La curcumine a été choisie comme modèle dans le but de développer une plateforme de livraison de molécules actives pour traiter les maladies du système nerveux central impliquant le stress oxydatif. Les NPs chargées en curcumine, montrent la même transition de taille et de morphologie lorsque le contenu en PEG dépasse 15% (poids/poids). Le taux de chargement en molécule active, l'efficacité de changement et les cinétiques de libérations ainsi que les coefficients de

diffusion de la curcumine montrent une dépendance à l'architecture des polymères. Les NPs ne présentent pas de toxicité et n'induisent pas de stress oxydatif lorsque testés in vitro sur une lignée cellulaire neuronale. En revanche, les NPs chargées en curcumine préviennent le stress oxydatif induit dans ces cellules neuronales. La magnitude de cet effet est reliée à l'architecture du polymère et à l'organisation de la NP.

En résumé, ce travail a permis de mettre en évidence quelques propriétés intéressantes des copolymères en peigne et la relation intime entre l'architecture des polymères et les propriétés physico-chimiques des NPs. De plus les résultats obtenus permettent de proposer de nouvelles approches pour le design des nanotransporteurs polymériques de molécules actives.

Mots-clés : Nanoparticules, Poly(lactique), Poly(éthylène glycol), XPS, NMR, Micelle-like, Microcalorimétrie, Chimie clic, Curcumine

Abstract

The goal set to nanotechnologies applied to pharmaceutical sciences is to improve drug delivery and benefits with the help of nanometer-sized vehicles. At this time different types of drug carriers had been proposed. Amongst them, block copolymer nanoparticles (NP) have been designed to allow, at the same time, efficient drug encapsulation and provide surface properties (hydrophilic layer) to the NP which are necessary for its interactions with biological systems by preventing the opsonisation and the subsequent recognition by the mononuclear macrophage system (MPS) and the rapid elimination of the drug carrier.

The most prominent polymer architecture in drug delivery application is the linear di-block copolymer architecture, such as poly(ethylene glycol) blocks (PEG) linked to a polyester hydrophobic chain. PEG is the gold standard to add a hydrophilic corona to drug carrier's surface, but its efficacy is directly linked to its surface organization and surface densities. In spite of limited success of diblock at the clinical stage, few studies have been devoted to other type of architecture such as comb-like copolymers, either for the exploration of new synthesis routes or for the characterization of particles prepared from alternative architecture polymers. We attempted in preamble of this work to define more closely the conceptual and technical framework allowing quantitative determination of PEG surface densities. This review work has been used in the experimental work to define the characterization methods.

Several synthesis strategies have been developed for the preparation of comb copolymers in this work. All strategies are based on random copolymerization of dilactide with small epoxy molecules with a pendant group suitable for subsequent PEG grafting, yielding a polyester-co-ether backbone. In a second step, PEG chains have been grafted on available pendant groups (alcohol groups or alkyne) to produce the final comb copolymers. ***In the first part of the experimental work***, esterification reaction by acylation and coupling (the Steglish reaction) allowed the preparation of a first comb-like copolymer library with PEG content varying from 5 to 50 % (w/w). The number of PEG chains (PEG grafting density) was varying while the lengths of the PEG chains and the hydrophobic PLA backbone were kept constant. The library of comb-like polymers was used to prepare nanocarriers with dense PEG

brushes at their surface, stability in suspension, and resistance to protein adsorption. The structural properties of nanoparticles (NPs) produced from these polymers by a surfactant-free method were assessed by DLS, zeta potential, and TEM and were found to be controlled by the amount of PEG present in the polymers. A critical transition from a solid NP structure to a soft particle with either a "micelle-like" or "polymer nano-aggregate" structure was observed when the PEG content was between 15 to 25% w/w. This structural transition was found to have a profound impact on the size of the NPs, their surface charge, their stability in suspension in presence of salts as well as on the binding of proteins to the surface of the NPs. The arrangement of the PEG-*g*-PLA chains at the surface of the NPs was investigated by ^{1}H NMR and X-ray photoelectron spectroscopy (XPS). NMR results confirmed that the PEG chains were mostly segregated at the NP surface. Moreover, XPS and NMR allowed the quantification of the PEG chain coverage density at the surface of the solid NPs. Concordance of the results between the two methods was found to be remarkable. Physical-chemical properties of the NPs such as resistance to aggregation in saline environment as well as anti-fouling efficacy, assessed by isothermal titration calorimetry (ITC), were related to the PEG surface density and ultimately to polymer architecture.

In the second part of this work, grafting of PEG chains on a polyester-co-ether backbone was directly performed using cyclo-addition of PEG azide on pendant alkyne groups. The new strategy was designed to understand the contribution of PEG chains grafted on PLA backbone ends. The new polymer library was composed of PEG-*g*-PLA with different PEG grafting densities and PEG molecular weights (750, 2000 and 5000 D). PEG chain grafting could only take place on pendant groups with this approach. NPs were produced by different methods of nanoprecipitation, including "flash nanoprecipitation" and microfluidic technology. Some formulation variables such as polymer concentration and speed of mixing were studied in order to observe their effects on NP surface characteristics. Unlike for the first copolymer library, here the NPs size and zeta potential were found to not be much affected by the PEG content (% w/w in polymer). Sizes were also not affected by the PEG chains length. TEM images show round shaped object and as expected sizes were found to decrease with polymer concentration in the organic phase and with a decrease in mixing time of the two

phases (for flash nanoprecipitation and microfluidic technology). PEG chain surface densities were assessed by quantitative ^{1}H NMR and XPS.

In the third experimental part, we explored the role of polymer architecture on drug encapsulation and release of curcumin from NPs. Curcumin has been chosen as a model with a view to develop a delivery platform to treat diseases involving oxidative stress affecting the CNS. As previously observed with blank NPs, a sharp decrease in curcumin-loaded NP size and morphology change occurred between 15 to 20 % w/w of PEG. Drug loading, Drug loading efficiency and the diffusion coefficients of curcumin in NPs are showing a dependence over the polymer architecture. NPs did not present any significant toxicity when tested *in vitro* on a neuronal cell line. Moreover, the ability of NPs carrying curcumin to prevent oxidative stress was evidenced and linked to polymer architecture and NPs organization.

In a nutshell, our study showed the intimate relationship between the polymer architecture and the biophysical properties of the resulting NPs and sheds light on new approaches to design efficient NP-based drug carriers. The results obtained lead us to propose PEG-*g*-PLA comb architecture copolymers for nanomedecine development as an alternative to the predominant polyester-PEG diblock polymers.

Keywords : Nanoparticle, Poly(lactic acid), Poly(ethylene glycol), XPS, NMR, Micelle-like, Microcalorimetry, Click chemistry, Curcumin

Table des matières

Liste des tableaux

Liste des figures

Chapitres 1 et 2

Chapitre 3

Liste des abréviations

AFM	Microscopie de force atomique (Atomic Force Microscopy)
AGE	Allyl glycidyl éther
ATR	Réflectance totale atténuée (Attenuated Total Reflectance, ATR)
BGE	Benzyle glycidyl Éther
BHE	Barrière Hémato-Encéphalique
CDB	Calorimétrie Différentielle à balayage (Differential Scanning Calorimetry, DSC)
Cryo-MET	Microscopie Électronique à Transmission à basse température
DCC	Dicyclohexylcarbodiinide
DCF	Dichloro-fluorosceine
DLS	Dynamic Light Scattering
DMAP	Diméthyliaminopyridine
DMSO	Diméthyl sulfoxyde
EE	Éfficacité d'encapsulation
EPR	Enhanced Permeation and Retention effect
FIB-MEB	Sonde ionique focalisée (« Focused ion beam ») associée à la Microscopie électronique à balayage
FTIR	Infrarouge à transformée de Fourier
GPC	Chromatographie à perméation de gel (Gel Permeation Chromatography)
GPE	Glycidyl Propargyl Éther
I.V.	Intraveineux
LDH	Lactate déshydrogénase
MEB	Microscopie électronique à balayage (SEM)
MET	Microscopie Électronique à Transmission (TEM)
NLS	Nanoparticules lipidiques solides (ou SLN)
NP	Nanoparticule
NT	Nano-transporteur de médicament

NTP	Nano-transporteur polymérique
PBS	Tampon Phosphate Salin (Phosphate Buffer Saline)
PCL	Poly(caprolactone)
PEG	Poly(ethylene glycol)
PLA	Poly(lactique)
PLGA	Poly(lactique-co-glycolique)
PEG-*g*-PLA	Polymère en peigne : chaine(s) de Poly(éthylène glycol) greffée(s) sur une chaine de poly(lactique)
PEG-*b*-PLA	Poly(éthylène glycol)-bloc-Poly(lactique), polymère dibloc linéaire
RMN	Résonance magnétique nucléaire (NMR)
ROP	Polymérisation par ouverture de cycle (Ring Opening Polymerization)
ROS	Dérivés réactif de l'oxygène (Reactive Oxygen Species)
RNS	Dérivés réactifs de l'azote (Reactive Nitrogen Species)
$SnOct_2$	Octanoate d'étain
TE	Taux d'encapsulation (DL. Drug loading)
Tg	Température de transition vitreuse
THF	Tétrahydrofurane
XPS	Spectrométrie de photoélectrons induits par rayons X

Même si un seul nom figure sur la page titre une thèse est un travail collectif et qui doit son existence à de nombreuses personnes proches ou éloignées de la recherche. Je dédie donc ce travail à toutes les personnes qui ont rendu possible ce travail aux cours des années.

Remerciements

Mes remerciements vont en premier lieu à mon directeur de recherche, le Pr Patrice Hildgen qui m'a fait confiance au moment où j'en avais besoin. Je lui dois beaucoup et bien au-delà de cette thèse de doctorat. Merci Patrice.

Je dois aussi remercier mon codirecteur, le Pr Xavier Banquy qui s'est joint à ce projet plus tardivement, mais qui m'a grandement aidé à finaliser les données, à me mettre sur de nouvelles pistes et m'a aidé à exploiter et mettre en forme les résultats obtenus. Merci Xavier

Je remercie les différents membres du jury pour le temps passé sur ce manuscrit et leur apport à l'affinage du document final, le Pr Michel Chérel, examinateur externe, le Dr Sophie Dorothée Clas, membre du Jury, le Pr FX Lacasse, Président du jury ainsi que mes co-directeurs. À vous tous merci.

Je me dois aussi de remercier les co-auteurs des articles figurant dans cette thèse, sans leur apport scientifique, littéraire et humain ces articles n'existeraient pas.

De nombreux collègues se sont succédé au courant des années dans le laboratoire, j'ai beaucoup appris de tous et toutes sans exception, merci à vous tous et toutes. Merci au « 4ème » et aux amis du « 4ème ».

Différents organismes m'ont soutenu financièrement. Je remercie le Fonds de recherche du Québec Nature et Technologie du gouvernement du Québec, le vice-décanat à la recherche de la Faculté de pharmacie, la Faculté des Études Supérieures de l'Université de Montréal. Je dois aussi remercier mes codirecteurs à cet égard; eux qui ont apporté les financements complémentaires et qui ont aussi apporté les moyens matériels afin de réaliser ces travaux.

Enfin, je veux remercier ma famille, mes parents, ma sœur, pour m'avoir soutenu et encouragé pendant toutes ces années. À toi aussi, pour m'avoir retardé un peu sur le chemin.

1 Introduction

1.1 Les nanotechnologies pharmaceutiques

1.1.1 Mise en contexte : les nanotechnologies et l'administration de médicaments

La galénique ou la science des technologies pharmaceutiques a pour but d'administrer de façon optimale une molécule active afin d'obtenir un effet thérapeutique maximal et des effets toxiques minimaux, par les moyens les plus acceptables possible par le patient. En regard de cet objectif général, la galénique s'est intéressée depuis trois décades environ à l'apport potentiel des nanotechnologies. Les nanotechnologies peuvent être définies comme la science de la conception, de la caractérisation et de l'utilisation de structures de tailles nanométriques (de 1 à quelques centaines de nanomètres) à différentes fins, dont en l'occurrence le transport, la libération et l'optimisation de l'action de molécules actives dans l'organisme [1, 2].

Dans le domaine pharmaceutique, les défis reliés à l'administration de médicament sont nombreux: les problèmes de solubilité en milieux aqueux, les problèmes de stabilité dans les milieux biologiques (notamment pour les médicaments biologiques), les limitations aux transports et à la biodistribution, les problèmes reliés à un index thérapeutique étroit. Ces problèmes ne sont pas nouveaux, mais sont de plus en plus fréquents, la chimie médicinale produisant des molécules plus puissantes et plus spécifiques, mais généralement moins solubles en milieu aqueux [3]. L'autre défi provient de la classe des médicaments biologiques, c'est à dire, les peptides, protéines et acide nucléiques, molécules plus volumineuses, plus chargées, plus fragiles que les molécules développées jusqu'à présent et souvent nécessitant un ciblage tissulaire, voire intracellulaire pour être pleinement actives.

L'objectif de l'utilisation des nanotechnologies en galénique est donc de modifier la pharmacocinétique (« ADME ») des molécules actives par leur inclusion dans des objets nanométriques, des nanotransporteurs (NT). Cette inclusion peut agir de différentes façons.

- ***L'absorption*** : Pour la voie orale, l'encapsulation des molécules actives peut favoriser leur passage à travers la barrière gastro-intestinale et donc augmenter la dose biodisponible [4].

- ***La distribution*** : Si la solubilité aqueuse de l'actif est un problème, son encapsulation dans un NT qui lui sera facilement dispersé dans les milieux biologiques permettra une meilleure distribution de l'actif. Dans ce cas en effet la biodistribution devient celle du transporteur en substituant les paramètres de pharmacocinétique du médicament à ceux du NT.

- ***L'élimination :*** Dans le cas de la voie i.v. l'encapsulation a pour conséquence de diminuer la concentration libre en circulation de l'actif et donc de le rendre moins susceptible à la filtration rénale et à la dégradation au niveau hépatique [5].

- ***Le métabolisme :*** La modification enzymatique des molécules actives sera aussi limitée à la partie non encapsulée, ce qui pour la voie orale signifie que les molécules actives seront protégées de la dégradation dans le tractus gastro-intestinal.

Si les NT présentent des caractéristiques pharmacocinétiques favorables pour l'administration de certaines molécules actives, il reste qu'en regard des molécules circulantes dans le sang et des espaces dans lesquels ils doivent circuler (capillaires, matrices extracellulaires, liquides tissulaires interstitiels, vésicules intracellulaires) ce sont des objets de grande taille. Cette taille, favorable sous certains aspects, pose aussi des limitations à la diffusion dans des milieux complexes et des limitations à la traversée des barrières biologiques [6, 7].

Pour atteindre les objectifs de modification de la pharmacocinétique et d'amélioration de l'efficacité ou de l'innocuité des traitements, les NT doivent répondre à plusieurs critères physico-chimiques particuliers. Ces critères peuvent varier selon la voie d'administration, la molécule à livrer, son site d'action et une pathologie donnée.

- **Efficacité d'encapsulation.** En premier lieu les NT doivent permettre une encapsulation efficace des molécules actives: en fonction de la physico-chimie des molécules. Différents transporteurs auront des caractéristiques les rendant propres à encapsuler tels ou tels types de molécules avec des efficacités variables.

- **Libération des molécules actives.** En second lieu les NT devront permettre un relargage efficace de la molécule active, un paramètre qui peut être en conflit avec le point précédent. En effet si l'encapsulation est trop stable l'actif ne sera jamais libéré et ne pourra pas engendrer d'action pharmacologique.

- **Stabilité des NT dans les milieux biologiques.** Les NT doivent être stables en milieu biologique ce qui signifie plusieurs choses, soient :
  - Rester sous forme de dispersion, sans précipitation, coagulation ou floculation en milieu isotonique [8] et en présence de fluide biologique [9, 10].
  - Un assemblage stable des composants du NT : pas de désagrégation des composants en milieu biologique ou uniquement sous l'influence de facteurs prédéterminés, tel que le pH d'un environnement tumoral ciblé [11-13].
  - Une dégradation contrôlée [14, 15]

- **Durée de circulation.** La longueur de la durée de circulation dans le sang peut être critique pour certaines applications :
  - Notamment les stratégies fondées sur l'effet EPR (« Enhanced Permeation and Retention Effect ») pour accumuler les NT dans des sites pathologiques tels que des tumeurs ou des sites d'inflammation comportant des systèmes vasculaires lacunaires [16].
  - Si le NT sert seulement de réservoir circulant de molécules actives dans le sang et procure son effet favorable en relâchant de façon contrôlé l'actif encapsulé. Il existe à ce jour de nombreuses évidences que les effets positifs de nombre de nanoformulations sont reliés à cet « effet réservoir », au-delà des effets potentiels de ciblage tissulaire [17].

- **Ciblage.** À ces critères peuvent également s'ajouter des objectifs de ciblage [17-19], de pénétration de tissus [20], de transport à travers des barrières biologiques [7], ou encore d'internalisation dans des cellules spécifiques.

1.1.2 Les différents types de nanotransporteurs (NT)

Pour atteindre ces objectifs, plusieurs types de NT avec des compositions chimiques variables ont été décrits et testés, les principales familles en sont les suivantes :

- **Les liposomes**, vésicules constituées de bicouches phospholipides [21], modifiés ou non par des chaînes de poly(éthylène glycol) [22, 23]. Ce type de systèmes se retrouve actuellement en clinique avec notamment le produit Doxil® une formulation de doxorubicine pour le traitement de certaines tumeurs [24].

- **Les micelles** constituées de molécules amphiphiles ou de polymères dibloc (micelles dites « polymériques ») [25]

- **Les micro- et nanoparticules** polymériques matricielles : intensivement étudiées, plusieurs essais cliniques sont en cours sur des NT avec des diblocs de type PEG-PLGA [26]

- **Les nanoparticules lipidiques solides (NLS ou SLN)** [27]

- **Les particules autoassemblées** : souvent par interactions électrostatiques pour encapsuler des acides nucléiques par exemple pour des applications de thérapie génique ou d'interférence de la transcription des gènes [28], ou fabriquées par un procédé « couche par couche » (« layer by layer ») [29]

- **Les dendrimères :** assemblage en forme d'arborescences capables d'encapsuler dans leurs espaces internes des molécules actives [30].

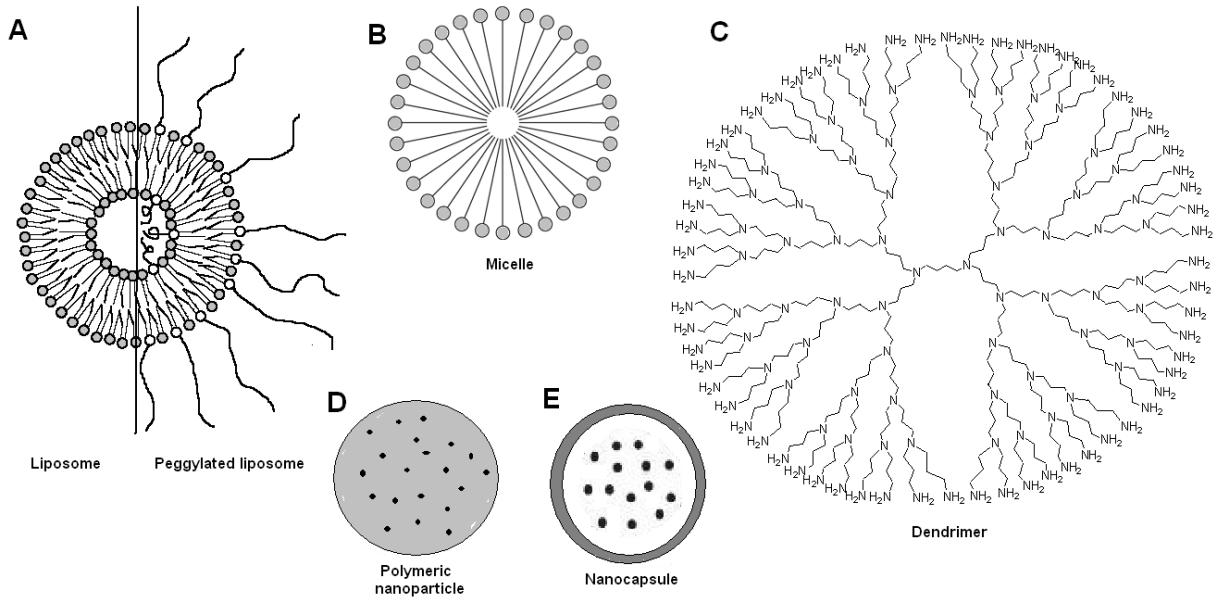

Figure 1.1. Représentation schématique de quelques nanotransporteurs (A) Liposomes, (B) Micelles (constituée de molécule de type surfactant), (C) Dendrimère, (D) Micro ou nanoparticules polymériques, (E) Capsules. (Figure extraite de notre revue [7])

En dépit de plusieurs décennies de recherche dans ce domaine, un nombre limité de produits a atteint les essais cliniques et encore moins nombreux sont les produits qui ont été mis en marché. Parmi ces derniers, on retrouve les liposomes PEGylés chargés en doxorubicine, disponibles depuis 1995 sous le nom de Doxil® en Amérique du Nord [24], les

nanoparticules d'albumine transportant du paclitaxel sur le marché depuis 2005 sous le nom d'Abraxane®,[31]. Il est à noter que la plupart des essais cliniques sur des technologies de nanoencapsulation actuellement en cours reposent sur ces mêmes technologies ou des variations de celles-ci [32]. Les bénéfices apportés par ces nanoformulations sont modestes, probablement du fait du peu de contrôle sur la libération des actifs, de leur stabilité limitée dans les milieux biologiques, d'un ciblage peu performant [33], ainsi que du fait de l'apparition de certains effets secondaires [5].

1.1.3 Les systèmes polymériques, nanotransporteurs polymériques (NTP)

Parmi les nombreux NT proposés, les nanotransporteurs polymériques (NTP) se démarquent de par leur stabilité et leur biocompatibilité [34]. Les NTP faits de copolymères sont réputés être plus biocompatibles et biodégradables que beaucoup des autres vecteurs, ce qui explique leur popularité pour le développement des systèmes de livraison de médicament. La stabilité de ces systèmes est appréciable en regard des exigences de longue circulation afin, de prendre avantage de l'effet de perméabilité et de rétention dans les tissus tumoraux (effet « EPR ») dans les applications liées au cancer [16], alors que les véhicules de type liposomal présentent des libérations prématurées de leur contenu limitant ainsi leur performance [17]. L'utilisation des NTP n'est pas limitée à la voie I.V. et plusieurs applications potentielles existent pour les voies orales et pulmonaires [7]. L'autre important avantage des NTP est la possibilité de moduler la libération du principe actif par la modulation des propriétés de la matrice polymérique [35]. Bien qu'attractives à plusieurs points de vue, le peu de résultats obtenus en clinique n'a pas permis la mise sur le marché de formes pharmaceutiques de ce type [26]. Ceci est en grande partie attribuable à l'approche largement empirique qui préside à leur conception ainsi qu'à une sous-estimation de la complexité biologique du transport de nanoparticules dans les milieux biologiques [5, 17]. La progression récente des connaissances sur les contraintes associées à la traversée des barrières physiologiques nous donne des indications plus précises sur les caractéristiques souhaitables pour ces vecteurs en regard de la taille, les propriétés de surface [7, 20, 33, 36].

Le manque de connaissances fondamentales décrivant les interactions des NTP avec le milieu biologique a fortement diminué l'efficacité thérapeutique des vecteurs développés jusqu'à présent. Il est clair que des paramètres physico-chimiques, tels que la structure interne de la particule et l'homogénéité de ses propriétés de surface doivent être mieux pris en compte durant les étapes de conceptions afin d'améliorer significativement leur biodisponibilité et biodistribution. Il serait profitable de passer d'une approche « essai-erreur » à une approche raisonnée basée sur l'élucidation des déterminants de l'organisation des chaînes polymériques et le recours à des approches d'ingénierie inverse pour la conception des polymères.

Les systèmes de livraison par la voie I.V. actuellement approuvés reposent essentiellement sur l'effet EPR, ciblage dit « passif » [7]. La possibilité d'augmenter cette accumulation au site d'action en utilisant des ligands de reconnaissance spécifique (ciblage dit « actif ») a donné à ce jour des résultats *in vivo* au mieux mitigés. Il est notamment difficile d'arriver à dépasser une accumulation de 5 à 10% de la dose injectée au site d'action, quelle que soit la stratégie employée [33]. Il semble clair, dans l'état actuel de la recherche, que l'ajout d'un ligand n'a qu'un effet marginal sur l'accumulation spécifique et son rôle semble plutôt de favoriser l'endocytose du nanovecteur [37]. C'est dans ce sens que le ciblage est improprement nommé comme « actif », car il n'y a pas d'énergie fournie au système pour faire augmenter le rendement de l'accumulation au site visé, mais seulement une rétention possible du vecteur dans le cas où il rencontre le récepteur adéquat suite à des processus de convection et diffusion [19].

Outre une meilleure connaissance de la biologie et de la physiopathologie, l'augmentation de l'efficacité du ciblage « actif » ne pourra donc reposer, lui aussi que sur des avancées au niveau fondamental de la compréhension de l'organisation de la structure du NTP, notamment au niveau de l'interface avec le milieu biologique [38].

Comme mentionné plus haut le fait de baser les NTP sur des matériaux polymériques biodégradables d'origine synthétique permet d'exploiter plusieurs de leurs propriétés clés :

- ***La stabilité chimique des polymères***

- ***La pureté et homogénéité des matériaux*** (vs les polymères d'origine naturelle)

- ***La versatilité des propriétés des matériaux polymériques*** dont les caractéristiques peuvent être modifiées à l'infini soient la taille des chaînes, leur architecture, la chimie de liaison, les groupes pendants, etc.

- ***La dégradation et l'élimination:*** le design permet de s'assurer de la possibilité de dégradation en sous-produits non toxiques et éliminables *in vivo* en vue de limiter les problèmes d'accumulation dans l'organisme.

Néanmoins il faut noter par ailleurs quelques facteurs limitants qui sont rattachés à ce type de système polymérique. Les trois principaux sont les suivants :

- ***La capacité d'encapsulation*** est largement limitée aux actifs hydrophobes et peu chargés et avec des taux de charge en molécule active (« Drug loading ») de l'ordre de 10 à 15 %, qui sont les rendements usuels, mais rarement dépassés. Ceci a deux conséquences : administration de quantité importante de polymères pour atteindre la dose efficace d'une part pour certaines molécules actives, ou la limitation de l'applicabilité de ces technologies à des actifs agissant à des doses faibles. Certaines approches semblent prometteuses pour augmenter les efficacités de chargement, notamment par « flash nanoprécipitation », mais n'ont pas encore de conséquences sur les produits développés.

- ***La libération contrôlée :*** l'atteinte d'une bonne balance entre la capacité d'encapsulation une molécule active de façon stable et la capacité à la libérer de façon précise dans l'espace et le temps n'est pas toujours facile à mettre en place. En effet, seule la molécule active libre a une action pharmacologique et de nombreux paramètres entrent en ligne de compte pour atteindre cet objectif : localisation de la NTP en fonction du temps, accès à la dose locale, vitesse de dégradation de la matrice, etc.

- ***Caractérisations structurales et chimiques :*** en dépit de leur nature artificielle, les systèmes ne sont pas suffisamment caractérisés, ce qui, en cas d'échec de la stratégie de livraison de la molécule active, ne permet par une analyse complète des raisons de l'échec et donc une adaptation de l'approche.

1.2 Les polymères synthétiques biodégradables, mise en contexte

1.2.1 Les polyesters

Les polymères synthétiques dégradables pour la préparation des transporteurs de médicament ont une histoire à rappeler brièvement pour situer nos travaux dans leur contexte. La nature dégradable des polymères synthétiques est conférée par la nature de la liaison chimique permettant l'enchaînement des monomères.

Plusieurs familles de polymère de ce type ont été décrites telles que les Poly(anhydrides), Poly(amide) [39]; Poly(cyanoacrylates) [40], [39, 41].

Mais à cet égard, les polyesters (Figure 1.2) sont les polymères qui ont été le plus étudiés. Poly(caprolactone) (ou PCL), Poly(lactique) (ou PLA), poly(glycolique) (ou PGA) et surtout le copolymère de ces derniers, le poly(lactique-co-glycolique) (ou PLGA) sont parmi les polyesters qui ont fait l'objet du plus d'études [42]. Les avantages des polyesters sont nombreux: 1) l'hydrolyse possible en milieu biologique des liaisons ester par voie enzymatique ou non enzymatique; 2) une vitesse de dégradation ajustable par la nature des monomères et leur ratio, ainsi que par la taille des chaines; 3) la facilité de synthèse; 4) des produits de dégradation généralement (les monomères) non toxiques et éliminables par les voies métaboliques normales.

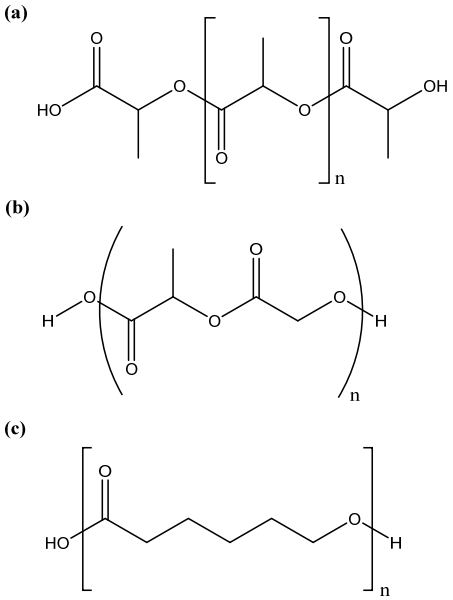

Figure 1.2. Structure des polyesters (a) PLA, (b) PLGA, (c) PCL

Par contre ces polymères forment des matrices hydrophobes dans lesquelles on encapsule de façon efficace quasi exclusivement des actifs hydrophobes. De plus ces polymères utilisés sans autres excipients conduisent à la production de particules solides qui ont une forte tendance à l'agrégation en milieu salin et qui sont facilement opsonisées [43], reconnues par le système des cellules macrophages et donc rapidement éliminées [44]. Ceci ne permet ni la libération ni le ciblage efficace des molécules actives [5]. Ces polymères doivent donc être modifiés pour l'usage pharmaceutique.

1.2.2 Les polymères blocs

Donc parallèlement des copolymères, de type dibloc, associant polyesters et poly(éthylène-PEG (Figure 1.3), ont été développés. L'ajout d'un bloc de PEG a pour fonction de conférer au copolymère formé des propriétés de surfactant, qui non seulement stabilise la particule, mais aussi prolonge sa durée de vie en circulation [45]. Selon la taille du bloc polyester, des micelles polymériques possédant une structure cœur-couronne (Polyester-PEG) ou encore des particules solides seront formées [46]. Dans les deux cas, le PEG permet de rajouter une couche hydrophile externe en surface de la particule permettant de diminuer le dépôt de

protéines à la surface du NTP, première étape vers la reconnaissance par les macrophages et leur élimination rapide [1, 47, 48].

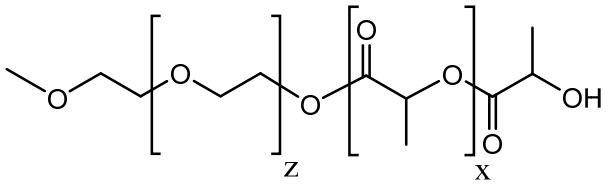

Figure 1.3. Structure d'un dibloc mPEG-*b*-PLA.

Les diblocs principalement explorés ont été les PEG-PLGA et PEG-PLA [26, 49]. L'optimisation des tailles des blocs, de la nature des monomères, de leur ratio a fait l'objet d'intenses travaux par l'équipe du Pr R Langer [26].

Les synthèses des diblocs sont réalisées principalement par deux approches : soit une réaction de couplage entre des chaines de PEG et des chaines polyesters [50]; soit l'élongation de chaîne polyester par polymérisation par couverture de cycle (« Ring Opening Polymerization, ROP ») à partir d'une chaîne de PEG agissant comme macroinitiateur de la chaîne polyester [51].

D'autres architectures « bloc » linéaires comportant des chaines de PEG et de polyesters ont été décrites, soit des triblocs, multiblocs synthétisés par des approches combinées de polymérisation et de couplages [52, 53].

1.2.3 Les polyesters fonctionnalisés : les approches de synthèse

Plusieurs méthodes ont été proposées pour ajouter des fonctionnalités aux chaînes polyesters. En effet, seuls les groupements terminaux étant accessibles, il y a une limite à l'introduction de fonctionnalités, leur nombre, ainsi qu'une limite importante à la variété de structure possible. Cette limitation plusieurs groupes se sont attachés à la surmonter en développant et testant des architectures alternatives. Notamment des structures branchées ont été proposées par le laboratoire du Pr Hildgen [54, 55], mais également par d'autres avec des structures du type $(PEG)_3$-PLA.[56]. Également des chaînes poly(lactique) possédant des structures branchées ont été décrites et il a été montré que les propriétés physiques des polymères différent en fonction de leur architecture [57].

Une stratégie pour fonctionnaliser les polyesters consiste en la polymérisation de dioxolanes fonctionnalisées. Beaucoup de synthèses de lactones fonctionnalisées ont été rapportées dans la littérature avec une large gamme de groupements fonctionnels [58, 59]. Le greffage des groupements fonctionnels latéraux sur les branches peut se faire soit sur le cycle qui porte ces dernières avant synthèse tel que décrit pour un monomère dilactide-PEG [60], soit après fonctionnalisation des branches. Cependant ces approches nécessitent la synthèse à grande échelle de dilactones modifiées.

Une autre approche est la synthèse de copolymère comportant des enchaînements polyesters et d'un monomère possédant un groupement pendant avec une fonction chimique modifiable. C'est cette dernière approche qui a été développée dans le laboratoire du Pr P Hildgen ces dernières années afin de produire des polymères branchés, « en peigne ». Les copolymères « peignes » sont constitués d'une chaîne principale sur laquelle seront greffées des chaines pendantes de différente nature.

1.2.4 Les approches de synthèse développées dans le laboratoire du Pr P. Hildgen

Nous avons, par le passé, développé la synthèse de polyester-co-éther branchés par copolymérisation de deux monomères, dont l'un est porteur d'une chaîne latérale modifiable post-polymérisation [54]. Brièvement, le dilactide est mélangé à un catalyseur ($SnOct_2$) en présence de l'allyl glycidyl éther pour obtenir un polylactide-co-éther portant des groupements latéraux allyle par polycondensation par ouverture de cycle [61]. Ces groupements sont soumis ensuite à une oxydation douce qui conduit à un groupement hydroxyle puis à une deuxième oxydation qui conduit à un groupement carboxylique. Sur ce dernier groupement sont fixés les ligands ou autres chaînes latérales par une réaction d'estérification, conduisant à des polymères branchés décrits dans plusieurs études [54, 62, 63].

Cette méthode conduit à des polymères aléatoires et dont le poids moléculaire peut être affecté par les modifications post-polymérisation. Plusieurs étapes sont nécessaires (Figure 1.4) pour aboutir au produit final ce qui conduit à des rendements plus faibles, ce qui dans une

perspective de translation est peu acceptable. Des approches permettant l'obtention du même type de polymères de façon plus rapide avec un nombre d'étapes réduit seraient donc une grande amélioration.

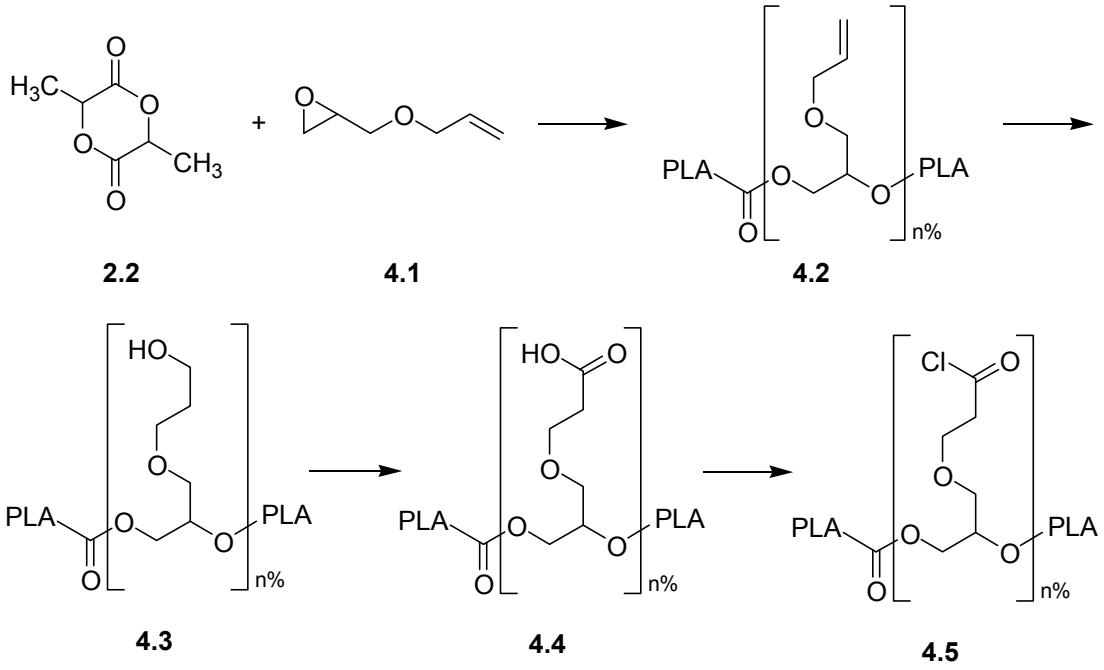

Figure 1.4. Synthèse complète des PLA fonctionnalisés. Le produit 4.5 est mis en présence d'un ligand présentant un hydroxyle libre qui réagit avec le chlorure d'acyle pour former une liaison ester. (Figure d'après [54])**.**

1.3 Méthodes de préparation des NTP

La fabrication des nanoparticules, entre 50 et 200 nm, à partir d'une solution de copolymères bloc, est abondamment décrite dans la littérature. Les deux principales techniques sont l'émulsion/évaporation de solvant [64, 65] et la nanoprécipitation [65, 66], ainsi que ces variantes comme la « nanoprécipitation flash » [67, 68] ou les techniques de microfluidique [69] [70].

La technique d'émulsion-évaporation de solvant repose sur la formation préalable d'une émulsion stable (au moins transitoirement) d'une solution organique de polymère dans une

phase externe aqueuse [65]. Les solvants organiques utilisés dans cette méthode sont pratiquement insolubles dans la phase aqueuse externe. Cette émulsion doit être stabilisée par des surfactants ou des stabilisants stériques. La diffusion du solvant organique dans la phase externe et puis son évaporation permet la solidification de la particule. Après lavages par dialyse ou par centrifugation de l'excès de molécules stabilisatrices, les particules peuvent être récupérées et caractérisées. Nous n'apporterons pas davantage d'informations sur l'émulsion/évaporation de solvant, car cette technique n'a pas été retenue dans notre étude pour différentes raisons, la principale étant la nécessité d'utilisation d'adjuvants tels que des surfactants. En général, ceux-ci sont difficiles à éliminer et donc compliquent les analyses chimiques de surface au cœur de cette étude.

1.3.1 Principe de la nanoprécipitation

Le procédé de nanoprécipitation consiste à injecter dans une phase externe aqueuse, d'une solution de polymère globalement hydrophobe, dispersée dans un solvant organique complètement soluble ou partiellement soluble dans l'eau, tel que l'Acétone, le DMSO ou le THF [71].

Ce procédé ne nécessite pas forcement l'utilisation de molécules stabilisatrices qui peuvent être requises cependant dans une perspective d'optimisation des tailles ou si on utilise des polymères de haut poids moléculaire (>50 000 g/mole) peu hydrophiles. Ceci est un grand avantage tel que nous le verrons par la suite dans notre projet. Globalement, c'est une méthode simple bien adaptée à l'échelle du laboratoire, mais dont la limitation provient de la difficulté à faire de la mise à l'échelle pilote ou industrielle.

Deux théories ont été proposées pour expliquer le mécanisme de formation des nanoparticules lors de la nanoprécipitation. La première, proposée par Quintana-Guerero *et coll.* [72], explique la formation de NP par des turbulences à l'interface entre la phase organique et la phase aqueuse. Ces turbulences sont provoquées par les différences de tension de surface entre les deux solvants et elles conduisent à la formation de microgouttelettes et à la

précipitation subséquente du polymère sous forme de particule, due à la fuite du solvant organique.

La seconde théorie est basée sur l'instabilité chimique du système lors du mélange des deux phases. Le passage quasi instantané du solvant organique dans la phase externe aqueuse provoque un phénomène de « supersaturation », le polymère étant à une concentration dans la phase composée d'eau et du solvant organique beaucoup plus élevée que sa concentration de solubilité maximum. Cette solution métastable évolue spontanément. Résultant de petites fluctuations locales de concentrations, une nucléation et une croissance de la nouvelle particule en formation par l'insertion de chaînes polymériques se produisent. Le résultat en est des particules de forme globulaire de taille nanométrique qui grossissent avec le temps. L'insertion de chaines continue jusqu'à ce que l'énergie nécessaire soit trop élevée et cela même si le système n'est pas à l'équilibre [65, 66]. Le système devient alors « gelé » et la taille de la particule est fixée et il ne se produit plus d'échange de chaîne de polymère.

De façon intéressante, celle-ci permet de prédire que le rayon des particules formées dépend de la supersaturation : à faible supersaturation, peu de particules sont formées tandis qu'à haute supersaturation de nombreuses particules plus petites sont formées [66]. Autrement dit, si le mélange des phases organiques (solvant) et aqueuses (non-solvant) est lent, les particules auront tendance à être plus grosses que si le mélange est rapide et qu'alors moins de chaines ont le temps de diffuser et de s'insérer dans le noyau en formation.

L'obtention de petites tailles et de faibles polydispersités nécessite que la nucléation se produise sur temps très bref, ce qui demande des temps de mélange très courts, de l'ordre de quelques millisecondes [67]. Ceci a amené le groupe de R Prud'homme notamment à développer des dispositifs d'auto-assemblage rapide des polymères bloc appelé « flash nanoprecipitation » [67, 68]. Ces dispositifs reposent sur la rencontre de deux jets (une phase de « non-solvant », une phase contenant le polymère dissous dans un bon solvant) se rencontrant dans une chambre de géométrie particulière permettant une diffusion rapide des deux phases [73].

Le mécanisme de nucléation et croissance n'est pas sans rappeler les étapes de formation des micelles, y compris les micelles faites à partir d'amphiphiles de haut poids moléculaires, tels que des polymères blocs. La formation des micelles, contrairement à la formation des particules, est complétée par une phase d'équilibration qui minimise l'énergie libre du système et implique un changement du nombre de micelles [74]. Cette étape ne se produit pas pour les systèmes « gelés » que sont les particules polymériques qui ne sont pas des systèmes dynamiques. Néanmoins ces systèmes ont été appelés « micelle-like » [8] ou « frozen-micelle » par plusieurs auteurs pour refléter le fait que leur structure rappelait les micelles formées par des surfactants. Le terme « crew-cut » micelle a été également introduit par le groupe d'Adi Eisenberg pour des particules formées par copolymère bloc dont le bloc hydrophile était beaucoup plus petit que le bloc hydrophobe formant le cœur de la particule « micellaire » [75].

Plus récemment des approches reposant sur la microfluidique, soit l'utilisation des principes de mécanique des fluides dans des canaux de taille micrométrique ont été mise de l'avant afin de mieux contrôler les paramètres de mélange des phases et afin de permettre une mise à l'échelle plus facile des procédés de fabrication [76, 77]. Le principe repose sur l'injection à des vitesses bien contrôlées dans des canaux distincts de quelques centaines de µm d'une phase organique et d'une phase aqueuse. Ces phases se rencontrent à des ratios prédéfinis dans une chambre de mélange qui prend différentes formes selon les systèmes pour favoriser leur mélange rapide. La rapidité de mélange de la phase organique et de la phase aqueuse est déterminante pour l'obtention de particules de petites tailles et de faible polydispersité tel que mentionné précédemment. On retrouve principalement deux types de design, soit des designs basés sur des flux coaxiaux d'une phase organique et d'une phase aqueuse [69], soit encore des designs impliquant de la tortuosité et des formes d'arrêtes de poisson perturbant l'écoulement des fluides, favorisant un mélange chaotique et rapide des deux phases [70]. Les nanoparticules liposomales, lipidiques [78, 79] ou polymériques obtenues sont par la suite collectées et purifiées [69]. Certains auteurs ont rapporté un meilleur

contrôle sur les tailles, la morphologie et l'efficacité d'encapsulation de molécules actives par ces méthodes [80].

1.3.2 Paramètres à contrôler

De façon pratique, selon la théorie basée sur la supersaturation, la taille des particules (et la dispersité de taille) dépend de la vitesse du mélange et de la concentration de polymère dans la phase organique, qui deviennent donc les paramètres primordiaux à contrôler.

La concentration, donc la quantité de chaînes dans un volume donné de phase organique, détermine la taille des particules formées. Cet effet est indissociable de la viscosité de la solution de polymère qui en augmentant favorise la production de particules de plus grande taille [71]. Le rôle du poids moléculaire du polymère ainsi que du type de solvant ont aussi été mis en évidence en relation avec la viscosité de la phase organique [81].

La vitesse d'injection de la phase organique contenant le polymère a peu d'influence en nanoprécipitation classique, le paramètre important étant dans cette configuration la rapidité du mélange des deux phases. Par contre en nanoprécipitation « flash » et en microfluidique, ce paramètre de débit des phases devient important pour contrôler la taille des particules obtenues [67, 69].

D'autres paramètres peuvent être négligés, tels que la température ou le ratio phase organique / phase aqueuse qui n'ont qu'une influence mineure sur la taille et la dispersité de taille [65].

1.3.3 Encapsulation de molécules actives.

L'incorporation de molécules dans une NP se fait au moment de sa fabrication. Lors de l'encapsulation de molécule active hydrophobe par nanoprécipitation, la situation est complexifiée, car il faut prendre en compte le comportement de la molécule à encapsuler, parallèlement au comportement du polymère. Plusieurs paramètres reliés à la molécule active sont importants : sa solubilité dans la phase organique et la phase aqueuse, la vitesse relative de précipitation du polymère et de la vitesse de précipitation de la molécule active, sa

concentration, son affinité pour l'un et l'autre des deux blocs du copolymère, décrit par le paramètre d'interaction de Flory-Huggins χ_{SP} [82], la vitesse de diffusion des solvants et des molécules.

Un phénomène souvent observé est une limite de solubilité de l'actif dans la matrice polymérique au-delà de laquelle, le système est déstabilisé, produisant des particules de taille micrométriques, une suspension dispersée ainsi que des particules d'actifs non encapsulées.

La co-solubilisation de la molécule active (dans le cas d'actif hydrophobe) et du polymère dans une phase organique et leur coprécipitation subséquente peut avoir plusieurs conséquences pour la molécule active, qui peut subir une séparation de phase et précipiter pour former des cristaux (ou des nanocristaux), se retrouver sous forme amorphe ou encore être dispersée en solution dans la matrice polymérique. Ces états physiques doivent être connus, car ils influencent la solubilité, la libération de l'actif, sa stabilité [83].

L'encapsulation et ces conséquences sur la structure de la particule sont à suivre pour toute nouvelle formation. En effet l'intercalation de molécules actives entre les chaines de polymères sous forme de molécules isolées, de nanocristaux ou de partie amorphe peut avoir des conséquences sur les transitions vitreuses des polymères, la possibilité de séparation de phase, la dégradation et les cinétiques de libérations des molécules actives.

1.4 Caractérisation des transporteurs polymériques

L'évaluation des nanotransporteurs polymériques (NTP) repose sur la mesure de différents paramètres physico-chimiques, soient la taille, la charge de surface, les propriétés de surface, la stabilité des suspensions, la structure interne (Table 1.1). Ces propriétés ont une influence directe sur l'efficacité de livraison de molécules actives par les NTP.

1.4.1 La taille

1.4.1.1 Rôle de la taille

La taille est une caractéristique essentielle des NTP, car elle détermine un nombre important de propriétés *in vivo*, notamment la biodistribution, la vitesse de libération des molécules actives encapsulées, les interactions avec les tissus et les cellules, le passage des barrières endothéliales, l'internalisation cellulaire. Il a été notamment montré dans de nombreuses études que les interactions entre les NTP et les macrophages, les cellules cibles, les membranes cellulaires étaient taille-dépendantes [84, 85]. Il en est de même pour l'internalisation dans les cellules alors que les différentes voies d'endocytose sont taille-dépendante [86]. Il en est de même pour la pénétration des barrières endothéliales: tractus gastro-intestinal, barrière hématoencéphalique, barrières vasculaires, que ce soit par transcytose ou de par l'existence de porosité traversant la barrière en question [7]. Finalement un exemple type du rôle primordial joué par la taille du NT nous est donné par effet d'accumulation par l'effet « Enhanced Permeation and Retention » (ou EPR). L'effet EPR permet l'accumulation de macromolécule ou de nanoparticules au site tumoral ou inflammatoire du fait de parois de vaisseaux sanguins déstructurées et poreuses. Cet effet est fortement dépendant de la taille des objets [16, 87].

1.4.1.2 Méthodes de mesure

Les techniques les plus usuelles dans le domaine sont la diffusion dynamique de la lumière (ou « Dynamic Light Scattering », DLS), la diffraction laser en suspension liquide. Les différentes méthodes de microscopies électroniques : MEB, MET et MFA (ou « AFM ») sont également largement utilisées dans la caractérisation des nanomatériaux. L'utilisation de méthodes reposant sur des principes physiques distincts est recommandée afin d'avoir une évaluation non biaisée des tailles des particules [88].

Les informations obtenues par ces différentes méthodes et les limites de ces méthodes sont développées dans l'article de revue, inclus dans ce mémoire [89]. Sans contredit, la

principale limitation de ces mesures est la difficulté à mesurer de façon adéquate la taille des NT dans des conditions physiologiques.

Table 1.1. Principales méthodes de caractérisation des nanoparticules

Propriétés	Méthode	Principe physique	Type d'information	Limitations
Taille	Diffusion dynamique de la lumière (« DLS »)	Mesure des variations de la lumière diffusée par les particules	Diamètre Hydrodynamique	- Particule sphérique - Échantillon homogène
	Laser Scattering (« LS »)	Diffraction laser à différents angles	Taille et distribution de taille (40 nm-2 mm)	Grande quantité de particules nécessaire
	Microscopie de Force Atomique (« AFM »)	Pointe oscillante interagissant avec la surface de l'échantillon	Représentation topographique et information sur la chimie de surface	Particules sèches Artefacts Durée
	Microscopie Électronique à Balayage (MEB)	Balayage d'un faisceau électronique	Taille des NP	Traitement image pour résultats statistiquement significatifs Traitement de surface des NPs
	Microscopie Électronique à Transmission (MET)	Faisceau d'électrons traversant l'échantillon	Taille des NPs par projection	Traitement d'images Particules sous vide
Charge	Mesure du potentiel Zêta	Mobilité électrophorétique	Mesure indirecte du potentiel de surface (mV)	Mesure très sensible aux conditions externes
Composition Chimique de surface	Résonance Magnétique Nucléaire (RMN)	Signaux de résonance des protons (^{1}H)	Quantitatif	Solvant deutérés, Détection des entités chimiques mobiles (solubilisés)
	Spectrométrie de photoélectrons induits par rayons X (« XPS »)	Détection électrons émis suite au bombardement de la surface par des photons X	Composition chimique en pourcentage (%)	Analyse semi-quantitative Profondeur d'analyse 10 nm Particules lyophilisées
	TOF-SIMS	Spectrométrie de masse de surface	Fragments SM	Profondeur d'analyse 1 nm Résolution 200 nm

Stabilité	DLS	Mesure des variations de la lumière diffusée par les particules	Mesure de la taille et l'agrégation	Sensibilité faible Pas possible en milieux biologiques
Structure interne	Microscopie électronique à transmission (MET)	Faisceau d'électron	Images à travers l'échantillon	Stabilité des matériaux Épaisseur limitée
	Diffraction de neutron (« SANS »)	Diffraction d'un faisceau de neutrons	Modèle d'organisation interne de la particule	Technique peu accessible, modèle dépendante
	Adsorption de gaz	Mesure de la quantité de gaz adsorbée par un soldie	Volume et dimension des pores (taille; A)	Matériaux secs
Structure de la surface	Microscopie électronique à balayage (MEB)	Faisceau d'électron balayant la surface d'un échantillon	Image de la surface de l'échantillon	Stabilité des matériaux Modification de la surface
	Microscopie de force atomique (AFM)	Pointe oscillante interagissant avec la surface	Image 3D de la surface Information chimique	Résolution

1.4.2 Charge de surface

1.4.2.1 Rôle des charges de surface

Les charges de surface ont une incidence sur la stabilité des nanosuspensions dans les milieux salins, mais elles déterminent aussi les interactions avec les milieux biologiques, en particulier les interactions avec les protéines plasmatiques [90]. Il est généralement considéré comme avantageux un potentiel proche de la neutralité pour éviter les liaisons spécifiques aux protéines et aux membranes cellulaires, qui ont pour conséquences une élimination rapide des NT de l'organisme ou encore des effets toxiques notamment dus aux charges cationiques [91].

Il faut noter qu'un potentiel neutre en absence d'autre modalité pour maintenir la stabilité de la nanosuspension peut poser des problèmes de coagulation et agrégation des particules en milieu salin tels que les milieux biologiques.

Dans les NPP préparées à partir de polyesters, il est généralement admis que les charges ont pour origine les groupes carboxyliques en bout de chaine [92].

1.4.2.2 Méthode de mesure : le potentiel zêta

Le potentiel électrique est mesuré par mesure du déplacement électrophorétique des particules dans un milieu conducteur en réponse à un champ électrique appliqué. Il est à noter que le potentiel mesuré n'est pas directement relié à la charge de surface. Il s'agit plutôt de la différence de potentiel entre le plan de cisaillement et le cœur de la solution (voir Figure 3.3 Chapitre 3 [89]). C'est donc une mesure indirecte des charges de surface.

Il résulte de la méthode de mesure que la mesure du potentiel dépend de la distance du plan de cisaillement de la surface de la particule ainsi que de la force ionique du milieu dans lequel la mesure est prise. Le premier peut être déplacé par la présence de chaînes polymériques hydrophiles qui s'étendent dans le milieu environnant, telles que des chaines de PEG ou des surfactants stériques tels que le PVA. La force ionique ainsi que le pH du milieu modifient la répartition des charges aux alentours de la particule, modifiant également le potentiel mesuré.

1.4.3 Composition chimique de surface

1.4.3.1 Importance de la surface

La surface du NT interagit avec le milieu biologique. Une grande partie de son devenir est dictée par ces interactions [93]. Plusieurs éléments sont à considérer tels que l'hydrophilicité (stabilité en milieux salins, interactions avec les protéines), la composition chimique (réaction immunogène, etc.), la présence de ligand de reconnaissance (ciblage), la topographie.

1.4.3.2 Les méthodes d'étude

La composition chimique de la surface de NTP a été étudiée par spectroscopie de photon (XPS) [89, 94] qui donne des résultats semi-quantitatifs sur une épaisseur de 5 à 7 nm. La spectroscopie de masse « TOF-SIMS » (ou « Time of flight secondary ions mass spectrometry »), qui analyse les surfaces sur une profondeur moindre encore (1 nm environ) a permis de confirmer la présence d'un ligand azoté en surface de nanoparticules a très faible concentration [95]. Ces techniques néanmoins ont un manque de résolution trop important pour cartographier des nanoparticules individuelles, les résultats obtenus sont des moyennes sur une grande population de particules.

En ce qui concerne les nanoparticules pegylées, la densité et la conformation du PEG en surface [96] ont été étudiées par plusieurs méthodes du fait de son rôle important dans le devenir de la particule *in vivo*. Une des méthodes directes est la quantification du PEG dans D_2O par RMN du proton [97, 98]; par fluorescence [99] ou encore par la mesure du potentiel zêta [92, 100]. Nous avons revu de façon exhaustive cet aspect de la quantification du PEG en surface des NTP récemment en détaillant les différentes approches de quantifications et leurs limites [89]. Cette revue est incluse à la fin de cette introduction.

1.4.4 Stabilité des systèmes

Tel que mentionnée dans les sections 1.4.2 et 1.4.3, la stabilité des préparations nanoparticulaires est conditionnelle à des propriétés de surface permettant aux forces de répulsion de dominer les forces d'attraction, tel que prédit par la théorie dite « DLVO ». Dans cette théorie, un rôle clé est attribué aux charges (répulsion électrostatique) et à la répulsion stérique (chaines polymériques hydrophiles en surface) pour s'opposer à l'agrégation causée par les forces attractives (hydrophobe, van der Walls).

Dans les milieux physiologiques, les NTP sont exposées à des concentrations salines (équivalent de 154 mM NaCl). Les particules de polyesters en l'absence de PEG présentent une surface largement négative, tandis que le rôle des sels cationiques est de faire écran et de neutraliser ces charges, diminuant les forces de répulsion.

Un critère pour évaluer la stabilité en milieu salin est la mesure de la concentration critique de coagulation ou de floculation («Critical Coagulation Concentration» ou «Critical Flocculation Concentration») en réponse à des concentrations croissantes de sels dans le milieu de suspension [101-103]. Ces informations peuvent être obtenues par la mesure de taille des particules en fonctions des forces ioniques.

1.4.5 Structure interne

Si la compréhension des surfaces est d'une importance primordiale pour le devenir du transporteur dans un milieu biologique, on ne peut négliger l'importance de la structure interne des objets nanométriques. Cette structure interne que l'on peut définir comme l'arrangement des chaînes polymériques joue un rôle dans la stabilité de l'objet, le taux d'encapsulation des molécules actives, leur taux et vitesse de relargage.

L'investigation de la structure interne est difficile. L'étude de microscopique de coupes transversales des particules est difficile à cette échelle de taille nanométrique, surtout dans le cas de particules molles telles que des formes pseudo-micellaires (« micelle-like particle »). La microscopie électronique à transmission (MET ou TEM) permet par des techniques de préparation d'échantillon congelés de visualiser les morphologies natives de ces objets [104].

La technique de « Small Angle Neutron Scattering ou SANS » est basée sur la diffraction de neutrons par les atomes constituants la particule. Riley *et coll*. ont démontré, par exemple, un modèle structural pour les particules dibloc de PLA-PEG en utilisant cette technique [46]. Le SANS a permis la modélisation des particules de type cœur-couronne (« core-shell »), cependant c'est une méthode peu accessible, nécessitant des équipements très spécialisés.

Une autre méthode qui a été développée dans le laboratoire du professeur P. Hildgen, mais qui est encore peu rapportée est l'adsorption de gaz pour étudier la porosité des particules polymériques solides [62, 64, 105]. Par cette méthode il a été possible de rapporter des liens

entre l'architecture des polymères et la taille et le volume de la porosité des nanoparticules solides ainsi que des relations avec les taux d'encapsulation et de libération [62].

1.4.6 Structure des surfaces

L'analyse fine de la structure des surfaces n'est pas non plus facilement accessible, surtout pour des particules « molles » telles que des agrégats micellaires.

La microscopie de force atomique (Atomic Force Microscopy ou AFM) [106] permet d'obtenir une image topographique des particules, mais également d'obtenir des informations sur la chimie de surface [100]. La microscopie électronique à balayage (Scanning electronic Microscopy, SEM) a également été

En ce qui concerne des particules solides, la rugosité peut être accessible par adsorption gazeuse pour des particules lyophilisées [62, 64]. La signifiance des informations fournies par des particules sèches sur la surface de particules hydratées et dans des conditions physiologiques néanmoins reste à démontrer.

1.4.7 Encapsulation et relargage de médicament.

Les propriétés d'encapsulation d'un NTP peuvent être définies par les informations suivantes, soient le taux d'encapsulation, l'efficacité d'encapsulation, l'état physique de la molécule active, le profil et les conditions de libération de la molécule active.

Le taux d'encapsulation (« Drug loading ») peut être défini comme la masse de molécules actives sur la masse totale de la formulation, (*Éq. 1.1*) :

$$TE = \frac{Poids\ d'actif\ dans\ les\ NPs}{Poids\ total\ de\ NPs} \times 100$$

L'efficacité d'encapsulation (« Loading efficiency ») peut être définie comme la masse d'actif effectivement dans la formulation finale sur la masse d'actif ajouté au début du processus de préparation de la formulation, (*Éq. 1.2*) :

$$EE = \frac{Poids\ d'actif\ dans\ les\ NPs}{Poids\ d'actif\ initial} \times 100$$

L'état physique de la molécule active (amorphe, cristallin ou dispersée dans la matrice polymère (« dispersée moléculairement ») est un paramètre important, car il détermine la solubilité et la libération de la molécule, la stabilité de la molécule dans la formulation. Cette information est accessible par l'analyse calorimétrique différentielle (ACD ou « DSC ») ou par l'analyse rayons X de la formulation et la comparaison des profils de diffraction [83].

Le profil de libération. La cinétique de libération de la molécule active détermine son efficacité, les paramètres à considérer sont l'importance de « burst », la vitesse de libération, la dose totale libérée, la durée de la libération [107, 108].

La stabilité de la molécule active encapsulée. Si la formulation n'est pas utilisée immédiatement, la stabilité du chargement lors du stockage de la formulation (l'absence de relargage prématuré) et la stabilité chimique de la molécule active sont des points importants dans la perspective d'un développement pharmaceutique.

2 Hypothèse de recherche et objectifs

2.1 Hypothèse

2.1.1 Mise en contexte

Si l'essentiel des travaux publiés sur les NTP repose sur l'utilisation de polymères diblocs linéaires tel que discuté dans l'introduction (section 1.3), nous avons développé pour notre part une famille de polymère, les polyesters-co-éthers greffés latéralement par des groupes fonctionnels divers [54] dans le but de préparer des nanotransporteurs de médicament pour différentes applications (section 1.5). Notre approche globale pour la préparation des NTP repose sur plusieurs considérations :

(1) Elle consiste en l'utilisation de polymères préformés avec leur multifonctionnalité, (furtivité, reconnaissance spécifique, détection), ce qui permet d'obtenir des NTP prêtes à l'usage en une seule étape d'émulsion/évaporation de solvant ou de nanoprécipitation. De ce fait, on s'affranchit des étapes de modifications sur des NTP préformés, étapes qui introduisent des variabilités dans les caractéristiques des lots et posent des problèmes de purification et de stabilité de l'encapsulation. Cette approche est avantageuse dans une perspective de mise à l'échelle (« scale-up ») vers la production de lots cliniques. Si les paramètres de préparation des NTP sont bien maîtrisés, il est en effet plus facile de contrôler la synthèse de polymère et de s'assurer d'obtenir des lots reproductibles et bien caractérisés. Par ailleurs, cette approche nécessite une compréhension du processus de formation et d'organisation de la NPP, dans son volume et à sa surface pour s'assurer de la conformation et de la quantification des différents éléments fonctionnels. Cet aspect sera la contribution essentielle de ce travail.

(2) Elle repose également sur l'utilisation exclusivement de matériaux déjà cliniquement validés, tels que le poly(éthylène glycol) (PEG) et des polyesters de type poly(lactique), des polymères déjà approuvés pour usage interne par les agences

réglementaires, ce qui diminue les risques et incertitudes dans une perspective de développement clinique et industriel.

(3) Elle repose finalement sur des architectures polymériques « en peigne », soit une chaîne principale de polyesters avec des chaines pendantes disposées de façon aléatoire. Cette architecture permet, contrairement aux formes polymériques linéaires, une densité de greffage ajustable, ainsi que la possibilité de greffer indépendamment des éléments de furtivité et de reconnaissance sur la même chaine. De plus l'architecture permet des variations qui peuvent modifier le comportement des polymères en solution et dans la NTP ce qui a des conséquences sur l'organisation des chaînes avec des effets sur la structure des particules (des particules solides aux micelles), leur porosité, les séparations de phase et les propriétés de surface [62, 100].

2.1.2 Hypothèse de recherche

Le développement futur des NTP préparés à partir de polymères branchés nécessite leur caractérisation structurale. La conception de NTP possédant des propriétés structurales internes et de surface bien définies nécessite l'utilisation de méthodes analytiques convergentes qui permettront de relier la chimie des polymères synthétisés et les paramètres de fabrication aux propriétés structurales et à la chimie des surfaces. La connaissance approfondie de la structure et des propriétés des NTP permettra de prévoir et de contrôler leur capacité de livraison de molécules actives. L'hypothèse centrale que nous voulons valider dans ce projet est donc la suivante :

Les nanoparticules polymériques s'organisent selon une structure complexe hétérogène qui ne dépend que de la nature des polymères et de leurs propriétés physicochimiques.

Les sous-hypothèses suivantes qui sont ses corolaires seront également testées :

La structure interne et superficielle des NTP à base de polyesters peut être contrôlée finement en utilisant des polymères de structures bien définies.

La synthèse de polymère polyesters branchés va permettre d'optimiser la structure de ces polymères sur la base des propriétés des particules obtenues, soient la taille, les propriétés de surface, l'encapsulation d'actif en vue de développer une plateforme pour la livraison d'actif au CNS.

2.2 Objectifs de recherche.

Pour valider ces hypothèses de recherche, nous proposons de poursuivre trois objectifs de recherches correspondant aux trois étapes principales du projet. Ces objectifs sont les suivants :

2.2.1 Objectif 1 : Conception et synthèse de polymères branchés PEGylés

Le premier objectif consistera à développer une librairie de polymères branchés à base d'acide lactique. Les branches seront constituées de groupes fonctionnels, sur lesquels seront greffés des quantités variables de PEG.

Cette librairie sera développée sur la base d'une évolution de la méthode en place pour s'affranchir de certaines de ces étapes limitantes, soit l'oxydation des groupes pendants allyls. Pour ce faire nous substituerons le groupement allyl par un groupement benzyloxy (voir Chapitre 4, Article 1). Une autre innovation sera l'utilisation de la chimie « clic » par cyclo-addition catalysée par le cuivre en substituant le groupement allyl cette fois par un groupement alcyne (voir Chapitre 5, Article 2).

L'objectif de ces nouvelles approches sera d'obtenir des copolymères bloc avec des structures définies possédant une architecture alternative aux copolymères bloc linéaires. Le résultat doit être une librairie avec une continuité sur une large gamme, en termes de nombre de chaines greffées, de taille du bloc hydrophobe et du contenu en PEG en pourcentage du poids du polymère.

2.2.2 Objectif 2 : Caractérisation des particules formées par ces polymères

Le second objectif de l'étude sera de formuler des NTP à partir de ces polymères par nanoprécipitation et de caractériser exhaustivement leurs propriétés structurales aussi bien en surface que dans le cœur. À l'aide des résultats obtenu nous développerons un modèle de la formation et de la structure des particules en fonction des propriétés structurales des copolymères.

Une des propriétés importantes des particules est leur propriété de surface conférée par la couronne hydrophile constituée de PEG. Nous nous sommes attaché dans un article de revue à donner un cadre théorique à cette problématique qui est, à notre point de vue, un peu négligée par les formulateurs. Nous avons donc révisé exhaustivement la littérature concernant la détermination quantitative des propriétés de surface notamment la densité (nombre de chaines par unités de surface) de PEG. Ce cadre a été repris dans les publications subséquentes lors de l'étude de propriétés de surface des NPs (Chapitre 3, Article de revue).

Ces objectifs de caractérisations structurales sont développés dans les Chapitres 4, 5 et 6 (Article 1 à 3) avec la mise au point de méthodes de quantification XPS et par RMN, de microcalorimétrie, et de microscopie électronique à transmission notamment.

2.2.3 Objectif 3 : Test d'une application potentielle MND

Le troisième objectif sera d'évaluer le potentiel de cette bibliothèque de polymères pour formuler une molécule active modèle pour des applications de livraison au Système Nerveux Central (SNC). La molécule active retenue est la curcumine qui *in vitro* a montré des propriétés antioxydantes ayant le potentiel de contribuer à un traitement des maladies neurodégénératives (MND) telle que la maladie d'Alzheimer (MA). De plus, la curcumine est une molécule peu soluble en milieu aqueux et instable chimiquement lorsque solubilisée, ce qui augmente l'intérêt de son encapsulation pour des fins thérapeutiques.

Ces propriétés d'encapsulation et de libération ainsi que son efficacité à combattre le stress oxydatif *in vitro* seront évalués (Chapitre 6, Article 3).

References (Chapitres 1 et 2)

1. Gref, R., et coll., *Biodegradable long-circulating polymeric nanospheres.* Science, 1994. **263**(5153): p. 1600-3.
2. Parveen, S., R. Misra, and S.K. Sahoo, *Nanoparticles: a boon to drug delivery, therapeutics, diagnostics and imaging.* Nanomedicine: Nanotechnology, Biology and Medicine, 2012. **8**(2): p. 147-166.
3. Lipinski, C.A., *Drug-like properties and the causes of poor solubility and poor permeability.* Journal of Pharmacological and Toxicological Methods, 2000. **44**(1): p. 235-249.
4. Florence, A.T., *Nanoparticle uptake by the oral route: Fulfilling its potential?* 2005. **2**(1): p. 75-81.
5. Bertrand, N. and J.-C. Leroux, *The journey of a drug-carrier in the body: An anatomo-physiological perspective.* Journal of Controlled Release, 2012. **161** (2): p. 152-163.
6. Crommelin, D.J.A. and A.T. Florence, *Towards more effective advanced drug delivery systems.* International Journal of Pharmaceutics, 2013(0).
7. Rabanel, J.M., et coll., *Drug-loaded nanocarriers: passive targeting and crossing of biological barriers.* Current Medicinal Chemistry, 2012. **19**(19): p. 3070-102.
8. Riley, T., et al., *Colloidal stability and drug incorporation aspects of micellar-like PLA–PEG nanoparticles.* Colloids and Surfaces B: Biointerfaces, 1999. **16**(1–4): p. 147-159.
9. Lu, J., S.C. Owen, and M.S. Shoichet, *Stability of Self-Assembled Polymeric Micelles in Serum.* Macromolecules, 2011. **44**(15): p. 6002-6008.
10. Owen, S.C., D.P.Y. Chan, and M.S. Shoichet, *Polymeric micelle stability.* Nano Today, 2012. **7**(1): p. 53-65.
11. Roux, E., et coll., *On the characterization of pH-sensitive liposome/polymer complexes.* Biomacromolecules, 2003. **4**(2): p. 240-8.
12. Schmaljohann, D., *Thermo- and pH-responsive polymers in drug delivery.* Advanced Drug Delivery Reviews, 2006. **58**(15): p. 1655-1670.
13. Gao, W., J.M. Chan, and O.C. Farokhzad, *pH-Responsive Nanoparticles for Drug Delivery.* Molecular Pharmaceutics, 2010. **7**(6): p. 1913-1920.
14. Göpferich, A., *Mechanisms of polymer degradation and erosion.* Biomaterials, 1996. **17**(2): p. 103-114.
15. Shive, M.S. and J.M. Anderson, *Biodegradation and biocompatibility of PLA and PLGA microspheres.* Adv Drug Deliv Rev, 1997. **28**(1): p. 5-24.
16. Fang, J., H. Nakamura, and H. Maeda, *The EPR effect: Unique features of tumor blood vessels for drug delivery, factors involved, and limitations and augmentation of the effect.* Adv Drug Deliv Rev, 2011. **63**(3): p. 136-51.
17. Kwon, I.K., et al., *Analysis on the current status of targeted drug delivery to tumors.* Journal of Controlled Release, 2012. **164**(2): p. 108-114.
18. Muro, S., *Challenges in design and characterization of ligand-targeted drug delivery systems.* Journal of Controlled Release, 2012. **164**(2): p. 125-137.

19. Ruenraroengsak, P., J.M. Cook, and A.T. Florence, *Nanosystem drug targeting: Facing up to complex realities.* Journal of Controlled Release, 2010. **141**(3): p. 265-276.
20. Jain, R.K. and T. Stylianopoulos, *Delivering nanomedicine to solid tumors.* Nature Reviews. Clinical Oncology, 2010. **7**(11): p. 653-664.
21. Gabizon, A., et al., *Long-circulating liposomes for drug delivery in cancer therapy: A review of biodistribution studies in tumor-bearing animals.* Advanced Drug Delivery Reviews, 1997. **24**(2-3): p. 337-344.
22. Moghimi, S.M. and J. Szebeni, *Stealth liposomes and long circulating nanoparticles: critical issues in pharmacokinetics, opsonization and protein-binding properties.* Prog Lipid Res, 2003. **42**(6): p. 463-78.
23. Sawant, R.R. and V.P. Torchilin, *Liposomes as 'smart' pharmaceutical nanocarriers.* Soft Matter, 2010. **6**(17): p. 4026-4044.
24. Barenholz, Y., *Doxil® — The first FDA-approved nano-drug: Lessons learned.* Journal of Controlled Release, 2012. **160**(2): p. 117-134.
25. Gaucher, G., et coll., *Block copolymer micelles: preparation, characterization and application in drug delivery.* Journal of Controlled Release, 2005. **109**(1-3): p. 169-188.
26. Hrkach, J., et al., *Preclinical Development and Clinical Translation of a PSMA-Targeted Docetaxel Nanoparticle with a Differentiated Pharmacological Profile.* Science Translational Medicine, 2012. **4**(128): p. 128ra39.
27. Gastaldi, L., et al., *Solid lipid nanoparticles as vehicles of drugs to the brain: current state of the art.* Eur J Pharm Biopharm, 2014. **87**(3): p. 433-44.
28. Suma, T., et al., *Smart Multilayered Assembly for Biocompatible siRNA Delivery Featuring Dissolvable Silica, Endosome-Disrupting Polycation, and Detachable PEG.* ACS Nano, 2012. **6**(8): p. 6693-6705.
29. de Martimprey, H., et al., *Polymer nanocarriers for the delivery of small fragments of nucleic acids: Oligonucleotides and siRNA.* European Journal of Pharmaceutics and Biopharmaceutics, 2009. **71**(3): p. 490-504.
30. Al-Jamal, K.T., C. Ramaswamy, and A.T. Florence, *Supramolecular structures from dendrons and dendrimers.* Advanced Drug Delivery Reviews, 2005. **57**(15): p. 2238-2270.
31. Gradishar, W.J., *Albumin-bound paclitaxel: a next-generation taxane.* Expert Opinion on Pharmacotherapy, 2006. **7**(8): p. 1041-1053.
32. *https://clinicaltrials.gov/*.
33. Bae, Y.H. and K. Park, *Targeted drug delivery to tumors: Myths, reality and possibility.* Journal of Controlled Release, 2011. **153**(3): p. 198-205.
34. Panyam, J., et al., *Polymer degradation and in vitro release of a model protein from poly(D,L-lactide-co-glycolide) nano- and microparticles.* J Control Release, 2003. **92**(1-2): p. 173-87.
35. Uhrich, K.E., et al., *Polymeric Systems for Controlled Drug Release.* Chemical Reviews, 1999. **99**(11): p. 3181-3198.

36. Alexis, F., et al., *Factors affecting the clearance and biodistribution of polymeric nanoparticles.* Molecular Pharmaceutics, 2008. **5**(4): p. 505-515.
37. Kirpotin, D.B., et al., *Antibody Targeting of Long-Circulating Lipidic Nanoparticles Does Not Increase Tumor Localization but Does Increase Internalization in Animal Models.* Cancer Research, 2006. **66**(13): p. 6732-6740.
38. Mahon, E., et al., *Designing the nanoparticle–biomolecule interface for "targeting and therapeutic delivery".* Journal of Controlled Release, 2012. **161**(2): p. 164-174.
39. Domb, A.J., J. Kost, and D.M. Wiseman, *Hanbook of Biodegradable Polymers*, ed. A.T. Florence and G. Gregoriadis. 1997: Hardwood academic publishers.
40. Vauthier, C., D. Labarre, and G. Ponchel, *Design aspects of poly(alkylcyanoacrylate) nanoparticles for drug delivery.* J Drug Target, 2007. **15**(10): p. 641-63.
41. Seyednejad, H., et al., *Functional aliphatic polyesters for biomedical and pharmaceutical applications.* Journal of Controlled Release, 2011. **152**(1): p. 168-176.
42. Perrin, D.E. and J.P. English, *Polyglycolide and polylactide*, in *Handbook of biodegradable polymers*, A.J. Domb, J. Kost, and D.M. Wiseman, Editors. 1997, Hardwood academic publishers.
43. Sempf, K., et al., *Adsorption of plasma proteins on uncoated PLGA nanoparticles.* Eur J Pharm Biopharm, 2013. **85**(1): p. 53-60.
44. Danhier, F., et al., *PLGA-based nanoparticles: An overview of biomedical applications.* Journal of Controlled Release, 2012. **161**(2): p. 505-522.
45. Owens, D.E., 3rd and N.A. Peppas, *Opsonization, biodistribution, and pharmacokinetics of polymeric nanoparticles.* Int J Pharm, 2006. **307**(1): p. 93-102.
46. Riley, T., et al., *Core−Shell Structure of PLA−PEG Nanoparticles Used for Drug Delivery.* Langmuir, 2003. **19**(20): p. 8428-8435.
47. Bazile, D., et al., *Stealth Me.PEG-PLA nanoparticles avoid uptake by the mononuclear phagocytes system.* J Pharm Sci, 1995. **84**(4): p. 493-8.
48. Gref, R., et al., *'Stealth' corona-core nanoparticles surface modified by polyethylene glycol (PEG): influences of the corona (PEG chain length and surface density) and of the core composition on phagocytic uptake and plasma protein adsorption.* Colloids Surf B Biointerfaces, 2000. **18**(3-4): p. 301-313.
49. Gu, F., et al., *Precise engineering of targeted nanoparticles by using self-assembled biointegrated block copolymers.* Proceedings of the National Academy of Sciences, 2008. **105**(7): p. 2586-2591.
50. Cheng, J., et al., *Formulation of functionalized PLGA-PEG nanoparticles for in vivo targeted drug delivery.* Biomaterials, 2006.
51. Riley, T., et al., *Physicochemical Evaluation of Nanoparticles Assembled from Poly(lactic acid)−Poly(ethylene glycol) (PLA−PEG) Block Copolymers as Drug Delivery Vehicles.* Langmuir, 2001. **17**(11): p. 3168-3174.
52. Peracchia, M.T., et al., *PEG-coated nanospheres from amphiphilic diblock and multiblock copolymers: Investigation of their drug encapsulation and release characteristics.* Journal of Controlled Release, 1997. **46**(3): p. 223-231.
53. Quesnel, R. and P. Hildgen, *Synthesis of PLA-b-PEG Multiblock Copolymers for Stealth Drug Carrier Preparation.* Molecules, 2005. **10**(1): p. 98-104.

54. Nadeau, V., et al., *Synthesis of new versatile functionalized polyesters for biomedical applications.* Polymer, 2005. **46**(25): p. 11263-11272.
55. Dhanikula, R.S. and P. Hildgen, *Influence of molecular architecture of polyether-co-polyester dendrimers on the encapsulation and release of methotrexate.* Biomaterials, 2007. **28**(20): p. 3140-52.
56. Ayen, W.Y., et al., *Effect of PEG chain length and hydrophilic weight fraction on polymersomes prepared from branched (PEG)3-PLA co-polymers.* Polymers for Advanced Technologies, 2011. **22**(1): p. 158-165.
57. Nouri, S., C. Dubois, and P.G. Lafleur, *Synthesis and characterization of polylactides with different branched architectures.* Journal of Polymer Science Part B: Polymer Physics, 2015. **53**(7): p. 522-531.
58. Trollsås, M., et al., *Hydrophilic Aliphatic Polyesters: Design, Synthesis, and Ring-Opening Polymerization of Functional Cyclic Esters.* Macromolecules, 2000. **33**(13): p. 4619-4627.
59. Leemhuis, M., et al., *Functionalized Poly(α-hydroxy acid)s via Ring-Opening Polymerization: Toward Hydrophilic Polyesters with Pendant Hydroxyl Groups.* Macromolecules, 2006. **39**(10): p. 3500-3508.
60. Castillo, J.A., et al., *Well-Defined Poly(lactic acid)s Containing Poly(ethylene glycol) Side Chains.* Macromolecules, 2011. **45**(1): p. 62-69.
61. Dechy-Cabaret, O., B. Martin-Vaca, and D. Bourissou, *Controlled Ring-Opening Polymerization of Lactide and Glycolide.* Chemical Reviews, 2004. **104**(12): p. 6147-6176.
62. Sant, S., M. Thommes, and P. Hildgen, *Microporous structure and drug release kinetics of polymeric nanoparticles.* Langmuir, 2008. **24**(1): p. 280-287.
63. Essa, S., J.M. Rabanel, and P. Hildgen, *Effect of polyethylene glycol (PEG) chain organization on the physicochemical properties of poly(D, L-lactide) (PLA) based nanoparticles.* European Journal of Pharmaceutics and Biopharmaceutics, 2010. **75**(2): p. 96-106.
64. Rizkalla, N., et al., *Effect of various formulation parameters on the properties of polymeric nanoparticles prepared by multiple emulsion method.* J Microencapsul, 2006. **23**(1): p. 39-57.
65. Mora-Huertas, C.E., H. Fessi, and A. Elaissari, *Influence of process and formulation parameters on the formation of submicron particles by solvent displacement and emulsification–diffusion methods: Critical comparison.* Advances in Colloid and Interface Science, 2011. **163**(2): p. 90-122.
66. Lepeltier, E., C. Bourgaux, and P. Couvreur, *Nanoprecipitation and the "Ouzo effect": Application to drug delivery devices.* Advanced Drug Delivery Reviews, 2014. **71**(0): p. 86-97.
67. Johnson, B.K. and R.K. Prud'homme, *Mechanism for Rapid Self-Assembly of Block Copolymer Nanoparticles.* Physical Review Letters, 2003. **91**(11): p. 118302.
68. Pustulka, K.M., et coll., *Flash Nanoprecipitation: Particle Structure and Stability.* Molecular Pharmaceutics, 2013. **10**(11): p. 4367-4377.

69. Karnik, R., et al., *Microfluidic Platform for Controlled Synthesis of Polymeric Nanoparticles.* Nano Letters, 2008. **8**(9): p. 2906-2912.
70. Stroock, A.D., et al., *Chaotic Mixer for Microchannels.* Science, 2002. **295**(5555): p. 647-651.
71. Galindo-Rodriguez, S., et al., *Physicochemical Parameters Associated with Nanoparticle Formation in the Salting-Out, Emulsification-Diffusion, and Nanoprecipitation Methods.* Pharmaceutical Research, 2004. **21**(8): p. 1428-1439.
72. Quintanar-Guerrero, D., et al., *A mechanistic study of the formation of polymer nanoparticles by the emulsification-diffusion technique.* Colloid and Polymer Science, 1997. **275**(7): p. 640-647.
73. Johnson, B.K. and R.K. Prud'homme, *Chemical processing and micromixing in confined impinging jets.* AIChE Journal, 2003. **49**(9): p. 2264-2282.
74. Nicolai, T., O. Colombani, and C. Chassenieux, *Dynamic polymeric micelles versus frozen nanoparticles formed by block copolymers.* Soft Matter, 2010. **6**(14): p. 3111-3118.
75. Zhang, L. and A. Eisenberg, *Multiple Morphologies and Characteristics of "Crew-Cut" Micelle-like Aggregates of Polystyrene-b-poly(acrylic acid) Diblock Copolymers in Aqueous Solutions.* Journal of the American Chemical Society, 1996. **118**(13): p. 3168-3181.
76. Valencia, P.M., et al., *Microfluidic technologies for accelerating the clinical translation of nanoparticles.* Nat Nano, 2012. **7**(10): p. 623-629.
77. Khan, I.U., et coll., *Microfluidics: A focus on improved cancer targeted drug delivery systems.* Journal of Controlled Release, 2013. **172**(3): p. 1065-1074.
78. Belliveau, N.M., et al., *Microfluidic Synthesis of Highly Potent Limit-size Lipid Nanoparticles for In Vivo Delivery of siRNA.* Mol Ther Nucleic Acids, 2012. **1**: p. e37.
79. Leung, A.K.K., et al., *Lipid Nanoparticles Containing siRNA Synthesized by Microfluidic Mixing Exhibit an Electron-Dense Nanostructured Core.* The Journal of Physical Chemistry C, 2012. **116**(34): p. 18440-18450.
80. Kolishetti, N., et al., *Engineering of self-assembled nanoparticle platform for precisely controlled combination drug therapy.* Proceedings of the National Academy of Sciences, 2010. **107**(42): p. 17939-17944.
81. Legrand, P., et al., *Influence of polymer behaviour in organic solution on the production of polylactide nanoparticles by nanoprecipitation.* Int J Pharm, 2007. **344**(1-2): p. 33-43.
82. Letchford, K., R. Liggins, and H. Burt, *Solubilization of hydrophobic drugs by methoxy poly(ethylene glycol)-block-polycaprolactone diblock copolymer micelles: Theoretical and experimental data and correlations.* Journal of Pharmaceutical Sciences, 2008. **97**(3): p. 1179-1190.
83. Panyam, J., et al., *Solid-state solubility influences encapsulation and release of hydrophobic drugs from PLGA/PLA nanoparticles.* Journal of Pharmaceutical Sciences, 2004. **93**(7): p. 1804-1814.
84. He, C., et al., *Effects of particle size and surface charge on cellular uptake and biodistribution of polymeric nanoparticles.* Biomaterials, 2010. **31**(13): p. 3657-66.

85. Walkey, C.D., et al., *Nanoparticle Size and Surface Chemistry Determine Serum Protein Adsorption and Macrophage Uptake.* Journal of the American Chemical Society, 2011. **134**(4): p. 2139-2147.
86. Rejman, J., et al., *Size-dependent internalization of particles via the pathways of clathrin- and caveolae-mediated endocytosis.* Biochem J, 2004. **377**(Pt 1): p. 159-69.
87. Matsumura, Y. and H. Maeda, *A new concept for macromolecular therapeutics in cancer chemotherapy: mechanism of tumoritropic accumulation of proteins and the antitumor agent smancs.* Cancer Res, 1986. **46**(12 Pt 1): p. 6387-92.
88. Gaumet, M., et al., *Nanoparticles for drug delivery: the need for precision in reporting particle size parameters.* Eur J Pharm Biopharm, 2008. **69**(1): p. 1-9.
89. Rabanel, J.-M., P. Hildgen, and X. Banquy, *Assessment of PEG on polymeric particles surface, a key step in drug carrier translation.* Journal of Controlled Release, 2014. **185**(0): p. 71-87.
90. Gessner, A., et al., *Influence of surface charge density on protein adsorption on polymeric nanoparticles: analysis by two-dimensional electrophoresis.* European Journal of Pharmaceutics and Biopharmaceutics, 2002. **54**(2): p. 165-170.
91. Dobrovolskaia, M.A., et al., *Method for Analysis of Nanoparticle Hemolytic Properties in Vitro.* Nano Letters, 2008. **8**(8): p. 2180-2187.
92. Gref, R., G. Miralles, and É. Dellacherie, *Polyoxyethylene-coated nanospheres: effect of coating on zeta potential and phagocytosis.* Polymer International, 1999. **48**(4): p. 251-256.
93. Nel, A.E., et coll., *Understanding biophysicochemical interactions at the nano-bio interface.* Nat Mater, 2009. **8**(7): p. 543-57.
94. Shakesheff, K.M., et al., *The adsorption of poly(vinyl alcohol) to biodegradable microparticles studied by x-ray photoelectron spectroscopy (XPS).* Journal of Colloid and Interface Science, 1997. **185**(2): p. 538-547.
95. Banquy, X., et al., *Selectins Ligand Decorated Drug Carriers for Activated Endothelial Cell Targeting.* Bioconjugate Chemistry, 2008. **19**(10): p. 2030-2039.
96. Vonarbourg, A., et al., *Parameters influencing the stealthiness of colloidal drug delivery systems.* Biomaterials, 2006. **27**(24): p. 4356-73.
97. Heald, C.R., et al., *Poly(lactic acid)-poly(ethylene oxide) (PLA-PEG) nanoparticles: NMR studies of the central solidlike PLA core and the liquid PEG corona.* Langmuir, 2002. **18**(9): p. 3669-3675.
98. Garcia-Fuentes, M., et al., *Application of NMR Spectroscopy to the Characterization of PEG-Stabilized Lipid Nanoparticles.* Langmuir, 2004. **20**(20): p. 8839-8845.
99. Perry, J.L., et al., *PEGylated PRINT Nanoparticles: The Impact of PEG Density on Protein Binding, Macrophage Association, Biodistribution, and Pharmacokinetics.* Nano Letters, 2012. **12**(10): p. 5304-5310.
100. Sant, S., S. Poulin, and P. Hildgen, *Effect of polymer architecture on surface properties, plasma protein adsorption, and cellular interactions of pegylated nanoparticles.* Journal of Biomedical Materials Research, Part A, 2008. **87A**(4): p. 885-895.

101. Trimaille, T., et al., *Poly(d,l-lactic acid) nanoparticle preparation and colloidal characterization.* Colloid and Polymer Science, 2003. **281**(12): p. 1184-1190.
102. Santander-Ortega, M.J., et al., *Colloidal stability of Pluronic F68-coated PLGA nanoparticles: A variety of stabilisation mechanisms.* Journal of Colloid and Interface Science, 2006. **302**(2): p. 522-529.
103. Rabanel, J.-M., et al., *"Effect of polymer architecture on the structural and biophysical properties of PEG-PLA nanoparticles"* ACS Applied Materials and Interfaces, Accepted April 24th 2015.
104. Cui, H., et al., *Elucidating the assembled structure of amphiphiles in solution via cryogenic transmission electron microscopy.* Soft Matter, 2007. **3**(8): p. 945-955.
105. Sant, S., V. Nadeau, and P. Hildgen, *Effect of porosity on the release kinetics of propafenone-loaded PEG-g-PLA nanoparticles.* J Control Release, 2005. **107**(2): p. 203-14.
106. Sitterberg, J., et al., *Utilising atomic force microscopy for the characterisation of nanoscale drug delivery systems.* European Journal of Pharmaceutics and Biopharmaceutics, 2010. **74**(1): p. 2-13.
107. Siepmann, J., et al., *Effect of the size of biodegradable microparticles on drug release: experiment and theory.* Journal of Controlled Release, 2004. **96**(1): p. 123-134.
108. Arifin, D.Y., L.Y. Lee, and C.-H. Wang, *Mathematical modeling and simulation of drug release from microspheres: Implications to drug delivery systems.* Advanced Drug Delivery Reviews, 2006. **58**(12–13): p. 1274-1325.

3 Article de revue “Assessment of PEG on Polymeric Particles Surface, a Key Step in Drug Carrier Translation”

Publié dans “Journal of Controlled Release”, Vol.185 pp71-87 (2014) 185

Dans cette revue nous nous attachés à réviser les méthodes analytiques rapportés pour examiner la couche de chaines de PEG installée à la surface de nanotransporteurs de médicament. Nous nous sommes particulièrement intéressés aux méthodes quantitatives afin de diriger nos travaux futurs.

Cette étude critique s’avérait un préalable obligé de ce projet de recherche qui consiste à mettre en évidence les relations entre l’architecture des matériaux que nous allions développés et les propriétés de surface des nanotransporteurs fabriqués par la suite.

En annexe 1, se retrouvent des informations complémentaires à cette étude, notamment les méthodes de calculs des densités de surface des chaines de poly(éthylène glycol) que nous avons par la suite intégrées dans les études décrites dans le Chapitre 4 et 5.

Assessment of PEG on Polymeric Particles Surface, a Key Step in Drug Carrier Translation

Jean-Michel Rabanel [1, 2], Patrice Hildgen [1], Xavier Banquy [2, ‡]

[1] *Laboratoire de Nanotechnologie Pharmaceutique, Faculté de Pharmacie, Université de Montréal, C.P. 6128, Succursale Centre-ville, Montréal, Québec, H3C 3J7, Canada*

[2] *Canada Research Chair in Bio-inspired materials, Faculté de Pharmacie, Université de Montréal, C.P. 6128, Succursale Centre-ville, Montréal, Québec, H3C 3J7, Canada*

[‡] *Corresponding author*

3.1 Abstract

Injectable drug nanocarriers have greatly benefited in their clinical development from the addition of a superficial hydrophilic corona to improve their cargo pharmacokinetics. The most studied and used polymer for this purpose is poly(ethylene glycol), PEG. However, in spite of its wide use for over two decades now, there is no general consensus on the optimum PEG chain coverage-density and size required to escape from the mononuclear phagocyte system and to extend the circulation time. Moreover, cellular uptake and active targeting may have conflicting requirements in terms of surface properties of the nanocarriers which complicates even more the optimization process. These persistent issues can be largely attributed to the lack of straightforward characterization techniques to assess the coverage-density, the conformation or the thickness of a PEG layer grafted or adsorbed on a particulate drug carrier and is certainly one of the main reasons why so few clinical applications involving PEG coated particle-based drug delivery systems are under clinical trial so far.

The objective of this review is to provide the reader with a brief description of the most relevant techniques used to assess qualitatively or quantitatively PEG chain coverage-density, conformation and layer thickness on polymeric nanoparticles. Emphasis has been made on polymeric particle (solid core) either made of copolymers containing PEG chains or modified after particle formation. Advantages and limitations of each technique are presented as well as methods to calculate PEG coverage-density and to investigate PEG chains conformation on the NP surface.

Key words: Poly(ethylene glycol), coverage-density, nanoparticle, surface analysis, DLS, Zeta potential, fluorescence quantification, NMR, XPS

3.2 Introduction

Poly(ethylene glycol) (PEGs) is extensively used as a surface modifier of particulate drug carriers to provide important biological properties such as reducing toxicity and extending circulation time [1, 2]. Amongst all drug carriers, polymeric "PEGylated" microparticles (MP) and nanoparticles (NP) are investigated for their potential use as drug delivery and targeting systems taking advantage of their stability in biological media, their prolonged period of circulation in the blood and their role in decreasing drug toxicity and clearance [3-7]. However, only a few nanocarrier platforms based on PEGylated particles have reached the market with, in several cases, limited improvements over already available formulations [8].

Controlling NP surface properties is a challenging task due to the many, often conflicting, constrains that are involved in the design of a particle surface. Such constraints involve the *simultaneous* specific recognition of targeted pathological sites and avoidance of non-specific recognition by serum proteins, cells, tissues and organs. While the former is conferred by elements such as antibodies, peptides, ligands, etc., the latter is usually conferred by a polymeric hydrophilic corona covering the entire particle surface.

Poly(ethylene glycol) has been for more than two decades the polymer of choice for such corona, even if alternatives are now emerging [9, 10]. PEG and PEG monomethyl ether are ones of the few polymers approved for internal use in humans by the FDA, which is an important consideration when developing new pharmaceutical formulations [11, 12]. Nonetheless, biocompatibility of new excipient created by PEG covalent coupling to various polymers needs to be documented before advancing to the clinical trials stage [7]. Its unique combination of properties such as biocompatibility, low immunogenicity, water and organic solvent solubility, have made PEG the gold standard since the beginning of the 90's. Indeed, Doxil®, a PEGylated liposomal formulation of doxorubicin was introduced on the US market as early as 1995 [13]. Since then, formulation development based on PEGylated polymeric particles has been confined to the clinical trial level, although some have recently shown promising outcomes [7, 14].

So far, optimal PEG surface coverage-density has been empirically determined for each system by varying the experimental conditions of carrier preparation, often with only a qualitative proof of PEG presence on the surface. Considering how critical PEG is for NP performance, routine but precise assessment of PEG surface coverage-density is a pre-requisite in drug carrier development, production and quality control.

The objective of this review is to provide the reader with available tools to assess qualitatively or quantitatively PEG surface coverage-density either directly or indirectly on polymeric MP or NP surfaces. Advantages and limitations of each technique will be presented as well as methods to calculate PEG density and to estimate PEG chains conformation.

3.3 PEGylation of polymeric particles

3.3.1 Particle fabrication methods and consequences on PEG distribution

Polymeric NPs have diverse morphologies, preparation methods, type of polymer matrix as well as intended uses [15-18]. Creation of a PEG coating on a NP surface can be achieved in different ways (Table 3.1) such as the segregation of (i) a hydrophilic segment of the core matrix polymer at the surface (ex: poly(lactic-co-glycolic)/PEG or poly(lactic)/PEG diblock polymers), or (ii) of additives with an amphiphilic structure (ex. PEG-oleate, PEG-stearate). Alternatively, it can also result from the addition of hydrophilic polymers on preformed particle by either (iii) physiosorption, electrostatic interactions (iv) covalent attachment (grafting-to approaches) of functional PEG to available surface reactive groups or (v) emulsion/copolymerization [3, 19].

When polymeric NPs are formed by emulsification techniques such as microfluidic techniques [20, 21] or nanoprecipitation, PEG can be introduced on the NP surface either as an amphiphilic molecule additive or as part of the polymer matrix (Fig. 1-B). It is ideally expected that PEG segments will segregate completely to the interface with water, while the hydrophobic part of the polymer will remain in the particle core. However, PEG segments can also remain in the particle core as well (Fig. 1-A), thus decreasing PEG concentration at the surface [22]. Several reasons can account for such phenomenon, such as entanglements, small polymeric chains lost in the external aqueous phase, physical processes involved in the NP preparation (such as diffusion of water and solvent, viscositycontrasts, polymer-polymer interactions, etc.), solidification processes, or the presence of aqueous cavities in the particle (Fig. 1 A).

Approaches based on the surface modification of preformed particles have the advantage of ensuring the presence of PEG exclusively at the surface. On the other hand, they may result in batch-to-batch variations of coupling yield and incomplete coverage due to steric constraints and reaction rates. PEG copolymer adsorption can be achieved by hydrophobic interactions [23, 24] or by electrostatic interactions with charged particle surfaces [25]. Such interactions can be too weak to guaranty strong anchoring of PEG chains on the NP surface *in vivo* [26]. Covalent grafting of

end-functionalized PEG chains on preformed particles is less reported (the "grafting-to" approach). Just to name a few, such approach can involve a carbodiimide coupling reaction between an activated COOH group and NH_2 to form amide bond [27, 28]; modified PEG reaction with thiols yielding to thioester bonds [29]; or more recently an alkyne/azide coupling reaction [30]. In all cases, the grafting density of PEG on preformed particles is expected to be rather low or at least insufficient to reach the brush conformation regime mainly due to steric limitations of the adsorption of the hydrophobic anchors or to the steric hindrance affecting the coupling reaction of neighboring bulky PEG chains. Moreover, tedious separation and purification steps have to be implemented to eliminate the excess of non-adsorbed or unreacted PEG chains. This particular step can be very problematic if the anchoring strength is weak as with physio-adsorbed polymers.

3.3.2 Relationship between PEG coverage-density and the NP biophysical properties

The PEG layer may have different roles in a particle biological fate, and all of them depend on the chain coverage-density. PEG coatings are known to prevent aggregation and to stabilize particles and colloidal suspensions in physiological salt concentration media by steric and hydration repulsions [31-33].

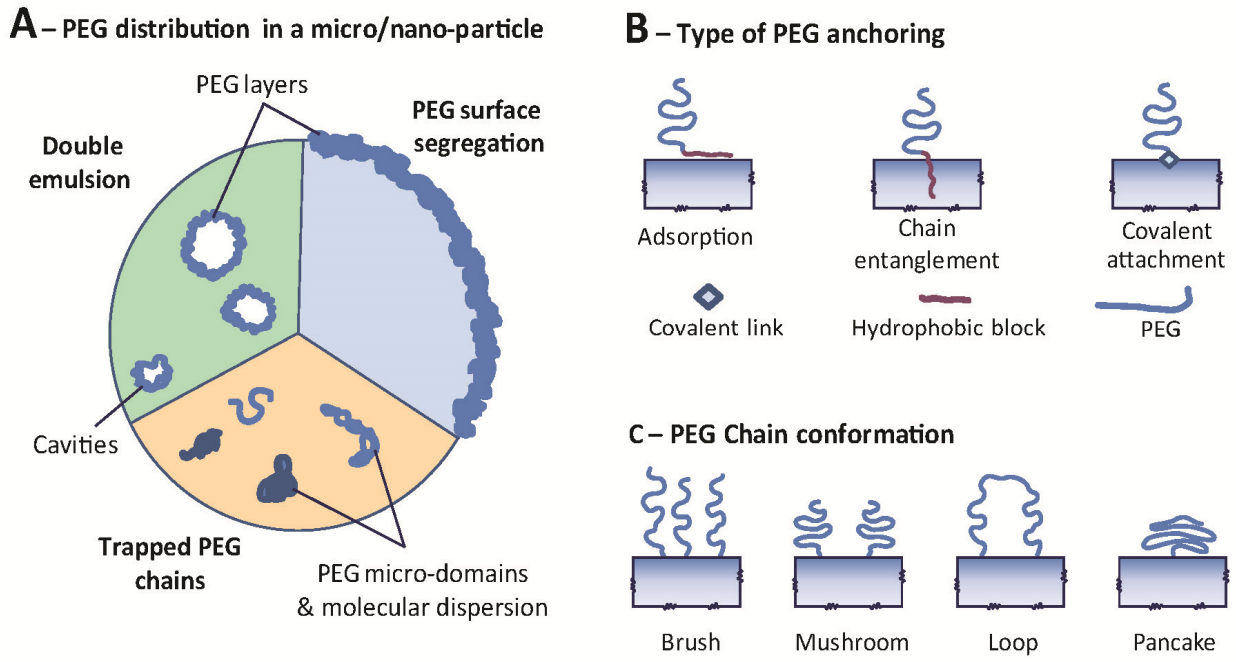

Figure 3.1. Pegalyted polymeric micro or nanoparticle: (A) PEG distributions in a polymeric particle depending on the fabrication process; (B) Schematic representation of the different types of PEG anchoring on a surface; (C) PEG conformations on a particle surface.

The resistance to non-specific absorption (opsonisation) of plasmatic proteins is the most important determinant of NP fate once injected in the host [34]. High resistance to protein adsorption leads to a decreased uptake by the Mononuclear Phagocytose System (MPS), decreased degradation and elimination rate leading to a longer half-life in the blood stream, which in turn influences drug pharmacokinetic (PK) parameters. The resistance to proteins binding (the so-called "antifouling effect") is dependent on PEG chains coverage conformation and is usually achieved at high coverage-density (Fig. 1-C), in the polymeric brushes regime [2, 35]. The optimal coverage-density is still a matter of debate as some studies showed protein repellency even at low coverage-density [36, 37]. Resistance to protein adsorption may also improve targeting capabilities by preventing blockade by steric hindrance of ligand recognition [38, 39]. The PEG layer on NP surface can also improve drug encapsulation by providing a physico-chemical barrier to drug escape and it could affect drug release pattern [40].

In addition to the abovementioned biological properties, it has been recently demonstrated that PEG surface coverage controls NP transport through biological matrices such as the gastrointestinal tract (GIT) mucus [41], the cervicovaginal mucus [42], the pulmonary mucus [43] and the tumor extracellular matrix [44]. Improving the ability of a NP to diffuse in a complex media can potentially greatly improve drug delivery efficacy, as electrostatic and steric hindrances prevent NP to cross mucosal barriers or to penetrate tissues beyond the perivascular region [45, 46]. Very dense coatings seem to be necessary (about 0.5-1 PEG/nm^2 for 200 nm diameter particle) to achieve particle transport coefficients in mucus comparable to those in liquid medium [43].

Table 3.1. Main PEGylation strategies for polymeric particles

	Advantages	Drawbacks	Interactions/bonding	Pegylated molecule	Ref.
Modification of preformed drug loaded particle surface					
Physisorption (non-covalent)	PEG presence limited to the surface Simple and convenient technique	Instability of anchorage Additional purification steps Coverage-density limited by steric hindrance	Hydrophobic interaction (hydrophobic surface) Electrostatic interaction (charged surface)	Poloxamer®, Poloxamine®, Pluronic®, PS-*b*-PEG PLL-PEG; pASP-PEG	[47] [24, 48] [25, 49-51]
Grafting to- (covalent)	Stability of the PEG layer	Requires a control of surface reactive group number Additional purification steps	COOH/NH_2 coupling	PEG-NH_2	[27, 28, 52]
		Coverage-density limited by steric hindrance	Grafting on NH_2 Click chemistry Thiol coupling	PEG-succinimidyl ester-PA PEG-N_3 PEG-SH	[53] [30] [54, 55]
Inclusion & affinity complexes	No chemical reaction involved	Steric limitation to coverage-density Complexes stability may be hampered by other potential biological guests	Cyclodextrine/Adamantane	PEG-Adamantane	[31, 56]
			Avidin/biotin	PEG-Biotin	[57]
Segregation of PEG during the formation stage (emulsion & nanoprecipitation)					
Pegylated matrix polymer	High stability of the PEG layer	Control of PEG segregation	Covalent link	Diblock polymer : PEG-PLA, PEG-PLGA; PEG-PACA; PEG-PIBCA;	[58-62]
	High coverage-density acheivable	Possible formation of microdomains		Triblock and multiblocks: PEG-PLA-PEG	[63, 64]
	Single step fabrication process			Comb copolymers: PEG-*g*-PLA	[65, 66]
Amphiphilic emulsifiers	Stability of the PEG layer by physical entanglement	Long term stability of the PEG layer	Physical link by chain entanglement	Diblock : PEG-Stearate DSPE-PEG SQ-PEG	[67] [68-70] [71] [70]
	Single step fabrication process	Residual free polymer in solution		Triblock : PEG-Distearate	[72]
Emulsion/polymerization					
	Single step fabrication process	Stability of encapsulated drug Additional purification steps	Covalent link	PIBCA-PEG PEG-acrylate PPhe-NH_2-PEG PEG-HEMA/HEMA-PLA	[37] [73] [74, 75]

Note : PLA; poly(lactic); PLGA: poly(lactic-co-glycolic); PLL: poly(L-Lysine); PS: poly(styrene); pASP-EPG: poly(asparctic acid)-PEG, SQ-PEG: Squalene-PEG; PACA: poly(alkylcyanoacrylate); PIBCA: poly(isobutylcyanoacrylate); PPhe-PEG: Poly(phenylalanine)-PEG; DSPE: 1,2-Distearoyl-sn-glycero-3-phosphoethanolamine; PEG-HEMA: 2-hydroxylethyl methacrylate-PEG

Target recognition and docking of ligand molecules located at the surface of a PEGylated particle are dependent on the density and thickness of the PEG layer and the positioning of the ligand [76-78]. It appears that long circulation time, low non-specific cellular uptake and active targeting have conflicting requirements in terms of NP surface properties which complicates the formulation process. Non-optimal properties of a NP layer can induce activation of the complement cascade and contribute to the "accelerated blood clearance" (ABC) associated to the production of antibodies directed to PEG, after repeated administered doses [79]. Noteworthy, the level of immunogenicity of PEG, as well as the biological effects of the immune response, are still a matter of debate [80].

Increase in PEG coating density or layer thickness seems to affect NP cellular uptake as well [81]. Low cellular uptake can be advantageous since it increases circulation time due to MPS avoidance. On the other hand, it may also decrease drug efficacy if the intended targeted cells are not internalizing efficiently the drug carriers. This step is critical for the efficacy of several types of drugs with intracellular target such as *si*RNA or drugs subjected to efflux pumps. This situation is referred as the "PEG dilemma" as addition of PEG is having simultaneously a positive impact on the biodistribution of the NP as well as a negative impact on the cellular uptake and endosomal escape of the NP [18, 82]. For example, conflicting results observed with nuclei acid carriers [83] could be explained by the lack of quantitative structural studies of these supra-molecular assemblies. More sophisticated approaches have been recently designed to overcome this "PEG dilemma" using sheddable PEG layer [84]. In this approach, surface grafted PEG chains are removed at the targeted site by enzymatic, hydrolytic or redox cleavage of chemical linkers [85-87]. Reported methods to assess PEGylation and de-PEGylation of the particles remain however largely qualitative at this point [51, 57].

In spite of the extensive use of PEG for three decades now, there is no general consensus on what is the optimum coverage-density, conformation and molecular weight (M_w) combination for a given carrier and application. [2, 19]

3.3.3 Current challenges in PEG dosage

Correlating particle biological performance and PEG coverage-density is an arduous task due to the lack of standard quantification tests. Qualitative and batch-to-batch relative quantification are the most commonly used approaches of reporting PEG surface content.

Part of this issue originates from the lack of convenient and reliable analytic techniques to dose surface-bound PEG chains, particularly on polymeric particles. One of the challenges with PEG quantification resides in the fact that it is not detectable directly by spectroscopic techniques. Indeed, detection by UV (or fluorescence) spectroscopy requires the coupling of PEG chains to a chromophore, resulting in laborious and complex procedures.

Another issue is to distinguish between the PEG located at the surface from the total PEG present in the carrier, either trapped in the polymeric matrix, or loosely bound to the surface. Complete segregation of PEG chains at the surface of the NP is often assumed without providing direct evidence, which in some cases could be justified by the preparation method used, as in the case of addition of PEG on preformed particles [37, 88]. But in other cases it is not clearly justified and results in an overestimation of PEG coverage-density. Direct assessment of PEG on intact particles is sough and possible to some extend by NMR (as discussed later in section 4). According to the preparation methods used to add the PEG corona on the NP, quantification methods may have to be adapted in order to differentiate surface PEG from total PEG. If PEG is added by grafting or adsorption on preformed particles, one has to make sure that loosely- bound or free PEG is not inferring with the dosage.

Lastly, procedures involving a purification step to separate bound from free PEG may introduce several methodological bias. On the other hand, with nanoprecipitation or emulsion-based preparation methods, it is clear that in most cases the total PEG content cannot simply be assumed to represent only surface PEG (Fig. 1).

3.3.4 PEG surface coverage parameters

The different PEG chains conformations at interfaces are presented in section S1.1. Calculation methods and error analysis regarding PEG coverage-density are presented in Supporting Information, sections S1.2 and S1.3 (available free of charge at http://www.sciencedirect.com). In what follows we provide some definitions of the commonly used parameters describing PEG coverage on a particle surface.

Weight coverage-density, is a PEG mass per surface unit, noted Γ ($\Gamma = \rho t$, where ρ is PEG layer volumetric density and t, layer thickness in wet or dry state according the analytical method used). ***Surface chain coverage-density***, σ is more generally expressed as PEG chain/nm^2 [35, 36, 58, 88, 89]. This expression of PEG density will be used in this review. ***Surface coverage***

represents the PEG coating efficiency, i.e. the percentage of total PEG found on the surface of a NP. It is expressed as a percentage of NP surface covered by PEG. ***PEG coating efficiency*** is referred to the percentage of PEG present at the surface in regard of total PEG in the particle [22, 90]. ***PEG coating density*** is similar to the PEG coating efficiency but is expressed in terms of weight quantities, for instance, in mg of PEG at the surface for 100 mg of particle [22].

PEG footprint, ***FP***, is the projected area of a single chain of PEG end-grafted on a NP surface. It is also defined and expressed by the relation (in nm^2/chain of PEG) which is the reciprocal of the coverage-density (in the brush regime only):

$$FP = A_{PEG} = \frac{1}{\sigma} = \frac{S}{N_{PEG}} \ (nm^2) \qquad \textbf{(1-1)}$$

The actual "occupied" area (i.e. the chain footprint) should be distinguished from area "available" to the chain (A_{PEG}). When $D > 2R_F$ the area occupied by a PEG chain is less than the available area (see Fig. 2A). When $D < 2R_F$, the area occupied by a PEG chain is equal to the available space (Fig. 2B-C). ***Distance between chains*** (or grafting distance, D, in nm) can be calculated when the PEG chain footprint is a circular area in a close packed hexagonal arrangement. The expression for D under these assumptions is:

$$D = 2\sqrt{\frac{A_{PEG}}{\pi}} \ (nm) \qquad \textbf{(1-2)}$$

It is important to stress that the number of PEG chains per particle is of limited usefulness as particle mean diameter may vary from batch to batch. It is more reliable for comparison purposes to use the surface coverage-density expressed as PEG/nm^2.

3.4 Indirect assessment of surface PEGylation efficiency

To assess the presence of PEG on a particle surface, many comparative measurements based on the changes in the physical or chemical properties of the particles induced by the addition of PEG have been used. The most popular techniques by far are the monitoring of the particle hydrodynamic diameter (D_H) or the zeta potential (ζ) upon PEGylation. Other indirect measurements worth mentioning are surface the measurements of hydrophilicity or protein binding on PEGylated NPs.

3.4.1 Particle size

Several techniques are available to measure particle diameters. Amongst them, the most used on a routine basis in the nanometer range (2 to 1000 nm) is Dynamic Light Scattering (DLS) also named Photon correlation spectroscopy (PCS).

The particle size measured by DLS is referred to as a "hydrodynamic radius" (R_H). The measured size is not only dependent on the core size of the NP but also on any polymer or solvent/ion molecules attached or loosely bound to the particle surface (Fig. 2). DLS measurements apply best to homogenous population, i.e. monomodal (single peak), spherical or near-spherical, monodisperse (narrow width of distribution) particle suspensions in the range of 2 nm to 2000 nm with a single refractive index.

Grafting of PEG on a NP surface results in an increase of the NP diameter equals to twice the thickness (L) of the PEG layer. As shown in the SI (SI-S1.1), L can be related to the coverage-density σ, in the brush regime. Measurement of NP hydrodynamic diameters before and after PEG grafting have shown, in several studies, a diameter increase compatible with the PEG layer thickness expected from the theory, particularly in the brush regime. For example, size measurements of silica NPs by DLS, before and after grafting of PEG 5kD showed differences in diameter consistent with the radius of gyration of PEG [91].

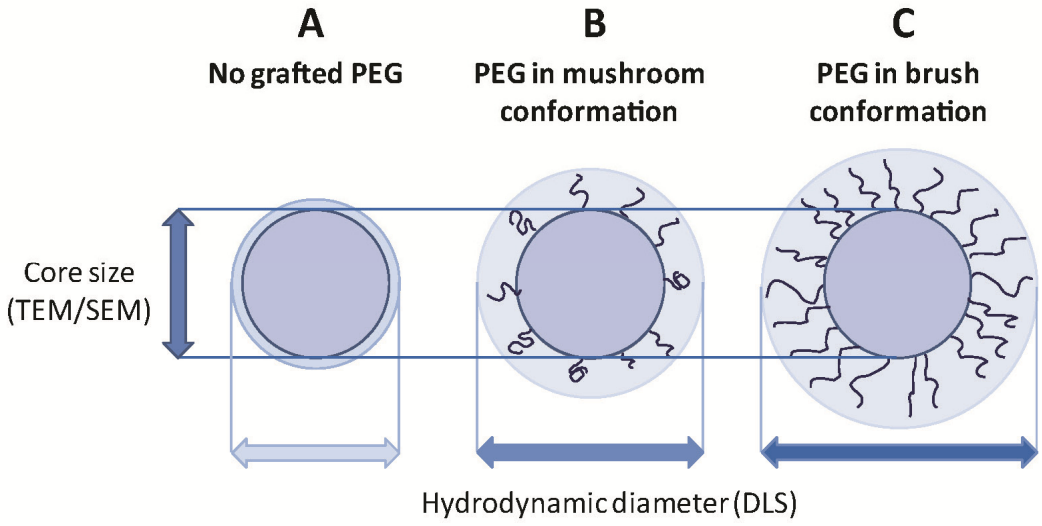

Figure 3.2. Hydrodynamic diameter and core diameter of naked vs. PEGylated NP. (A): "Naked" particle; (B): PEGylated particle (mushroom regime); (C): PEGylated particle (brush regime).

Similarly gold NPs of different sizes were functionalized with mixtures of PEG of different molecular weights. DLS size results were related to PEG layer composition, ratio of long and short PEG chains reacted to the gold surface [92].

Stolnik *et al.* adsorbed small diblock PLA-PEG_{2000}, PLA-PEG_{5000} and Poloxamine 908® to poly(styrene) (PS) or poly(lactic-co-glycolic) (PLGA) preformed NPs to create an adsorbed coating of PEG coating. The authors reported a coating layer thickness of 2 to 10 nm, consistent with value of L for PEG chains lengths used [47]. Similarly, Redhead *et al.* prepared PLGA particles and incubated them with Poloxamine 908®. Results showed an increase in mean particle size upon physisorption but with lower values (4-6 nm layer thickness) [24].

It is clear that R_H overestimates the core particle radius R_C which is the key parameter to estimate the total surface on which PEG is attached or anchored. It is however, very much in use and the most reported radius value is usually *z*-average value, even if it is strongly affected by the presence of a small number of large particles. For NP surface characterization, it is more recommended to retain the mean radius from particle size distribution in number. Moreover, it provides values more comparable to size values obtained by technique such as TEM.

DLS can also put in evidence the effect of steric stabilization of a PEG layer on particle in suspension. This can be achieved by monitoring the decrease in particle size as the concentration of PEG derivatives, used in the preparation method destined to be adsorbed on the particle surface, is increased in the medium [51]. In several studies, PEG surface coverage has been correlated to aggregation kinetics (assess by DLS) at different salts concentration of the medium [31, 32].

The technique has limitations both as an analytical tool and in the type of particle that can be characterized. Firstly as mentioned above, only uniform (non-structured) spherical NPs can be analyzed. Measurements on NPs with other shapes (elliptical, rod) or structure (core-shell, vesicle) should be performed with other methods, such as microscopy. The sensitivity of DLS is limited, mainly by two factors. First the PEG layer thickness is dependent on both PEG M_w and coverage-density and it usually varies between 1 and 10 nm. This small difference in the layer thickness may not be detected, or be considered as significant, when measuring particle size well above this range (> 100-200 nm). However, for smaller particles (<20 nm), this difference may be significant providing that the polydispersity index (PDI) is constant before and after grafting. Indeed, it is essential to compare batches with low and similar PDI, as pointed out by several authors [91, 93]. Molecular species interacting with the particles and/or altering the properties of the suspension stabilizer, can impact the measurements as well [94]. Viscosity, pH, salts concentrations changes,

release of surfactants from particles surface, as well as temperature and NP concentration can strongly impact the measurements and should be controlled to maintain similar conditions [95]. Finally characterization of mixtures of NP populations of different sizes or sizes above 1 µm should be avoided due to the lack of precision of most standard equipment in resolving such complex systems [93].

Correlations between NP hydrodynamic diameter and PEG surface coverage are not always straightforward because particle size assessed by DLS is measured at the shear plane between the particle and the surrounding fluid. The position of this shear plane is *a priori* different from the unperturbed chain length (see Fig. 3). Moreover, the increase of D_H is not always consistent with the scaling theory prediction of a PEG layer thickness in all cases [96], other contributions, such as aggregation state might be considered.

Finally, assessment of PEG presence by DLS is recommended only in the case of a PEG layer added *after* the formation of the NP. Nanoprecipitation or emulsion-based processes will generate very different NP sizes in presence or absence of PEGylated polymers that can act as surfactants.

Other sizing techniques are available to obtain hydrodynamic diameters (from particles suspended in liquid medium), such as Laser light diffraction, more adapted to multi-modal particle populations sizes up to 2000 µm in size. Nonetheless, this technique is limited to particle populations whose diameters is above 20 nm and to requires large sample volumes. Several other sizing techniques based on individual particles analysis, such as Particle Tracking Analysis (PTA) [97], Tunable Resistive Pulse Sensor (TRPS) or Scanning Ion Occlusion Sensing (SIOS) [98, 99] are still under evaluation to quantify PEG surface coverage.

Microscopy and related imaging techniques are rather limited for the characterization of PEG layer thickness measurement using particle size. Scanning electronic microscopy (SEM) and transmission electronic microscopy (TEM) allow to measure particle size (Fig. 3), with a resolution between 1 and 5 nm, if enough NP are analyzed to reach statistical significance [100]. Soft polymeric layers on NPs are not easily visible by TEM and SEM, even with positive and negative staining procedures such as the ones using heavy metals salts. Indeed, polymeric layers on NP are prone to collapse in vacuum and present low electronic density. Microscopy measurements are useful to assess the size of the core of the particles (see section S1.2 and S1.3 in SI about PEG coverage-density calculations). Similar issues are encountered when imaging with atomic force microscopy (AFM), as particles are usually imaged in the dry state [101, 102].

3.4.2 Surface hydrophilicity

3.4.2.1 Contact angle methods

Measures of changes in surface hydrophilicity are used on a routine basis to follow modifications of otherwise hydrophobic, flat substrates after grafting or derivatization with hydrophilic polymer such as PEG. Hydrophobicity of a surface is usually expressed by the three phase-contact angle value, of a liquid (usually water) droplet. In the case of micro- or nanoparticle it is a very difficult experiment, as the determination of contact angle is not usually possible at this scale. Indirect methods have been proposed as surrogate measurements such as production of polymer and "particles" films, followed by measures of the static contact angle.

Films made from the same polymeric material (or material mix) as the particles can be studied for their surface properties. However, to be meaningful, the technique to produce the films should be representative of the NP preparation method. The general method used to obtain polymeric film is spin coating, although the surface properties created at the organic phase/air interface is not representative of the organic phase/water interface polymer organization found in emulsion-based or nanoprecipitation processes used to produce polymeric particles. A lower segregation of hydrophilic chains toward the air interface can be expected compared to the water interface.

Alternatively, it has been proposed to use "particle films" by spin coating a particle suspension on a glass substrate and to subsequently measure static contact angles with a goniometer. Using this approach several studies report correlations between contact angles with PEG surface density [90, 103]. However, contact angle is sensitive to surface energy/chemistry and roughness. Wetting will thus depend on particle size and state of aggregation of NP in the films as well as on the PEG content.

3.4.2.2 Chromatographic techniques

Chromatography has been used to assess the addition of a PEG layer on hydrophobic particles such as PLA or PS particle [47, 104, 105]. Hydrophobic interaction chromatography (HIC) allows separation of PLA and PEG-PLA NP on phenyl-agarose (high hydrophobicity scale) and butyl-agarose (low hydrophobicity scale) columns. The hydrophocity of NP samples was quantified by the percentage of particles retained on either of the column tested under phosphate

buffer saline (PBS) elution conditions. PLA NP were found to be strongly retained on both type of support, while PEG-PLA were only slightly retained [105]. Hydrophilicity of PLGA particle modified with various amounts of PEG-PLA was also assessed by HIC [47] and similar results were obtained with PEGylated cyano-acrylates particles [37]. This technique provides evidence for the modification of the NP surface properties by PEG, but tend to give broad chromatographic peaks due to either the limited resolution of the column or/and particle surface heterogeneity.

3.4.3 Zeta potential

3.4.3.1 Principle of measurement

Surface charges present on the surface of a NP create at the close vicinity of the particle a diffuse layer of ions of opposite charge (see Fig. 3). Additionally, diffusing particles are "escorted" by a layer of solvent molecules strongly bound to their surface which increases effectively their hydrodynamic radius. The zeta potential (ζ) is the electrostatic potential of the NP measured at the interface between the strongly bound layer of solvent molecules and ions and the bulk liquid, also called the shear plane.

High ionic strength of the bulk liquid decreases the measured potential by effect of electrostatic screening. High ionic strength could also affect PEG conformation on the particle surface and alter the position of the shear plane [37]. Furthermore, ζ potential is not only dependant on salts concentration, but also on pH and the type of buffer [106]. Therefore all these parameters, ionic strength, pH and type of buffers have to be controlled to be able to compare adequately NP batches.

Several studies have reported a shift in the ζ potential upon adsorption of PEGylated macromolecules on different type of particles [24, 47] [51, 57]. Increasing the *surface coverage-density of PEG* chains can cause an increase of the PEG layer thickness, which results in a further decrease of ζ (Fig. 3 C) [27].

Similar results could be obtained with the increase of *PEG chain lengths*. Gref *et al.* showed that for PEG-PLA diblock polymeric NP, addition of 2 kD and 5 kD PEG never completely screened the ζ potential, even at high PEG weight percentage in the copolymer. On the other hand, 20 kD PEG have a stronger effect on ζ potential when PEG weight percentage is increased in the copolymer, and could even result in a total screening of the surface charge [107]. Similarly, an addition of small PLA-PEG diblock on preformed PLGA particle results in a ζ potential correlated to PEG chain length increase [47]. Rahme *et al.* reported a non-linear

relationship between PEG M_w and ζ potential of gold particles, with a plateau (a zeta potential minimum) at around 20 kD PEG [108].

The variation of the zeta potential with the ionic strength has been indirectly related to PEG thickness in the case of liposomes [109, 110]. The "Fixed aqueous layer thickness" (or "FALT"), layer of water bound to the liposome surface and moving along with the particle can be calculated from the equation (2.1):

$$\ln \zeta = \ln A - kL \qquad (2.1)$$

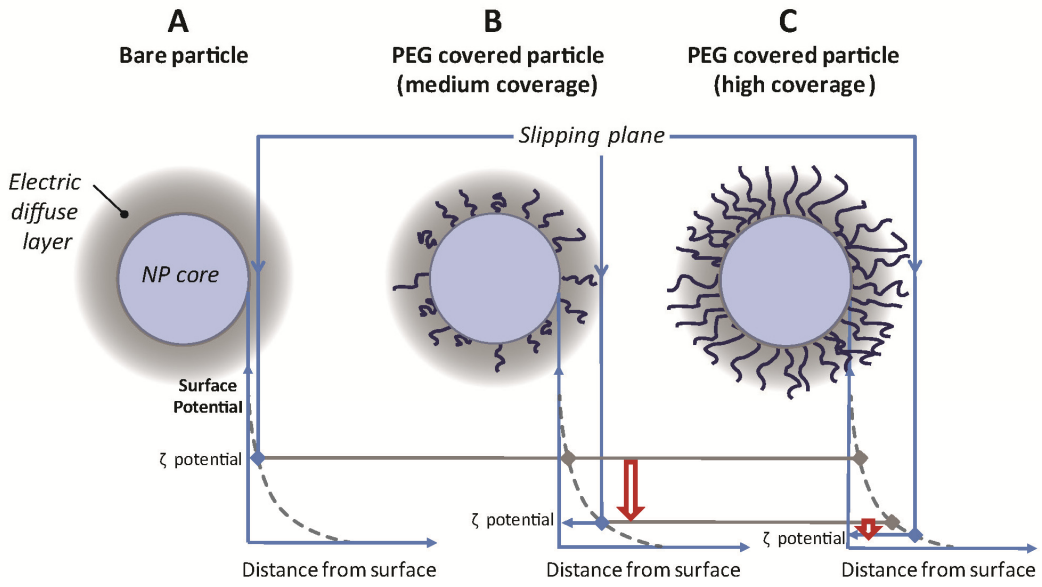

Figure 3.3. Effect of PEGylation on the position of the slipping plane and zeta potential. (A) Bare negatively charged nanoparticle (ex. PLA NP); (B) Negatively charged NP after PEGylation (C) Negatively charged NP with a high surface density of PEG chains. Light grey area represents the electrostatic double layer moving along with the particle. The position of the slipping/shear plane is shifted outward from the particle surface as the length or the grafting density of the PEG chains is increased.

where L is the position of the shear plane (measured in nm from the particle surface); A is the surface potential and k is the inverse Debye length, which depends on the molality of electrolytes in solution. By measuring ζ at different ionic strength (different k), Sadzuka *et al*. were able to estimate the position of the shear plane L for different molecular weights of grafted PEG chains as well as for molecular weight mixture ratio for liposomal preparations [109, 110]. This approach was also used with poly(hexadecyl cyanoacrylates) (PHDCA) PEGylated nanoparticles [111].

3.4.3.2 Limitations of the method

The use of zeta potential measurement to assess PEG layer structure has several limitations. Zeta potential depends on pH, buffer type and salts concentration which may interfere with the effect of PEG layer [106]. It remains thus difficult to compare results acquired in different environments. For instance measurements PLA or PLGA nanoparticle PEGylation have been shown to weakly affect their zeta potential which stays strongly negative in spite of the addition of significant amount of PEG, even if the PEG amount on the surface is significant enough show a biological effect such as protein repellency and increased circulation time [105, 112].

Little evidences of quantitative correlations between PEG coverage-density and ζ have been reported so far, with the exception of the work of Meng *et al.* [27] describing PEG grafting onto PS particle. In this study a linear relationship was found between PEG surface concentration and ζ [27]. On the other hand, upon addition of PEG-PLA diblock on NP made of PLA, a plateau of the zeta potential value is reached rapidly at about 2% weight of PEG content [35]. In another study, polyplexes bearing cyclodextrins (CD) that were modified by PEG-Adamantane (PEG-AD) were reported to exhibited a maximal decrease in zeta potential up to a CD/PEG-AD ratio of 40% [31].

But unfortunately correlations between zeta potential and PEG grafting are not always evident. For example, grafting of PEG on gelatin nanoparticles was reported to have a modest effect on the zeta potential even if 90% of amino group available for grafting were coupled with PEG [96].

3.4.4 Protein binding

PEG coverage-density and conformation are known to control protein binding [2, 19]. Protein binding could thus be used as an indirect evidence for PEG layer presence on the particle surface.

Protein binding on the surface of NP increases the hydrodynamic diameter (and of PDI). Such increase has been reported to be more pronounced for bare PLA particles, particle without any PEG attached on the surface compared to particles exhibiting PEG on their surface [113]. However, such assay is not sensitive in PEG coverage-density or PEG chain length effect [35, 47]. Several studies showed a correlation between the quantity of bound proteins as detected by bicinchoninic acid assay (BCA dosage) and PEG surface-coverage and PEG chain length [114, 115].

Adsorption patterns of plasmatic proteins have been explored in 1D and 2D western blot and appeared to be well correlated to NP surface hydrophilicity [116]. Western blots also showed that the correlation is not valid for all proteins species [117]. Binding of proteins on NP surface have been related to surface properties by ITC microcalorimetry [36, 118].

PEG density and length have also been related to complement consumption activity in *in vitro* assays for PEG grafted on poly(isobutyl 2-cyanoacrylate) NP [2, 37] and for surface modified Poloxamine-PS NP [119]. Nitrogen content of particle surface quantified by X-rays photoelectrons spectroscopy (XPS) can be related to the concentration of adsorbed protein and therefore to efficacy of the PEG layer [120, 121]. More detailed information about XPS technique is presented in section 6.

One of the issues with proteins binding assay is the optimization of the separation method to isolate particle-proteins complexes. The method should be able to remove loosely bounded proteins while, maintaining biologically relevant interactions (even weak ones). If the conditions are too harsh, only the protein "hard corona" [122] will be evidenced. If the conditions are too mild, irrelevant protein interactions may be detected and quantified as well.

In a nutshell, although, indicative and useful on a routine basis to assess presence of PEG layer, indirect methods do not provide quantification of PEG and thus do not provide coverage-density, conformation and thickness data allowing comparison of different systems. They could be used as quality control of products but they are insufficient at the development stage of new particulate devices, where quantitative data are needed. They often provide poor correlation with PEG coverage, as evidenced in DLS, Zeta potential and protein adsorption data [35], particularly in the brush regime.

3.5 Direct assessment of surface PEGylation efficiency based on solution dosage

In term of methodology, PEG quantification can be performed by:

(1) Direct quantification on native particle (Fig. 4-A).

In this case, the method should allow a quantitative reaction (or detection) with tethered or grafted PEG chains and it should not be affected by the presence of the particle itself.

(2) Indirect quantification in solution, after the dissociation of PEG chains from the particle (Fig. 4-B).

The major limitation of this approach, considering that PEG can be also located in the particle core as well, is that only total PEG quantities are obtained rather than surface PEG quantities. The measurement method should work in a dissociation media (often an organic solvent) and additional preparation steps are needed to distinguish surface bound from total PEG.

(3) Differential quantification (Fig. 4-C).

In the case of a grafting reaction or adsorption on a bare particle, it is possible to quantify the initial concentration of PEG as well as the residual concentration after grafting and to deduce the amount grafted by difference.

3.5.1 PEG and PEG copolymer dosage by colorimetric methods

3.5.1.1 Detection of coordination complexes

Analytical methods to quantify PEG molecules or conjugates have been reviewed recently by Cheng *et al.* [123]. Iodine/potassium iodide colorimetric assay or Baleux's assay involves the coordination reaction between Iodine and PEG yielding a blue compound which is quantified by spectrophotometry [124], In order to quantify PEG concentration at the surface and in the core of diblock PLA-PEG particles, Bazile *et al.* used an alkaline hydrolysis to degrade selectively the PLA and release the PEG from the NP. The authors found that all the PEG chains were quickly released from the NP confirming that the polymer was located mainly at the surface of the particle and not in the core [58]. The authors also proposed a calculation method to estimate PEG coverage-density from their dosage results (see further details in Supporting Information section). A similar method has been used to assess PEG content in poly(cyanoacrylate) NP [125], and in NP made of PEG-*b*-PLA to quantify methoxy-PEG amounts [126, 127].

The Baleux assay has been adapted by D'Addio *et al.* [128] to characterise and measure directly PEG surfactants (PEG attached to PS, PLA or PCL) deposition on latex NP (Fig. 5-A). The authors were able to correlate quantitative measurements of PEG coverage-density to NP clearance *in vivo* [128]. The same group characterized PEG coverage-density of PS-*g*-PEG adsorbed on latex particles and unbound surfactant in supernatants after centrifugation with the same assay [48].

Another colorimetric method worth mentioning for the extend of its use, is the aqueous ferro-thiocyanate assay. It is used for PEG conjugate or non-ionic PEGylated surfactant detection based on partition of PEG in an organic phase and forming a colored complex [123, 129, 130]. An optimized version of the test [130] has been used to follow the depletion of Poloxamine907® in

the bulk solution upon absorption onto PS particles. Surface coverage-density and conformation can be then assessed at equilibrium from the adsorption isotherms [119, 131].

Limits of detection (LOD) of colorimetric methods are generally high. These methods often exhibit a limited sensitivity and a slow decay of absorbance over time. Great care has to be taken to get reliable data which requires fresh solutions and precise measurement time point [48]. Moreover, the described methods so far quantify PEG in solution only, which may require the degrafting of PEG from the NP surface.

3.5.1.2 Enzymatic detection

A special case of colorimetric detection by enzymatic reaction has been used to indirectly assess PEG surface coverage [132]. PLGA was blended with palmitate-avidin to obtain NP exhibiting avidin proteins on their surface. The affinity of avidin for biotin was used to "graft" PEG chains of the NP surface ligand-receptor interaction [132]. Attachment of PEG was studied by a two steps procedure, involving first the quantification of avidin present on the NP surface by protein assay. After "grafting", a biotin-Horseradish peroxidase (HRP) conjugate was allowed to bind to still accessible avidin sites on the NP surface. The conversion of a chromogenic substrate by the enzyme was detected by spectrophotometry. The absorbance was inversely proportional to the number of biotin-PEG present on the surface [132].

3.5.1.3 Antibody detection

Anti-PEG monoclonal antibodies, with specificity for methoxy terminal group or PEG monomer units, have been developed for PEG and PEG derivatives quantification [123]. The major advantage of antibody detection is the sensitivity of the assay usually in the picomolar range for free PEG or PEG small conjugate quantitation. Several modalities of colorimetric detection have been proposed either by direct detection or by competitive assays to yield quantifiable colored products [133-135]. For example, enzyme linked immuno-sorbent assay (ELISA) allows for the detection of PEG either in its free form or conjugated [135]. Reports of PEG quantification on intact particulate system are scarce. Cheng *et al.* reported quantitation of PEG on pegylated quantum dots and pegylated liposomes [133]. Although of interest because of the low limit of detection and the possibility to perform the assay in complex biological matrices, this approach has never been used to determine PEG surface coverage-density. It is unclear at this time if quantitative antibody binding can be obtained at high PEG chain coverage-density considering steric hindrance effects. A more suitableuse of this approach could be in the development of a more sensitive quantitation of dissociated PEG chains from NP surfaces.

3.5.2 Chromatographic quantification methods

Chromatographic detection of free and un-grafted PEG chains is usually done with refractive index (RI) or viscosimetric detectors rather than UV, as PEG is not quantifiable by UV detection.

Zillies *et al.* quantified grafted PEG chains on gelatin NP [136]. The author quantified unreacted PEG (non-attached to the gelatin NP) directly from the reaction mixture containing the gelatin NP and PEG (Fig. 4-C). Free PEG chains were separated from NP by asymetric flow field-flow fractionation (AF4) [137] and the effluents were analyzed by HPLC. Unreacted PEG was detected and quantified by GPC coupled to a refractive index (RI) detector. PEG grafting density was calculated by difference between the initial PEG quantity and the unreacted PEG quantified by HPLC [136].

Free PEG can also be detected and quantified by HPLC coupled with an evaporative light scattering detection (ELSD) as proposed by Zabaleta *et al.* [138]. Separation was provided by a size exclusion chromatography (SEC) column with a mobile phase gradient system suitable to separate PEG from other components [138]. ELSD detectors can detect and quantify non-volatile molecules without requiring any chromophore [139]. Similarly to the above mentioned strategy (Fig. 4- C), the amount of PEG grafted on NP was calculated as the difference between the initial PEG and PEG recovered in the supernatant of the suspension after washing. The results obtained by SEC-ELSD analysis were found to be quantitatively similar to ^{1}H NMR analysis results (see section 5) [138].

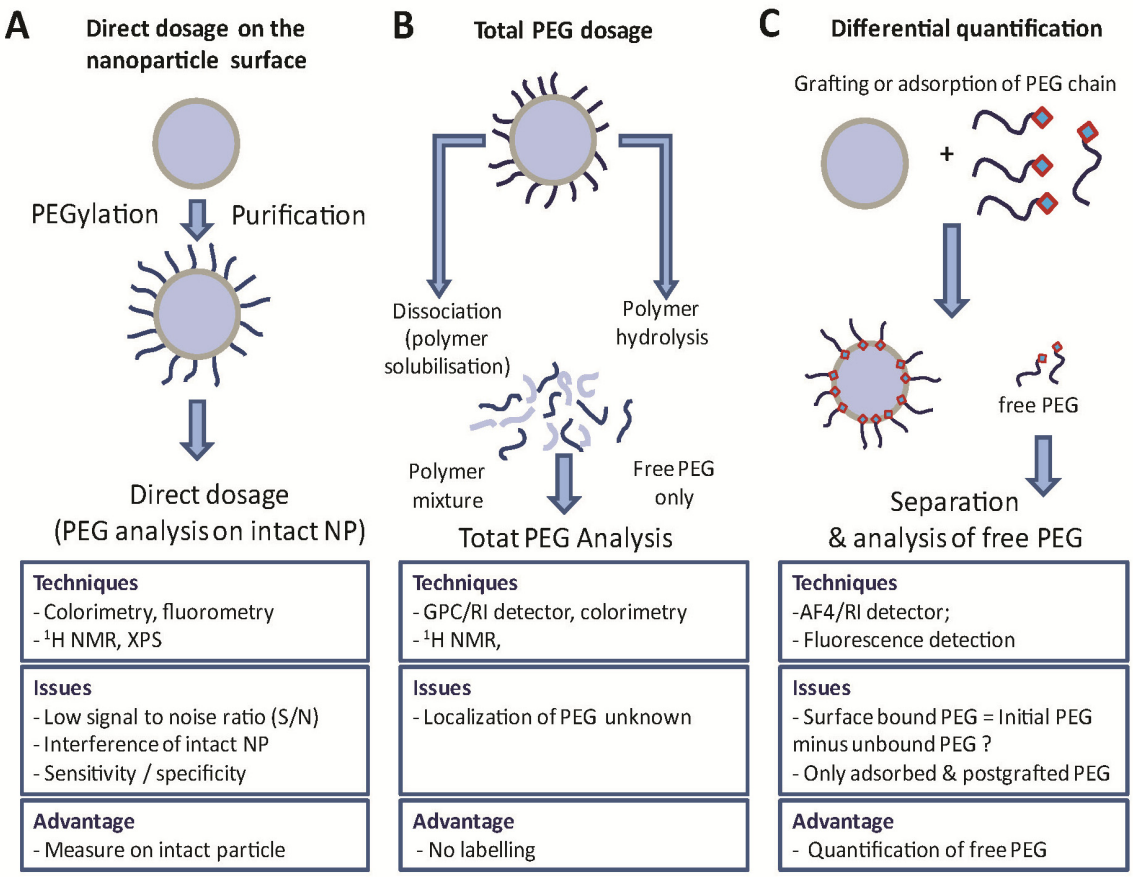

Figure 3.4. Different PEG quantification strategies

Quantification methods of Poloxamer® (PEG derivatives) by ELSD and LC-MS detectors were found to have better sensitivity than RI and with less interference [140]. Indeed, RI detectors are very sensitive to contaminant and other environmental factor such as temperature and flow which results in low sensitivity, unstable baseline, high limit of detection and long equilibration time. As expected, ESI-MS method provided higher sensitivity. But, on the other hand, SEC-ELSD is easier and less expensive to operate than ESI-MS. It is also easier to transfer from a research environment to a manufacturing facility [140].

3.5.3 PEG quantification by UV and Fluorescence spectroscopy

UV and fluorescence quantification has been reported using different strategies by coupling of PEG with a chromophore or fluorophore. A critical point in the validation of the dosing procedure is to clearly identify the location of the dosed PEG (in solution or on the NP surface). In term of methodology and potential issues, the different situations could be summarized as follow (Fig. 5):

(1) *UV/fluorescent PEG conjugates are attached on the particle surface (Fig. 5-A)*

Quantification by UV/fluorescence can be done on purified NP preparation (Fig. 5-A1, Direct quantification), or on the un-grafted PEG (Fig. 5-A3, Differential quantification) or on dissolved particle as well (Fig. 5-A2, Quantification in solution). The potential problems common to all of these approaches arise from the modification of PEG physical-chemical properties caused by the UV/fluorescent tag, which could affect grafting yield, chain conformation and ultimately surface coverage.

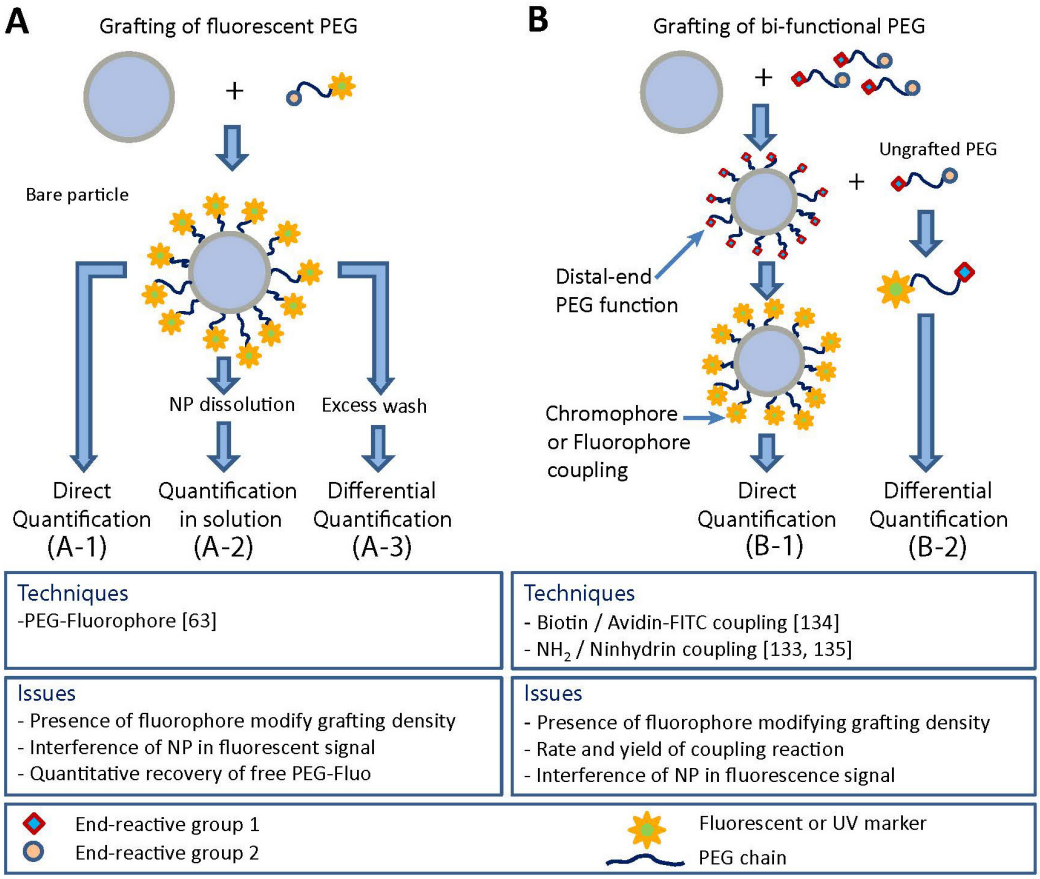

Figure 3.5. Strategies of PEG quantification by fluorescence or UV spectroscopy**.** (A) Grafting of fluorescently labeled PEG; (B) Labeling of grafted PEG chains

Direct quantification of grafted PEG chains using fluorescein-PEG 5 kD was recently reported on PRINT® NPs (hydrogel particle). [36] Bound PEG molecules were assessed by fluorescence spectroscopy using a calibration curve of serial dilution of free fluoroscein-PEG (Fig. 5-A1).

(1) Post-modification of grafted PEG (Fig. 5-B)

This approach requires the availability of a reactive group at the distal end of the PEG chain. Since reactive end groups may not be readily accessible for coupling, it is important point to make sure that the yield and rate of coupling are important enough to obtain quantitative measurements.

End-functionalized PEGs are often used to attach fluorescent dye or specific ligand for active targeting. In the case of NH_2 terminated PEG, amino groups can be quantify by the Kaiser test [141], a primary amine dosage test based on the reaction of NH_2 with ninhydrin, resulting in a deep blue color (Fig. 5-B-2) [142]. The assay allows the quantification of bound PEG and hence coverage-density if the coupling reaction is complete. Trinitrobenzene sulfonic acid (TNBS) assay, another reactive for primary amine, was also proposed as an alternative to ninhydrin to dose unreacted diamino-PEG [27].

Coupling of a fluorescent marker to PEG chain end can be performed using a ligand receptor complexe such as biotin-avidin [143]. In such case, the avidin protein carries the fluorophore (usually FITC). If PEG grafting density is important, steric hindrance can between avidin proteins can impede binding and thus lead to an underestimate of PEG amounts.

Xia *et al.* reported the use of several complementary methods of PEG quantification using UV or fluorescence spectroscopies to determine PEG coverage-density on gold NP by dosing either PEG bound to the particle or free (unreacted) in solution [144]. In the study, the authors used bi-functional PEG (HS-PEG-NH_2) covalently attached to a gold particle by their thiol end.

The coupling reaction yield was determined by reacting the *remaining free PEG* in solution via their primary amine with either fluorescamine (a marker becoming fluorescent upon coupling reaction with primary amine) or ninhydrin, the UV marker for the Kaiser test ("differential quantification" strategy illustrated in Fig. 5-B2). Using this approach, the authors were able to follow the decrease of free PEG concentration over time which was associated to the progress of PEG attachment to the NP. In another assay, fluorescein-isothiocyanate (FITC) was reacted with the available NH_2 group on grafted PEG on gold NP [144].

After purification and dissolution of the particles, and measurement of the fluorescence signal, coverage-density was determined. The authors showed very large differences in PEG quantification between methods using free PEG quantification by fluorescamine coupling and direct reaction of FITC on surface tethered PEG chain. The authors attribute this difference to the insufficient reactivity of NH_2 groups on PEG chains. It is however clear from these examples than

even carefully controlled quantification method ought to be cautiously interpreted, and, complementary dosing methods are necessary to get a reliable value of the coverage-density.

To conclude, UV/florescence approaches are having the downsides to require preparation of specially labeled particles. These particles may not be completely representative of the "real" particles used in biological assays. The quantification method depends on the yield of the conjugation reaction and on the effect of interfacial properties of conjugated PEG. Availability of technique permitting a dosage without modification of the target (a label-free method) and *in situ* would be more advantageous. NMR and XPS analysis offer some of these advantages.

3.6 Direct assessment of surface PEGylation based on quantitative NMR

^{1}H NMR is a quantitative analytical method, as the integrated peak surface is directly proportional to the number of proton being detected. Over the years, NMR has been refined with processing and instrument to the point it can be used to determine minute concentrations of metabolite and fine chemicals in biological samples. Practical considerations as well as specific parameters such as optimisation of signal, pulse sequences, gain, relaxation time, choice of internal standard, etc. are beyond the scope of this review and readers are referred to specialized literature on the subject [145, 146].

Three main approaches can be followed to quantify attached PEG chains: (i) the use of an internal standard whose signal does not interfere with PEG signal and soluble in the deuterated solvent; (ii) the electronic referencing by generation of an electronic calibrated signal avoiding contamination of the product (the signal is calibrated from previous product reference analysis, so it requires a two-steps calibration); (iii) use of an external standard. It is worth emphasizing the importance of having a clean and stable baseline (starting point of good peak integration) and to introduce relaxation delay (D_1) long enough in the pulse program (usually five time the PEG T_1) to get quantitative results [147].

3.6.1 Total PEG dosage

Total PEG quantification by NMR is well described by Nance *et al.* [44]. The authors prepared PS particles and then modified their surface with PEG chains and later dissolved them completely in $CDCl_3$. The quantification by NMR was performed using an internal standard added to the deuterated solvent [44]. Internal standards have also been used to determine total PEG in

PEG/PLGA NP [106]. In this last study, the standard was a component of the particles, as the amount of PEG was calculated relatively to the amount of the PLGA polymer methylene proton. The molar ratio of the two species (PEG and PLGA) was well correlated to the theoretical PEG content allowing for the percentage of PEG incorporated in the NP to be established [106]. A similar approach was proposed with PEGylated PS particles, using PS signals as internal reference [52].

Lastly, NMR spectra of polypeptide-PEG NP dissolved in d-TFA–d-chloroform, acquired before and after PEG layer degrafting allowed to calculate the PEG coverage-density. The amount of detached PEG was evaluated in reference to the polypeptide signals from the particle core [55].

The doped ("spiked") sample method has been reported to estimate the total PEG-lipid content in NPs [112]. Known aliquots of PEG-lipid doped into the NP sample were yielding a linear increase of the protons PEG signal. The linear correlation was then used to determine the initial mass of PEG-lipid in the sample.

The use of external standards has also been reported to determine the total concentration of PEG in NPs by measuring the ratio of ethylene glycol protons signals (at δ=3.51 ppm) of NP completely dissolved in DMSO-d6 to the same signal for known amounts of free PEG analyzed in the same conditions [148]. By this technique, PEG grafted onto PS particle were quantified by the weight percentage using an external calibration curve with mixtures of known amounts of PEG and PS dissolved in $CDCl_3$ [27].

It is important to note that after NP dissolution in a deuterated solvent, PEG chains from the core and from the surface become indistinguishable in the NMR spectrum. The signal obtained can represent the surface-bound PEG only if PEG is grafted or adsorbed *exclusively* on the surface.

3.6.2 Surface-bound PEG dosage

More interestingly, NMR can assess directly surface-bound PEG on intact particles suspended in D_2O without any post-modification (Fig. 4-A). ^1H NMR of NP suspended in D_2O has been proposed for the first time by Hkrach *et al.* to qualitatively characterize NPs made of PEG-PLA diblock [149]. The authors demonstrated that only the anchored PEG could be seen in ^1H NMR, with a similar signal compared to free PEG in deuterated water. The polymeric solid inner core mainly composed of hydrophobic PLA segments gave no NMR signals (Fig. 6). NMR confirmed that diblock PEG-PLA NP are structured around a hydrophobic core (mainly composed

of PLA), surrounded by a hydrophilic layer of PEG [149-151]. Similar observations were made with lipid NPs containing PEG-stearate [67], or polymeric NP made of comb PEG-g-PLA [66, 152].

Surface PEG quantification methods based on ^{1}H NMR have been developed relying on different calibration methods: (i) internal standard directly dissolved in deuterated water [22, 54, 67, 74], (ii) quantification referenced to a separated signal acquisition of a known quantity of PEG in the same conditions [148], (iii) external standard constituted by a narrow bore tube containing the reference placed coaxially within the tube containing the sample [150].

To determine PEG coating efficacy (% of total PEG found on the surface) of PLA-PEG NP, Sheng *et al.* calculated the ratio of surface PEG obtained in D_2O analysis to the total PEG obtained from NP dissolved in $CDCl_3$ [90].

Polymer mobility will vary from the anchoring point on the NP surface to its distal end in the bulk volume. This affects the relaxation time (T_1) of the polymers along the chain resulting in peak broadening which ultimately affects integration boundaries and quantification (Figure 3.7).

A potential problem associated with particle is the aggregation at the freeze-dried stage resulting in particle coalescence. To avoid such problem, addition of cryo-preservatives (usually carbohydrates) is commonly used but could interfere with PEG or internal standard NMR signals. PEGylated NP tendency to aggregate could result in a decrease of accessible surface to analysis and potentially to an underestimation of surface-bound PEG. This problem can be addressed by directly producing NP by emulsification-based method in D_2O containing a hydrophilic internal standard [89].

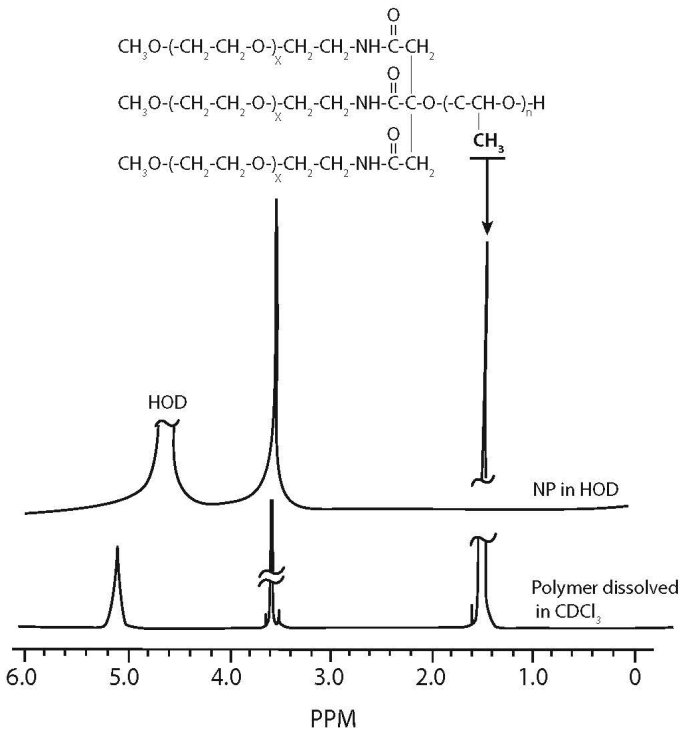

Figure 3.6. ^{1}H NMR spectra of PEG-PLA branched multiblock copolymer (PLA, M_n=71, 000 g/mol. attached to three blocks of PEG M_n=5,000 g/mol.) suspended in $CDCl_3$; and ^{1}H NMR spectra of nanoparticles prepared with the same polymer by emulsification-solvent evaporation and suspended in D_2O. Figure adapted from [149].

3.7 Direct assessment of surface PEGylation by XPS

X-rays photoelectron spectroscopy (XPS) is an analytic technique to assess chemical composition of surfaces [153, 154]. This technique has been introduced to study polymeric NP by Brindley *et al.* investigating PS NP [73] and Shakesheff *et al.* working on PLA NP and associated surfactant [155].

3.7.1 Principles of XPS

In XPS, a monochromatic source of X-rays is directed toward the surface and inducts emission of photoelectron from the matter under investigation. The emitted photoelectrons from the core level orbitals are collected and identified for their energy and quantified by a detector. The detection is quantitative in atomic relative percentage, and those data can be converted to relative mass percentage of surface component. The error margin, in routine conditions is about 10 to 20% [156].

The thickness of the upper layer accessible to the XPS analysis depends on several factors such as the nature of the element (C, O), angle of emission, nature of the material and its density. As electrons have a limited ability to penetrate polymeric materials, the maximum sampling depth, accounting for 99% of the observed signal, is around 10 nm for carbon electrons and 8 nm for oxygen electrons [157]. Two types of surface analysis can be performed in XPS, (i) survey scan allowing elemental compositions analysis and (ii) high resolution scan allowing chemical bond identification and quantifications.

3.7.2 Survey scan and elemental analysis

Survey scan is a low resolution scan over à range of 1000 eV, aimed at identify elements present on the surface and quantify them by peak integration as relative percentage with a sensitivity of about 0.1 atomic %.

Kingshott *et al.* correlated PEG presence with O/C peak integration ratio obtained from the survey scans [120]. Quantification of relative presence of PEG based on elemental analysis is of a limited precision on polymeric NP as both PEG and polymeric segments of the copolymer have close carbon and oxygen compositions. Also, carbon contamination by environmental exposure of the samples during transfer can cause difficulties in the interpretation of the scans. Lastly, C1s and O1s sampling depth are different which can also increase discrepancies in results. On the other hand, if PEG has a functional group at the distal end or at the attachment point to the particle surface comprising heteroatom such as nitrogen (N) or sulfur (S) atoms, not present in any other particle components, the atoms can be identified and quantified.

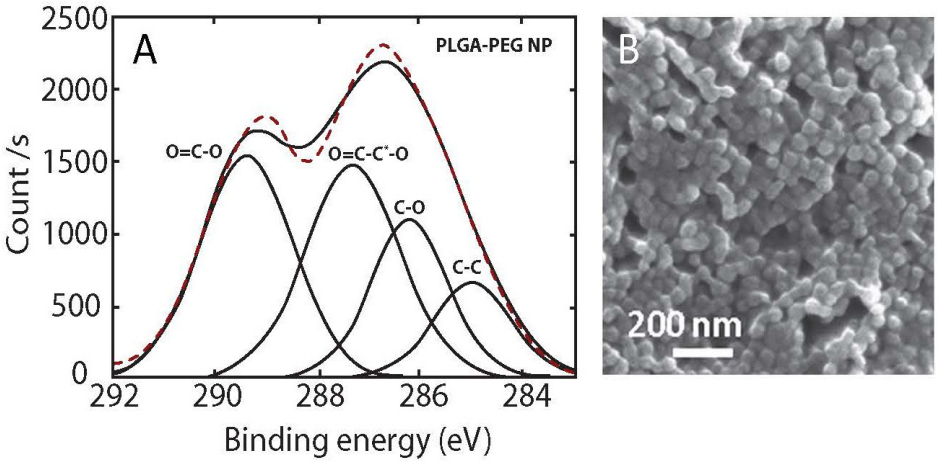

Figure 3.7. (A) High resolution C1s (right) scans of PLGA-PEG nanocapsules with peaks deconvolution and signal assignment (dashed line represents the acquired signal while solid lines

represent deconvoluted signals). (B) SEM image of the nanocapsules analyzed. Adapted from [158].

3.7.3 High resolution spectra and chemical bonds quantification

High resolution scans are realized over a narrower range of electron energy (10eV), around signals of interest, usually carbon, oxygen and nitrogen. Deconvolution of the signals allows identification of the relative percentage of the different chemical states of an atom, and thus the chemical functionalities present at the NP surface (see in Fig. 7 an example of C1s spectra for PLGA-PEG nanocapsules). High resolution spectrum allows the calculation of the relative contributions of different chemical bonds and the quality of the data generated is dependent on the positioning of the peak of interest and the determination of the peak width. For example, if no other ether compounds are found in the particle, ether bond are specific to PEG (C-O-C peak) and the signal integration is correlated to PEG concentration [73].

XPS has been used to establish the presence of PEG at the surface of poly(cyano-acrylate) NP [159], diblock and multiblock NPs [160]; diblock PEG-PLA particles [161] or PEG-PLGA nanocapsules [158]. The presence of PEG derivatives such as Poloxamine® on NP made of PLGA was also reported using XPS [162]. Lacasse *et al.* prepared by spray-drying, 1-3 µm PLA microparticles (MP) in presence of a surface modifier, PEG distearate, a triblock polymer composed of stearate-PEG-stearate. The authors found that PEG segments were segregated at the surface and evidenced a correlation between the quantity of PEG distearate added during the preparation stage and PEG amounts determined by XPS on the MP surface [72]. Similarly, XPS data showed an enrichment of the surface in PEG compared to the bulk PEG-*g*-PLA polymer in the case of NP prepared by emulsion/solvent evaporation. This enrichment was correlated to the content of PEG copolymer [66, 113].

Likewise, additions of covalently linked amino-PEG 5 kD and 20 kD to core shell NP lead to an increase of the C-O-C signal in high resolution survey scan of C1s confirming presence of PEG [163]. XPS also confirmed the successful grafting reaction of amino-PEG on the surface of polystyrene nanobeads [163]. End-functionalized amino PEG was quantified using the signal from 1s electron of the nitrogen at the binding energy expected for an amide bond.

XPS measurements only give access to a relative quantification of the different components detected at the NP surface [154]. By combining NMR and XPS analytical techniques, Ebbesen *et al.* showed that it is possible to calculate the relative enrichment in PEG of the particle

surface by calculating of the ratio of total PEG determined by qNMR to surface PEG concentration, detected by XPS. The authors found a three to ten times higher concentration of PEG on the NP surface, depending on the nature of the PEGylated polymers added on PEG-PLGA particles [106].

3.7.4 Measurement of the PEG layer thickness by XPS

Core shell organization can be qualitatively estimated by recording XPS signal attenuation of specific core polymer signals by a a PEG corona of increasing chain length [74].

Furthermore, PEG coverage-density on NP surfaces can be calculated from XPS data by measuring the thickness of the PEG layer on the NP [50, 164, 165]. In the case of carbonaceous polymer particles, the attenuation of the carbon electron signal when covered by PEG can be related to the PEG layer thickness [164]. Knowing the thickness and volumetric-density of PEG (around 1.08 to 1.13g/cm^3), the surface concentration (Γ: g/nm^2) can be calculated as $\Gamma = \rho L$; as well as the distance between grafted chain, *D*. This approach has been primarily developed for flat surfaces but was later extended to PEGylated MP such as Sephadex® MP [166]; Alginate/chitosan MP [167] or silica MP [168]. Its validity with NPs, which have a higher radius of curvature, is still to be demonstrated.

Quantification of PEG on particle surfaces by XPS has several limitations. The technique measures only surface PEG and the quantification is always relative not absolute. So far, XPS measurements are performed on a collapsed dehydrated PEG layer (in vacuum). The quantification of PEG can be extremely complicated with a multi-component surface especially when other ether compounds are present. Moreover, the effect of drying on PEG layer thickness and surface distribution is still unknown, but can have incidence on XPS results. Noteworthy, XPS is not strictly a surface analysis technique as the signal recorded is coming from the 8-10 nm upper layer of the particle. For a 100 nm diameter nanoparticle (50 nm radius), the volume accessible to XPS analysis represents about 48% of the volume of the particle.

3.8 Assessment of polydispersed PEG layer

PEG, as any polymeric material, has an intrinsic polydispersity. Formally, every PEG layers on a NP surface are composed of a mixture of different molecular weights. Small polydispersity has little consequences on quantification in most techniques. However, polydispersed PEG chains, such as mixed population of 2 kD and 5 kD PEG chains, are

increasingly proposed to improve pegylated surface properties such as selectivity of active targeting [169].

Studies performed on flat surfaces exhibiting a short "underbrush" layer of 2kD PEG mixed with PEG 5kD, have shown a decrease in non-specific protein absorption [170-172] as well as an inhibition of endothelial cell outgrowth [173]. Similarly, it can be expected the same trend for nanocarriers surface, although it has not been intensively studied. Some studies on liposomes showed the benefits of this approach which induces an increase in circulation time [109, 110]. Colloidal stability of gold NP of different sizes has been improved using mixed molecular weights PEG layer as well [92]. Likewise, “hetero-brush” PEG surface (with 2 kD “underbrush” and 5 to 20 kD PEG chains) on peptidic nanospheres show greater protein resistance and stability in serum media compared to “homo-brush” PEG surface with either 2 kD or 5 kD chains [29, 54].

Direct quantification of mixed layers after grafting (PEG chains number and ratio) has yet to be reported. The simultaneous quantification of both PEG molecular weights to ensure that the optimal ratio is maintained throughout the preparation process is a real challenge. Finally assessment of the uniformity of the two chain populations on the entire surface of the particle [174] to avoid any possible phase separations or surface heterogeneity.

3.9 Perspectives and conclusions

Drug nanocarriers are not progressing to the clinical stage as fast as expected based on earlier promises [8, 175]. One of the main reasons for that failure can be attributed to the lack of complete surface characterization of these objects, the other major cause being the lack of knowledge about the biology of tissues and biological barriers [176, 177] governing the host-surface nanocarrier interactions at the nano-bio interface.

Combinatory approaches have been recently proposed to optimize drug carriers based on lipid NP [178] or diblock polymer particles [179] with high throughput screening. This approach is powerful but necessitates testing of hundreds of combinations. A complementary approach will be to build analytical tools to adequately report key properties and compare platform in order to build a knowledge-based framework for surface optimization.

Direct quantification of PEG on the surface of drug carriers is not trivial and the availability of convenient techniques for polymeric NP is still limited. Specific methods for PEG surface assessments are needed, and existing methods need to be validated and standardized for this purpose. Sources of error should be more exposed and discussed. This is not the case in most

publications at the present time (see supporting information sections *S1.2* and *S1.3* for discussions on coverage-density calculation and error analysis). Two points are to be highlighted: firstly, rigorous care should be taken during NP size characterization, particularly for small particles (below 150 nm), secondly as mentioned in *SI*, section *S1.3*, the PEG coverage-density is mostly reported as a mean value, without any associated standard deviation, or interval.

Table 3.2. Characterization methods of PEG layer

Methods	Parameter measured	Advantages	Disadvantages	Detection limit/sensitivity	References
	Indirect quantification methods				
DLS	Size	Accessible technique, easy to perform	Low sensitivity, affected by media composition	ND	[24, 47]
Zeta Potential	Electric potential	Accessible technique, easy to perform	For charged particle only, qualitative, affected by ionic strength and pH	ND	[24, 51, 107]
Chromatography	Surface hydrophilicity	Separation of particle populations	Sensitivity, qualitative	ND	[105] [104]
Western blot & proteins dosage	Protein surface binding	Routine techniques in bio labs	Sensitive to separation conditions to keep NP-protein complexes intact	ND	[115] [116]
	Direct quantification methods				
Coupling fluo or UV marker	UV, Fluorescence intensity	Sensitivity	PEG modification necessary	5-10ng/ml	[144] [36]
Colorimetric	Light absorbance	Easy to perform	High background noise	1-10µg/ml	[58, 128]
HPLC/GPC	Refractive index	Accessible technique and instruments	Sample preparation, Low sensitivity	10-100µg/ml	[138]
AF4/GPC	Refractive index	In line separation of NP and free PEG	Low sensitivity, differential calculations could introduce error	10-100µg/ml	[136]
NMR	Proton chemical displacements	Highest sensitivity and versatility, intact particle in suspension	Particle resuspension in D_2O	mM range*	[22, 44, 54, 55, 67, 148]
XPS	Electron energy	Semi-quantitative/relative, intact dry particle	Dry state, Specialized equipment and personnel	0.1 % in mass	[72, 106, 155]

* *In routine NMR conditions (400 MHz frequency)*

Most quantification techniques require the production of "special" batches of NP (ex: particle in D_2O for NMR, addition of marker for fluorescence), and as mentioned earlier, those batches may or may not be representative of particle batches made for biological assays. Table 3.2 summarizes the advantages and disadvantages of the main techniques discussed in this regard. Some additional techniques are presented in SI-S3. Since all the techniques so far have severe flaws, more efforts should be invested in the use of complementary techniques [54, 144].

Combination of techniques and standardization of assays should be implemented to confirm results. Several methods discussed here are not part of a characterization routine in most laboratories, nor easily accessible. Up to date and albeit some limitations, quantitative NMR appears as the best compromise between accessibility and quality of results. However, choices of techniques depend on MP/NP system to be investigated and particle preparation method. Beside total PEG and surface PEG quantification, the quantification of internal PEG, i.e. PEG chains found on internal cavities surface, into micro-domains or molecularly dispersed in the core matrix should be considered as it may have implications in NP organization and drug delivery (Fig. 1).

Development of NP drug delivery systems is hampered by the lack of understanding and investigations of their physico-chemical properties. This shortcoming may have consequences on *in vivo* development, as performances cannot be related to well-characterized properties, limiting development process on trial-and-error basis. Implementation of precise PEG quantification to characterize stealth nanocarriers, should be included in all development process. The concerns of a better quantitative characterization of surface-tethered PEG chains are shared by many other fields of research. For instance, biomaterial for tissues engineering, biofiltration, biosensors, etc. are all domains in which the use and development of anti-fouling surfaces are at the center of the attention.

Increasing number of standardized protocols to characterize nanomaterial are available through the work of the USA National Cancer Institute's Nanotechnology Characterization Laboratory (NCL) (information available at http://ncl.cancer.gov). However, standardized methods for NP surface characterization have yet to be implemented. As pointed out by Crist *et al.* from the NCL: "*Another common mistake observed in understanding a material's composition is erroneously assuming the presence, covalent attachment and/or quantitation of surface ligands (functionalized groups, coatings, targeting moieties, etc.)"* [180]. This is best illustrated by the case-study published by the NCL, showing that the batch-to-batch variations of a nanocarrier toxicity appeared to be due to batch-to-batch variations of PEG coverage-density, variations which were not expected *a priori* [181]. Clinical translation of next generation of vehicles is strongly dependent on methods and analytical tools. Those are to be improved and developed if any significant progress could be made toward a more extensive use of NP at the clinical level.

Recently the commonly accepted effect of PEGylation has been challenged, as some reports showed contradictory results regarding PEG effects. Indeed PEGylation did not and will not resolve all problems. In particular number of studies has shown that PEG does not abolish

proteins opsonization but only decreases it. The controversy, thus, about the magnitude of the effects of PEG may originate from incomplete surface characterizations of NP making comparison between studies with conflicting results very difficult. So before questioning the PEGylation strategy, it is worth to establishing more firmly and quantitatively its effects. To conclude, we will quote Pr. Kinam Park for whom "There is no questions whether PEGylation is beneficial or not. Rather the question is how to pegylate" [182].

ACKNOWLEDGMENTS

XB acknowledges financial support from the Canada Research Chair program. JMR would like to acknowledge the FRQ-NT (Québec, Canada) and the Faculty of pharmacy of the Université de Montréal for their support through doctoral fellowships. The authors declare no competing interests.

REFERENCES

1. Moghimi, S.M. and J. Szebeni, *Stealth liposomes and long circulating nanoparticles: critical issues in pharmacokinetics, opsonization and protein-binding properties.* Prog Lipid Res, 2003. **42**(6): p. 463-78.
2. Vonarbourg, A., et al., *Parameters influencing the stealthiness of colloidal drug delivery systems.* Biomaterials, 2006. **27**(24): p. 4356-73.
3. Gref, R., et al., *The controlled intravenous delivery of drugs using PEG-coated sterically stabilized nanospheres.* Advanced Drug Delivery Reviews, 1995. **16**(2–3): p. 215-233.
4. Mosqueira, V.C.F., et al., *Biodistribution of long-circulating PEG-grafted nanocapsules in mice: Effects of PEG chain length and density.* Pharmaceutical Research, 2001. **18**(10): p. 1411-1419.
5. Brigger, I., C. Dubernet, and P. Couvreur, *Nanoparticles in cancer therapy and diagnosis.* Advanced Drug Delivery Reviews, 2012. **64,** Supplement(0): p. 24-36.
6. Danhier, F., et al., *PLGA-based nanoparticles: An overview of biomedical applications.* Journal of Controlled Release, 2012. **161**(2): p. 505-522.
7. Hrkach, J., et al., *Preclinical Development and Clinical Translation of a PSMA-Targeted Docetaxel Nanoparticle with a Differentiated Pharmacological Profile.* Science Translational Medicine, 2012. **4**(128): p. 128ra39.
8. Bae, Y.H. and K. Park, *Targeted drug delivery to tumors: Myths, reality and possibility.* Journal of Controlled Release, 2011. **153**(3): p. 198-205.
9. Knop, K., et al., *Poly(ethylene glycol) in drug delivery: pros and cons as well as potential alternatives.* Angew Chem Int Ed Engl, 2010. **49**(36): p. 6288-308.
10. Estephan, Z.G., P.S. Schlenoff, and J.B. Schlenoff, *Zwitteration As an Alternative to PEGylation.* Langmuir, 2011. **27**(11): p. 6794-6800.
11. *Polyethylene glycol*, in *United States Pharmacopeia and National Formulary (USP 36 -NF 31)*. 2013, The United States Pharmacopeial Convention: Rockville, MD, USA. p. 2139-2141.

12. *Polyethylene Glycol Monomethyl Ether*, in *United States Pharmacopeia and National Formulary (USP 36-NF 31)*. 2013, The United States Pharmacopeial Convention: Rockville, MD, USA. p. 2142-2145.
13. Barenholz, Y., *Doxil® — The first FDA-approved nano-drug: Lessons learned.* Journal of Controlled Release, 2012. **160**(2): p. 117-134.
14. Davis, M.E., *The First Targeted Delivery of siRNA in Humans via a Self-Assembling, Cyclodextrin Polymer-Based Nanoparticle: From Concept to Clinic.* Molecular Pharmaceutics, 2009. **6**(3): p. 659-668.
15. Soppimath, K.S., et al., *Biodegradable polymeric nanoparticles as drug delivery devices.* Journal of Controlled Release, 2001. **70**(1–2): p. 1-20.
16. Vauthier, C. and K. Bouchemal, *Methods for the Preparation and Manufacture of Polymeric Nanoparticles.* Pharmaceutical Research, 2009. **26**(5): p. 1025-1058.
17. Kamaly, N., et al., *Targeted polymeric therapeutic nanoparticles: design, development and clinical translation.* Chemical Society Reviews, 2012. **41**(7): p. 2971-3010.
18. Wang, T., J.R. Upponi, and V.P. Torchilin, *Design of multifunctional non-viral gene vectors to overcome physiological barriers: Dilemmas and strategies.* International Journal of Pharmaceutics, 2012. **427**(1): p. 3-20.
19. Owens, D.E., 3rd and N.A. Peppas, *Opsonization, biodistribution, and pharmacokinetics of polymeric nanoparticles.* Int J Pharm, 2006. **307**(1): p. 93-102.
20. Valencia, P.M., et al., *Microfluidic technologies for accelerating the clinical translation of nanoparticles.* Nat Nano, 2012. **7**(10): p. 623-629.
21. Khan, I.U., et al., *Microfluidics: A focus on improved cancer targeted drug delivery systems.* Journal of Controlled Release, 2013. **172**(3): p. 1065-1074.
22. Vila, A., et al., *Transport of PLA-PEG particles across the nasal mucosa: effect of particle size and PEG coating density.* J Control Release, 2004. **98**(2): p. 231-44.
23. Moghimi, S.M., A.C. Hunter, and J.C. Murray, *Long-Circulating and Target-Specific Nanoparticles: Theory to Practice.* Pharmacological Reviews, 2001. **53**(2): p. 283-318.
24. Redhead, H.M., S.S. Davis, and L. Illum, *Drug delivery in poly(lactide-co-glycolide) nanoparticles surface modified with poloxamer 407 and poloxamine 908: in vitro characterisation and in vivo evaluation.* Journal of Controlled Release, 2001. **70**(3): p. 353-363.
25. VandeVondele, S., J. Vörös, and J.A. Hubbell, *RGD-grafted poly-l-lysine-graft-(polyethylene glycol) copolymers block non-specific protein adsorption while promoting cell adhesion.* Biotechnology and Bioengineering, 2003. **82**(7): p. 784-790.
26. Neal, J.C., et al., *In vitro displacement by rat serum of adsorbed radiolabeled poloxamer and poloxamine copolymers from model and biodegradable nanospheres.* J Pharm Sci, 1998. **87**(10): p. 1242-8.
27. Meng, F., G.H.M. Engbers, and J. Feijen, *Polyethylene glycol–grafted polystyrene particles.* Journal of Biomedical Materials Research Part A, 2004. **70A**(1): p. 49-58.
28. Suh, J., et al., *PEGylation of nanoparticles improves their cytoplasmic transport.* International Journal of Nanomedicine, 2007. **2**(4): p. 735-41.
29. Matsumoto, M., M. Matsusaki, and M. Akashi, *Preparation of Biodegradable Peptide Nanospheres with Hetero PEG Brush Surfaces.* Macromolecular Bioscience, 2014. **14**(1): p. 142-150.
30. Breed, D.R., et al., *Functionalization of Polymer Microspheres Using Click Chemistry.* Langmuir, 2009. **25**(8): p. 4370-4376.
31. Pun, S.H. and M.E. Davis, *Development of a Nonviral Gene Delivery Vehicle for Systemic Application.* Bioconjugate Chemistry, 2002. **13**(3): p. 630-639.

32. Guo, X. and F.C. Szoka, *Steric Stabilization of Fusogenic Liposomes by a Low-pH Sensitive PEG−Diortho Ester−Lipid Conjugate.* Bioconjugate Chemistry, 2001. **12**(2): p. 291-300.
33. Dos Santos, N., et al., *Influence of poly(ethylene glycol) grafting density and polymer length on liposomes: Relating plasma circulation lifetimes to protein binding.* Biochimica et Biophysica Acta - Biomembranes, 2007. **1768**(6): p. 1367-1377.
34. Nel, A.E., et al., *Understanding biophysicochemical interactions at the nano-bio interface.* Nat Mater, 2009. **8**(7): p. 543-57.
35. Gref, R., et al., *'Stealth' corona-core nanoparticles surface modified by polyethylene glycol (PEG): influences of the corona (PEG chain length and surface density) and of the core composition on phagocytic uptake and plasma protein adsorption.* Colloids Surf B Biointerfaces, 2000. **18**(3-4): p. 301-313.
36. Perry, J.L., et al., *PEGylated PRINT Nanoparticles: The Impact of PEG Density on Protein Binding, Macrophage Association, Biodistribution, and Pharmacokinetics.* Nano Letters, 2012. **12**(10): p. 5304-5310.
37. Peracchia, M.T., et al., *Complement consumption by poly(ethylene glycol) in different conformations chemically coupled to poly(isobutyl 2-cyanoacrylate) nanoparticles.* Life Sciences, 1997. **61**(7): p. 749-761.
38. Salvati, A., et al., *Transferrin-functionalized nanoparticles lose their targeting capabilities when a biomolecule corona adsorbs on the surface.* Nat Nano, 2013. **8**(2): p. 137-143.
39. Mirshafiee, V., et al., *Protein corona significantly reduces active targeting yield.* Chemical Communications, 2013. **49**(25): p. 2557-2559.
40. Fontana, G., et al., *Amoxicillin-loaded polyethylcyanoacrylate nanoparticles: Influence of PEG coating on the particle size, drug release rate and phagocytic uptake.* Biomaterials, 2001. **22**(21): p. 2857-2865.
41. Lai, S.K., Y.-Y. Wang, and J. Hanes, *Mucus-penetrating nanoparticles for drug and gene delivery to mucosal tissues.* Advanced Drug Delivery Reviews, 2009. **61**(2): p. 158-171.
42. Lai, S.K., et al., *Rapid transport of large polymeric nanoparticles in fresh undiluted human mucus.* Proceedings of the National Academy of Sciences of the United States of America, 2007. **104**(5): p. 1482-1487.
43. Tang, B.C., et al., *Biodegradable polymer nanoparticles that rapidly penetrate the human mucus barrier.* Proceedings of the National Academy of Sciences, 2009. **106**(46): p. 19268-19273.
44. Nance, E.A., et al., *A Dense Poly(Ethylene Glycol) Coating Improves Penetration of Large Polymeric Nanoparticles Within Brain Tissue.* Science Translational Medicine, 2012. **4**(149): p. 149ra119.
45. Stylianopoulos, T., et al., *Diffusion Anisotropy in Collagen Gels and Tumors: The Effect of Fiber Network Orientation.* Biophysical Journal, 2010. **99**(10): p. 3119-3128.
46. Stylianopoulos, T., et al., *Diffusion of Particles in the Extracellular Matrix: The Effect of Repulsive Electrostatic Interactions.* Biophysical Journal, 2010. **99**(5): p. 1342-1349.
47. Stolnik, S., et al., *Surface Modification of Poly(lactide-co-glycolide) Nanospheres by Biodegradable Poly(lactide)-Poly(ethylene glycol) Copolymers.* Pharmaceutical Research, 1994. **11**(12): p. 1800-1808.
48. Budijono, S.J., et al., *Block copolymer surface coverage on nanoparticles.* Colloids and Surfaces A: Physicochemical and Engineering Aspects, 2010. **360**(1–3): p. 105-110.
49. Kim, S.H., et al., *Target-Specific Cellular Uptake of PLGA Nanoparticles Coated with Poly(l-lysine)−Poly(ethylene glycol)−Folate Conjugate.* Langmuir, 2005. **21**(19): p. 8852-8857.

50. Ogaki, R., et al., *Temperature-Induced Ultradense PEG Polyelectrolyte Surface Grafting Provides Effective Long-Term Bioresistance against Mammalian Cells, Serum, and Whole Blood.* Biomacromolecules, 2012. **13**(11): p. 3668-3677.
51. Suma, T., et al., *Smart Multilayered Assembly for Biocompatible siRNA Delivery Featuring Dissolvable Silica, Endosome-Disrupting Polycation, and Detachable PEG.* ACS Nano, 2012. **6**(8): p. 6693-6705.
52. Zhan, X., K.K. Tran, and H. Shen, *Effect of the Poly(ethylene glycol) (PEG) Density on the Access and Uptake of Particles by Antigen-Presenting Cells (APCs) after Subcutaneous Administration.* Molecular Pharmaceutics, 2012. **9**(12): p. 3442-3451.
53. Zahr, A.S., M. de Villiers, and M.V. Pishko, *Encapsulation of Drug Nanoparticles in Self-Assembled Macromolecular Nanoshells.* Langmuir, 2004. **21**(1): p. 403-410.
54. Matsumoto, M., M. Matsusaki, and M. Akashi, *Safe Control of Construction-Deconstruction of High-density PEG Brushes on the Surface of Peptide Nanospheres by Thermally Induced Shrinkage of PEG-SS-PEG.* Chemistry Letters, 2013. **42**(4): p. 344-346.
55. Waku, T., et al., *Complete surface control of peptide nanospheres with detachable and attachable polymer brush layers.* Chemical Communications, 2010. **46**(37): p. 7025-7027.
56. Guo, M.Y., M. Jiang, and G.Z. Zhang, *Surface modification of polymeric vesicles via host-guest inclusion complexation.* Langmuir, 2008. **24**(19): p. 10583-10586.
57. Poon, Z., et al., *Layer-by-Layer Nanoparticles with a pH-Sheddable Layer for in Vivo Targeting of Tumor Hypoxia.* ACS Nano, 2011. **5**(6): p. 4284-4292.
58. Bazile, D., et al., *Stealth Me.PEG-PLA nanoparticles avoid uptake by the mononuclear phagocytes system.* J Pharm Sci, 1995. **84**(4): p. 493-8.
59. Karnik, R., et al., *Microfluidic Platform for Controlled Synthesis of Polymeric Nanoparticles.* Nano Letters, 2008. **8**(9): p. 2906-2912.
60. Choi, Y.K., Y.H. Bae, and S.W. Kim, *Block Copolymer Nanoparticles of Ethylene Oxide and Isobutyl Cyanoacrylate.* Macromolecules, 1995. **28**(24): p. 8419-8421.
61. Calvo, P., et al., *Long-Circulating PEGylated Polycyanoacrylate Nanoparticles as New Drug Carrier for Brain Delivery.* Pharmaceutical Research, 2001. **18**(8): p. 1157-1166.
62. Vauthier, C., et al., *Poly(alkylcyanoacrylates) as biodegradable materials for biomedical applications.* Advanced Drug Delivery Reviews, 2003. **55**(4): p. 519-548.
63. Luck, M., et al., *Plasma protein adsorption on biodegradable microspheres consisting of poly(D,L-lactide-co-glycolide), poly(L-lactide) or ABA triblock copolymers containing poly(oxyethylene). Influence of production method and polymer composition.* J Control Release, 1998. **55**(2-3): p. 107-20.
64. De Jaeghere, F., et al., *Cellular uptake of PEO surface-modified nanoparticles: Evaluation of nanoparticles made of PLA : PEO diblock and triblock copolymers.* Journal of Drug Targeting, 2000. **8**(3): p. 143-153.
65. Nadeau, V., et al., *Synthesis of new versatile functionalized polyesters for biomedical applications.* Polymer, 2005. **46**(25): p. 11263-11272.
66. Sant, S., S. Poulin, and P. Hildgen, *Effect of polymer architecture on surface properties, plasma protein adsorption, and cellular interactions of pegylated nanoparticles.* Journal of Biomedical Materials Research, Part A, 2008. **87A**(4): p. 885-895.
67. Garcia-Fuentes, M., et al., *Application of NMR Spectroscopy to the Characterization of PEG-Stabilized Lipid Nanoparticles.* Langmuir, 2004. **20**(20): p. 8839-8845.
68. Lobovkina, T., et al., *In Vivo Sustained Release of siRNA from Solid Lipid Nanoparticles.* ACS Nano, 2011. **5**(12): p. 9977-9983.

69. Hatakeyama, H., H. Akita, and H. Harashima, *A multifunctional envelope type nano device (MEND) for gene delivery to tumours based on the EPR effect: A strategy for overcoming the PEG dilemma.* Advanced Drug Delivery Reviews, 2011. **63**(3): p. 152-160.
70. Mura, S., et al., *Novel Isoprenoyl Nanoassembled Prodrug for Paclitaxel Delivery.* Bioconjugate Chemistry, 2013. **24**(11): p. 1840-1849.
71. Díaz-López, R., et al., *Quantification of pegylated phospholipids decorating polymeric microcapsules of perfluorooctyl bromide by reverse phase HPLC with a charged aerosol detector.* Journal of Pharmaceutical and Biomedical Analysis, 2008. **48**(3): p. 702-707.
72. Lacasse, F.X., P. Hildgen, and J.N. McMullen, *Surface and morphology of spray-dried pegylated PLA microspheres.* International Journal of Pharmaceutics, 1998. **174**(1–2): p. 101-109.
73. Brindley, A., et al., *Polystyrene Colloids with Surface-Grafted Polyethylene Oxide as Model Systems for Site-Specific Drug Delivery: I. Preparation and Surface Chemical Characterization Using SIMS and XPS.* Journal of Colloid and Interface Science, 1995. **171**(1): p. 150-161.
74. Waku, T., et al., *PEG Brush Peptide Nanospheres with Stealth Properties and Chemical Functionality.* Macromolecules, 2007. **40**(17): p. 6385-6392.
75. Colombo, C., et al., *Tunable Degradation Behavior of PEGylated Polyester-Based Nanoparticles Obtained Through Emulsion Free Radical Polymerization.* Industrial & Engineering Chemistry Research, 2014.
76. Sawant, R.R., et al., *The architecture of ligand attachment to nanocarriers controls their specific interaction with target cells.* Journal of Drug Targeting, 2008. **16**(7-8): p. 596-600.
77. Hak, S., et al., *The Effect of Nanoparticle Polyethylene Glycol Surface Density on Ligand-Directed Tumor Targeting Studied in Vivo by Dual Modality Imaging.* ACS Nano, 2012. **6**(6): p. 5648-5658.
78. Stefanick, J.F., et al., *A Systematic Analysis of Peptide Linker Length and Liposomal Polyethylene Glycol Coating on Cellular Uptake of Peptide-Targeted Liposomes.* ACS Nano, 2013.
79. Abu Lila, A.S., H. Kiwada, and T. Ishida, *The accelerated blood clearance (ABC) phenomenon: Clinical challenge and approaches to manage.* Journal of Controlled Release, 2013. **172**(1): p. 38-47.
80. Schellekens, H., W. Hennink, and V. Brinks, *The Immunogenicity of Polyethylene Glycol: Facts and Fiction.* Pharmaceutical Research, 2013. **30**(7): p. 1729-1734.
81. Mishra, S., P. Webster, and M.E. Davis, *PEGylation significantly affects cellular uptake and intracellular trafficking of non-viral gene delivery particles.* European Journal of Cell Biology, 2004. **83**(3): p. 97-111.
82. Hong, R.-L., et al., *Direct Comparison of Liposomal Doxorubicin with or without Polyethylene Glycol Coating in C-26 Tumor-bearing Mice: Is Surface Coating with Polyethylene Glycol Beneficial?* Clinical Cancer Research, 1999. **5**(11): p. 3645-3652.
83. Tagalakis, A.D., et al., *PEGylation improves the receptor-mediated transfection efficiency of peptide-targeted, self-assembling, anionic nanocomplexes.* Journal of Controlled Release, (0).
84. Li, S.D. and L. Huang, *Stealth nanoparticles: high density but sheddable PEG is a key for tumor targeting.* J Control Release, 2010. **145**(3): p. 178-81.
85. Hatakeyama, H., et al., *Development of a novel systemic gene delivery system for cancer therapy with a tumor-specific cleavable PEG-lipid.* Gene Ther, 2007. **14**(1): p. 68-77.
86. Romberg, B., W. Hennink, and G. Storm, *Sheddable Coatings for Long-Circulating Nanoparticles.* Pharmaceutical Research, 2008. **25**(1): p. 55-71.

87. Gao, W., R. Langer, and O.C. Farokhzad, *Poly(ethylene glycol) with Observable Shedding.* Angewandte Chemie International Edition, 2010. **49**(37): p. 6567-6571.
88. Vittaz, M., et al., *Effect of PEO surface density on long-circulating PLA-PEO nanoparticles which are very low complement activators.* Biomaterials, 1996. **17**(16): p. 1575-1581.
89. Xu, Q., et al., *Scalable method to produce biodegradable nanoparticles that rapidly penetrate human mucus.* Journal of Controlled Release, 2013. **170**(2): p. 279-286.
90. Sheng, Y., et al., *In vitro macrophage uptake and in vivo biodistribution of PLA–PEG nanoparticles loaded with hemoglobin as blood substitutes: effect of PEG content.* Journal of Materials Science: Materials in Medicine, 2009. **20**(9): p. 1881-1891.
91. Thierry, B. and H.J. Griesser, *Dense PEG layers for efficient immunotargeting of nanoparticles to cancer cells.* Journal of Materials Chemistry, 2012. **22**(18): p. 8810-8819.
92. Liu, T. and B. Thierry, *A Solution to the PEG Dilemma: Efficient Bioconjugation of Large Gold Nanoparticles for Biodiagnostic Applications using Mixed Layers.* Langmuir, 2012. **28**(44): p. 15634-15642.
93. Gaumet, M., et al., *Nanoparticles for drug delivery: the need for precision in reporting particle size parameters.* Eur J Pharm Biopharm, 2008. **69**(1): p. 1-9.
94. Fillafer, C., M. Wirth, and F. Gabor, *Stabilizer-Induced Viscosity Alteration Biases Nanoparticle Sizing via Dynamic Light Scattering.* Langmuir, 2007. **23**(17): p. 8699-8702.
95. Hackey, V.A. and J.D. Clogston, *Measuring the size of nanoparticles in aqueous media using batch-mode dynamic light scattering*. 2010, NIST-NCL Joint Assay Protocol, PCC-1, version 1.1.
96. Kommareddy, S. and M. Amiji, *Biodistribution and pharmacokinetic analysis of long-circulating thiolated gelatin nanoparticles following systemic administration in breast cancer-bearing mice.* J Pharm Sci, 2007. **96**(2): p. 397-407.
97. Filipe, V., A. Hawe, and W. Jiskoot, *Critical Evaluation of Nanoparticle Tracking Analysis (NTA) by NanoSight for the Measurement of Nanoparticles and Protein Aggregates.* Pharmaceutical Research, 2010. **27**(5): p. 796-810.
98. Vogel, R., et al., *Quantitative Sizing of Nano/Microparticles with a Tunable Elastomeric Pore Sensor.* Analytical Chemistry, 2011. **83**(9): p. 3499-3506.
99. Yang, L., M. Broom, and I. Tucker, *Characterization of a Nanoparticulate Drug Delivery System Using Scanning Ion Occlusion Sensing.* Pharmaceutical Research, 2012. **29**(9): p. 2578-2586.
100. Bonevich, J.E. and W.K. Haller, *Measuring the size of nanoparticles using transmission electron microscopy (TEM)*. 2010, NSIT-NCL Joint Assay Protocol, PCC-7, version 1.1.
101. Sitterberg, J., et al., *Utilising atomic force microscopy for the characterisation of nanoscale drug delivery systems.* European Journal of Pharmaceutics and Biopharmaceutics, 2010. **74**(1): p. 2-13.
102. Roe, G., L. McDonnell, and A. Ghanem, *A method for measuring the size distribution of latex particles by scanning force microscopy.* Ultramicroscopy, 2004. **100**(3–4): p. 319-329.
103. Cao, S., et al., *A novel approach for the preparation of acrylate–siloxane particles with core–shell structure.* Polymer International, 2007. **56**(3): p. 357-363.
104. Carstensen, H., B.W. Müller, and R.H. Müller, *Adsorption of ethoxylated surfactants on nanoparticles. I. Characterization by hydrophobic interaction chromatography.* International Journal of Pharmaceutics, 1991. **67**(1): p. 29-37.
105. Tobio, M., et al., *Stealth PLA-PEG Nanoparticles as Protein Carriers for Nasal Administration.* Pharmaceutical Research, 1998. **15**(2): p. 270-275.

106. Ebbesen, M.F., et al., *Surface Analysis of PEGylated Nano-Shields on Nanoparticles Installed by Hydrophobic Anchors.* Pharmaceutical Research, 2013: p. 1-10.
107. Gref, R., G. Miralles, and É. Dellacherie, *Polyoxyethylene-coated nanospheres: effect of coating on zeta potential and phagocytosis.* Polymer International, 1999. **48**(4): p. 251-256.
108. Rahme, K., et al., *PEGylated gold nanoparticles: polymer quantification as a function of PEG lengths and nanoparticle dimensions.* RSC Advances, 2013. **3**(17): p. 6085-6094.
109. Sadzuka, Y., et al., *Effects of mixed polyethyleneglycol modification on fixed aqueous layer thickness and antitumor activity of doxorubicin containing liposome.* International Journal of Pharmaceutics, 2002. **238**(1–2): p. 171-180.
110. Sadzuka, Y., et al., *Characterization and cytotoxicity of mixed polyethyleneglycol modified liposomes containing doxorubicin.* International Journal of Pharmaceutics, 2006. **312**(1–2): p. 83-89.
111. Fang, C., et al., *In vivo tumor targeting of tumor necrosis factor-[alpha]-loaded stealth nanoparticles: Effect of MePEG molecular weight and particle size.* European Journal of Pharmaceutical Sciences, 2006. **27**(1): p. 27-36.
112. Duncanson, W.J., et al., *Targeted binding of PLA microparticles with lipid-PEG-tethered ligands.* Biomaterials, 2007. **28**(33): p. 4991-4999.
113. Essa, S., J.M. Rabanel, and P. Hildgen, *Effect of polyethylene glycol (PEG) chain organization on the physicochemical properties of poly(D, L-lactide) (PLA) based nanoparticles.* European Journal of Pharmaceutics and Biopharmaceutics, 2010. **75**(2): p. 96-106.
114. Goppert, T.M. and R.H. Muller, *Protein adsorption patterns on poloxamer- and poloxamine-stabilized solid lipid nanoparticles (SLN).* Eur J Pharm Biopharm, 2005. **60**(3): p. 361-72.
115. Gessner, A., et al., *Protein rejecting properties of PEG-grafted nanoparticles: Influence of PEG-chain length and surface density evaluated by two-dimensional electrophoresis and bicinchoninic acid (BCA)-proteinassay.* Die Pharmazie - An International Journal of Pharmaceutical Sciences, 2006. **61**(4): p. 293-297.
116. Aggarwal, P., et al., *Nanoparticle interaction with plasma proteins as it relates to particle biodistribution, biocompatibility and therapeutic efficacy.* Adv Drug Deliv Rev, 2009. **61**(6): p. 428-37.
117. Blunk, T., et al., *Colloidal carriers for intravenous drug targeting: Plasma protein adsorption patterns on surface-modified latex particles evaluated by two-dimensional polyacrylamide gel electrophoresis.* Electrophoresis, 1993. **14**(1): p. 1382-1387.
118. Cedervall, T., et al., *Understanding the nanoparticle-protein corona using methods to quantify exchange rates and affinities of proteins for nanoparticles.* Proceedings of the National Academy of Sciences of the United States of America, 2007. **104**(7): p. 2050-2055.
119. Al-Hanbali, O., et al., *Concentration Dependent Structural Ordering of Poloxamine 908 on Polystyrene Nanoparticles and Their Modulatory Role on Complement Consumption.* Journal of Nanoscience and Nanotechnology, 2006. **6**(9-1): p. 3126-3133.
120. Kingshott, P., H. Thissen, and H.J. Griesser, *Effects of cloud-point grafting, chain length, and density of PEG layers on competitive adsorption of ocular proteins.* Biomaterials, 2002. **23**(9): p. 2043-2056.
121. Rouzes, C., et al., *Influence of polymeric surfactants on the properties of drug-loaded PLA nanospheres.* Colloids and Surfaces B: Biointerfaces, 2003. **32**(2): p. 125-135.

122. Monopoli, M.P., et al., *Physical-chemical aspects of protein corona: relevance to in vitro and in vivo biological impacts of nanoparticles.* J Am Chem Soc, 2011. **133**(8): p. 2525-34.
123. Cheng, T.-L., et al., *Analytical Measurement of PEGylated Molecules.* Bioconjugate Chemistry, 2012. **23**(5): p. 881-899.
124. Baleux, B., *Colorimetric determination of non-ionic polyoxyethylene surface using iodoiodated solution.* Comptes Rendus Hebdomadaires des Séances de l'Academie des Sciences Serie, 1972. **274**: p. 1617–1620.
125. Brigger, I., et al., *Near Infrared with Principal Component Analysis as a Novel Analytical Approach for Nanoparticle Technology.* Pharmaceutical Research, 2000. **17**(9): p. 1124-1132.
126. Sims, G.E.C. and T.J. Snape, *A method for the estimation of polyethylene glycol in plasma protein fractions.* Analytical Biochemistry, 1980. **107**(1): p. 60-63.
127. Zambaux, M.F., et al., *Protein C-loaded monomethoxypoly (ethylene oxide)–poly(lactic acid) nanoparticles.* International Journal of Pharmaceutics, 2001. **212**(1): p. 1-9.
128. D'Addio, S.M., et al., *Effects of block copolymer properties on nanocarrier protection from in vivo clearance.* Journal of Controlled Release, 2012. **162**(1): p. 208-217.
129. Nag, A., G. Mitra, and P.C. Ghosh, *A Colorimetric Assay for Estimation of Polyethylene Glycol and Polyethylene Glycolated Protein Using Ammonium Ferrothiocyanate.* Analytical Biochemistry, 1996. **237**(2): p. 224-231.
130. Al-Hanbali, O., et al., *Modification of the Stewart biphasic colorimetric assay for stable and accurate quantitatitive determination of Pluronic and Tetronic block copolymers for application in biological systems.* Analytical Biochemistry, 2007. **361**(2): p. 287-293.
131. Hamad, I., et al., *Distinct Polymer Architecture Mediates Switching of Complement Activation Pathways at the Nanosphere−Serum Interface: Implications for Stealth Nanoparticle Engineering.* ACS Nano, 2010. **4**(11): p. 6629-6638.
132. Cu, Y. and W.M. Saltzman, *Controlled Surface Modification with Poly(ethylene)glycol Enhances Diffusion of PLGA Nanoparticles in Human Cervical Mucus.* Molecular Pharmaceutics, 2008. **6**(1): p. 173-181.
133. Cheng, T.-L., et al., *Monoclonal Antibody-Based Quantitation of Poly(ethylene glycol)-Derivatized Proteins, Liposomes, and Nanoparticles.* Bioconjugate Chemistry, 2005. **16**(5): p. 1225-1231.
134. Su, Y.-C., et al., *Sensitive Quantification of PEGylated Compounds by Second-Generation Anti-Poly(ethylene glycol) Monoclonal Antibodies.* Bioconjugate Chemistry, 2010. **21**(7): p. 1264-1270.
135. Chuang, K.-H., et al., *Measurement of Poly(ethylene glycol) by Cell-Based Anti-poly(ethylene glycol) ELISA.* Analytical Chemistry, 2010. **82**(6): p. 2355-2362.
136. Zillies, J.C., et al., *Method for Quantifying the PEGylation of Gelatin Nanoparticle Drug Carrier Systems Using Asymmetrical Flow Field-Flow Fractionation and Refractive Index Detection.* Analytical Chemistry, 2007. **79**(12): p. 4574-4580.
137. Fraunhofer, W. and G. Winter, *The use of asymmetrical flow field-flow fractionation in pharmaceutics and biopharmaceutics.* European Journal of Pharmaceutics and Biopharmaceutics, 2004. **58**(2): p. 369-383.
138. Zabaleta, V., M.A. Campanero, and J.M. Irache, *An HPLC with evaporative light scattering detection method for the quantification of PEGs and Gantrez in PEGylated nanoparticles.* Journal of Pharmaceutical and Biomedical Analysis, 2007. **44**(5): p. 1072-1078.

139. Arndt, J.H., T. Macko, and R. Brüll, *Application of the evaporative light scattering detector to analytical problems in polymer science.* Journal of Chromatography A, 2013. **1310**(0): p. 1-14.
140. Nair, L.M., et al., *Comparison of electrospray ionization mass spectrometry and evaporative light scattering detections for the determination of Poloxamer 188 in itraconazole injectable formulation.* Journal of Pharmaceutical and Biomedical Analysis, 2006. **41**(3): p. 725-730.
141. Kaiser, E., et al., *Color test for detection of free terminal amino groups in the solid-phase synthesis of peptides.* Analytical Biochemistry, 1970. **34**(2): p. 595-598.
142. Sacchetti, C., et al., *Surface Polyethylene Glycol Conformation Influences the Protein Corona of Polyethylene Glycol-Modified Single-Walled Carbon Nanotubes: Potential Implications on Biological Performance.* ACS Nano, 2013. **7**(3): p. 1974-1989.
143. Onyskiw, P.J. and O. Eniola-Adefeso, *Effect of PEGylation on Ligand-Based Targeting of Drug Carriers to the Vascular Wall in Blood Flow.* Langmuir, 2013. **29**(35): p. 11127-11134.
144. Xia, X., et al., *Quantifying the Coverage Density of Poly(ethylene glycol) Chains on the Surface of Gold Nanostructures.* ACS Nano, 2011. **6**(1): p. 512-522.
145. Huang, Y., et al., *Improving the efficiency of quantitative 1H NMR: An innovative external standard–internal reference approach.* Journal of Pharmaceutical and Biomedical Analysis, 2014. **88**(0): p. 1-6.
146. Rizzo, V. and V. Pinciroli, *Quantitative NMR in synthetic and combinatorial chemistry.* Journal of Pharmaceutical and Biomedical Analysis, 2005. **38**(5): p. 851-857.
147. Vernooij, E.A.A.M., et al., *1H NMR Quantification of poly(Ethylene Glycol)-Phosphatidylethanolamine in Phospholipid Mixtures.* Pharmaceutical Research, 1999. **16**(10): p. 1658-1661.
148. Yoncheva, K., E. Lizarraga, and J.M. Irache, *Pegylated nanoparticles based on poly(methyl vinyl ether-co-maleic anhydride): preparation and evaluation of their bioadhesive properties.* European Journal of Pharmaceutical Sciences, 2005. **24**(5): p. 411-419.
149. Hrkach, J.S., et al., *Nanotechnology for biomaterials engineering: structural characterization of amphiphilic polymeric nanoparticles by 1H NMR spectroscopy.* Biomaterials, 1997. **18**(1): p. 27-30.
150. Heald, C.R., et al., *Poly(lactic acid)-poly(ethylene oxide) (PLA-PEG) nanoparticles: NMR studies of the central solidlike PLA core and the liquid PEG corona.* Langmuir, 2002. **18**(9): p. 3669-3675.
151. Vila, A., et al., *PEG-PLA nanoparticles as carriers for nasal vaccine delivery.* J Aerosol Med, 2004. **17**(2): p. 174-85.
152. Sant, S., V. Nadeau, and P. Hildgen, *Effect of porosity on the release kinetics of propafenone-loaded PEG-g-PLA nanoparticles.* J Control Release, 2005. **107**(2): p. 203-14.
153. Briggs, D. and M.P. Seah, *Practical Surface Analysis: Auger and X-ray photoelectron spectroscopy*. 1990, Chichester, United Kingdom: John Wiley & Sons. 657.
154. Briggs, D. and J.T. Grant, *Surface Analysis by Auger and X-ray Photoelectron Spectroscopy*. 2003, Chichester, West Sussex, United Kingdom: IM Publications LLP. 899.
155. Shakesheff, K.M., et al., *The adsorption of poly(vinyl alcohol) to biodegradable microparticles studied by x-ray photoelectron spectroscopy (XPS).* Journal of Colloid and Interface Science, 1997. **185**(2): p. 538-547.

156. Powell, C.J. and M.P. Seah, *Precision, accuracy, and uncertainty in quantitative surface analyses by Auger-electron spectroscopy and x-ray photoelectron spectroscopy.* Journal of Vacuum Science & Technology A, 1990. **8**(2): p. 735-763.
157. Tanuma, S., C.J. Powell, and D.R. Penn, *Calculations of electron inelastic mean free paths. V. Data for 14 organic compounds over the 50–2000 eV range.* Surface and Interface Analysis, 1994. **21**(3): p. 165-176.
158. Diou, O., et al., *Long-circulating perfluorooctyl bromide nanocapsules for tumor imaging by 19FMRI.* Biomaterials, 2012. **33**(22): p. 5593-5602.
159. Peracchia, M., et al., *Pegylated Nanoparticles from a Novel Methoxypolyethylene Glycol Cyanoacrylate-Hexadecyl Cyanoacrylate Amphiphilic Copolymer.* Pharmaceutical Research, 1998. **15**(4): p. 550-556.
160. Peracchia, M.T., et al., *PEG-coated nanospheres from amphiphilic diblock and multiblock copolymers: Investigation of their drug encapsulation and release characteristics.* Journal of Controlled Release, 1997. **46**(3): p. 223-231.
161. Kim, S.Y., I.G. Shin, and Y.M. Lee, *Preparation and characterization of biodegradable nanospheres composed of methoxy poly(ethylene glycol) and dl-lactide block copolymer as novel drug carriers.* Journal of Controlled Release, 1998. **56**(1–3): p. 197-208.
162. Scholes, P.D., et al., *Detection and determination of surface levels of poloxamer and PVA surfactant on biodegradable nanospheres using SSIMS and XPS.* Journal of Controlled Release, 1999. **59**(3): p. 261-278.
163. Zahr, A.S., C.A. Davis, and M.V. Pishko, *Macrophage Uptake of Core−Shell Nanoparticles Surface Modified with Poly(ethylene glycol).* Langmuir, 2006. **22**(19): p. 8178-8185.
164. Popat, K.C., S. Sharma, and T.A. Desai, *Quantitative XPS Analysis of PEG-Modified Silicon Surfaces.* The Journal of Physical Chemistry B, 2004. **108**(17): p. 5185-5188.
165. Baer, D.R. and M.H. Engelhard, *XPS analysis of nanostructured materials and biological surfaces.* Journal of Electron Spectroscopy and related Phenomena, 2010. **178–179**(0): p. 415-432.
166. Damodaran, V.B., et al., *Conformational Studies of Covalently Grafted Poly(ethylene glycol) on Modified Solid Matrices Using X-ray Photoelectron Spectroscopy.* Langmuir, 2010. **26**(10): p. 7299-7306.
167. Zheng, J., et al., *Enhancement of Surface Graft Density of MPEG on Alginate/Chitosan Hydrogel Microcapsules for Protein Repellency.* Langmuir, 2012. **28**(37): p. 13261-13273.
168. Chen, A., et al., *Particle-by-particle quantification of protein adsorption onto poly(ethylene glycol) grafted surfaces.* Biofouling, 2008. **24**(4): p. 267-273.
169. Wang, S. and E.E. Dormidontova, *Selectivity of Ligand-Receptor Interactions between Nanoparticle and Cell Surfaces.* Physical Review Letters, 2012. **109**(23): p. 238102.
170. Uchida, K., et al., *A Reactive Poly(ethylene glycol) Layer To Achieve Specific Surface Plasmon Resonance Sensing with a High S/N Ratio: The Substantial Role of a Short Underbrushed PEG Layer in Minimizing Nonspecific Adsorption.* Analytical Chemistry, 2005. **77**(4): p. 1075-1080.
171. Uchida, K., et al., *Creation of a mixed poly(ethylene glycol) tethered-chain surface for preventing the nonspecific adsorption of proteins and peptides.* Biointerphases, 2007. **2**(4): p. 126-130.
172. Nagasaki, Y., *Construction of a densely poly(ethylene glycol)-chain-tethered surface and its performance.* Polym J, 2011. **43**(12): p. 949-958.
173. Satomi, T., et al., *Density Control of Poly(ethylene glycol) Layer To Regulate Cellular Attachment.* Langmuir, 2007. **23**(12): p. 6698-6703.

174. Bosker, W.T.E., et al., *BSA adsorption on bimodal PEO brushes.* Journal of Colloid and Interface Science, 2005. **286**(2): p. 496-503.
175. Crommelin, D.J.A. and A.T. Florence, *Towards more effective advanced drug delivery systems.* International Journal of Pharmaceutics, 2013(0).
176. Rabanel, J.M., et al., *Drug-loaded nanocarriers: passive targeting and crossing of biological barriers.* Current Medicinal Chemistry, 2012. **19**(19): p. 3070-102.
177. Bertrand, N., et al., *Cancer nanotechnology: The impact of passive and active targeting in the era of modern cancer biology.* Advanced Drug Delivery Reviews, 2014. **66**: p. 2-25.
178. Akinc, A., et al., *A combinatorial library of lipid-like materials for delivery of RNAi therapeutics.* Nat Biotech, 2008. **26**(5): p. 561-569.
179. Siegwart, D.J., et al., *Combinatorial synthesis of chemically diverse core-shell nanoparticles for intracellular delivery.* Proceedings of the National Academy of Sciences, 2011. **108**(32): p. 12996-13001.
180. Crist, R.M., et al., *Common pitfalls in nanotechnology: lessons learned from NCI's Nanotechnology Characterization Laboratory.* Integrative Biology, 2013. **5**(1): p. 66-73.
181. Adiseshaiah, P.P., J.B. Hall, and S.E. McNeil, *Nanomaterial standards for efficacy and toxicity assessment.* Wiley Interdisciplinary Reviews: Nanomedicine and Nanobiotechnology, 2010. **2**(1): p. 99-112.
182. Park, K., *To PEGylate or not to PEGylate, that is not the question.* Journal of Controlled Release, 2010. **142**(2): p. 147-148.

4 Article 1 “Effect of Polymer Architecture on the Structural and Biophysical Properties of PEG-PLA Nanoparticles”

Accepté dans ACS Applied Materials and Interfaces, le 22 avril 2015
ACS Appl. Mater. Interfaces 2015, 7, 10374–10385, DOI: 10.1021/acsami.5b01423

Dans cet article nous décrivons la synthèse d’une bibliothèque de copolymères PEGylés avec une architecture « peigne ». Ces polymères sont caractérisés puis par la suite utilisés pour fabriquer des nanoparticules par nanoprécipitation.

Les propriétés structurales des particules sont étudiées dans le but de faire un lien entre l’architecture des copolymères et l’organisation interne et de surface des particules.

Les propriétés de stabilité en milieu salin et d’interactions avec les protéines sont également étudiées en lien avec la structure des copolymères utilisés et des nanoparticules obtenues.

Effect of Polymer Architecture on the Structural and Biophysical Properties of PEG-PLA Nanoparticles

Jean-Michel Rabanel[1,2], Jimmy Faivre[2], Soudeh F. Tehrani[1], Augustine Lalloz[1,2], Patrice Hildgen[1,] , Xavier Banquy[2,*]*

[1] Laboratoire de Nanotechnologie Pharmaceutique,
Faculté de Pharmacie, Université de Montréal,
C.P. 6128, Succursale Centre-ville, Montréal, Québec, H3C 3J7, Canada
[2] Canada Research Chair on Bio-inspired Materials and Interfaces
Faculté de Pharmacie, Université de Montréal,
C.P. 6128, Succursale Centre-ville, Montréal, Québec, H3C 3J7, Canada
** Corresponding authors*

4.1 Abstract

Polymers made of poly(ethylene glycol) chains grafted to poly(lactic acid) chains (PEG-*g*-PLA) were used to produce stealth drug nanocarriers. A library of comb-like PEG-*g*-PLA polymers with different PEG grafting densities was prepared in order to obtain nanocarriers with dense PEG brushes at their surface, stability in suspension, and resistance to protein adsorption. The structural properties of nanoparticles (NPs) produced from these polymers by a surfactant-free method were assessed by DLS, zeta potential, and TEM and were found to be controlled by the amount of PEG present in the polymers. A critical transition from a solid NP structure to a soft particle with either a "micelle-like" or "polymer nano-aggregate" structure was observed when the PEG content was between 15 to 25% w/w. This structural transition was found to have a profound impact on the size of the NPs, their surface charge, their stability in suspension in presence of salts as well as on the binding of proteins to the surface of the NPs. The arrangement of the PEG-*g*-PLA chains at the surface of the NPs was investigated by ^{1}H NMR and X-ray photoelectron spectroscopy (XPS). NMR

results confirmed that the PEG chains were mostly segregated at the NP surface. Moreover, XPS and quantitative NMR allowed quantifying the PEG chain coverage density at the surface of the solid NPs. Concordance of the results between the two methods was found to be remarkable. Physical-chemical properties of the NPs such as resistance to aggregation in saline environment as well as anti-fouling efficacy were related to the PEG surface density and ultimately to polymer architecture. Resistance to protein adsorption was assessed by isothermal titration calorimetry (ITC) using lysozyme. The results indicate a correlation between PEG surface coverage and level of protein interactions. The results obtained lead us to propose such PEG-*g*-PLA polymers for nanomedecine development as an alternative to the predominant polyester-PEG diblock polymers.

Keywords: Poly(lactic) acid, poly(ethylene glycol), nanoparticle, micellar particle, XPS, NMR, ITC

4.2 Introduction

Polymeric nanoparticles (NPs) have been intensively investigated for their potential use as drug delivery and targeting systems because of their stability in biological media, drug encapsulation and release capabilities, as well as their compatibility with various routes of administration[1-3]. However, the high expectations generated by the NP-based therapies (including liposomes, micelles, particles, etc.) are not currently matched by clinical successes. Only a handful of products have reached the market with, in several cases, limited improvement over preexisting formulations. These drug delivery approaches are now seriously questioned and many of their biological properties such as organ clearance, [4] organ targeting and biodistribution, [5, 6] ability to cross biological barriers, [7] ability to evade the complement system, [8] and ability to diffuse into tissue interstitium [9] are under scrutiny. One of the most significant issues of NP-based systems is the limited accumulation of NPs at the pathological site, regardless of the nature of the NPs. It appears that only 5 to 10% of an I.V. injected dose of NPs does accumulate at the desired site, with 90 to 95% of the dose distributing non-specifically to organs such as the liver and spleen [10].

Many elements have been put forth to explain these disappointing results. One of them is the lack of systematic quantitative characterization of the properties of the particles used in drug delivery in spite of efforts put forward by many research teams [11].

In order to fulfill their promise as drug delivery systems, polymeric NPs should not only be composed of biocompatible, excretable and/or degradable materials, but also possess a well-defined structure and adequate surface properties. Adequate surface properties can be conferred by a polymeric hydrophilic corona. In the case of polymeric NPs, such hydrophilic corona can be formed during the NP fabrication process either by self-assembly of the polymer chains carrying hydrophilic moieties or by postgrafting of hydrophilic polymer chains at the surface of the NP. The self-assembly process, due to its simplicity, is by far the most commonly used method to produced NPs with a hydrophilic corona.

The use of PEG as a corona-forming polymer effect is well established. The resistance of NPs to non-specific absorption (opsonisation) of plasmatic proteins is a key element to determine their fate in the human body. The anti-fouling properties of NPs control the half-life as well as other pharmacokinetic parameters of the NPs [12], their targeting capabilities [5, 13] and their therapeutic action (pharmacodynamics). Denser PEG coatings have been shown to improve the diffusion of NPs in the extra cellular matrix (ECM) and across the mucosa barrier, which in turn should improve drug delivery efficacy [14], [15]. High resistance to protein adsorption as well as NP diffusion in complex media are obtained at high PEG surface densities, where the polymer chains are organized as brushes.[14, 16] Resistance to protein adsorption has been extensively studied both at the fundamental level[17, 18] and in the context of pharmaceutical sciences[12].

While the effect of surface PEGylation on the biological outcome of nano-based drug delivery systems has been extensively investigated in the literature, the correlations between the PEG copolymer architecture and its biological effects have yet to be explored. To date, the polymer architecture of choice is a linear diblock copolymer composed of a hydrophobic segment, usually a biodegradable polymer such as poly(lactic acid) (PLA) or poly(caprolactone) (PCL), and a hydrophilic segment, usually poly(ethylene glycol) (PEG). [19] The possible control of surface PEGylation and particle structure by alternative PEG copolymer architecture is an intriguing possibility that has received little attention.

Moreover, the PEG surface densities are often ill-characterized in the literature. This lack of characterization makes it difficult to compare the performance of different delivery systems and establish the optimal PEG surface density. In general, the PEG moieties are assumed to be completely segregated at the surface of the NPs based on indirect evidences such as increase in NP hydrodynamic diameter and decrease of zeta potential. Such an assumption leads to in an overestimation of PEG density and incorrect appreciation of the PEG layer conformation. Direct quantification and assessment of polymer conformation are not trivial and the number of techniques suitable for polymeric NPs is indeed limited [20]. For example, ^{1}H NMR of NPs suspended in D_2O has been proposed for the first time by Hkrach *et al.* to qualitatively characterize PEG-*b*-PLA NPs[21]. Later, surface PEG quantification methods based on ^{1}H NMR have been proposed relying on internal standards [22, 23]. X-ray photoelectron spectroscopy (XPS) allowing analysis of NPs in the dried state has also been proposed to semi-quantify polymers attached at the surface of polystyrene NPs[24] and PLA NPs [25-27].

We previously developed a family of comb-type copolymers having PEG chains branching along a linear polymeric backbone of PLA. This architecture had been proposed to increase the number of functionalities present on a single polymer chain and to help control the number and density of functionalities at the NP periphery. These polymers were used to produce stealth NPs in a one-step process that avoided the grafting of PEG chains post NP fabrication and facilitated purification. PEG segregation toward the surface was observed for these NPs[27]. However, assessment of PEG density and optimization of the stealth behavior of the NPs are still lacking.

In this study, a library of branched/comb PEG-*g*-PLA with controlled PEG contents was synthesized in order to establish correlations between polymer architecture and NP properties. A diblock PEG-*b*-PLA was also synthesized and used to compare the performance of the different polymers. The conformation of the PEG chains at the surface of the NPs was investigated by quantitative ^{1}H NMR and XPS. The performance of the PEGylated NPs was assessed by protein adsorption isotherms and colloidal stability assays. Correlations between the surface coverage afforded by PEG and the properties of the NPs allowed establishing

criteria for the design and preparation of PEGylated polymeric NPs based on comb-shaped polymers.

4.3 Experimental methods

4.3.1 Materials

All chemicals were purchased from Sigma-Aldrich (Oakville, ON Canada) unless otherwise stated in the text. Dilactide was recrystallized in toluene and dried overnight in vacuum before use. Solvents were from Fisher Scientific (Whitby, ON Canada) and used as received.

4.3.2 Polymer synthesis and characterization.

- ***Polyester-co-ether backbone polymer synthesis (benzyl-g-PLA)***

Polymer synthesis was carried out as previously described [28] with minor modifications. Briefly, random copolymerizations of D,L-dilactide and benzyl glycidyl ether (BGE) were obtained by ring-opening polymerization catalyzed by stannous 2-ethyl hexanoate (molar ratio of 1/5000 relative to lactic monomer) at 150^{o}C under argon atmosphere and mechanical stirring for 6 hours. At the end of the reaction, the crude polymer melt was dissolved in dichloromethane (DCM) and the polymer was precipitated in hexanes (HEX) twice to yield polymer **(1)** shown in Scheme 1. (Total yield: 90-95%). The BGE/lactic acid ratio was varied from 0.5 to 3 % to yield PLA backbone polymers with different benzyl side chain densities.

Example of Polymer (**1**), Benzyl-g-PLA, at 1.1 % Benzyl to lactic monomer ratio:

FTIR: (cm^{-1}): 3512.6; 2994.4; 2944.9; 2880.5; 1745.2; 1451.7; 1380.5; 1363.8; 1319.1; 1268; 1183.7; 1127.6; 1080.3; 1049; 956.1; 863.7; 746.9; 699.3 ^{1}H NMR (400 MHz, DMSO-d6): δ: 1.3-1.5 (m, 3H, CH_3); 4.48 (m 2H, CH_2); 3.58 (m, 2H); 4.2 (m, 2H); 5.2 (m, 1H, CH); 7.3 (m, 5H, benzylic); GPC : M_n 18,500 g/mol; M_w 31,700 g/mol.

- ***Benzyl-g-PLA debenzylation (HO-g-PLA)***

Alcohol pendant group was deprotected by catalytic hydrogenation in presence of Pd/Carbon 5% (1 g of carbon powder for each mmole of benzyl group) in ethyl acetate (EtAc) under constant H_2 flow for 48 hours. Pd/Carbon was removed on a filtration column (Celite® Standard Super-Cel® NF, Acros Organics, Thermo Fisher Scientific, USA). Polymer **(2)** was recovered after solvent evaporation, dissolution in DCM, precipitation in HEX, and drying under vacuum (Scheme 1). Complete removal of benzyl groups was confirmed by ^{1}H NMR. (Total yield: 95%).

Example of characterization of Polymer (**2**) after debenzylation (HO-g-PLA, 1.1% pendant OH) FTIR (cm^{-1}): 2998.8; 2947.4; 1744.1; 1450.3; 1362; 1267.8; 1183.8; 1126.8; 1078.1; 954.7; 863.3; 745.2; 704.8 ^{1}H NMR (400 MHz, $CDCl_3$) δ: 1.3-1.5 (m, 3H, CH_3); 3.58 (m, 2H); 4.19 (m, 2H); 5.2 (m, 1H, CH); GPC : M_n 16,200 g/mol; M_w 28,900 g/mol.

- ***Methoxy-PEG carboxyl preparation***

Methoxy-PEG-OH (mPEG-OH, 2kD) was oxidized by Jones reaction in acetone with 2.5 molar equivalent of CrO_6 (equivalent to OH present), H_2SO_4, and H_2O for 4 hours at room temperature under high speed stirring. The reaction was stopped by addition of 1N HCl and isopropanol. The acetone was removed by evaporation. The polymer solution was then extracted and dialyzed to remove Cr. The mPEG-COOH was recovered by freeze-drying as a white fluffy material. The mPEG-COOH was kept in presence of P_2O_5 under vacuum before use.

mPEG-COOH

FTIR (cm^{-1}) 3484.9; 2883.2; 2741.7; 1964.8; 1740.1; 1466.4; 1454.1; 1359.2; 1340.3; 1279.1; 1240.5; 1148; 1105.1; 1060.1; 946.4; 841.1; 667.5 ^{1}H NMR (400 MHz, $CDCl_3$) : δ 3.38 (s, 3H, CH_3); 3,64 (m, 2H, CH_3); 4.16 (m, 2H, CH_2)

- ***Grafting of mPEG-COOH on Polymer (2) (PEG grafted PLA or PEG-g-PLA)***

mPEG-COOH (2kD) was finally grafted onto PLA-OH polymers by acylation to yield PEG-g-PLA (polymer **(3)** in scheme 1). Briefly, weighed carboxy PEG was incubated under stirring with excess of thionyl chloride in $CHCl_3$ under argon atmosphere for 2 hours. After solvent removal and drying under vacuum, dry polymer (**3**) was added along with anhydrous

pyridine in dry $CHCl_3$ stabilized by amylene and stirred for 24 hours under argon atmosphere. The PEG-*g*-PLA polymers were recovered after washing, precipitation, rotary evaporation of solvent, and drying. The PEG content in the polymers was controlled by either varying the BGE content in the polymer backbone, and thus available hydroxyl grafting sites, or by controlling mPEG-COOH to OH-*g*-PLA ratio during the acylation reaction.

Example of characterization of PEGylated Polymer (**4**), PEG-g-PLA

FTIR (cm^{-1}) 2994.2; 2944.7; 2884.4; 2741.9; 2694.8; 1964.9; 1748.2; 1453.3; 1380.8;. 1359.6; 1342.4; 1276; 1241.1; 1185.7; 1083.3;1059.8; 962.4; 862.9; 841.9; 748.5; 698.8 ^1H NMR (400 MHz, $CDCl_3$) : δ: 1.3-1.5 (m, 3H, CH_3); 3.38 (s, 3H, CH_3); 3.65 (m, 2H CH_2); 4.18 (m, 1H); 4.35 (m, 2H); 5.2 (m, 1H, CH); GPC : M_n 16,200 g/mol; M_w 28,900 g/mol.

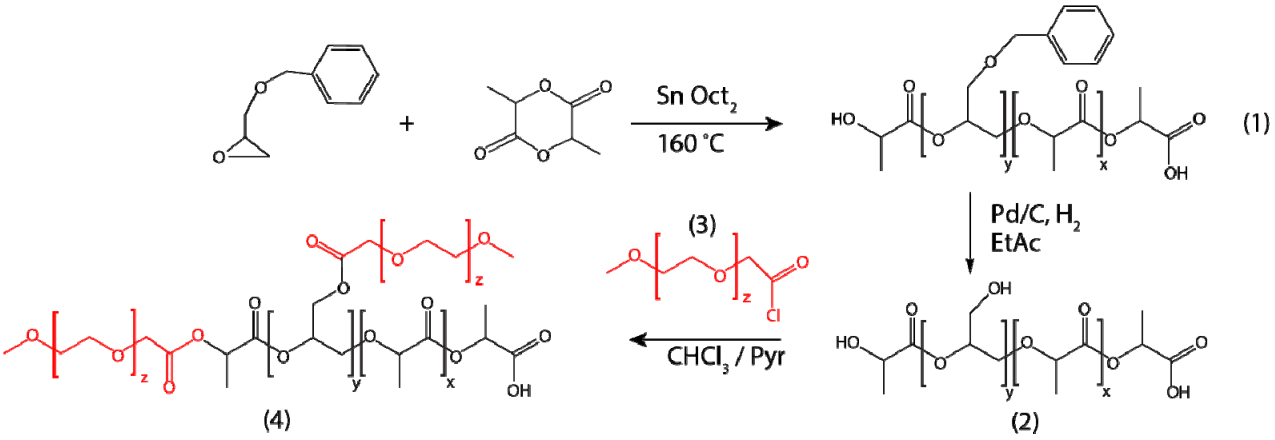

Scheme 1. PEG-*g*-PLA synthesis scheme by acyl chloride grafting

- ***PEG grafting by DCC coupling.***

Alternatively, the PEG chains were grafted by esterification with dicyclohexylcarbodiimide (DCC) as the coupling reagent and dimethylaminopyridine (DMAP) as the catalyst [29]. The number of available OH groups on OH-*g*-PLA (lateral and terminal) was estimated. A 1.1 equivalent of mPEG-COOH was added and dissolved in DCM stabilized by amylene. DMAP and DCC (1 M in DCM) were added at a ratio of 1.2 molar equivalent to available OH groups. The reaction was kept under stirring for 48 hours at room temperature.

PEGylated polymers were purified by filtration on a fritted glass (fine grade) funnel to remove DCU salt, followed by successive extractions with 0.5 M HCl (twice), saturated $NaHCO_3$, and finally MilliQ water. The organic phase was dried with anhydrous sodium sulfate and the polymers were precipitated in HEX. The polymers were dried under vacuum for 48 hours before analysis.

The number of available OH groups on OH-*g*-PLA was calculated as follow: the number of lateral OH groups per chain was taken as the number of benzyl groups present before catalytic hydrogenation as determined by ^1H NMR. The number of terminal OH groups/g of polymer was estimated based on M_n obtained by GPC. The PEG grafting calculations from NMR results are described in *SI*.

- ***Diblock synthesis (PEG-b-PLA)***

mPEG-OH 2kD was used as a macro-initiator in the ring-opening polymerization of dilactide in presence of $SnOct_2$ as previously described [30].

FTIR (cm^{-1}) 2993; 2943.5; 2879.2; 1747.2; 1452; 1381; 1363.4; 1268.1; 1182.2; 1126.4; 1080; 1043.3; 956.4; 862.3; 752.1; 701.8 ^1H NMR (400 MHz, $CDCl_3$) : δ: 1.3-1.5 (m, 3H, CH_3); 3.38 (s, 3H CH_3), 3.65 (m, 2H); 5.2 (m, 1H, CH); GPC: M_n 20,700 g/mol; M_w 29,400 g/mol.

- ***Polymer characterization (NMR, GPC, FTIR)***

The average molecular weights by weight (M_w) and by number (M_n) of the polymers were obtained by gel permeation chromatography (GPC) in either THF or $CHCl_3$. A Waters liquid chromatography system equipped with a refractive index detector, GPC columns (Styragel 5µm, Phenomenex, USA), and Breeze II® software (Waters Corporation, Milford, MA, USA) was used. Flow rate was set at 1 mL/min and column temperature at 40ºC. Linear polystyrene standards (M_w 600 to 400 000 g/mol) were used to construct the calibration curves.

Infrared spectra were recorded on a Nicolet iS10 FTIR (Thermo-Scientific, Canada) equipped with a SMART iTR attenuated total reflectance (ATR) sampling accessory with a ZnSe plate. Data were acquired and analyzed using the OMNIC® interface.

^{1}H NMR, ^{13}C NMR and 2-D $^{1}H/^{1}H$ (400 MHz) analyses were performed on Bruker Advanced 300 MHz or 400 MHz spectrometers (Bruker, Germany) and analyzed using the Mestrec® software. Samples were dissolved either in DMSO-d6 or $CDCl_3$.

Differential scanning calorimetry (DSC) measurements were performed on a DSC Q2000 (TA Instruments – Waters LLC, USA) connected to a refrigerated cooling system Q1000 RCS (TA Instruments – Waters LlC, USA). Polymer and NP samples (approximatively 5 mg) were placed in crimped aluminum pans. DSC analysis was carried out under nitrogen flow by heating the samples from -40°C to 80°C at 10°C min^{-1}, holding for 1 minute, cooling to -40°C at 20°C min^{-1}, and reheating to 80°C at 10°C min^{-1}. T_g (glass transition temperature) and PEG fusion peak were determined from the second heating run in case of the polymers and from the first heating run in case of the NP samples. Analysis was done using the TA instruments Universal Analysis 2000, version 4.5A (TA Instruments – Waters LLC, USA) software.

Polymer density was determined using a helium Ultrapycnometer 1000 (Quantachrome Instrument, Boynton Beach, FL, USA). Ten measurements were averaged.

4.3.3 Nanoparticle preparation and characterization

● ***Nanoprecipitation.*** NPs were prepared by a nanoprecipitation method without addition of surfactants. Polymers were dissolved in acetone at concentrations ranging from 5 to 20 mg/mL (0.5-2% w/v) and injected at a constant flow of 30 mL/h in an aqueous phase (organic to aqueous phase ratio 1:5) under stirring. After solvent evaporation and dialysis (SpectraPor membranes, 6-8 kD, Spectra Laboratories, USA) against a 100-fold volume of MilliQ water (Millipore Canada Ltd, Etobicoke ON, Canada) for 12 hours, twice; the suspension was kept at 4°C until use.

● ***Concentration of NP preparation.*** NP preparations were concentrated for NMR and microcalorimetry experiments using either tangential flow filtration or reverse osmosis. Tangential flow filtration was used for NPs having an average diameter of 70 to 150 nm. It was carried out using a polysulfone filtration column (pore 0.05 µm, Spectra Laboratories, USA) at a flow rate of 3 mL/min for 2 hours. This approach typically yielded a 5 to 7-fold concentration increase. As described elsewhere [31], particles batches NPs with sizes below

70 nm were concentrated by reverse osmosis against a 500 kD dextran solution (10 g/100 mL in MilliQ water), with dialysis membranes of 6-8 kD (SpectraPor, Spectra Laboratories). Typically, concentration increases of 10 to 20-fold were obtained over a 72 to 96-hour period. The concentrates were examined for aggregation and size change by dynamic light scattering (DLS).

● ***Size measurements.*** The NP size was determined by photon correlation spectroscopy (PCS) on a Malvern Zetasizer (Malvern, Worcester, UK) at a diffraction angle of 173^{o} in triplicate in either MilliQ water or 10 mM PBS, pH 7.4

● ***Zeta potential measurements.*** NPs (0.3 mg) were suspended in 1 mL of 5 mM NaCl and placed in a disposable folded capillary cell to measure ζ potential on a Malvern Zetasizer (Malvern, Worchester, UK). Measurements were done in triplicate.

● ***Determination of NP concentration.*** A fixed volume of vortexed NP suspension (500 µL) was placed in a tared Eppendorf tube and freeze-dried. The tube was weighed again after complete drying of the material to obtain the weight of NPs.

4.3.3 XPS surface analysis

NPs were freeze-dried without any cryoprotectant to obtain a fine fluffy powder. The powder was pressed on a doublesided tape and mounted onto a sample rod. XPS survey analysis was performed on a Excalab MK II (VG Scientific, Thermo Scientific) with a Mg Kα X-ray source (1253.6 eV) powered at 200 W, an electron take-off angle of 0°, and steps of 1.0 eV for an energy pass of 1000 eV. High resolution spectra were acquired on a Kratos Axis Ultra (Kratos analytical, Manchester, UK) with a Mg Kα X-ray source used at 120 W (12kV, 10 mA), with steps of 0.05 eV for an energy pass of 20 eV. A flood gun was used to offset the surface charges.

Relative atomic percentage was calculated using the Advanced® software (VG Scientific, ThermoFisher) from the low resolution spectra. The high resolution spectra were analyzed by curve deconvolution of the C_{1s} and O_{1s} signals on software Advanced® (VG scientific, ThermoFisher). The background was subtracted by the Shirley method using the Wagner sensitivity factor table. All spectra were calibrated on the C-C aliphatic carbon

binding energy peak set at 285.0 eV to compensate for surface charging effects. Peak fitting was performed as previously described [25] and based on data obtained for pure PLA and PEG [32]. The conversion of relative atomic percentages to mass percentages and to PEG surface densities is described in details in the Supporting Information (Section S5).

4.3.4 Determination of PEG surface density by NMR analysis

● ***Determination of PEG proton relaxation time***. The relaxation time of the PEG signal in D_2O was first assessed. D_1 was then set at 5 sec during the quantitative experiments, as previously reported by for PEG-DSPE [33].

● ***Total and surface PEG quantification***. PEG content at the surface of the NPs was determined by two methods. The first method consisted in producing the NPs directly in deuterated solvents. Briefly 20 mg of polymer were dissolved in 1 mL acetone-d and injected into 5 ml of deuterium oxide (with 0.75% 3-(trimethlysilyl) propionic-2,2,3,3-d4 sodium salt as internal standard) under stirring. After acetone evaporation on a rotary evaporator, 1 mL of the nanosuspension was transferred to an NMR tube and analyzed by ^{1}H NMR (AV400 Advanced, Bruker, Germany). Another ml of the nanosuspension was freeze-dried in a tared Eppendorf tube in order to determine the mass concentration of NPs for PEG surface density calculations. The same sample was dissolved in $CDCl_3$ and analyzed by ^{1}H NMR (AV400 Advanced, Bruker, Germany) in reference to the internal standard TMS and a PEG calibration curve in $CDCl_3$ to determine the total PEG content of the sample. The second method relied on diluting a concentrated NP suspension in D_2O. The methods to concentrate the NP suspensions and determine NP concentration were described earlier. Either 200 or 500 µL of concentrated NP suspension were added to respectively 800 and 500 µL of deuterium oxide (with internal standard) and analyzed. NP suspensions in D_2O and H_2O/D_2O were analyzed by ^{1}H NMR (AV400 Advanced, Bruker, Germany). Quantifications were conducted in reference to an mPEG-OH 2 kD calibration curve and internal standard peak intensity.

● ***PEG surface density evaluation by NMR calculation.*** See supporting information for more details on PEG chain surface density calculations.

4.3.5 Transmission electron microscopy (TEM)

● ***Sample preparation for TEM***. NP suspensions in MilliQ water (1 to 2 mg/mL) were deposited on carbon films on 400 mesh copper grids (Electron Microscopy Sciences, Hatfield, PA USA) as droplets of about 2 to 4 µL. The droplets were allowed to sit for 5 minutes before excess liquid was removed with a filter paper. Grids were allowed to air dry for 1 to 2 hours before image acquisition. No staining procedure was used.

● ***TEM image acquisition.*** TEM image acquisition was done in bright field mode in a JEM-2100F Field Emission electron microscope (Jeol Ltd, Tokyo, Japan) equipped with a sample holder cooled by liquid nitrogen (Gatan inc. Warrendale, Pittsburg, PA, USA). The grids were maintained at -170ºC throughout the acquisition with a temperature controller (Smart Set Model 900 Cold Stage controller; Gatan inc. Warrendale, Pittsburg, PA, USA). In brief, the grids were introduced in the microscope column under vacuum. Liquid nitrogen was added to the sample holder and temperature recorded. The sample was exposed to the electron beam only after the temperature had reached -170ºC. The acceleration voltage was set at 200 kV. Images were recorded with a digital camera at low electron dose to prevent damages to the heat-sensitive particles (current densities between 5 and 15 pA/cm^2). Images were acquired at a 0º angle. In few cases, images were also acquired at either 15 or 30º angles. Images were transferred, adjusted, and analyzed using the ImageJ software [21].

4.3.6 Colloidal stability in saline

Colloidal stability was evaluated by measuring the Critical Coagulation Concentration (CCC) by DLS. Different NaCl solutions with concentrations from 10mM to 2 M were tested. A known volume of NPs, V, was added to 1 mL of saline solution and rapidly stirred. Final NP concentration was 1 mg NP/mL. Particle size was immediately measured during 15 min at 2-min intervals (3 measurements of 4 runs at 25°C). The volume of each NP formulation to add to the saline solution was estimated using equation 1. :

$$V = \frac{4.\pi.r^3.d.N_{part}}{3.C} \qquad \text{(Eq. 1)}$$

where V is the volume of formulation pipetted to adjust the particles number in the sample, r is the mean NP radius as measured in Milli-Q water by DLS, d is the density of NPs (g cm^{-3}), N_{part} is the targeted number of NPs in solution (namely 4.7×10^{14} NPs/mL) and C is the NP concentration in the stock suspension (g mL^{-1}).

4.3.7 Protein binding assays

● ***Protein binding isotherms.*** Proteins binding isotherms were measured by incubating a fixed amount of NPs with increasing concentrations of either fluorescent bovine serum albumin (BSA) or fluorescent lysozyme (LYZ). BSA coupled with fluorescein isothiocyanate (BSA-FITC) was from Sigma-Aldrich. Lysozyme coupled with rhodamine isothiocyanate (RITC) was prepared as follows. One gram of egg white lysozyme was dissolved in 160 mL of borate buffer pH 8.3. RITC (100 mg) was dissolved in 40 mL of the same buffer. The two solutions were mixed at a lysozyme/RITC molar ratio of 2.8 and stirred for 24 hours at 10°C. The protein was purified by repeated dialysis (SpectraPor RC membrane, 6-8 kD cut-off, Spectrum Laboratories) against MilliQ water to remove unreacted RITC and freeze-dried. NP batches were prepared in phosphate buffered saline (PBS) (15 mM, pH 7.4) as described above and dialyzed against PBS before use. NP concentration was determined by freeze-drying 1 mL of NP suspension and NP diameter was measured by DLS to calculate total surface area (nm^2/mg of NP). Stock solutions of BSA-FITC and LYZ-RITC were prepared in PBS at 1 mg/mL and serially diluted. Aliquots (200 µL) of either 2 mg/mL NP suspensions or PBS (as control) were placed into vials with 40 µL of fluorescent the protein solutions. The final protein concentrations ranged between 0 to 160 µg/mL (0 to 2400 nM) for BSA and 0 to 130 µg/mL (0 to 8840 nM) for LYZ. The solutions were incubated in an orbital shaker at 37°C during 24 hours under constant stirring at 50 rpm, and then centrifuged at 20,000 g during 20 minutes. The pellets were washed and dissolved in 1.3 mL dimethylformamide. Fluorescence was measured at λ_{ex}=490 nm and λ_{em}=530 nm for BSA-FITC and λ_{ex}=550 nm and λ_{em}=570 nm for LYZ-RITC. The measurements were recorded with a F2710 fluorescence spectrophotometer (Hitachi, Tokyo, Japan). The amount of protein adsorbed to the NPs was calculated using a calibration curve and expressed as the number of protein adsorbed per nm² of NP (protein/nm²), as a function of the free-protein concentration in solution (nM), the difference between initial protein concentration and the concentration removed from the solution by

protein binding on the NP surface. Every test was performed in triplicate and results are reported as mean value ± standard error.

● ***Isothermal titration calorimetry*** **(ITC)** The heat of adsorption (*Q*) of lysozyme (LYZ) on the surface of NPs was measured by microcalorimetry. The experiments were carried out on a Microcal VP-ITC instrument (GE Healthcare Life sciences, Pittsburg, PA, USA). The volume of the sample cell was 1.4 mL. NP suspensions (5 to 10 g/L (0.1 to 10 nM) in 15 mM PBS pH 7.4) were placed in the sample cell under constant stirring (350 rpm). A LYZ (Sigma-Aldrich, St-Louis, MA, USA) solution at 1 g/L in 15 mM PBS 7.4 was filtered, degassed, and placed in the injection syringe. Titrations were performed by adding 1 × 2 µL and 12 × 20 µL of LYZ solution (total volume of 242 µL). The equilibration time between injections was set to 1200 s and the temperature was kept constant at 25ºC. The reference cell was filled with 15 mM PBS pH 7.4. The heat of dilution of LYZ was determined by titrating LYZ over 15 mM PBS pH 7.4. The heat of dilution of LYZ was used as reference and subtracted from all the binding isotherms. In a control experiment a LYZ solution (1g/L in PBS 15 mM pH 7.4) was titrated over a solution of mPEG-OH (2kD) in 15 mM PBS, pH 7.4.

4.4 Results and Discussion

4.4.1 Polymer synthesis and characterization

Copolymer synthesis was carried out according to a modified procedure based on the copolymerization of dilactide with BGE (Scheme 1). Compared to the original approach developed in our laboratory[28], the present procedure avoided the oxidation steps necessary to insert carboxyl moieties on the pendant groups. These oxidation steps were found to significantly affect the PLA backbone integrity with a substantial decrease in M_w. In the present approach, catalytic hydrogenation of the benzyl pendant groups under mild conditions was able to recover hydroxyl groups (see Section S1 in supporting information). No decrease in M_w was seen by GPC (see Table S1 for information on PLA backbones synthesis), suggesting that this approach maintains the integrity of the polymer backbones and allows a better control over molecular mass of the copolymer chain. Different PEGylated polymer batches were synthesized with varying PEG content (polymer structure in **Scheme 1**) and

characterized as shown in Table 4.1. Grafting of PEG was performed by either acyl chloride reaction (Scheme 1) [28] or DCC/DMAP coupling (Scheme S1) [29]. The PLA backbone chain length was chosen to be long enough to achieve NP structural integrity yet short enough to ensure adequate speed of hydration, erosion, and release of active ingredients from the polymeric matrix. This aspect is further developed in an upcoming paper dealing with hydrophobic drug encapsulation.

Table 4.1. Polymer characteristics depending on their architecture and grafting method

Polymer architecture	**Grafting Method**	**M*n*** [a] **OH-g-PLA**	**M*w*** [a] **OH-g-PLA**	**PDI**	**Grafting ratio PEG chain/LA**	**PEG chain/ PLA chain**	**M*w*** [c] **polymer**	**% PEG w/w**
		g/mol	*g/mol*		*% 100* [b]		*g/mol*	*% w/w*
Comb	DCC	18 500	28 300	1.53	0.31	0.8	29 890	**7.9**
Comb	DCC	24 300	40 300	1.66	0.473	1.6	43 520	**11.6**
Comb	DCC	18 500	28 300	1.53	0.63	1.62	31 540	**14.9**
Comb	DCC	24 330	33 890	1.39	0.63	2.13	38 150	**14.9**
Comb	DCC	13 400	19 820	1.48	0.89	1.66	23 100	**19.8**
Comb	DCC	18 500	28 300	1.53	0.93	2.39	33 080	**20.5**
Comb	DCC	14 180	23 990	1.69	1.26	2.48	28 950	**25.9**
Comb	DCC	22 200	30 700	1.38	1.5	4.63	39 950	**29.4**
Comb	EDC	15 700	22 700	1.45	1.6	3.49	29 680	**30.8**
Comb	DCC	17 000	25 300	1.49	1.76	4.16	33 600	**32.8**
Comb	DCC	15 700	22 700	1.45	2	4.36	31 420	**35.7**
Comb	Acyl Chloride	23 600	34400	1.46	0.33	1.08	36 560	**8.0**
Comb	Acyl Chloride	23 600	34400	1.46	0.56	1.84	38 070	**11.1**
Comb	Acyl Chloride	22 500	29800	1.32	0.75	2.34	34 490	**13.3**
Comb	Acyl Chloride	22 500	29800	1.32	0.96	3	35 800	**16.5**
Diblock	ROP **	NA	NA		0.4	1	23 800	***5.1***

Notes. [a] *determined by GPC*

[b] *determined by ^{1}H-NMR*

[c] *calculated based on GPC results*

** *ring-opening polymerization*

With the DCC coupling method, the grafting ratios obtained are in accordance with esterification of the secondary terminal OH PLA group as well as the primary pendant alcohol groups (see Table S1 in Supporting Information for the calculated number of available OH in each polymer batches). However, with the acyl chloride method, the grafting ratios were consistent with a grafting occurring predominately on the pendant alcohol groups only.

4.4.2 Preparation and characterization of NPs.

4.4.2.1 Particle size

Figure 4.1A shows the evolution of NP diameter with PEG content in the polymer (for a same PEG chain length of 2 kDa). Our results show that from 5 to 15% w/w PEG, large solid particles are formed with sizes that tend to decrease as PEG content increases (Figure 4.1A). Above 15% w/w, significantly smaller particles are formed as observed by both DLS (Figure 4.1A) and TEM imaging (Figure 4.2). Starting from 25% w/w PEG, the trend is reversed and the size of the particles increases linearly with PEG content. This increase in size could result from a stretching of the PEG chains due to a higher surface PEG chain density[34] or to an increase in the aggregation number of the particles.

The transition from large NPs to smaller particles was found to occur in a narrow range of PEG content situated between 15 and 20% w/w. Such sharp transition is contrasting with the smooth/continuous transition reported for diblock polymers (see Figure 4.1A).[35] Such differences in behavior demonstrate the importance of polymer architecture on NP structuration. The linear increase in size in the higher PEG content regime (i.e., >20% w/w PEG content) was also reported by Logie *et al.* who studied the effect of PEG content of comb-shaped polymers (from 0.6 to 6 PEG chains per polymer) on micelle stability and size by DLS and TEM [36].

4.4.2.2 Zeta potential

The zeta potential, ζ, of NPs produced using PEGylated polymers prepared via the acyl chloride grafting method was found to be largely negative and inferior to -30 mV (Figure 4.1B). On the other hand, the ζ of NPs produced with PEGylated polymers synthesized via the DCC coupling method was found to be significantly higher ranging from -20 mV to 0 mV. Polymers exhibiting PEG chains at the end of the PLA backbone (diblocks or polymer synthesized by the DCC method) present values of ζ much closer to neutrality compared to polymers exhibiting PEG chains well distributed on the PLA backbone (polymer synthesized by the acyl chloride method). These findings suggest that the position of the PEG chain in the PLA backbone plays a crucial role in the composition of the NP-medium interface. Independently of the synthetic method used, it appears that ζ tends to increase from - 40 mV to almost 0 mV with PEG content which confirms the screening of the surface charges on the NP surface by PEG chains.

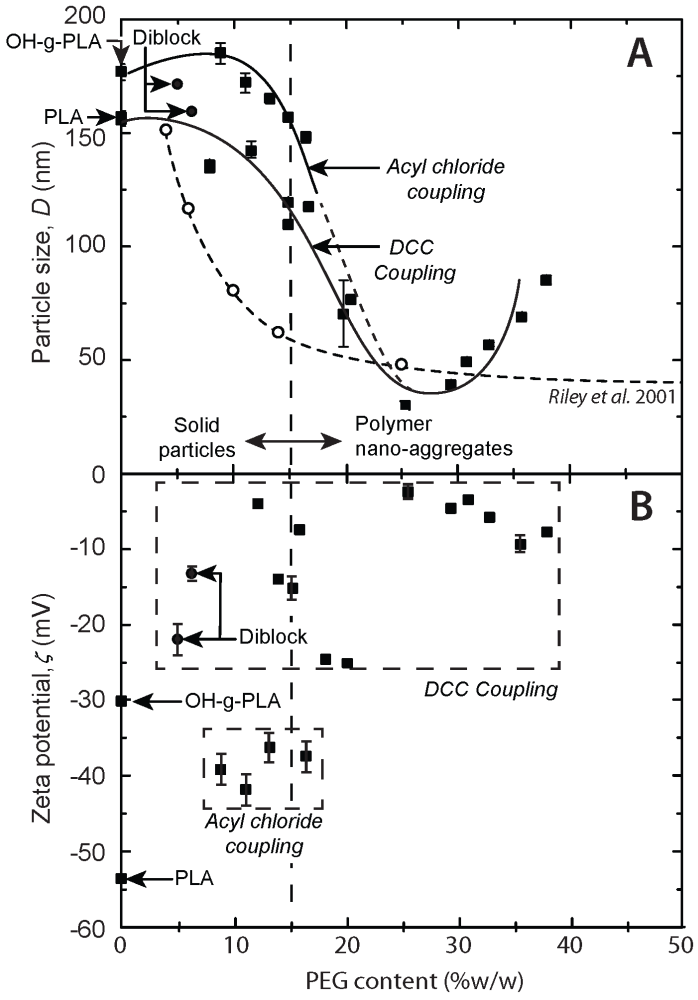

Figure 4.1. (A) Particle size dependence over total PEG content. Solid squares represent particle batches produced for this study while empty circles reproduce data from Riley *et al.* [35] obtained with a diblock PEG-*b*-PLA polymer with a PEG segment of 5000 g/mol. **(B)** Zeta potential dependence over total PEG. Nanoparticle zeta potential measured in 5 mM NaCl increases sharply with PEG content in the particle regime and stays constant in the micellar regime. Lines represent 4th order polynomial fit ($R^2 = 0.91$).

4.4.2.3 Structure and morphology of particles

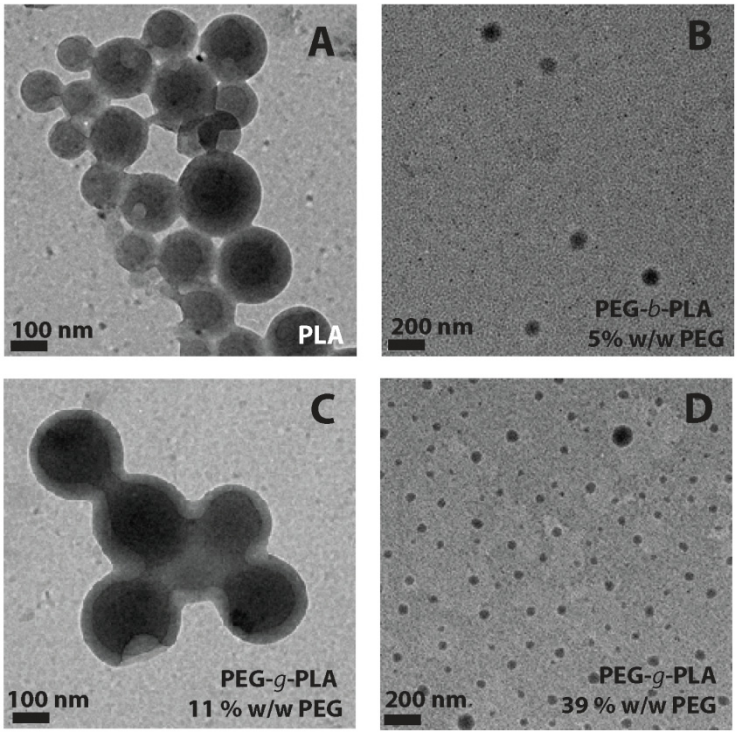

Figure 4.2. Representative cryo-TEM images of nanoparticles fabricated from PLA, PEG-*b*-PLA diblock copolymer, and PEG grafted copolymers. (A) PLA NPs, (B) diblock PEG-*b*-PLA NPs, (C) Solid PEG-*g*-PLA NPs with a PEG content of 11% w/w, (D) PEG-*g*-PLA Polymer nano-aggregate with a PEG content of 38% w/w.

Effect of PEG content and polymer architecture

The relationship between the NP formation process and the NP internal structure is still poorly understood. With the goal of improving our knowledge of such a relationship, we performed cryo-TEM imaging of the NPs. Cryo-TEM images confirmed the existence of two particle structures, i.e. solid core particles at PEG contents below 15% w/w (Figure 4.2A and C) and "polymer nano-aggregates" or soft particles at PEG contents above 15% w/w (Figure 4.2D). Soft particles were also obtained for the diblock polymers (Figure 4.2B). The particle sizes measured by cryo-TEM were in agreement with DLS analysis (using a size distribution by number). The PLA and PEG-*g*-PLA solid particles displayed an apparent core-shell

structure (Figure 4.2A and C). Pustulka *et al.* reported a similar core-shell structure for NPs made of diblock PEG-*b*-PLGA prepared by flash nano-precipitation and encapsulating hydrophobic derivatives of paclitaxel [37]. The authors suggested that the observed structure was the result of a drug-rich core surrounded by a PLGA shell and a PEG corona. In our case however, the structures were observed regardless of the presence of hydrophilic polymer blocks or encapsulated hydrophobic compounds. We found that the shape of the core-shell interface and its position could be changed by simply tilting the substrate during imaging. Such changes in shape and position were found to be consistent with a solid NP in flat contact with the substrate (see Figure S11 in SI). Polymer nano-aggregate particles did not exhibit any core-shell like features on cryo-TEM images (Figure 4.2B and D), which is an indication of significant deformation of the NPs on the substrate upon deposition on the carbon grids. Such significant deformation is favored by the lower glass transition temperature (T_g) of the most PEGylated polymers compared to PLA (see calorimetric data, Table S4 in SI). The PEG corona itself is neither dense enough nor thick enough to be seen by TEM and other analytical methods should be used for its characterization.

Nature of the particles

NPs produced from comb-shaped polymers with low PEG content (<15% w/w) were observed as solid particles while NPs produced from polymers with higher PEG content (>15%) were observed as soft "micelle-like" or "polymer nano-aggregate" particles (Figure 4.2). From TEM imaging, it appears that the later particles are soft (at room temperature) and that they flatten upon dehydration during sample preparation and under vacuum. The structural organization of the polymeric chains forming the particles containing over 15% w/w PEG is not clearly defined yet. By analogy with other block copolymer NPs, the term "micelle-like" could be used to describe them [38, 39]. However, such term may not be appropriate since it defines a thermodynamically stable structure, which is certainly not the case of the present NPs which appear as kinetically frozen, as already mentioned previously.[19, 40] A micellar phase is characterized by the independence of the micelle size over polymer concentration as well as a narrow micelle size distribution. Both properties were not observed with the polymers under study as we found large polydispersity (PDI) for polymer nano-aggregate (PDI $\geq$ 0.25) as shown in Table S5. Particle preparations using

different polymer concentrations in the organic stock solution showed significant variations of NP size indicative of a NP formation mechanism more related to precipitation/aggregation than micellization (data not shown). PEG polymer content could also affect the polymer solution viscosity in organic solvent, which is a determinant of the particle size produced by nanoprecipitation (Figure S6).

Effect of PEG grafting method

We found differences in NP properties whether PEGylation was achieved by DCC or acyl chloride coupling reactions, even at similar PEG content. NPs prepared from polymers obtained by DCC coupling appeared similar to NPs prepared from the diblock polymer in terms of zeta potential (ζ) and TEM morphology. NPs prepared from acyl chloride polymers seemed similar to plain PLA and OH-*g*-PLA NPs. The differences are mostly due to the difference in polymer architecture obtained by the two coupling methods. Acyl chloride coupled polymers have well distributed PEG branches characteristic of the comb-like architecture. On the other hand, DCC polymers, even if they have PEG lateral grafted chains, have properties more related to diblock polymers because of PEG segment present at the PLA chain end. These structural differences might explain why NPs prepared with DCC polymers have sizes and ζ more closely related to those obtained with the diblock polymers compared to the acyl chloride polymers.

4.4.3 Calorimetric properties of pegylated polymers and nanoparticles

As already reported by Sant *et al.,* [41] the T_g of PEG-*g*-PLA polymers depends strongly on the PEG content in the polymer (Table S4). First and second runs of DSC scannings of representative polymers are shown in Figures S10 and S11. The main difference between the first and second runs was the disappearance of the polymer chain relaxation endotherm [37, 41]. The T_g of the polymers was determined as the midpoint of the extrapolated tangent of the baseline and was located between -5 ^oC and 30^oC (Table S4).

DSC scans of freeze-dried NPs presented striking differences compared to the bulk polymers. The presence of PEG dispersed in PLA was evidenced by a reduction of T_g in PEG-

g-PLA NPs compared to PLA NPs and by the absence of PEG fusion endotherm (data not shown). T_g shifts have also been observed in drug-loaded NPs as a result of polymer-drug interactions [42]. The presence of PEG chains in the particle core was also supported by the NMR quantification data as will be detailed below (Figure 4.3). T_g recorded for all NPs appeared independent on the PEG content (Table S4). This could result from a near constant amount of PEG, acting as a plasticizer, in the NP core.

4.4.4 Quantification of PEG distribution at the nanoparticle surface and in its core

4.4.4.1 NMR studies

The presence of PEG at the NP surface was confirmed by ^{1}H NMR analysis in D_2O. In D_2O, the PEG signals are sharp and well defined indicating that the PEG chains are at the surface of the NPs and highly hydrated while the PLA signals cannot be resolved (an example NMR spectrum is shown in Figure S9) [21, 37]. The absence of PLA signals supports a strongly dehydrated PLA core characteristic of solid NPs. No PLA signal was seen for the polymer nano-aggregates also, suggesting a kinetically frozen core with no exchange of unimers with the surrounding media. For instance, NPs made with PEG-*b*-PLA diblock have been shown to display a solid core when the molar mass of the PLA hydrophobic segment was above 6000 g/mol, while a liquid core was found for hydrophobic blocks below 4000 g/mol [22]. The NPs obtained at a PEG content >15% w/w having a kinetically frozen core, the use of "polymer nano-aggregate" is justified to designate them [40].

The exact PEG percentage at the surface and PEG surface density was quantified by NMR. Two sample preparation methods were tested, namely the nanoprecipitation of the dissolved polymer in deuterated acetone into deuterium oxide and the preparation of NPs in pure water followed by their dilution in D_2O. The first method has the advantage of producing ready-to-analyze particles and of generating NMR spectra exempt of a broad H_2O peak that could interfere with the integration of the PEG peak (Figure S9). However, this method produced NPs with smaller diameters compared to nano-precipitation in H_2O (Table 4.2) and NP preparations with residual organic solvent. D_2O and H_2O differ in surface tension,

viscosity, and density, parameters that affect the nano-precipitation process. The second method used closely reproduces the normal the preparation procedure of the NPs. However, it requires concentrating the NP suspension after nanoprecipitation, which can generate a potential problem in the control of NP size and which complicates the quantitative analysis by NMR due to the presence of H_2O in the suspension medium. To minimize this last issue, the suspensions were concentrates so as to minimize residual H_2O in the sample. The stability of the nano-suspensions after particle concentration by either tangential filtration or reverse osmosis was assessed by DLS (see Table S5 for sizes of NPs measured before and after concentration).

Table 4.2. NMR and XPS quantification of PEG surface density of solid particles

		^{1}H-NMR[a]				**XPS**[a]	
		NPs prepared in D_2O		*NPs concentrated & suspended in D_2O*			
Polymer Architecture	**PEG content**	**Diameter**[b]	**Surface density**	**Diameter**[b]	**Surface density**	**Diameter**[b]	**Surface density**
	% w/w	*nm*	*PEG/nm^2*	*nm*	*PEG/nm^2*	*nm*	*PEG/nm^2*
Comb	8.9	87.6	0.5	157.1	0.45	128.3	0.47
		95	0.55	--	--	149.1	0.43
		--	--	--	--	101.1	0.42
		--	--	--	--	100.9	0.39
Comb	11.1	--	--	134.8	0.97	87.5	0.57
						99.53	0.91
Comb	13.3	116.8	1.2	132.8	1.04	135.4	1.03
		99.5	1.07	--	--	101.1	1.02
Comb	16.5	--	--	113.8	0.88	97.6	1.02
Diblock	5	83.9	0.22	--	--	74.4	0.30
		64.3	0.22	--	--	67.7	0.32

[a] *Density calculations are detailed in the supporting information Sections S5 and S6*

[b] *Average size based on a distribution by number*

The percentage of PEG found at the surface of the NPs was calculated as the ratio of the mass of PEG detected by NMR over the total PEG content present in the sample (see Figure 4.3A). The percentage of PEG found at the surface increased with PEG content in the

solid particle regime (i.e. between 9 to 20% w/w of PEG) and reached a maximum at around 90%. In the polymer nano-aggregate regime (i.e. when the PEG content was increased above 20% w/w), the PEG percentage found at the surface of the NPs decrease to about 75% and remained constant thereafter, revealing that a significant portion of the PEG chains were located inside the particle core (Figure 4.3A). In contrast Riley *et al.* found a higher percentage (80 to 100%) of total PEG at the surface of NPs prepared with diblock polymers of different PLA block sizes (Figure 4.3A) [43]. Small Angle Neutron Scattering (SANS) studies also confirmed the presence of PEG in the particle core for polyester-PEG diblock polymer NPs. [44] In light of these differences, it appears that the comb-like architecture is imposing constrains to the migration of PEG chains towards the surface during NP formation.

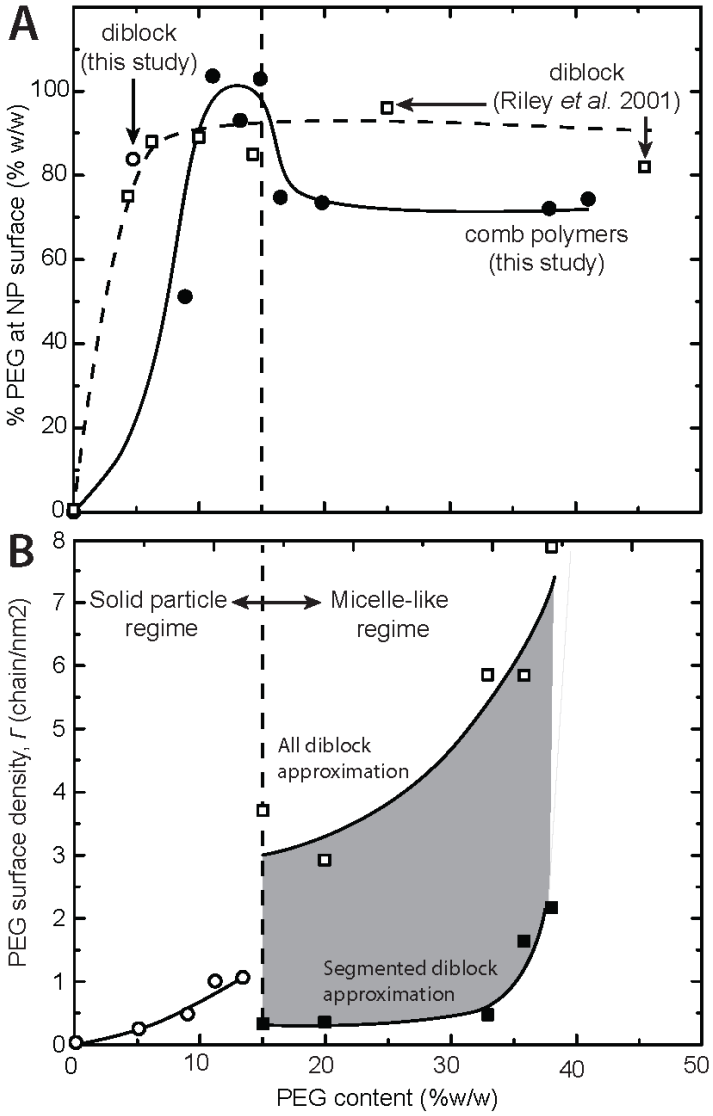

Figure 4.3. (A) Evolution of the % PEG at the surface of the NPs and (B) PEG surface densities determined by quantitative NMR as a function of PEG content in the polymer for solid *and* polymer nano-aggregate particles. In (B) open squares represent the calculated PEG surface density base on the "all diblock" approximation; the closed squares represent the calculated PEG surface density base on the "segmented diblock" approximation. Error bars are smaller than the symbols used.

PEG surface density, Γ, was calculated using the following equation (Eq. 2):

$$\Gamma = \frac{R^3}{R_c^2} . \%PEG(surface) . \%PEG(polymer) . \rho_p . \frac{N_A}{M_w} \qquad \text{(Eq. 2)}$$

Where R is the hydrodynamic radius of the NP, R_c the radius of the core of the NP, ρ_p refers to the polymer density, M_w its molecular weight, and N_A is the Avogadro number. %PEG (surface) refers to the fraction of polymer at the surface of the NP while %PEG (polymer) refers to the PEG content in the polymer.

^{1}H NMR analysis of NPs suspended in D_2O allowed determining the surface density of PEG, Γ (Table 4.2 and Figure 4.3B). For the solid particles, we used the approximation $R \simeq R_c$ and found that Γ increased with PEG content almost linearly to reach a value of $\Gamma \simeq 1$ chain/nm^2 at 15% w/w PEG content, which is well above the theoretical brush regimen threshold of 0.01-0.005 chain/nm^2. Other calculation methods were tested leading to similar results (see Section S6 and SI in [20]). Of note, the PEG surface density was found to be insensitive to PEG contents between 9 to 15% w/w.

In the micellar/polymer aggregate regime (i.e. at PEG contents > 15 to 20 % w/w), accurate density values could not be obtained given that the core radius, R_c, was not experimentally available in this regime. R_c was estimated using the star polymer approximation for polymeric micelles [45]. We used two possible effective architectures to calculate the number of hydrophilic and hydrophobic segments. In the first approximation, we considered all the ethylene oxide monomers per chain to form a single hydrophilic bloc. We called this first approximation the "all diblock" approximation. In the second approximation, each PEG segment was considered as an individual chain associated with a fraction of the PLA chain. We called this second approximation the "segmented diblock" approximation. Both approximations allowed upper and lower bound values for Γ to be obtained as shown in Figure 4.3B (respectively represented by open and closed squares).

Despite the large differences between the upper and lower boundaries defined by these two approximations, they both predict an eventual increase of Γ with PEG content. Our

approach does not allow identifying any dramatic change in PEG surface density at the transition from solid particles to polymer nano-aggregates as was observed for the % of PEG at the surface of NPs and for the NP diameter.

4.4.4.2 XPS studies

Qualitatively, XPS high resolution spectra of NPs showed an enrichment of PEG at the surface compared to the PEG-*g*-PLA polymer bulk as calculated in weight % based on chemical bond quantification (see Figure S7 and Table S3 of *SI*). These data support the orientation of PEG moieties towards the surface of the NPs and are in accordance with the NMR results [27].

Calculations based on the C_{1s} high resolution spectra give a semi-quantitative result that can be translated into PEG surface density, as the particle volume analyzed is a two-component substrate (PLA and PEG). Details of the calculation method can be found in the supporting information (Section S5). Two main assumptions were used in the calculation: 1) the polymer volumes analyzed by XPS were homogeneous and 2) all the PEG chains detected and quantified were localized at the surface of the NPs.

The PEG surface density results obtained by XPS are presented in Table 4.2. The results are found to be in close agreement with the NMR results, in spite of the difference in state of the NPs (dry vs. wet state) and the different assumptions made in the calculation methods. The PEG detected by XPS belongs to a layer of about 10 nm in depth at the surface of the NPs. As mentioned above, we assumed for the sake of calculation that the PEG chains detected were all at the surface of the NPs. However, it cannot be excluded that some of this PEG is buried just underneath the surface. This is why discrepancies can be expected between XPS and NMR results.

Of note, XPS analysis was not performed on polymer nano-aggregate particles as the radius of the particles decrease rapidly. Assuming that the layer accessible to the XPS analysis is 10 nm deep, the volume examined by XSP is about 35% of the total volume of a particle of 150 nm in diameter. For particles of about 50 nm in diameter, this volume percentage increases to about 80%. In the latter case, XPS analysis becomes less pertinent to give insight about the surface properties of the NPs.

4.4.5 Colloidal stability studies

The colloidal stability of NP suspensions was assessed by monitoring their aggregation kinetics in salt solution (Figure 4.4 and insert). The critical salt concentration of coagulation (or *CCC*) at which rapid aggregation of the particles occurred was used as stability criteria. CCC was determined when rapid aggregation occurs, i.e. when the rate of aggregation was found to be positive.

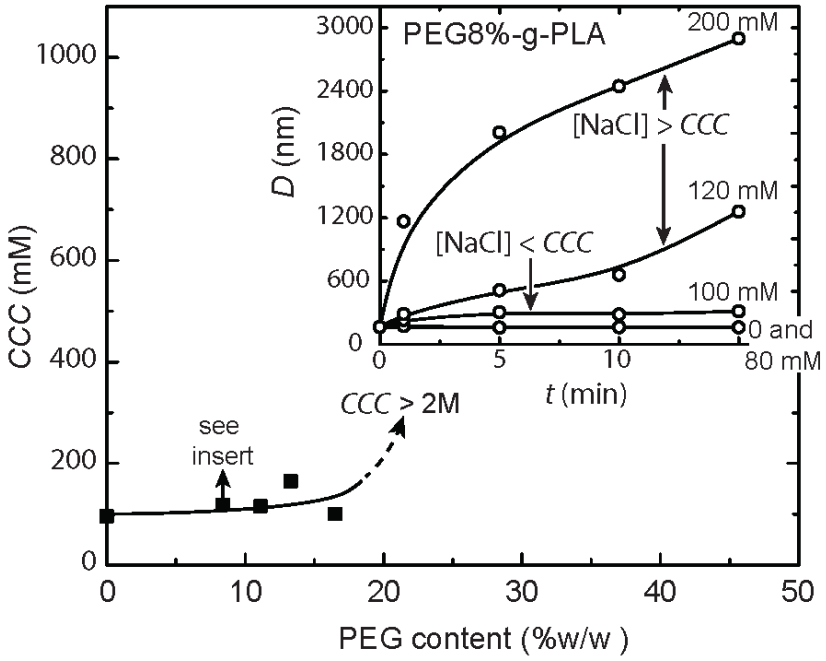

Figure 4.4: Critical coagulation concentration (*CCC*) of NP suspensions of PEG-*g*-PLA polymers. ***Insert****:* Aggregation kinetics of NPs composed of PEG8%-*g*-PLA in presence of different NaCl concentration as measured by DLS. Error bars are smaller than the symbols used.

In the solid particle regime, the *CCC* increased slightly with the PEG content of the polymer. Above a PEG content of 20% w/w, the *CCC* increased dramatically, indicating that the polymer nano-aggregate are extremely stable. In that regime, colloidal stability was maintained even at very high salt concentrations (> 2M NaCl). The extreme stability of the particles can be explained by the presence of strong repulsive steric forces originated from the presence of a dense layer of PEG chains in the brush conformation, as suggested by our

findings. Also, it is worth noting that at such high salt concentrations, other repulsive forces due to ion correlations may be expected to play a role as well.

4.4.6 Protein binding studies

4.4.6.1 Protein absorption isotherms

Human serum albumin (HSA) is the most abundant protein in serum (35 g/L). *In vivo*, it plays a role in creating a protein corona at the surface of particles, promoting their recognition by macrophage cells and their elimination. BSA is a protein similar to HSA. BSA has a molecular weight of 66.5 kD, ia diameter of about 3.8 nm, and an iso-electric point of 4.7-5.1, making it a negatively charged protein at physiological pH. LYZ has a molecular weight of 14 703 g/mol and an iso-electric point of 11, making it a positively charged protein at physiological pH.

As a reference, the theoretical monolayer protein values were calculated using surface values of 45 nm^2 and 12.6 nm^2 for BSA and LYZ, respectively (see Table S5). A BSA monolayer thus corresponds to a surface density of 0.022 BSA/nm^2 while the value is 0.08 LYZ/nm^2 for a LYZ monolayer. Experimentally, the binding of LYZ yielded a non-saturated isotherm of absorption (Figure 4.5). The LYZ surface densities obtained were below the monolayer surface density. In contrast, BSA binding saturated rapidly. Again, the values obtained were far below the protein monolayer surface density. At any given protein concentration, LYZ adsorbed to the NPs 10 to 15 times more than BSA did. This difference could be attributed to electrostatic interactions favoring binding of LYZ to the negatively charged NP surface (Figure 4.2b). Polymer nano-aggregates appeared more efficient at preventing BSA and LYZ binding than solid NPs. The protein binding values decreased with increasing PEG content of the polymers composing the NPs (Figure 4.5).

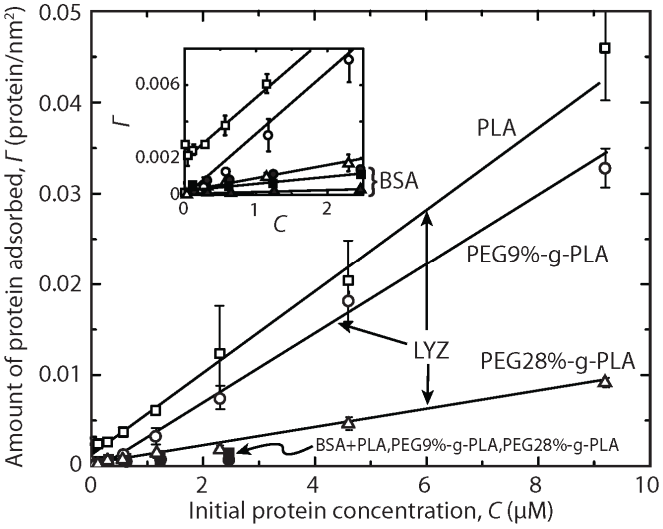

Figure 4.5. Adsorption isotherms of BSA and LYZ at the surface of NPs. For all NPs tested, BSA adsorbed at the surface of the NPs to a lesser extent than LYZ. ***Insert:*** enlarged portion of the adsorption isotherms. Lines represent linear fits (R^2= 0.93)

4.4.6.2 Isothermal Titration Calorimetry

BSA binding studies

Binding of proteins at the surface of the NPs was also studied by ITC. This technique is well suited to evaluate particle stealthness as previously proposed [46, 47]. However, initial adsorption studies with BSA failed to produce a significant thermal signal (data not shown). Surface hydrophilicity, particle concentration (1 to 50 mg/mL), temperature (15 to 25°C), and protein concentration (0.5 to 2 mg/mL) were varied, but still did not yield a significant signal. At the pH of the experiments and in the absence of divalent cations in the PBS buffer used, BSA was negatively charged and had limited attraction to the negatively-charged surface of the NPs. Lindman *et al*. studied the binding of a range of proteins (including human albumin) on hydrophilic acrylamide-based NPs by ITC. Contrary to our findings, the authors did record exothermic signals generated by the adsorption of proteins at the surface of the NPs [46].

Knowing that protein binding did occur (as evidenced by the adsorption isotherms shown in Figure 4.5 and by the change in zeta potential of the NPs measured after ITC experiments, see Table S6), the absence of calorimetric signal indicates that the protein

adsorption energy and binding constants are very weak. Lindman *et al.* hypothesized that protein adsorption occurs without enthalpy change, i.e. the adsorption is strictly entropy driven due to release of water from the NP and protein surfaces [46].

LYZ binding studies

When LYZ was used as model protein, an exothermic signal could be recorded by ITC, confirming the existence of stronger interactions between the NPs and the positively charged protein. This observation is in agreement with the adsorption isotherms presented in Figure 4.5. The complex shapes of the thermograms shown in Figure 4.6 indicate that a more complex mechanism of interaction is at play than simple electrostatic interactions between the NPs and the proteins. For the PEGylated NPs, the maximum exothermic values reached in the binding isotherm decreased with increasing PEG content in the NP. This indicates that the strength of the interactions between the surface of the NPs and LYZ decreased as the PEG surface density increased. Moreover, the saturation concentration, defined as the inflexion point of the binding isotherm, increased with PEG content until the signal reached the baseline (Figure 4.6). Interestingly, NPs with PEG contents higher than 15% w/w did not present any detectable calorimetric interactions. This is in agreement with the adsorption isotherms. Of note, visual examination of the samples after completion of the ITC experiments revealed flocculation of the NPs containing less than 15% w/w PEG. Such bridging of NPs in presence of LYZ was not observed in the case of the polymer nano-aggregate particles.

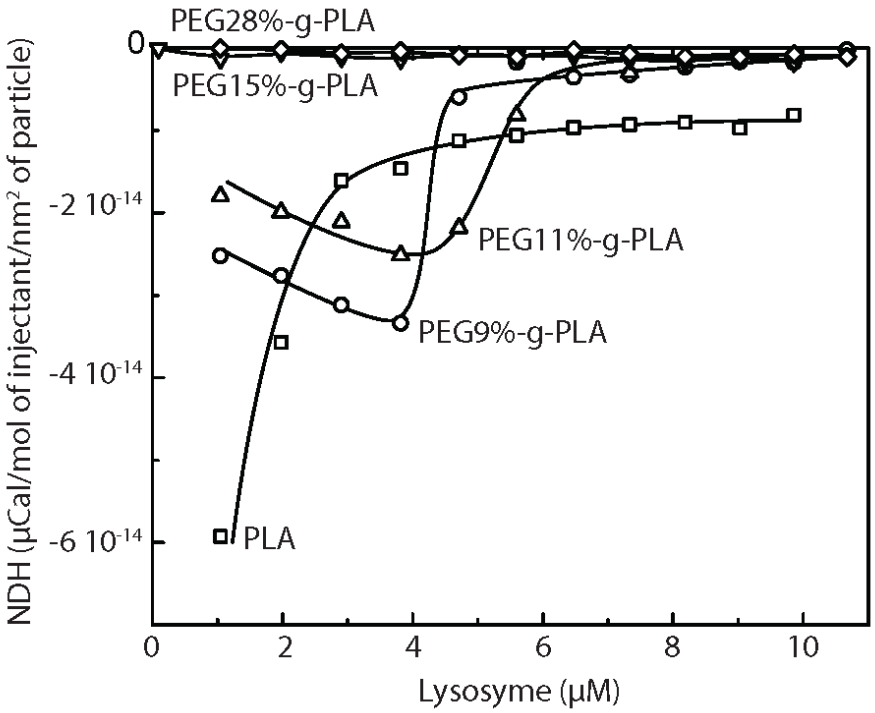

Figure 4.6. ITC assays performed by adding a 1 mg/mL LYZ solution to NPs with different PEG contents. The integrated calorimetric signal was normalized to the NP surface.

The contribution of the interaction between LYZ and PEG to the observed results was investigated. ITC experiment trying to evidence interactions between free PEG chains in solution and LYZ in similar concentration conditions did not show any significant signal (data not shown). This result demonstrates the absence of direct interactions between LYZ and the PEG chains of the NP corona. This result actually argues in favor of the penetration of the protein through the PEG brush and direct interaction between LYZ and the PLA core of the NP. This "primary adsorption" is favored by the small size of the protein (Table S4). Secondary (inside the brush) and tertiary (on the top of the brush) adsorptions are less likely to occur due to the lack of interaction signal between PEG and LYZ [48].

As shown herein, comb polymers could be advantageous alternatives to other polymer architectures to confer high protein resistance to NPs. This is supported by another study showing that a PLL-*g*-PEG polymer with a 20-kDa PLL backbone and 3.5 2-kDa PEG pendant chains is conferring higher protein resistance to cationic metallic surfaces than similar

polymers with other architectures [49]. In another recent study, increased stability in biological medium was also shown for micelles made from comb-shaped polymers with increasing PEG grafting densities [36].

4.5 Conclusion

The organization of the polymer chains of NPs prepared by nanoprecipitation seems to differ whether the polymers are comb-shaped or diblock. The characterization carried out in this study shows a discontinuity in size and zeta potential dependence when a critical PEG content is reached. The PEG content (% w/w) determines two apparent regimes: a solid particle regime and a polymer nano-aggregate regime. Interestingly, we found that only about 75% of the total PEG content was present at the surface of the NPs surface for both solid particles and polymer nano-aggregates. The implications of having PEG chains present inside the particle core remain to be investigated, but it may be that the PEG chains would play a role in drug encapsulation and release. Finally, protein adsorption and calorimetric studies indicate that the comb architecture could be advantageous over other polymer architectures to confer high protein resistance to NPs.

This paper represent a starting point toward the development of a nano-carrier platform for drug delivery. We are currently formulating these polymers for the delivery of active compounds to the central nervous system. All the NP properties reported in the present manuscript are very relevant to evaluate the potential use of the NPs as drug carriers. We believe that NP morphology, colloidal stability and protein adsorption are key design parameters that have to be evaluated before encapsulating any active compounds in the formulation. This manuscript reveals that these key properties are intrinsically linked to polymer architecture and composition.

ASSOCIATED CONTENT

Supporting Information

^{1}H NMR, GPC and FTIR characterizations of representative polymers, methods of calculations of surface densities from quantitative ^{1}H-NMR and XPS, supplementary TEM images and information on NP batches characterization before and after concentration. This material is available free of charge via the Internet at http://pubs.acs.org.

AUTHORS INFORMATION

Corresponding authors: E-mail: ; Tel. +1 (514) 343-2470; E-mail: ; Tel. +1 (514) 343-6448

Author Contributions. The manuscript was written through contributions of all authors. All authors have given approval to the final version of the manuscript.

Notes. Authors declare no competing financial interest

ACKNOWLEDGMENTS

JMR wishes to thank the "Fonds de Recherche du Québec – Nature et Technologie" (FRQ-NT, Government of Québec, Canada) and the Faculty of pharmacy of the Université de Montréal for doctoral fellowships. XB acknowledges the support of Canada Research chair program of the government of Canada. PH acknowledges the support of FRQ-NT (Québec, Canada).

The authors wish to thanks Suzie Poulin and Josianne Lefebvre (Laboratoire d'analyse de surface, École Polytechnique, Montréal, Québec, Canada) with their help with XPS analysis. TEM imaging was performed at the "Centre de Caractérisation Microscopique des Matériaux" (CM^2) of the École Polytechnique (Montréal, Québec, Canada) with the help of Jean-Philippe Massé. Dr. Savoji Mohammad Taghi, Pr. Julian Zhu, Sylvain Essiembre and Pierre Ménard-Tremblay help for GPC and DSC analysis is acknowledged. Johanne Habr technical assistance in NP batches preparation is also acknowledged. Pr. V. Gaêlle Roullin help with the optimization of NP preparation and concentration procedures was greatly appreciated. Editing of this article by Dr. MH Dufresne is greatly acknowledged.

4.6 References

1. Brigger, I., C. Dubernet, and P. Couvreur, *Nanoparticles in cancer therapy and diagnosis.* Advanced Drug Delivery Reviews, 2012. **64, Supplement**(0): p. 24-36.
2. Danhier, F., et al., *PLGA-based nanoparticles: An overview of biomedical applications.* Journal of Controlled Release, 2012. **161**(2): p. 505-522.
3. Hrkach, J., et al., *Preclinical Development and Clinical Translation of a PSMA-Targeted Docetaxel Nanoparticle with a Differentiated Pharmacological Profile.* Science Translational Medicine, 2012. **4**(128): p. 128ra39.
4. Bertrand, N. and J.-C. Leroux, *The journey of a drug-carrier in the body: An anatomo-physiological perspective.* Journal of Controlled Release, 2012. **161** (2): p. 152-163.
5. Ruenraroengsak, P., J.M. Cook, and A.T. Florence, *Nanosystem drug targeting: Facing up to complex realities.* Journal of Controlled Release, 2010. **141**(3): p. 265-276.
6. Kwon, I.K., et al., *Analysis on the current status of targeted drug delivery to tumors.* Journal of Controlled Release, 2012. **164**(2): p. 108-114.
7. Rabanel, J.M., et al., *Drug-loaded nanocarriers: passive targeting and crossing of biological barriers.* Current Medicinal Chemistry, 2012. **19**(19): p. 3070-102.
8. Moghimi, S.M., et al., *Complement activation cascade triggered by PEG-PL engineered nanomedicines and carbon nanotubes: The challenges ahead.* Journal of Controlled Release, 2010. **146**(2): p. 175-181.
9. Jain, R.K. and T. Stylianopoulos, *Delivering nanomedicine to solid tumors.* Nature Reviews. Clinical Oncology, 2010. **7**(11): p. 653-664.
10. Bae, Y.H. and K. Park, *Targeted drug delivery to tumors: Myths, reality and possibility.* Journal of Controlled Release, 2011. **153**(3): p. 198-205.
11. Crist, R.M., et al., *Common pitfalls in nanotechnology: lessons learned from NCI's Nanotechnology Characterization Laboratory.* Integrative Biology, 2013. **5**(1): p. 66-73.
12. Vonarbourg, A., et al., *Parameters influencing the stealthiness of colloidal drug delivery systems.* Biomaterials, 2006. **27**(24): p. 4356-73.
13. Salvati, A., et al., *Transferrin-functionalized nanoparticles lose their targeting capabilities when a biomolecule corona adsorbs on the surface.* Nat Nano, 2013. **8**(2): p. 137-143.
14. Nance, E.A., et al., *A Dense Poly(Ethylene Glycol) Coating Improves Penetration of Large Polymeric Nanoparticles Within Brain Tissue.* Science Translational Medicine, 2012. **4**(149): p. 149ra119.
15. Ensign, L.M., et al., *Mucus Penetrating Nanoparticles: Biophysical Tool and Method of Drug and Gene Delivery.* Advanced Materials, 2012. **24**(28): p. 3887-3894.
16. Gref, R., et al., *'Stealth' corona-core nanoparticles surface modified by polyethylene glycol (PEG): influences of the corona (PEG chain length and surface density) and of the core composition on phagocytic uptake and plasma protein adsorption.* Colloids Surf B Biointerfaces, 2000. **18**(3-4): p. 301-313.
17. Degennes, P.G., *Conformation of polymers attached to an interface.* Macromolecules, 1980. **13**(5): p. 1069-1075.

18. Jeon, S.I., et al., *Protein surface interactions in the presence of polyethylene oxide.1.Simplified theory.* Journal of Colloid and Interface Science, 1991. **142**(1): p. 149-158.
19. Letchford, K. and H. Burt, *A review of the formation and classification of amphiphilic block copolymer nanoparticulate structures: micelles, nanospheres, nanocapsules and polymersomes.* European Journal of Pharmaceutics and Biopharmaceutics, 2007. **65**(3): p. 259-269.
20. Rabanel, J.-M., P. Hildgen, and X. Banquy, *Assessment of PEG on polymeric particles surface, a key step in drug carrier translation.* Journal of Controlled Release, 2014. **185**(0): p. 71-87.
21. Hrkach, J.S., et al., *Nanotechnology for biomaterials engineering: structural characterization of amphiphilic polymeric nanoparticles by 1H NMR spectroscopy.* Biomaterials, 1997. **18**(1): p. 27-30.
22. Heald, C.R., et al., *Poly(lactic acid)-poly(ethylene oxide) (PLA-PEG) nanoparticles: NMR studies of the central solidlike PLA core and the liquid PEG corona.* Langmuir, 2002. **18**(9): p. 3669-3675.
23. Garcia-Fuentes, M., et al., *Application of NMR Spectroscopy to the Characterization of PEG-Stabilized Lipid Nanoparticles.* Langmuir, 2004. **20**(20): p. 8839-8845.
24. Brindley, A., et al., *Polystyrene Colloids with Surface-Grafted Polyethylene Oxide as Model Systems for Site-Specific Drug Delivery: I. Preparation and Surface Chemical Characterization Using SIMS and XPS.* Journal of Colloid and Interface Science, 1995. **171**(1): p. 150-161.
25. Shakesheff, K.M., et al., *The adsorption of poly(vinyl alcohol) to biodegradable microparticles studied by x-ray photoelectron spectroscopy (XPS).* Journal of Colloid and Interface Science, 1997. **185**(2): p. 538-547.
26. Lacasse, F.X., P. Hildgen, and J.N. McMullen, *Surface and morphology of spray-dried pegylated PLA microspheres.* International Journal of Pharmaceutics, 1998. **174**(1–2): p. 101-109.
27. Sant, S., S. Poulin, and P. Hildgen, *Effect of polymer architecture on surface properties, plasma protein adsorption, and cellular interactions of pegylated nanoparticles.* Journal of Biomedical Materials Research, Part A, 2008. **87A**(4): p. 885-895.
28. Nadeau, V., et al., *Synthesis of new versatile functionalized polyesters for biomedical applications.* Polymer, 2005. **46**(25): p. 11263-11272.
29. Neises, B. and W. Steglich, *Simple Method for the Esterification of Carboxylic Acids.* Angewandte Chemie, International Edition in English 1978. **17**(7): p. 522-524.
30. Quesnel, R. and P. Hildgen, *Synthesis of PLA-b-PEG Multiblock Copolymers for Stealth Drug Carrier Preparation.* Molecules, 2005. **10**(1): p. 98-104.
31. Vauthier, C., B. Cabane, and D. Labarre, *How to concentrate nanoparticles and avoid aggregation?* Eur J Pharm Biopharm, 2008.
32. Beamson, G. and D. Briggs, *High resolution XPS of organic polymers The Scienta ESCA300 Database.* 1992, West Sussex, England: John Wiley & Sons Ltd.,.
33. Vernooij, E.A.A.M., et al., *1H NMR Quantification of poly(Ethylene Glycol)-Phosphatidylethanolamine in Phospholipid Mixtures.* Pharmaceutical Research, 1999. **16**(10): p. 1658-1661.

34. de Gennes, P.G., *Polymers at an interface; a simplified view.* Advances in Colloid and Interface Science, 1987. **27**(3–4): p. 189-209.
35. Riley, T., et al., *Physicochemical Evaluation of Nanoparticles Assembled from Poly(lactic acid)−Poly(ethylene glycol) (PLA−PEG) Block Copolymers as Drug Delivery Vehicles.* Langmuir, 2001. **17**(11): p. 3168-3174.
36. Logie, J., et al., *PEG-Graft Density Controls Polymeric Nanoparticle Micelle Stability.* Chemistry of Materials, 2014. **26**(9): p. 2847-2855.
37. Pustulka, K.M., et al., *Flash Nanoprecipitation: Particle Structure and Stability.* Molecular Pharmaceutics, 2013. **10**(11): p. 4367-4377.
38. Riley, T., et al., *Colloidal stability and drug incorporation aspects of micellar-like PLA–PEG nanoparticles.* Colloids and Surfaces B: Biointerfaces, 1999. **16**(1–4): p. 147-159.
39. Zhang, L. and A. Eisenberg, *Multiple Morphologies and Characteristics of "Crew-Cut" Micelle-like Aggregates of Polystyrene-b-poly(acrylic acid) Diblock Copolymers in Aqueous Solutions.* Journal of the American Chemical Society, 1996. **118**(13): p. 3168-3181.
40. Johnson, B.K. and R.K. Prud'homme, *Mechanism for Rapid Self-Assembly of Block Copolymer Nanoparticles.* Physical Review Letters, 2003. **91**(11): p. 118302.
41. Sant, S., M. Thommes, and P. Hildgen, *Microporous structure and drug release kinetics of polymeric nanoparticles.* Langmuir, 2008. **24**(1): p. 280-287.
42. Essa, S., J.M. Rabanel, and P. Hildgen, *Effect of aqueous solubility of grafted moiety on the physicochemical properties of poly(D,L-lactide) (PLA) based nanoparticles.* International Journal of Pharmaceutics, 2010. **388**(1-2): p. 263-273.
43. Riley, T., et al., *Core−Shell Structure of PLA−PEG Nanoparticles Used for Drug Delivery.* Langmuir, 2003. **19**(20): p. 8428-8435.
44. Yang, B., et al., *Small Angle Neutron Scattering Studies on the Internal Structure of Poly(lactide-co-glycolide)-block-poly(ethylene glycol) Nanoparticles as Drug Delivery Vehicles.* Biomacromolecules, 2014.
45. Halperin, A., *Polymeric micelles: a star model.* Macromolecules, 1987. **20**(11): p. 2943-2946.
46. Lindman, S., et al., *Systematic Investigation of the Thermodynamics of HSA Adsorption to N-iso-Propylacrylamide/N-tert-Butylacrylamide Copolymer Nanoparticles. Effects of Particle Size and Hydrophobicity.* Nano Letters, 2007. **7**(4): p. 914-920.
47. Cedervall, T., et al., *Understanding the nanoparticle-protein corona using methods to quantify exchange rates and affinities of proteins for nanoparticles.* Proceedings of the National Academy of Sciences of the United States of America, 2007. **104**(7): p. 2050-2055.
48. Halperin, A., *Polymer Brushes that Resist Adsorption of Model Proteins: Design Parameters.* Langmuir, 1999. **15**(7): p. 2525-2533.
49. Kenausis, G.L., et al., *Poly(l-lysine)-g-Poly(ethylene glycol) Layers on Metal Oxide Surfaces: Attachment Mechanism and Effects of Polymer Architecture on Resistance to Protein Adsorption†.* Journal of Physical Chemistry. B, 2000. **104**(14): p. 3298-3309.

Table of content graphic.

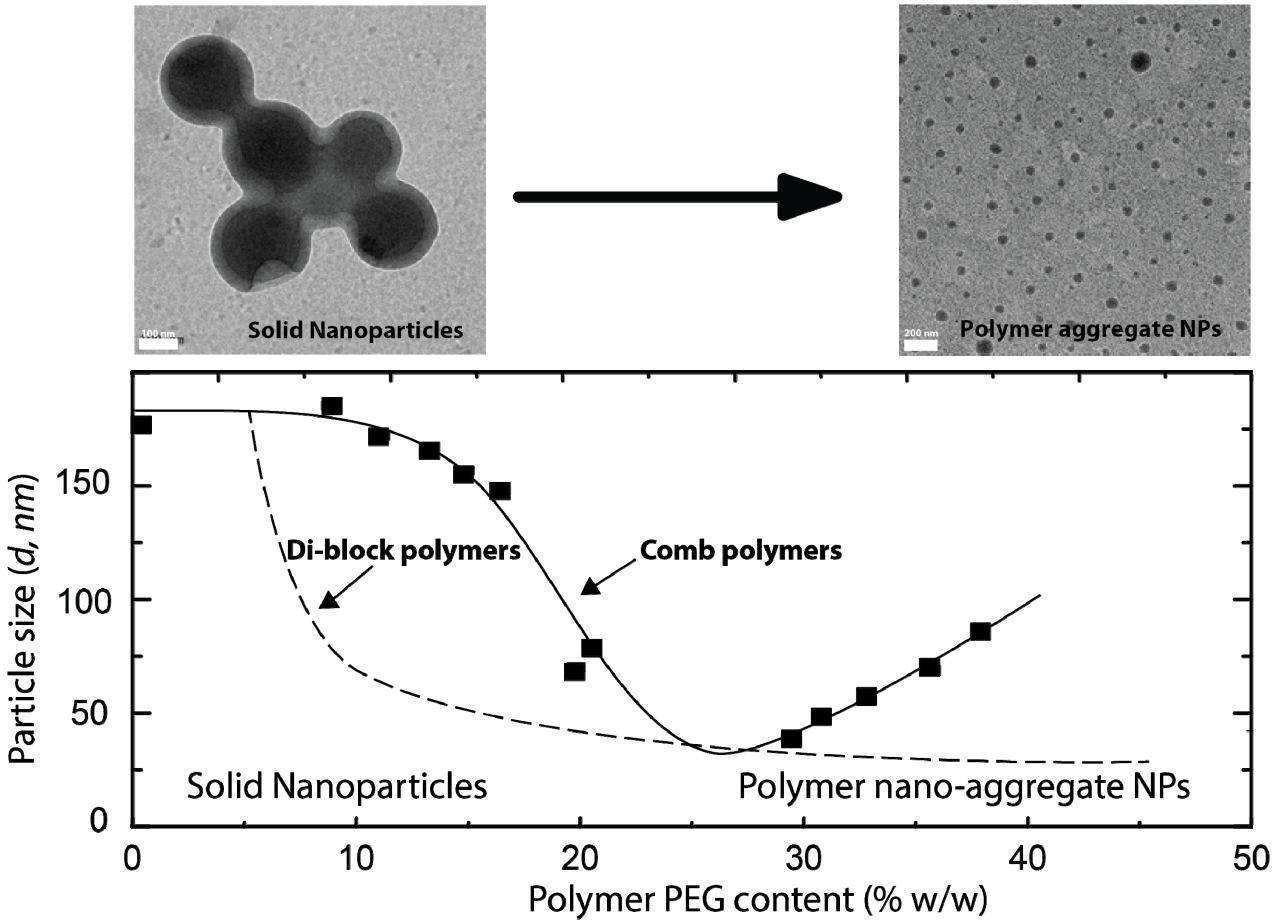

5 Article 2 « Effect of Formulation Parameters and Polymer Architecture on the Surface Properties of Nanoparticles Prepared from Clickable Comb-like Copolymers»

Manuscrit en préparation (avril 2015)

Ces travaux s'inscrivent dans la suite des améliorations à la synthèse des copolymères en peigne utilisant la stratégie de copolymérisation pour introduire des groupes latéraux fonctionnalisés dans la chaine de PLA (Chapitre 4).

Dans cette étude, nous avons eu recourt à la « chimie clic » par cyclo-addition catalysée par le cuivre de mPEB-N_3 sur des groupes latéraux de type alcyne. Cela nous permet de générer une nouvelle bibliothèque de copolymère en peigne PEGylées caractérisée par une structure sans blocs hydrophiles greffés en bout de la chaine. Un autre but poursuivi par cette étude est de comparer les propriétés de surface de particules préparées à partir de copolymères PEGylés à celle dont les surfaces ont été PEGylées ***après*** la formation de la particule, ce que permet la chimie clic. Cette approche peut avoir un intérêt en formulation.

L'effet de l'architecture du polymère sur la taille, la morphologie et les propriétés de surface des NPs fabriquées par différents procédés de fabrication est étudié également.

Ce manuscrit est en préparation et certaines données de caractérisation de surface par RMN sont incomplètes. Néanmoins les informations recueillies permettent de mettre en lumière des correspondances avec les données du Chapitre 4 et 6 sur le rôle de l'architecture des polymères dans la structuration des particules.

Effect of Formulation Parameters and Polymer Architecture on the Surface Properties of Nanoparticles Prepared from Clickable Comb-like Copolymers

Jean-Michel Rabanel[1,2], Patrice Hildgen[1], Xavier Banquy[2,§]

[1] Laboratoire de Nanotechnologie Pharmaceutique,

Faculté de Pharmacie, Université de Montréal,

C.P. 6128, Succursale Centre-ville, Montréal, Québec, H3C 3J7, Canada

[2] Canada Research Chair on Bioinspired Materials and Interfaces

Faculté de Pharmacie, Université de Montréal,

C.P. 6128, Succursale Centre-ville, Montréal, Québec, H3C 3J7, Canada

[§] Corresponding author

Graphical abstract:

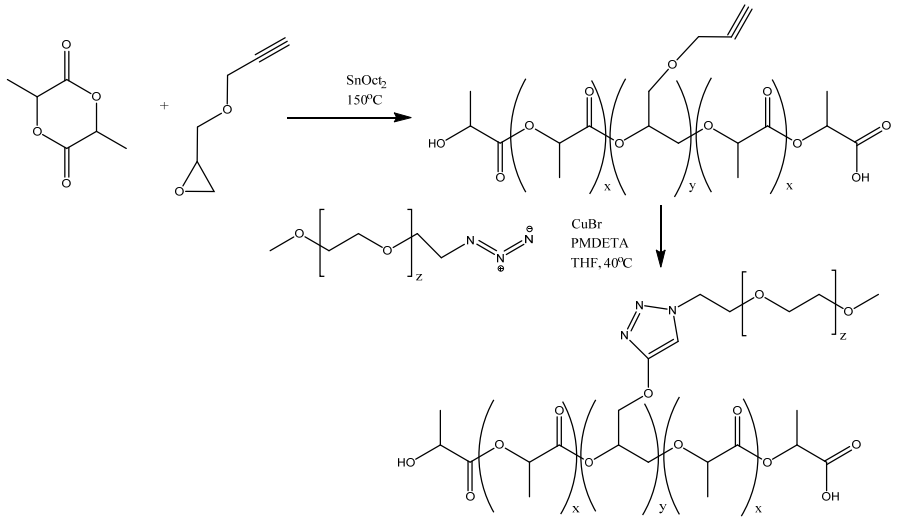

5.1 Abstract

A combination of ring-opening polymerization (ROP) and copper-catalyzed azide–alkyne cycloaddition (CuAAC) is described as an efficient route to synthesize a library of comb-like grafted copolymers containing poly(ethylene glycol) (PEG) as pendant groups (PEG-*g*-PLA). The library is composed of copolymers with different

PEG grafting densities and PEG with different molecular weights (750, 2000 and 5000 D). All intermediates and final products were characterized by ^{1}H-NMR, FTIR and GPC.

Polymeric nanoparticles (NP) assembly from comb-like polymers was performed by different methods: nanoprecipitation, "flash nanoprecipitation" and microfluidic technology. Some formulation variables such as polymer concentration and speed of mixing were studied in order to observe their effects on NP surface characteristics. Particle morphologies and sizes were assessed by TEM and DLS. Surface chemical analyses were performed by ^{1}H NMR and XPS. The NPs size and zeta potential were found to not be affected by PEG content (% w/w in polymer) and PEG chain length. TEM images show round shaped object and as expected, NPs sizes were found to decrease with polymer concentration in the organic phase and with a decrease in mixing time of the two phases for "flash nanoprecipitation" and microfluidic technology. PEG chain surface densities were assessed by quantitative ^{1}H NMR and XPS.

Taken together, these results support the interest of branched PEGylated polymer, as an alternative to linear diblock copolymers, to prepare stable polymeric drug nanocarriers.

Key words: Poly(lactic) acid, poly(ethylene glycol), click chemistry, nanoparticle, XPS

5.2 Introduction

Polymeric nanoparticles (NPs) are investigated for their potential in drug delivery and drug targeting for at least two decades now and some nanoformulations have reached the clinical stage studies [1]. A lot of different polymers have been proposed for this purpose and with very diverse chemical compositions [2, 3]. Those polymers should have a number of properties including, biocompatibility, a well-defined structure conferring adequate surface properties to the particles and be compatible with drug encapsulation and release.

One of the key surface properties for a drug carrier is the escape from recognition by serum proteins causing opsonisation of the NPs and premature elimination of the device [4, 5]. The most common surface modification used to achieve this is the addition

of a polymeric hydrophilic corona, usually a layer of polyethylene glycol (PEG) present at an adequate surface density and conformation [6].

The PEG layer could be the result of direct addition of PEG blocks after particle formation by either physioadsorption or covalent attachment. The latter approach may result however in low coupling yield and incomplete grafting due to steric constraints; while instability of the hydrophilic layer have been reported in case of physioadsorption. Additionally, in both cases, post-preparation modifications require the addition of one or several purification steps, steps that could be laborious and inefficient with nanoparticle batches.

Alternatively, the PEG layer could be the result of PEG chain segregation at the NP surface during the preparation stage. The use of copolymers tailored (in terms of architecture and chemical composition) to produce the desired surface properties as soon as the particle is formed, could be of great advantages in term of quality control of the drug carrier devices, but also in term of clinical translation.

Association of polyesters polymers such as poly(lactic) (PLA) or poly(lactic-co-glycolic) (PLGA) with PEG have been extensively studied for their advantages. For one, the polyester chain is fully degradable while the PEG usually used in drug carriers (<10 kD) is easily excreted by the kidney. PEGylated polyesters have also interesting drug encapsulation and release properties. Finally, as mentioned above, they have the ability to produce PEGylated surface NPs in a single step without the addition of surfactants. While diblock PEG-PLA and PEG-PLGA are prominent polymers in the development of drug nanocarriers up to the clinical stages [7, 8], other copolymer structures have been proposed in the past such as triblock or multiblock architecture [9, 10] and comb polymer architecture [11-13]. The resistance to protein binding is dependent on the PEG layer conformation and is obtained at high surface density, resulting in polymeric brushes [14]. The organization of such polymer brushes are dependent upon several variables such as area available for each PEG chains, their length, their packing and finally the hydrophobic block length, PEG points of attachments and chemical composition (in case of block copolymers). In other words, the PEG surface organization is largely dependent on the copolymer architecture.

Click chemistry and the combination of click chemistry with polymerization processes have been proposed to synthesize PEG copolymers. Several strategies have been put forth, the most reported being the polymerization of alkyne-functionalized lactones [15-17]. Combination of ring-opening polymerization and click chemistry has been proposed using various approaches [18, 19]. Finally, CuAAC has been also proposed to chemically modify the surface of pre-formed particles [20, 21].

We have previously developed a family of comb-type copolymers containing PEG branching along a linear polymeric backbone of PLA. This was obtained through copolymerization of dilactide and a co-monomer composed of functional pendant group attached to an oxirane ring. After copolymerization, chemical modification of pendant groups was allowing the grafting of PEG [11, 13]. The pendant groups functionalization produces a distribution of chemical modifications along the polymer backbones. The obtained architectures have structural features, distinctive from the usual diblock or block copolymer. They can strongly influence NPs sizes and morphology [13].

Herein, using a similar approach, alkyne pendant group were inserted in a growing PLA backbone and were used to covalently attach PEG chains of different length at different grafting density (PEG-to-lactic acid monomer ratio) by azide-alkyne click chemistry. These branched/comb PEG-*g*-PLA polymers were used to produce stealth NP in a one step process, advantageous in a translational point of view. PEG segregation toward the surface was shown as well as the dependence of surface PEG density on polymer structure. Branched/comb polymers PEG-*g*-PLA produced by click chemisty were shown to be alternative candidate to PEG-*b*-PLA polymer for preparation of polymeric drug carriers.

5.3 Experimental methods

5.3.1 Materials

All chemicals were from Sigma-Aldrich (Oakville, ON Canada) unless otherwise stated in the text. Solvents were from Fisher scientific (Whitby, ON Canada). THF was purified over an alumina column (Pure Solv System, Innovative Technology inc.,

Newburyport, MA, USA) before use. DMF anhydrous was from Acros (Fisher scientific, Whitby, ON Canada).

5.3.2 Polymer synthesis and characterization.

Synthesis of copolymer (Alkyne-g-PLA)

Copolymer synthesis of dilactide and glycidyl ethers were carried out as previously described[11] with modifications. Briefly, random copolymerizations of D,L dilactide (5 g, 3,47 10^{-2} moles) with glycidyl propargyl ether (GPE) present in variable molar ratios in the reaction vessel (GPE/lactic acid ratio of 0,5 to 2%) were carried out by ring-opening polymerization catalyzed by stannous 2-ethyl hexanoate (molar ratio with lactic acid monomer of 1/5000) at 150°C under argon atmosphere and mechanical stirring. Polymers were purified by dissolution of the melt in Dichloromethane (DCM) and repeated precipitations in hexanes (HEX) to yield a light yellow polymer **(1)** after solvent evaporation and drying under vacuum for 48 hours (Scheme 1). The synthesis and recovery yield was about 4.5 g (90%).

Copolymer (**1**)

^{1}H NMR (400 MHz, $CDCl_3$): δ (ppm) 1.3-1.5 (m, 3H, CH_3); 2.5 (s, 1H ≡CH), 4.15 (m, 2H CH_2), 5.1 (m, 1H CH). ^{13}C NMR (300 MHz, $CDCl_3$): δ (ppm) 16 (CH_3), 69 (CH), 169 (C=O). FTIR (cm^{-1}) 660.6; 706.6; 749.5; 842.6; 863.8; 962.5; 1060.5; 1081.9; 1184.3; 1276.3; 1341.9; 1359.8; 1381.2; 1453.0; 1747.7; 2890.1; 2946.1; 2997.6 GPC: M_n 42,680 $g.mol^{-1}$ M_w 58,820 $g.mol^{-1}$ PDI 1,38

Synthesis of Methoxy-PEG-mesylate

PEG-azides were synthesized as described previously with modifications [22]. Previously dried Methoxy-PEG (mPEG-OH, 750 D; 2kD or 5 kD) were used as starting material. For instance, mPEG-OH 2kD (20 g, 0.01 moles) were derived with 4 equivalents of methanesulfonyl chloride (3.1 ml, 0.04 moles) in presence of freshly distilled triethylamine (5.1 ml, 0.04 moles) in 100 ml anhydrous THF (purified on activated alumina column, Pure Solv System, Innovative Technology Inc., Newburyport, MA, USA). The solution was kept under argon atmosphere and under stirring for 24 h.

After partial THF evaporation, saturated 100 ml NaCl aqueous solution was added and extracted 5 times with 100 ml DCM. After partial organic phase evaporation, mPEG-mesylate was precipitated in cold diethyl ether twice, collected on a Buchner funnel and dry under vacuum. The typical yield was about 95 %.

mPEG-Mesylate

^{1}H NMR (400 Mhz, $CDCl_3$) : δ (ppm) 4.36 (m, 2H CH_2), 3.63 (m, 2H, CH_2), 3.4 (s, 3H, O-CH_3); 3.06 (s, 3H, CH3) ^{13}C NMR (300 MHz, $CDCl_3$) FTIR (cm^{-1}): 730; 841.32; 946.57; 1060; 1098; 1146.52; 1174.60; 1240.42; 1279; 1340.74; 1359.23; 1413; 1455; 1466; 1965; 2694; 2740; 2982 cm^{-1}

Synthesis of mPEG-N_3 ***(2)***

mPEG-mesylate 2kD (15 g, 7.5 mmoles) was redissolved in 100 ml anhydrous DMF and reacted with sodium azide (1.95 g, 0.03 moles) under stirring for 24 hours to yield mPEG-N_3. Purification was carried out by partial evaporation of DMF on a rotary evaporator, addition of saturated aqueous NaCl to aqueous DMF phase and repeated extractions with 100 ml DCM (5X). After partial solvent evaporation, mPEG-N_3 was precipitated in 10 volume of diethyl ether (2X). After filtration on a Buchner funnel, PEG-N_3 **(2)** was freeze-dried to yield a white fluffy material kept in presence of P_2O_5 under vacuum before use.

PEG-N_3, polymer (**2**)

^{1}H NMR (400 Mhz, $CDCl_3$) : δ: 3.6 (2H, CH2), 3.38 (m, 3H, CH_3); 3.38 (m, 2H, CH_2) ^{13}C NMR (300 Mhz, $CDCl_3$) : FTIR (cm^{-1}) 841; 946.2; 958; 1059.5; 1095.1; 1145.3; 1240.3; 1278.5; 1340.4; 1359.4; 1413; 1455; 1466.1; 1962.1; 2097.3; 2740.9; 2740.9; 2859.6; 2859.6; 2876.4

Synthesis of PEG-g-PLA

mPEG-N_3 (750 D, 2kD or 5 kD) was finally grafted by click chemistry to yield PEG-*g*-PLA (polymer **(3)** in scheme 1). For example, alkyne-*g*-PLA, with 0.5% alkyne pendent groups (2 g, 1.39 10^{-4} moles of alkyne) is dissolved in THF previously degassed by argon bubbling for 20 minutes. Weighed 2 kD mPEG-N_3 (0.278 g, 1.4 10^{-4} moles).

PMDETA and Cu(I) bromide (99,999% pure), were pre-incubated in 5 ml degassed THF to form a royal-blue solution. The solution was added at a 10% molar ratio relative to available alkyne groups. The reaction was carried out at 45°C and under stirring for 48 hours.

After partial THF evaporation, 50 ml DCM was added and the organic phase was washed repeatedly in a separation funnel with 100 ml distilled water to remove Cu and ungrafted PEG chains. After drying the organic phase with Na_2SO_4, the organic phase is removed on a rotary evaporation and the obtained copolymer is dried under vacuum.

In order to confirm the effective % of PEG grafting, NP were formed by nanoprecipitation (see section below for conditions) and then extensively dialysed in regenerated cellulose membrane tubes (50 kD cut-off, SpectraPor, Spectrum Laboratories, USA) for 3 days with at least 3 dialysis media change (MilliQ® water), before being freeze-dried, resuspended in deuterated solvent and evaluated by ^{1}H NMR.

PEG-*g*-PLA, Polymer (**3**)

^{1}H NMR (400 MHz, $CDCl_3$) : δ: 1.3-1.5 (m, 3H, CH_3); 5.1 (m, 1H, CH), 3.6 (m, 2H CH_2), 3.4 (s, 3H CH_3), ^{13}C NMR (300 MHz, $CDCl_3$) : FTIR (cm^{-1}): 699.3; 749.6; 842.1; 863.9; 962.3; 1081.9; 1183.6; 1270.8; 1342.1; 1359.7; 1381.1; 1452.9; 1747.8; 2884.4; 2945.2; 2994.8 cm^{-1}

Polymer characterization (NMR, GPC, FTIR, DSC)

The average molecular weights (M_w) and average molecular number (M_n) of the polymers were characterized by GPC in THF with PS standards, on a Waters liquid chromatography system equipped with a refractive index detector, GPC columns (Styragel 5µm) and analysed using Breeze II® software (Waters Corporation, Milford, MA, USA). Flow rate was set at 1 ml/min, column temperature at 40°C. Linear PS standards (M_w 600 to 200 000 g $mole^{-1}$) were used to construct the calibration curve.

The infrared spectra were recorded on a Nicolet iS10 FTIR (Thermo-Scientific, Canada) equipped with a SMART iTR attenuated total reflectance (ATR) sampling accessory with a ZnSe plate. Data were acquired and analysed using the OMNIC® interface.

^{1}H NMR, ^{13}C NMR and 2-D $^{1}H/^{1}H$ (400 MHz) analysis were performed, on a Bruker Advanced 300 Mhz or 400 Mhz (Bruker, Germany) and analyzed on Mestrec® software. Samples were dissolved in $CDCl_3$.

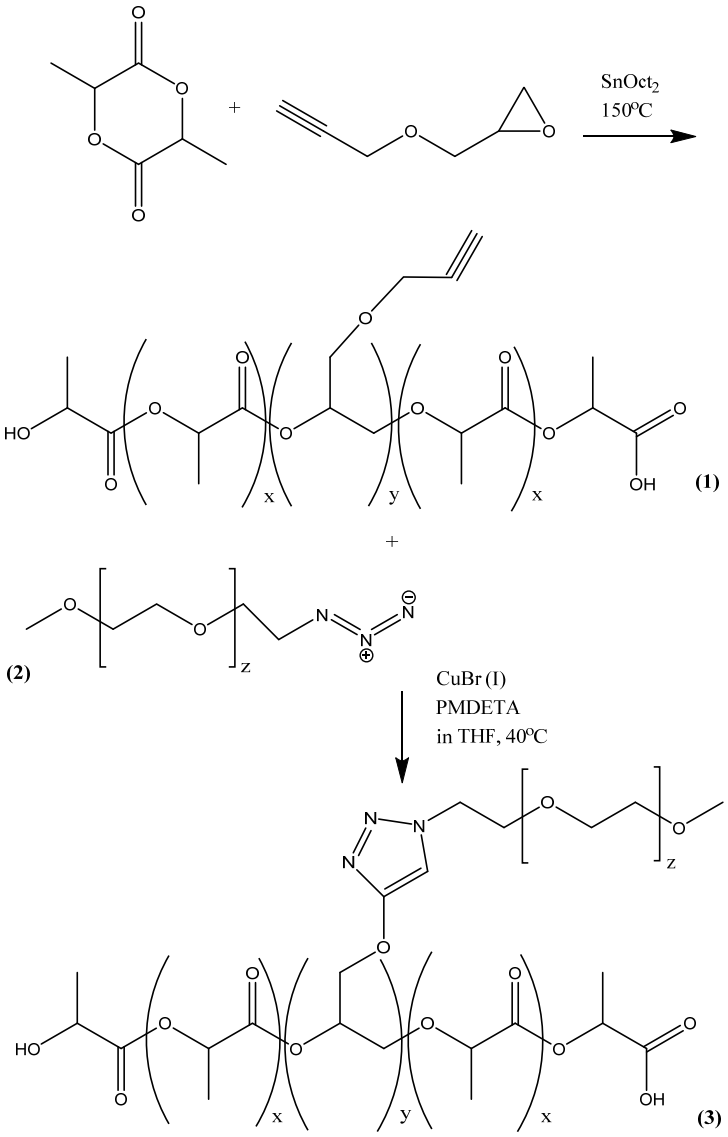

Scheme 5.1. PEG-*g*-PLA comb polymer synthesis. In copolymerization *y* was varied (0.5 to 2% relative to lactic acid monomer); *z* (PEG) = 17, 45 or 114.

Differential scanning calorimetry (DSC) assays were performed on a Jade DSC apparatus (Perkin-Elmer, Waltham, MA USA) connected to a cooling system. Polymer and NP samples (approximatively 5 mg) DSC analysis were performed in crimped

aluminum pan under nitrogen flow from 0°C to 100°C at 10°C min^{-1}, hold for 1 minute and cooled at a rate of 20°C min^{-1} to 0°C and reheated to 150°C at 10°C min^{-1}. Tg onsets (glass transition temperature) were determined from the second run.

5.3.3 Nanoparticle preparation and characterization

Nanoprecipitation.

NPs were prepared by nanoprecipitation: polymers (either Alkyne-*g*-PLA or PEG-*g*-PLA) were dissolved in acetone at 0.5 or 2% weight/volume concentration and injected in the aqueous phase under stirring (organic to aqueous phase ratio of 5). The speed of injection was set at 30 mL/h. The newly formed nanoparticle suspension was immediately quenched by dialysis in freshly distilled water (SpectraPor 50 kD, Spectrum Laboratories, USA), for 48 hours with media change every 12 hours. The suspension was either freeze-dried or kept at 4°C for future use.

Flash nanoprecipitation

"Flash nanoprecipitation" was performed using a mixing chamber precisely described by [23] and built in-house. The mixing chamber was connected to two syringe pumps, delivering respectively an aqueous phase and an organic phase. The pumps' injection speeds were set to adjust the ratio of the two phases and the overall flow rate. Polymer concentrations in the organic (acetone phase) were set at 0.5 or 2 % w/v The phase ratio was set at 3:1 and 5:1 respectively. The overall flow rate was set at 4, 8 or 12 ml/min.

Microfluidic method.

The microfluidic assays were conducted with a NanoAssemblr® device (Precision Nano, Vancouver, Canada), using the patented microfluidic chips based on chaotic mixing of the aqueous and the organic phase in converging micro-channels [24]. The ratios of the two phases, as well as the speed of injections, were adjusted using the provided software. The polymer concentration was set at 0.5 w/v, the ratio of the two phases at 3:1 and the overall flow rate was between 4 and 16 ml/min.

PEG grafting on NP made of GPE-PLA by click chemistry

Surface addition of PEG chain was carried out on suspension of NPs made of alkyne-*g*-PLA. The NPs was at a concentration of 2-3 mg/mL (NP prepared from polyesters-co-ether with different ratios of GPE) along with $CuSO_4$ 1 mM and sodium ascorbate 5 mM. Moreover, in selected assays, an hydrosoluble copper ligand was added to the medium at a concentration of 1mM The reaction was carried at room temperature for 24 h under stirring. PEG derived NPs were purified by extensive dialysis (SpectraPor 50 kD, Spectrum Laboratories, USA). PEG grafting was evaluated by ^{1}H-NMR. The nanosuspension was freeze-dried and the dried material was dissolved in CDCl3 for ^{1}H NMR quantification.

NPs size measurements. The NP sizes (hydrodynamic diameter) were determined by photo correlation spectroscopy (PCS) on a Malvern Zetasizer (Malvern, Worchester, UK) in triplicate and averaged.

Zeta potential measurements. NPs (0.3 mg) were suspended in 1 mL of PBS 0.1X pH 7.4 (about 15 mM NaCl) to measure ζ potential on a Malvern Zetasizer (Malvern, Worchester, UK) in triplicate.

5.3.4 Transmission Electronic microscopy.

TEM procedures were as described in [13]. Briefly, NPs suspension in MilliQ water at a concentration of 1 to 2 mg/mL was deposited on a carbon film 400 square mesh copper grids (Electron Microscopy Sciences, Hatfield, PA USA). No staining procedure was used. TEM image acquisition were conducted in bright filed mode in a JEM-2100F, Field Emission electron microscope (Jeol Ltd, Tokyo, Japan) equipped with a sample holder cooled by liquid nitrogen (Gatan inc. Warrendale, Pittsburg, PA, USA). The grids were maintained at -170°C throughout the acquisition with a temperature controller (Smart Set Model 900 Cold Stage controller; Gatan inc. Warrendale, Pittsburg, PA, USA). The acceleration voltage was set at 200 kV. Images were recorded with a digital camera at low electron dose to prevent damages to the heat-sensitive particles (current densities between 5 and 15pA/cm^2).

5.3.5 X-rays Photoelectron Spectroscopy.

Sample preparation.

NPs were lyophilized without cryoprotectant and the obtained fine fluffy powder was pressed on a double side tape and mounted onto a sample rod.

XPS survey analysis.

XPS survey analysis was performed on a Kratos Axis Ultra (Kratos Analytical, Manchester, UK) with a Mg Kα X-ray source used at 120 W (12kV, 10 mA), with an electron take off angle of 0°, steps of 1.0 eV for an energy pass of 1000 eV.

High Resolution spectra.

High resolution spectra were acquired on a Kratos Axis Ultra (Kratos Analytical, Manchester, UK) with a Mg Kα X-ray source used at 120 W (12kV, 10 mA), with steps of 0.05 eV for a pass energy of 20 eV. Flood gun was used to offset the surfaces charges. Relative atomic percentages were calculated using the Advanced® software (VG Scientific, ThermoFisher) from low resolution spectra. High resolution spectra were analysed by curve deconvolution of C_{1s} and O_{1s} signals on software Advanced® (VG scientific, ThermoFisher). Background was removed by the Shirley method, the Wagner sensitivity factor table was used. All spectra were corrected on C-C aliphatic carbon binding energy peak set at 285.0 eV to compensate for surface charging effect. Peak fitting was performed as previously described [25] and based on data obtained on pure PLA and PEG[26]. The conversion of relative atomic percentages to mass percentages and to PEG surface density estimates is described in detail in the Supporting information of previously published work [13].

5.3.6 NMR quantification.

Samples preparation (concentration of NP preparation). NP preparation were concentrated for NMR experiments using tangential flow filtration (Polysulfone filtration column, pore 0,05 μm,, Spectra Laboratories, USA) at a flow rate of 3 ml/min for two

hours. This approach typically yields to 5 to 7-fold concentration. The concentrates were examined for aggregation and size changes by DLS before and after the concentration.

NP total PEG quantification. One ml of nanosuspension was freeze-dried in a weighed Eppendorf tube to determine the mass concentration of particles for PEG surface density calculations. The same sample was dissolved in $CDCl_3$ and analyzed by ^1H NMR (AV400 Advanced, Bruker, Germany) relative to the internal reference, standard TMS and a PEG calibration curve in $CDCl_3$ to determine total PEG content of the sample.

NP surface PEG quantification. After determination of mass concentration of the concentrated nanosuspension, either 200 or 500µl of suspension were added respectively to 800 and 500µl of deuterium oxide (Deuterium oxide with 0.75% 3-(trimethlysilyl) propionic-2,2,3,3-d4 sodium salt as an internal standard) and analyzed. NP suspensions in D_2O or H_2O/D_2O were analyzed by ^1H NMR (AV400 Advanced, Bruker, Germany). Quantifications were conducted in reference to mPEG-OH 750, 2kD or 5 kD calibration curve and internal standard peak intensity.

PEG surface densities quantification by NMR calculation. PEG chain surface density calculations were previously reported [13].

5.4 Results and discussion

5.4.1 Polymer synthesis and characterization

Copolymer synthesis was carried out according to Scheme 1 based of random copolymerization of dilactide with glycidyl propargyl ether (GPE). Propargyl insertion was monitored by ^1H NMR using the signals at δ. 2.5 ppm for alkyne proton and 4.15 for CH_2 belonging to the pendent group. Insertion of GPE was tested over a range of 0.5 to 2 % (molar ratio GPE/LA monomer). This approach maintained the integrity of the polymer backbones and demonstrated control over molecular mass of the polymeric chain, as seen in the GPC results (Table 1). The use of azide-alkyne chemistry reduces the number of reaction step and provided greater control over reaction rate and final molecular weight.

Table 5.1. Table of PLA backbone polymer characterizations (alkyne-g-PLA).

Polymer batches	GPE* Feed ratio	Alkyne insertion	*GPC* M_n	M_w	PDI
	% (/LA)	*% (/LA)*	*g/mole*	*g/mole*	
1	1	0.5	28240	39350	1.39
2	1	0.6	31970	45200	1.42
3	1	0.7	31800	46000	1.45
4	1	0.8	22680	33110	1.5
5	2	1.1	22110	34090	1.54
6	2	1.7	42680	58820	1.38

* *glycidyl propargyl ether.*

The ^{1}H-NMR, FTIR analyses of mPEG-Mesylate and mPEG azide are shown in Fig S1, S2. PEG-*g*-PLA structures were confirmed as well by ^{1}H and ^{13}C NMR (Figure S3). Different polymer batches were synthesized with varying M_n and PEG content (polymer structure in **Scheme 5.1**) and characterized as shown in Table 5.2.

Table 5.2. Characteristic of PEGylated polymers (PEG-*g*-PLA)

Alkyne-g-PLA				PEG-g-PLA			Nanoparticle			
M_n	M_w	PDI	% alkyne	PEG *Mw*	PEG grafting	PEG content	PEG grafting	PEG content	PEG number	M_w Polymer
(GPC)	(GPC)		(NMR)		(NMR)		(NMR)			(calculated)
g/mole	*g/mole*		*% /LA*	*g/mole*	*% /LA*	*% mass*	*% /LA*	*% mass*	*PEG/ chain*	*g/mole*
31800	46000	1.45	0.7	750	0.6	6	0.34	3.4	1.50	47126
31800	46000	1.45	0.7	2000	0.41	10	0.35	8.9	1.55	49092
31800	46000	1.45	0.7	5000	0.7	33	0.7	32.7	3.09	61458
22110	34090	1.54	1.1	750	0.04	0.04	0.02	0.2	0.06	34136
22110	34090	1.54	1.1	2000	0.15	4	0.14	3.7	0.43	34950
22110	34090	1.54	1.1	5000	0.49	26	0.17	10.6	0.52	36700
42680	58820	1.38	1.7	750	0.39	3.4	0.34	3.4	2.02	60332
42680	58820	1.38	1.7	2000	1.9	33	1,8	33,3	10,67	80160
42680	58820	1,38	1,7	5000	1.46	51	1.45	50.2	8.60	101796

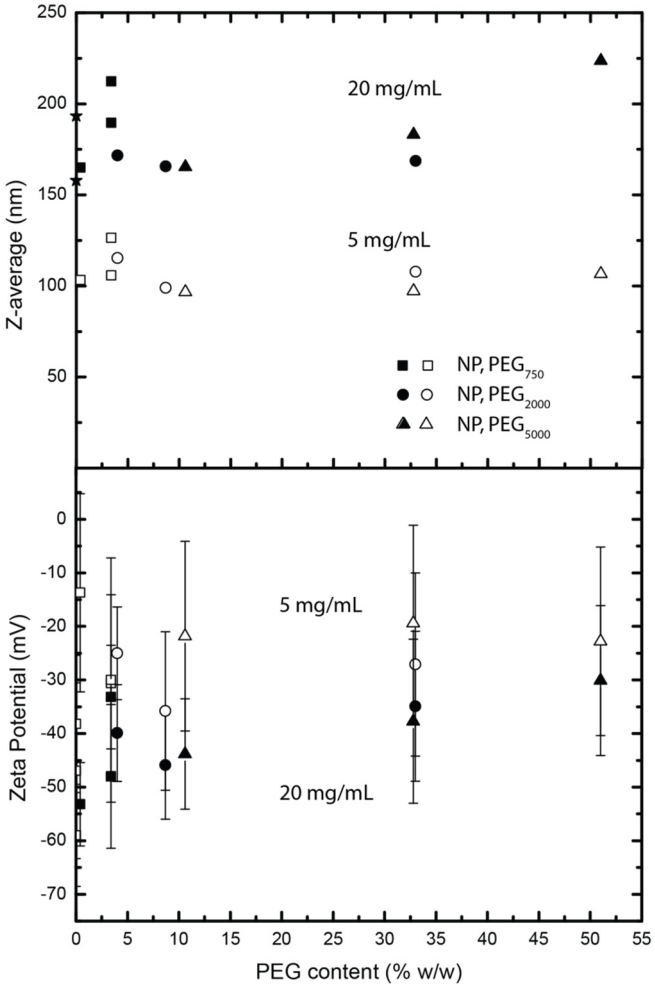

Figure 5.1. Nanoprecipitation (a) Particle Size dependence over PEG length and content (PEG % w/w in the polymer) using classical nanoprecipitation at polymer concentration (5 and 20mg/ml) (b) Zeta potential dependence over PEG content. Square represents NP made from PEG_{750}-*g*-PLA; Circle represents NP made form PEG_{2000}-*g*-PLA and Triangle represents NP made of PEG_{5000}-*g*-PLA. Star represents NP made from alkyne-*g*-PLA. Open symbol: nanoprecipitation made from a polymer solution at 5 mg/mL, Closed symbol: 20 mg/mL

5.4.2 Nanoparticle preparation and characterization

Nanoprecipitation

Preparation of NP by "classical" nanoprecipitation is straightforward and conditions used in a previous work were used as a reference [13]. As expected a lower polymer concentration yielded smaller particles (Figure 5.1 (a)). On the other hand, the NP size profiles are different from the profiles obtained with PEGylated polymers described previously [13]. The size transition, with drastic size decrease, in the vicinity of 15% PEG content observed for the other comb-like copolymer library is not present. It is not either observed an exponential size decay as observed for diblock copolymer by Riley *et al.* [27]. This could be due to two factors: firstly, the size of the hydrophobic (PLA) block which is larger in this study; and secondly the structure of PEG grafting. Herein there are only lateral PEG chains attached to the PLA backbone while with the method used previously, PEG grafting could also take place on the PLA chains end-groups.

The zeta potentials recorded in PBS (0.1X pH 7.4) show only a very minor decrease with increasing PEG length and content. The smaller particles tend to have less charge (Figure 5.1 (b)). Nonetheless, zeta potentials stay largely negative even for high PEG content NP. This could be attributed to the number of carboxyl end-groups still present on each PLA backbone chains.

"Flash" Nanoprecipitation

The device used here is based on dimensions given in [23]. We tested different flow rates and polymer concentrations in the organic phase. The dependence of NPs size over flow rate is shown in Figure 5.2 (A), The size PDI is less sensitive to flow rate and decreases significantly only at very low flow rate (1mL/min) (data not shown). As expected an increase in polymer concentration lead to a corresponding increase in particle diameter for all the copolymers (Figure 5.2 (B)). Sizes are not very sensitive over PEG total content (Figure 5.2(C) with only a modest decrease in diameter from PEG 750 to PEG 5000. This is similar to what was observed in nanoprecipitation (Figure 5.1). In figure 52 (D), we observed that the particle sizes are not trending with PEG molecular weight. Other factors seem in charge to define the particle size as we observed large difference in size for the same PEG chain length.

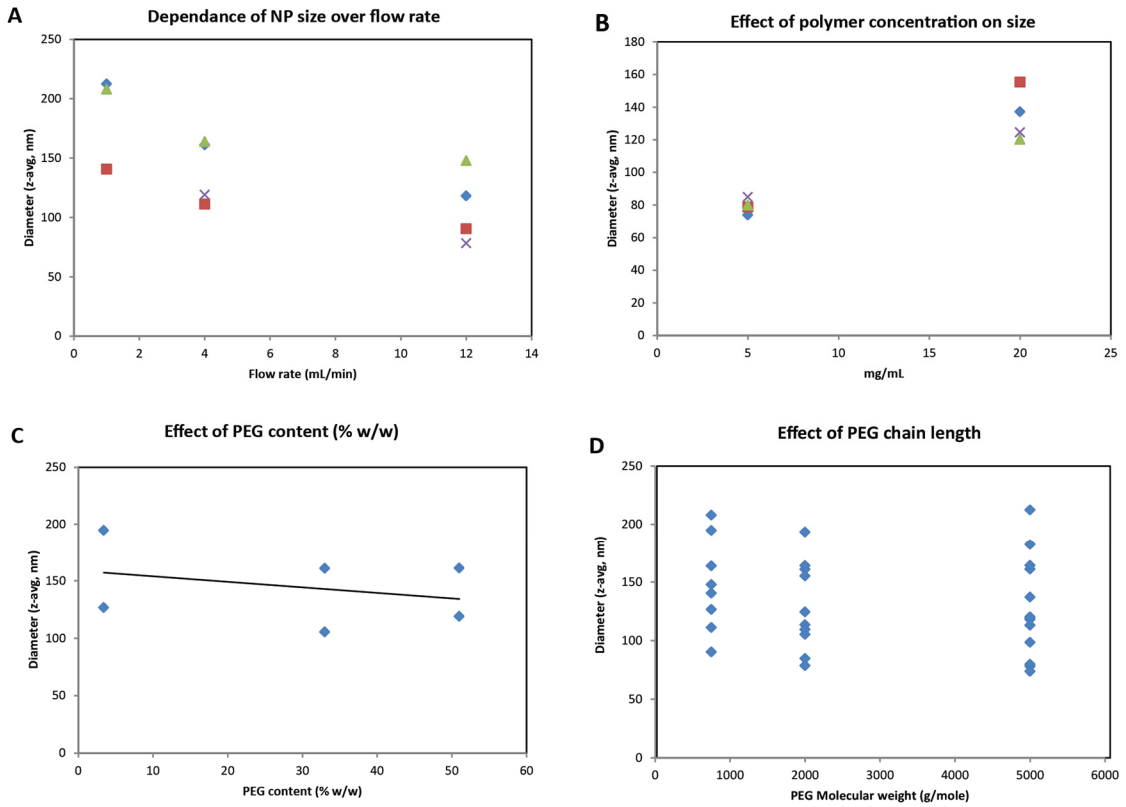

Figure 5.2. Nanoprecipitation "flash" (a) Particle Size dependence over flow rate (A); polymer concentration (B); PEG content % w/w in the polymer (C) and PEG chain length (D) using nanoprecipitation flash at polymer concentration (5 and 20mg/ml)

Microfluidic.

The geometry of the microfluidic devices is based on [24] and an integrated device including variable speed injections system has been developed in Peter Cullis' laboratory, to produced solid lipid nanoparticles and liposomes [28]. Different flow rates and polymer concentrations were chosen to compare the NPs physico-chemical properties made by the three preparation methods.

Of note, high concentration polymers (above 5 mg/ml) or non-PEGylated polymers tend to show precipitation in the mixing part of microchannels. In these cases, particles tend to grow until it forms bulk precipitated material. It can be explained because the NPs are not quenched fast enough and also because NPs are not stabilized by hydrophilic corona. Soft unquenched nanoparticles tend to collide and fuse, plugging the microchannel mixing chamber.

We tested a range of injection speeds and concentration with the PEGylated polymers. The size and zeta potential results are reported in Figure 5.3. We observe a decline of size with the increase of PEG content and PEG chain lengths. However, the decline is much slower compared to what was observed with comparable copolymer architecture produced by coupling reaction [13].

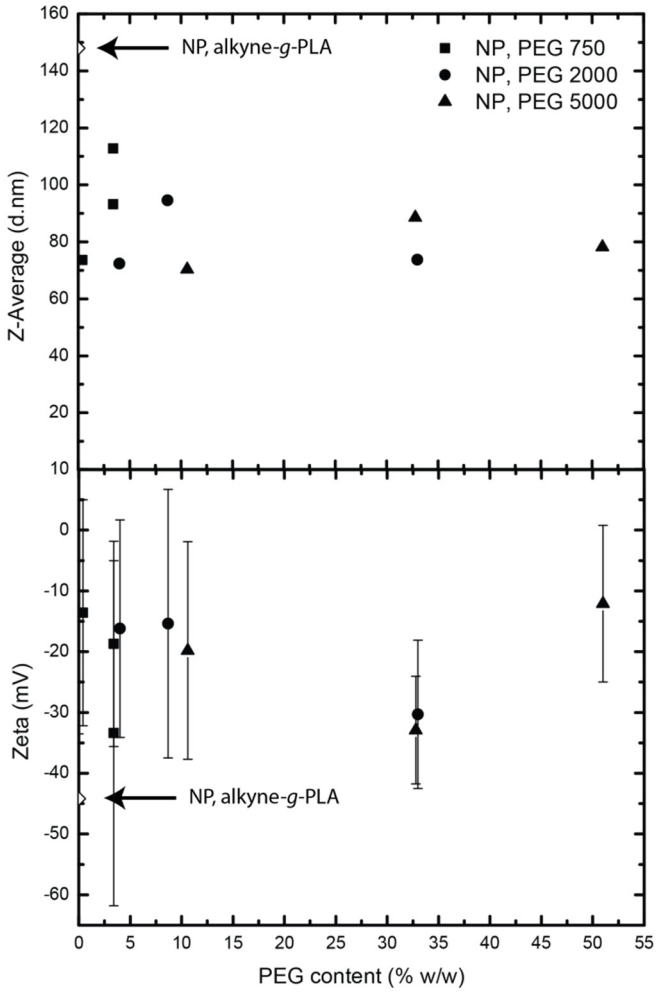

Figure 5.3. Nanoparticle prepared by microfluidic. Size (z-average) and zeta potential of NPs produced by microfluidic method (5 mg/mL polymer in organic phase, ratio 3:1 (aqueous/organic phases) at a flow rate of 4 mL/min.

The "grafting-to" approach.

Instead of using PEGylated copolymers to directly prepare drug-loaded particles, in some case it could be advantageous to produced NP from non-PEgylated polymer. This could happen for reasons related to encapsulation efficiency optimization. In this case PEG chains could be grafted after NP formation. We evaluated the possibility of installing a PEG surface layer on pre-formed alkyne-g-PLA NPs by click chemistry in an aqueous environment.

The aim here was to compare PEG densities that can be obtained by direct preparation of NP with pre-synthesized copolymers with PEG surface densities that can be reach by a "Grafting to" approach. NPs, made of alkyne-g-PLA (with 0.8 and 1.1% insertion ratio), were produced by nanoprecipitation. They were characterized for size and zeta potential (Table 5.3). Copper catalyzed cyclo-addition of mPEG-N_3 was performed on NP aqueous suspensions. The results (Table 5.3) are showing very little or no PEG grafting after click reaction and extensive dialysis. The PEG detected in the purified nanosuspensions appears as essentially a residual amount.

This can be explained by the lack of availability of alkyne pendant groups at the surface. They may be buried under the surface or because of their close proximity with the PLA backbones they can be locked in a position that does not allow the reaction to proceed. Moreover, it well known that reactions on a 2D surface are more difficult to achieve that reactions in solution. Changes in size and zeta do not appeared to be caused by the addition of a PEG layer on the NP surface.

The changes in NP apparent size as measured by DLS could be the result of the change of medium. The changes in zeta potential could be explained by cation salts adsorbed on to the PLA surface after the reaction. An alternative approach could be to have a more hydrophilic pendant groups, giving the alkyne more access to the surface and more flexibility.

Table 5.3. Apparent mPEG-N_3 grafting on NP surface ("grafting-to" approach)

% Alkyne	mPEG-N_3	$CuSO_4$	NaAsc	Ligand	% PEG*	Yield	Diameter**	PDI**	Zeta Potential	SD
(% /LA)		*mM*	*mM*	*mM*	*(%/AL)*	*%*	*Z-avg, nm*		*mV*	
1.1							157.9	0.161	-30.5	8.96
1.1	2000	1	5		0.073	6.6		*Nanoparticle aggregation*		
1.1	2000	1	5	1	0.073	6.6	196.3	0.117	-18.6	7.34
1.1	2000		5	1	0.067	6.1	159.7	0.09	-24.9	7.73
0.8							164.9	0.046	-23.6	8.61
0.8	2000	1	5		0.072	9.0		*Nanoparticle aggregation*		
0.8	2000	1	5	1	0.063	7.9	191.4	0.055	-17.3	7.52
0.8	2000		5	1	0.056	7.0	181	0.056	-19.9	7.84

** Determined by ^{1}H-NMR; ** determined by DLS*

5.4.3 Morphologies of NP

The morphology of NP produced by nanoprecipitation was examined by TEM as a function of PEG content and PEG length in the comb-like copolymers.

The obtained particles are solid and spherical and for diameters above 100 nm they show the apparent core-shell feature attributed to particle contact with the carbon film [13]. The particle sizes decrease as PEG length and total PEG content (% w/w) increase, confirming the DLS results. In comparison with previously comb-like polymers synthesized in our laboratory, we observed striking differences in NP morphology. The particles prepared with copolymers synthesized by acylation of coupling reactions showed a soft and "micelle-like" appearance when the PEG content was above 15% [13]. One possible source of difference is the polymer architecture. In this work we have strictly comb-like polymers, with only lateral PEG chains grafted onto the PLA backbone. In our previous work, we obtained diblock polymers having supplementary lateral PEG chains.

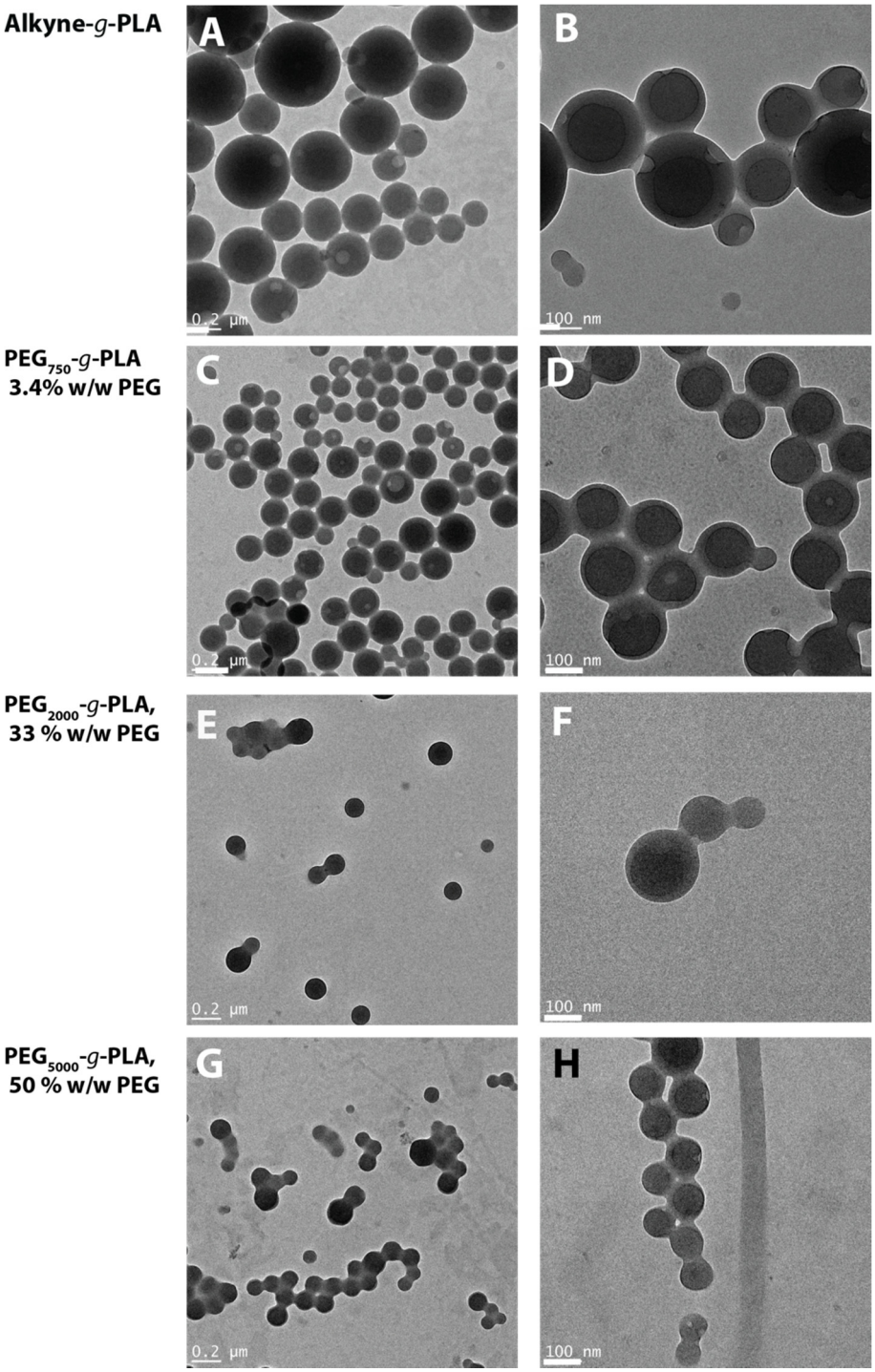

Figure 5.4. TEM imaging of NP prepared by nanoprecipitation (polymer concentration 20mg/mL) with different polymers having different PEG chain lengths grafted by click chemistry onto the same alkyne-g-PLA backbone. (A and B) Alkyne-g-PLA NPs (C and D), PEG_{750}-*g*-PLA NPs (E and F) PEG_{2000}-*g*-PLA NPs, (G and H) PEG_{5000}-*g*-PLA NPs

The effect of the preparation method on the NPs morphology was studied also by TEM (Fig 5.5). In this experiment, the same polymer (PEG_{2000}-*g*-PLA, 32% PEG) was used at a concentration of 5 mg/ml in the acetone phase, with a 3:1 ratio between the organic phase and aqueous phase for the three different methods. The sizes are smaller than the particles showed in Figure 5.4 due to the lower polymer concentration used. Nanoprecipitation and flash nanoprecipitation yielded comparable particle sizes, while the particles obtained by microfluidic are smaller. There are no differences in morphologies of the NPs between the three different methods. The NP produced by microfluidics however have a tendency to aggregate and appeared as fused particles, in the conditions of the preparation of the grids.

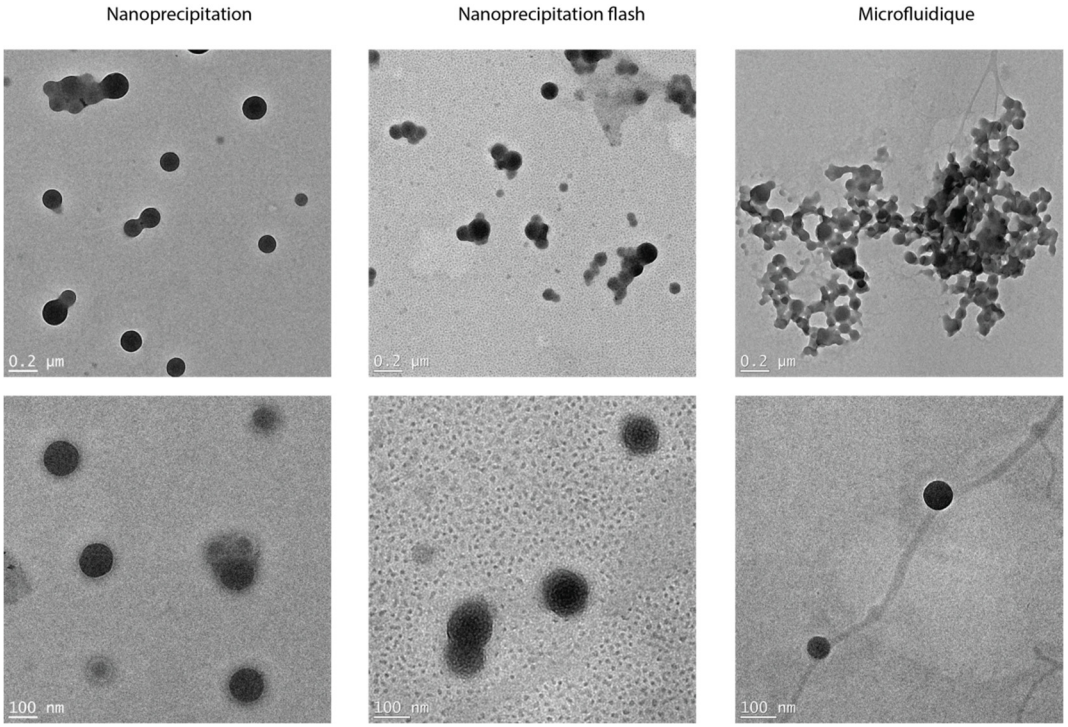

Figure 5.5. Comparison of NPs morphology (TEM imaging at two different magnifications). NPs were prepared by different methods using the same PEG_{2000}-*g*-PLA polymer: (A) Nanoprecipitation (left panel); (B) Nanoprecipitation flash (central panel), (C) Microfluidic (NanoAssemblr®, Precision Nanosystem) (right panel).

All particles produced by nanoprecipitation appear as solid NPs in TEM in contrast to previous results. At PEG contents around 30 to 50% (w/w), NPs made from PEGylated comb-like copolymers described previously were found to have "micelle-like" or "polymer nano-aggregate" aspects by cryo-TEM [13], Moreover their size as determined by DLS and TEM were much lower (25-50 nm in diameter). Two hypothesis are put forth to explain this difference: 1) the size of the PLA hydrophobic block which is slightly larger in this study (30-35 kD vs 20-25 kD on average in previous works [13]). A larger hydrophobic chain results in an increase of the NP core diameter and therefore a stabilization of the structure; 2) the structure of the comb-like copolymers in this study has some differences with polymer prepared in the previous work [13]. The synthesis strategy used herein removed the possibility to have PEG chain grafted on PLA terminal end-group resulting in a mixed architecture (diblock/comb copolymer). Here the only possibility of PEG grafting is on lateral pendant alkyne groups. 3) The last hypothesis for a different chain arrangement could be attributed to the stiffness of the triazole ring linking PEG to the PLA backbones. The constraints on the chain near the junction with the PLA backbones may limit the movement of the PEG chain, therefore contributing to an increase in chains number in each NPs.

5.4.4 PEG surface density: RMN quantification

The calculation for the total PEG present in the NPs is obtained from ^{1}H NMR using the relative quantification of PEG to the PLA block. The quantification of surface PEG was determined on NPs suspended in D_2O with an internal standard (Figure 5.6).

Nanoprecipitation.

Nanoprecipitations were performed at two polymer concentrations: 5 and 20 mg/mL, using same phase ratio, injection and mixing speeds. After concentration by tangential flow filtration, NP sizes were assessed by DLS and were found unchanged (Table S.1). Surface PEG quantification was done by diluting the NP suspension in D_2O. Moreover, to avoid H_2O interference in the quantification of the PEG peak, the residual water signal was presaturated before acquisition. The results are shown in Table 5.4,

Table 5.4. PEG surface density and percentage of PEG at the surface as determined by quantitative ^{1}H NMR for NPs prepared by nanoprecipitation (20 mg/mL polymer in acetone).

Id	PEG *Mw*	Polymer PEG content	NP Diameter	PEG surface density	Surface PEG
	g.mol^{-1}	*%*	*number, nm*	*PEG/nm^2*	*%*
1	**750**	3.4	157.0	0.56	62.5
2	**2000**	33	119.8	1.64	66.0
3	**5000**	51	114.6	0.65	44.4
4	**750**	3.4	135.8	0.19	25.2
5	**2000**	8.7	112.6	0.23	36.9
6	**5000**	32.8	112.9	0.27	29.2
7	**750**	0.4	112.1	0.00	0.0
8	**2000**	4	134.4	0.08	25.1
9	**5000**	10.6	123.0	0.13	39.2

PEG attached to a surface, adopts, according to the generally accepted model [29] a random coil configuration at low density (mushroom configuration). If the chain movements are restricted by the neighbor chains they switch to a brush model. The chain backbones are stretched and the extent of stretching is proportional to the PEG surface density.

PEG surface densities appear to reflect copolymer PEG content and PEG chains length (Table 5.4). The comparison of results for NPs made with a copolymer of about 33% PEG content, with either PEG 2kD or PEG 5kD (line 2 and 6, Table 5.4) show a decrease of PEG surface density that could attributed to the PEG chain footprint effect. This limits the access of more PEG 5kD chains to the surface compared to the PEG 2kD chains. This is reflected by the percentages of PEG on the surface. The decrease of PEG surface density cannot solely be attributed to the fact that for a same weight of PEG, there are 2.5-fold more PEG 2kD chains than PEG 5kD chains.

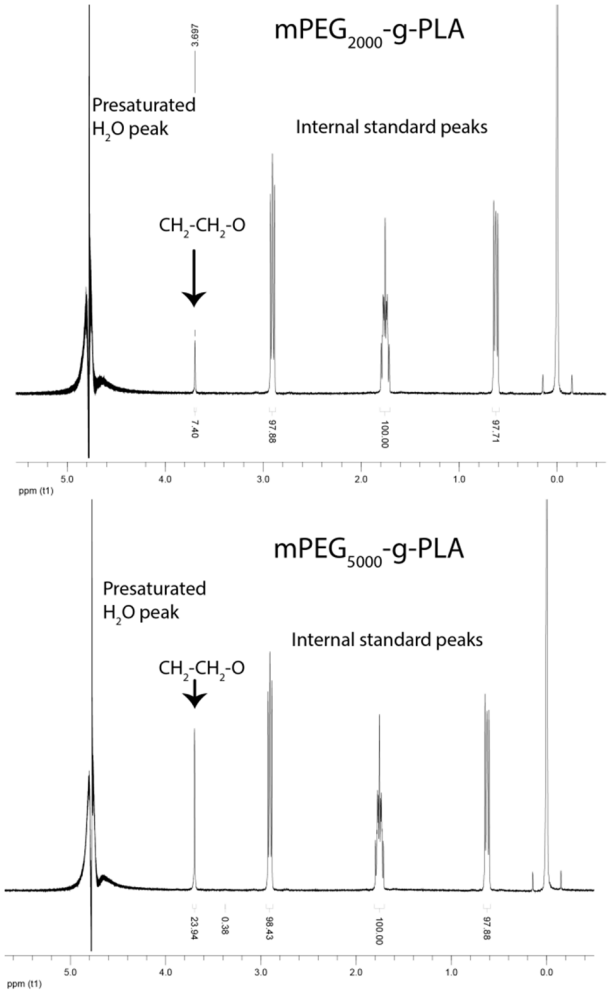

Figure 5.6. Example of surface PEG quantification of mPEG-*g*-PLA NPs by ^{1}H-NMR, (A) NP in D_2O prepared with a PEG 2kD copolymer; (B) NP in D_2O prepared with a PEG 5kD copolymer. Presaturated water signal is clearly seen at the left of the spectra.

Flash nanoprecipitation and microfluidic.

Preliminary data of PEG surface density are also available for other preparation methods. The table 5.5 shows some of the quantification results available. The nanoprecipitation results showed in this table are distinct from the results presented previously in sections above and represent duplication of fabrication batches.

Table 5.5 Comparison of preparation methods: NMR quantification results

Method*	PEG Mw	Polymer PEG content	Diameter	PEG surface density	Surface PEG
	g.mol-1	*%*	*number, nm*	*PEG/nm2*	*%*
1-NP	**750**	3.4	171.5	0.45	46.0
2-NP	**2000**	33	136.9	0.88	31.2
3-NP	**5000**	51	120.3	0.79	51.0
4-NP	**2000**	0.4	121.2	0.08	NA
5-MF	**2000**	33	128.1	0.61	22.9
6-MF	**2000**	33	128.1	0.79	29.9
7-NF	**2000**	33	105.1	0.81	37.3
8-NF	**750**	0	100.5	0.00	0.0
9-NF	**2000**	0.4	105.2	0.06	NA
10-NF	**5000**	4	94.2	0.11	117.0

** NP=Nanoprecipitation; MF=Microfluidic; NF=Nanoprecipitation Flash*

The comparison of preparation method using the same polymer (PEG 2kD, PEG content of 33%, line 2, 6 and 7) shows similar results for PEG surface density regardless of the preparation method. The small differences could be ascribed to the differences in total surface area which is a consequence of different NP diameters obtained for particles prepared using the different methods.

5.4.5 PEG surface density: XPS analysis of surface.

XPS analysis of NP surfaces were conducted only on NPs prepared by "classical" nanoprecipitation at polymer concentration of 20 mg/mL in acetone.

Survey analyses

In the survey analyses we were interested primarily in the detection of nitrogen as indicative of the presence of triazole ring and PEG grafting. The N1s peak was indeed detected for some PEGylated NP batches (Table 5.6) but the signal was very low. This is not surprising as the nitrogen content of the PEG-*g*-PLA in weigh is close to the detection limit of XPS. An enrichment of the nitrogen content could be expected at the NP surface compared to the bulk polymer content, as a result of PEG chain segregation at the surface of the particles. However, the nitrogen would be located at the junction between the core

of the particle and the PEG layer; its signal could be partially attenuated by the surface PEG brush. An unexpected contamination by Si atom has been attributed to silicone grease contamination. The origin of the contamination is still unknown.

High resolution spectra.

Nitrogen was detected in some samples, however, it was not possible to perform high resolution analyses to confirm the type chemical bonding as the amount of nitrogen is very low and samples were sensitive to multiple scans. The presence of the azide group was confirmed on mPEG-N_3 (see Figure S5). The disappearance of the peak at 404 eV (due to N^+ of the azide group) can be used to follow the click reaction and generation of the triazole ring resulting from the Cu-catalysed cyclo-addition of PEG. However, the signals recorded for the NP samples were too noisy to be conclusive to explain the disappearance of this peak and to obtain direct evidence of the presence of the triaozole ring.

In most cases, PEG surface enrichment was confirmed by XPS (Table 5.7). We converted the semi-quantitative results into quantitative results as described in [13] and obtained PEG surface densities values. The results are plotted in Figure 5.7 showing the dependence of the PEG surface density and the percentage of PEG surface content on the total PEG content in the copolymer. The density values in Figure 5.7 were similar with the NMR data listed in Table 5.5. For instance if we compare PEG_{2000}-*g*-PLA with the same PEG content of 33%, we have obtained similar surface density, ie. 0.7-0.8 PEG/nm^2.

This is also reflected by the percentage of total PEG found on the surface which decrease as a function of increased PEG content in the copolymer. It is particularly striking for PEG 5kD and may reflect a limited space for supplementary PEG chains at the surface due to the steric constraints imposed by the dense PEG brush.

Table 5-6. Survey analysis of alkyne-*g*-PLA and PEG-*g*-PLA NPs samples

		BE	Relative Atomic percentage											
		eV	%											
PEG length	*g.mol^{-1}*		0	750	2000	5000	0	750	2000	5000	0	750	2000	5000
PEG	*% (w/w)*		0	3.4	33	51	0	3.4	8.7	32.8	0	0.4	4	10.6
O1s		532.9	48.29	50.09	46.17	46.68	56.17	54.73	50.35	46.87	45.10	55.46	55.13	53.65
N1s		402.3	0	0	0.54	0	0	0	0	0.52	0	0	0.24	0.32
C1s		286.1	42.59	43.72	49.21	51.36	41.77	40.98	45.95	51.09	31.49	43.64	44.63	42.26
Si2p		102.1	8.81	6.19	4.08	1.97	2.06	4.29	3.70	1.53	5.03	0.90	0	3.77

Data from one sample, atomic percentages are reported as the average of XPS spectra taken at 3 different positions

Table 5.7 C1s relative atomic percentage (% of total carbon)

		BE	Relative Atomic percentage											
		eV	%											
PEG length	*g.mol^{-1}*		0	750	2000	5000	0	750	2000	5000	0	750	2000	5000
PEG content	*% (w/w)*		0	3.4	33	51	0	3.4	8.7	32.8	0	0.4	4	10.6
C-C (PLA)		285.0	42.15	34.65	25.91	22.19	35.13	30.91	27.85	24.48	35.60	30.91	29.89	28.62
C-O (PEG)		286.0	0.00	**11.31**	**32.48**	**40.36**	0.00	**11.18**	**15.95**	**31.00**	0.00	**11.18**	**15.50**	**15.71**
C-O (PLA)		287.0	28.38	26.03	21.15	19.64	30.98	29.36	27.12	21.93	30.20	29.36	26.59	28.82
O-C+O (PLA)		289.0	29.47	28.01	20.46	17.81	33.89	28.54	29.08	22.59	34.20	28.54	28.02	26.86

Data from one sample, atomic percentages are reported as the average of XPS spectra taken at 3 different positions

Table excludes the contribution of C-Si found in some samples

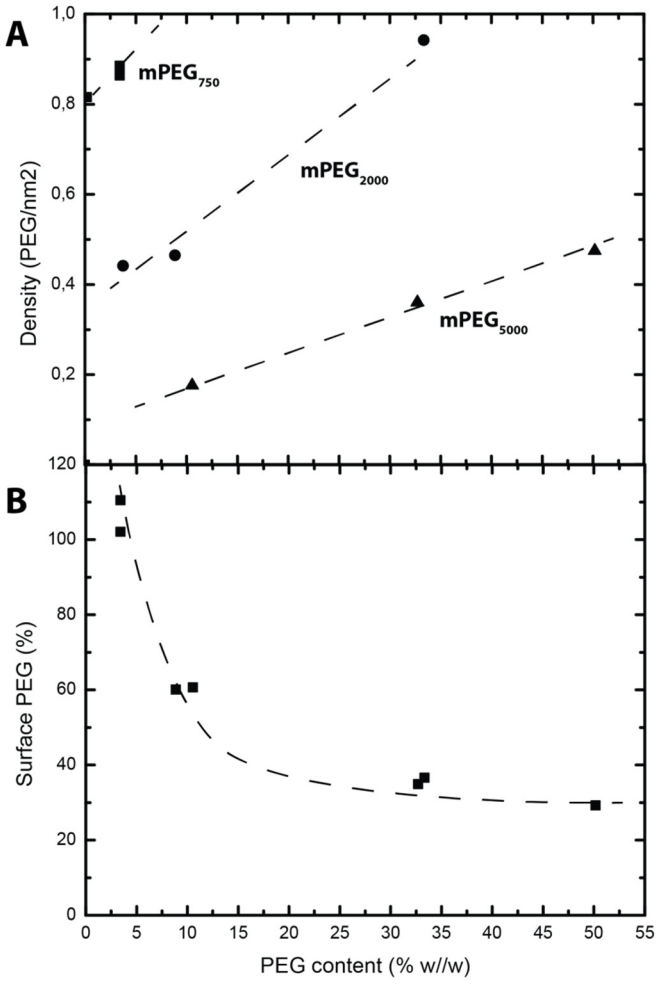

Figure 5.7. XPS analysis (A) PEG Surface density; (B) Surface PEG % as calculated from XPS data. All PEG M_w were pooled in these data.

5.5 Conclusion

In this work we synthetized comb-like copolymers by a combination of ring-opening polymerization (ROP) and copper-catalyzed azide–alkyne cycloaddition (CCAAC). The library of comb-like grafted copolymers containing poly(ethylene glycol) (PEG) as pendant groups (PEG-*g*-PLA) of different molecular weights was used to produced NPs using different preparation methods: "classical" nanoprecipitation, "flash" nanoprecipitation and microfluidic. The effects of polymer architecture and preparation on the size, morphology and surface physico-chemical properties were assessed.

The NPs size and zeta potential were not significantly dependant on the PEG content (% w/w in polymer) and PEG chains length in the copolymers. PEG chain surface densities were assessed by quantitative ^{1}H NMR and XPS. Preliminary data indicated that the effect of the preparation methods was limited to NP size, while PEG surface densities were found to be a function of the hydrophobic backbones (PLA), the total PEG content and the length of the pendant PEG chains. As with previously described comb-like copolymers [13], the position of the hydrophilic block in the chain appears to play an important role in NP structural arrangements. Taken together, the results support the importance of developing stable polymeric drug carriers with different polymer architecture from the linear diblock copolymers.

ACKNOWLEDGMENTS

JMR was the recipient of a doctoral grant from FQRNT (Québec, Canada). The authors wish to thanks Sonia Blais, Irene Kelsey (Université de Sherbrooke, Sherbrooke, Canada) and Josianne Lefebvre (Laboratoire d'analyse de surface, École Polytechnique, Montréal, Qc Canada) with their help with XPS analysis. XB acknowledges financial support from the Canada Research Chair program. PH acknowledges the support of FRQ-NT (Quebec, Canada). We wish to thank Precision Nanosystem (Vancouver, Canada) for the use of NanoAssemblr™ in microfluidic experiments.

5.6 References

1. Danhier, F., et al., *PLGA-based nanoparticles: An overview of biomedical applications.* Journal of Controlled Release, 2012. **161**(2): p. 505-522.
2. Cheng, J., et al., *Formulation of functionalized PLGA–PEG nanoparticles for in vivo targeted drug delivery.* Biomaterials, 2007. **28**(5): p. 869-876.
3. Andrieux, K. and P. Couvreur, *Polyalkylcyanoacrylate nanoparticles for delivery of drugs across the blood–brain barrier.* Wiley Interdisciplinary Reviews: Nanomedicine and Nanobiotechnology, 2009. **1**(5): p. 463-474.
4. Vittaz, M., et al., *Effect of PEO surface density on long-circulating PLA-PEO nanoparticles which are very low complement activators.* Biomaterials, 1996. **17**(16): p. 1575-1581.

5. Owens, D.E., 3rd and N.A. Peppas, *Opsonization, biodistribution, and pharmacokinetics of polymeric nanoparticles.* Int J Pharm, 2006. **307**(1): p. 93-102.
6. Vonarbourg, A., et al., *Parameters influencing the stealthiness of colloidal drug delivery systems.* Biomaterials, 2006. **27**(24): p. 4356-73.
7. Cheng, J., et al., *Formulation of functionalized PLGA-PEG nanoparticles for in vivo targeted drug delivery.* Biomaterials, 2006.
8. Hrkach, J., et al., *Preclinical Development and Clinical Translation of a PSMA-Targeted Docetaxel Nanoparticle with a Differentiated Pharmacological Profile.* Science Translational Medicine, 2012. **4**(128): p. 128ra39.
9. Peracchia, M.T., et al., *PEG-coated nanospheres from amphiphilic diblock and multiblock copolymers: Investigation of their drug encapsulation and release characteristics.* Journal of Controlled Release, 1997. **46**(3): p. 223-231.
10. Quesnel, R. and P. Hildgen, *Synthesis of PLA-b-PEG Multiblock Copolymers for Stealth Drug Carrier Preparation.* Molecules, 2005. **10**(1): p. 98-104.
11. Nadeau, V., et al., *Synthesis of new versatile functionalized polyesters for biomedical applications.* Polymer, 2005. **46**(25): p. 11263-11272.
12. Logie, J., et al., *PEG-Graft Density Controls Polymeric Nanoparticle Micelle Stability.* Chemistry of Materials, 2014. **26**(9): p. 2847-2855.
13. Rabanel, J.-M., et al., *Effect of Polymer Architecture on the Structural and Biophysical Properties of PEG-PLA Nanoparticles.* ACS Applied Materials and Interfaces, 2015. **7**(19): p. 10374–10385.
14. Gref, R., et al., *'Stealth' corona-core nanoparticles surface modified by polyethylene glycol (PEG): influences of the corona (PEG chain length and surface density) and of the core composition on phagocytic uptake and plasma protein adsorption.* Colloids Surf B Biointerfaces, 2000. **18**(3-4): p. 301-313.
15. Parrish, B., R.B. Breitenkamp, and T. Emrick, *PEG- and Peptide-Grafted Aliphatic Polyesters by Click Chemistry.* Journal of the American Chemical Society, 2005. **127**(20): p. 7404-7410.
16. Jiang, X., et al., *"Clickable" Polyglycolides: Tunable Synthons for Thermoresponsive, Degradable Polymers.* Macromolecules, 2008. **41**(6): p. 1937-1944.
17. Yu, Y., et al., *Functional Polylactide-g-Paclitaxel–Poly(ethylene glycol) by Azide–Alkyne Click Chemistry.* Macromolecules, 2011. **44**(12): p. 4793-4800.
18. Riva, R., et al., *Combination of Ring-Opening Polymerization and "Click Chemistry": Toward Functionalization and Grafting of Poly(ε-caprolactone).* Macromolecules, 2007. **40**(4): p. 796-803.
19. Teske, N.S., J. Voigt, and V.P. Shastri, *Clickable Degradable Aliphatic Polyesters via Copolymerization with Alkyne Epoxy Esters: Synthesis and Postfunctionalization with Organic Dyes.* Journal of the American Chemical Society, 2014. **136**(29): p. 10527-10533.
20. Baier, G., et al., *Surface Click Reactions on Polymeric Nanocapsules for Versatile Functionalization.* Macromolecules, 2012. **45**(8): p. 3419-3427.
21. Breed, D.R., et al., *Functionalization of Polymer Microspheres Using Click Chemistry.* Langmuir, 2009. **25**(8): p. 4370-4376.

22. Hiki, S. and K. Kataoka, *A Facile Synthesis of Azido-Terminated Heterobifunctional Poly(ethylene glycol)s for "Click" Conjugation.* Bioconjugate Chemistry, 2007. **18**(6): p. 2191-2196.
23. Han, J., et al., *A simple confined impingement jets mixer for flash nanoprecipitation.* Journal of Pharmaceutical Sciences, 2012. **101**(10): p. 4018-4023.
24. Stroock, A.D., et al., *Chaotic Mixer for Microchannels.* Science, 2002. **295**(5555): p. 647-651.
25. Shakesheff, K.M., et al., *The adsorption of poly(vinyl alcohol) to biodegradable microparticles studied by x-ray photoelectron spectroscopy (XPS).* Journal of Colloid and Interface Science, 1997. **185**(2): p. 538-547.
26. Beamson, G. and D. Briggs, *High resolution XPS of organic polymers The Scienta ESCA300 Database.* 1992, West Sussex, England: John Wiley & Sons Ltd.,.
27. Riley, T., et al., *Physicochemical Evaluation of Nanoparticles Assembled from Poly(lactic acid)−Poly(ethylene glycol) (PLA−PEG) Block Copolymers as Drug Delivery Vehicles.* Langmuir, 2001. **17**(11): p. 3168-3174.
28. Belliveau, N.M., et al., *Microfluidic Synthesis of Highly Potent Limit-size Lipid Nanoparticles for In Vivo Delivery of siRNA.* Mol Ther Nucleic Acids, 2012. **1**: p. e37.
29. de Gennes, P.G., *Polymers at an interface; a simplified view.* Advances in Colloid and Interface Science, 1987. **27**(3–4): p. 189-209.

6 Article 3 “Effect of polymer architecture on Curcumin encapsulation and release from pegylated polymer nanoparticles: toward a drug delivery nano-platform to the CNS”

Article actuellement en révision au « European Journal of Pharmaceutics and Biopharmaceutics » (version révisée acceptée le 7 septembre 2015).

Dans cette partie, nous avons d’étudié le rôle de l’architecture du polymère sur les propriétés d’encapsulation et de libération d’une molécule active, la curcumine. Les copolymères testés sont ceux appartenant à la première bibliothèque de copolymères (PEG-*g*-PLA) obtenus par couplage et acylation (décrits dans le Chapitre 4).

Le but est de faire un lien entre les propriétés physicochimiques des particules, mises en évidence dans les chapitres précédents et l’efficacité d’une molécule active. Un second objectif était d’explorer les possibilités offertes par cette bibliothèque de copolymères pour concevoir un véhicule pour cibler à terme le système nerveux central.

Effect of polymer architecture on Curcumin encapsulation and release from pegylated polymer nanoparticles: toward a drug delivery nano-platform to the CNS.

Jean-Michel Rabanel[1,2 ‡], Jimmy Faivre[1 ‡], Ghislain Djiokeng Paka[3], Charles Ramassamy[3,*], Patrice Hildgen[2, *] Xavier Banquy,[1, *]

[1] *Canada Research Chair on Bio-inspired materials, Faculté de Pharmacie, Université de Montréal, C.P. 6128, Succursale Centre-ville, Montréal, Québec, H3C 3J7, Canada*

[2] *Laboratoire de Nanotechnologie Pharmaceutique, Faculté de Pharmacie, Université de Montréal, C.P. 6128, Succursale Centre-ville, Montréal, Québec, H3C 3J7, Canada*

[3] *INRS-Institut Armand-Frappier, 531, Boulevard des Prairies Laval, Québec H7V 1B7, Canada*

[*] *Corresponding author*

[‡] *These authors contributed equally to this work*

6.1 Abstract

We developed a nanoparticles (NPs) library from poly(ethylene glycol)-poly lactic acid comb-like polymers with variable amount of PEG. Curcumin was encapsulated in the NPs with a view to develop a delivery platform to treat diseases involving oxidative stress affecting the CNS. We observed a sharp decrease in size between 15 to 20 % w/w of PEG which corresponds to a transition from a large solid particle structure to a "micelle-like" or "polymer nano-aggregate" structure. Drug loading, loading efficacy and release kinetics were determined. The diffusion coefficients of curcumin in NPs were determined using a mathematical modelling. The higher diffusion was observed for solid particles compared to "polymer nano-aggregate" particles. NPs did not present any significant toxicity when tested in vitro on a neuronal cell line. Moreover, the ability of NPs carrying curcumin to prevent oxidative stress was evidenced and linked to polymer architecture and NPs organization. Our study showed the intimate relationship between the polymer architecture and the biophysical

properties of the resulting NPs and sheds light on new approaches to design efficient NP-based drug carriers.

TOC graphic

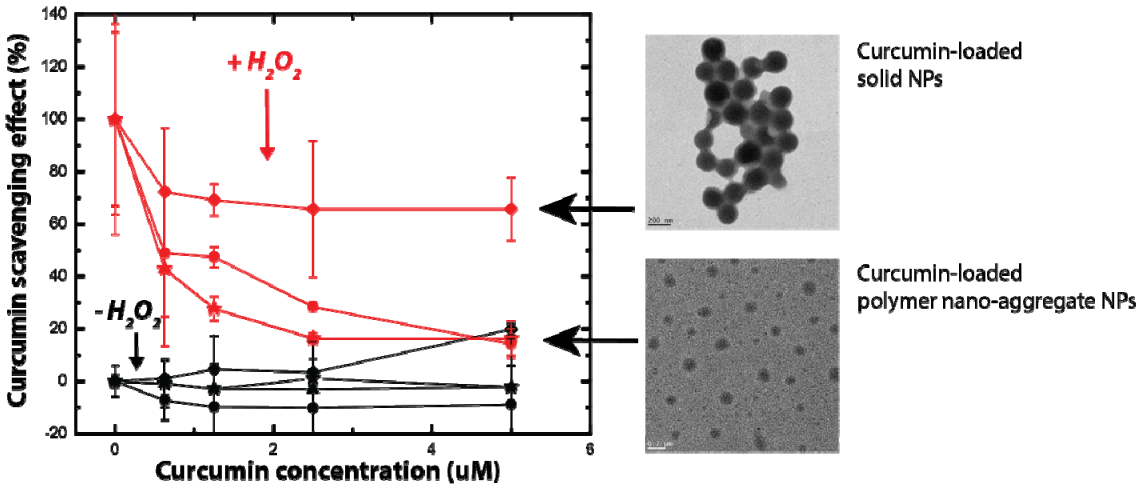

Key words: poly(lactic); poly(ethylene glycol), comb-polymer, nanoparticle, micelle-like, nanoaggregate, curcumin, toxicity, ROS, CNS

6.2 Introduction

Neurodegenerative disorders (NDD) are an increasing burden for the health systems and amongst all NDD, Alzheimer disease (AD) represents the most common disease. Besides the complexity of the pathophysiology of these diseases, NDD and AD are also particularly difficult to treat due to the limited permeability of the blood-brain barrier (BBB). Indeed, the BBB is very efficient to prevent the entry of foreign compounds in the central nervous system (CNS), thanks to a very tight endothelial structure and the action of efflux pumps [1, 2]. Moreover, the drugs available for the treatment of AD are in limited number and are symptomatic drugs associated with unwanted peripheral secondary effects. Finally, considering the number of mechanisms involved in AD progression, delivery of compounds with pleiotropic properties is a promising strategy. For instance, several studies have pointed out that curcumin, a phyto-polyphenol with anti-oxidative, anti-inflammatory activities and

low toxicity, could alter several mechanisms involved in AD such as the amyloid-beta cascade, the phosphorylation of Tau protein as well as the development of oxidative stress [3]. However, curcumin brain bioavailability is low due to its poor stability in physiological media [4] and poor permeability across the BBB [5, 6].

Curcumin encapsulation in nanocarriers has been extensively studied for different therapeutic applications, mainly in an effort to by-pass the BBB but also to improve its solubility limitation and chemical instability. Liposomes, micelles, lipids or albumin particles [3, 7-9], as well as polyester-based carriers [5, 10] and poly(cyanoacrylate) based carriers [11] have been proposed to deliver curcumin and other substances to the CNS. Curcumin encapsulated in PLGA NPs showed an increased accumulation in CNS tissues compared to free curcumin [12].

Nanoparticle-mediated efficient uptake of active substances into the CNS represents the new field of nanomedecine with great challenge and could represent a major breakthrough in the management of different CNS disorders. Although several proofs of concept have been put forward, the main goal stays elusive, mainly for reasons linked to the dose levels actually delivered, accumulation of polymeric material in the host, more complex cellular environment and interspecies differences between models [13]. Amongst those reasons, one that has been clearly underestimated is the structural properties of the particle. The relationships between the polymer architecture and the resulting NP structural organization are still a matter of debate in spite of several decades of research. In the area of pharmaceutical polymeric nanocarrier, diblock polymers are the most commonly used polymers to form NPs [14, 15]. On the other hand, few systematic studies focusing on establishing the relationship between the polymer architecture and the performances of the nano-carriers in term of encapsulation efficiency, release profile and more generally drug efficacy, are available.

The ability of PEGylated NP to penetrate into the brain tissue through the BBB is still a matter of debate. It is well established that drug carriers must be PEGylated in order to circulate for an extended period of time in the blood stream and to provide enough time to the different transport mechanisms to improve NP brain accumulation. “Naked” NPs are usually rapidly opsonized resulting in an increase of liver uptake and macrophage elimination. This

strongly decreases their distribution in other organs and tissues, including brain tissues. The influence of PEGylation on the BBB crossing mechanisms is not well documented yet. It has been reported that PEGylated poly(alkylcyanoacrylate) NP penetrate the brain tissues more efficiently than any other nanoformulation using other surface modifications [14, 16]. The specific crossing of a non-compromised BBB (in absence of brain injury or inflammation creating gaps between endothelial cells.) involves passage through a layer of endothelial cells via endocytosis, lysosomal escape and exocytosis on the brain parenchyma side [17, 18]. Modification of NP surface properties using polymers such as Poloxamer®, polysorbates and PEG have been shown to favour adsorption of serum ApoE on the NP surface [13]. ApoE can be used as a targeting ligand allowing translocation of the NP across the BBB via the ApoE receptor present on endothelial cell surfaces [7]. The effect of PEG surface densities and PEG surface organization on BBB crossing efficiency is not well documented. To our knowledge, systematic exploration of these parameters is yet to be conducted.

Considering the often opposite properties a NP has to display for a successful clinical outcome [19], the development of innovative polymer architectures is necessary to maximize the efficacy of delivery to the CNS. We previously developed a library of polymers based on a comb-like architecture exhibiting a backbone of polylactic acid with pendant polyethylene glycol chains. We showed that by systematically varying the amount of PEG in the polymer, we were able to control the NP structure from solid particles to soft, polymer nano-aggregate or "micelle-like" particles [20].

In this work, we used this library of PEG-g-PLA polymers to prepare nano-vectors loaded with curcumin. The effect of polymer architecture on the structure of the particle, drug encapsulation efficiency, drug loading, the drug release and its modeling taking in account curcumin degradation, were studied. The suitability of these NP for antioxidant delivery was evaluated on a neuronal cell line. This work represents the first step toward the development of an efficient drug delivery system to the CNS. Moreover, our library of NP with a systematic variation of PEG content and PEG surface densities may provide a tool to explore the role of PEG in the NP crossing of the BBB.

6.3 Materials and Methods

6.3.1 Materials

The synthesis of the different polymers used in this study was described elsewhere [20]. Briefly, random copolymerization of D,L-dilactide and benzyl glycidyl ether (BGE) was performed by ring-opening polymerization catalyzed by stannous 2-ethyl hexanoate (SnOct2). The BGE/lactic acid ratio was varied from 0.5 to 3 % to yield PLA chains with different densities of benzyl pendant moities. Alcohol pendant groups were deprotected by catalytic hydrogenation in presence of Pd/Carbon to yield OH-g-PLA. mPEG-COOH (2kD) was grafted onto OH-g-PLA polymers by acylation to yield PEG-g-PLA (polymer A and C in Figure 1). Alternatively, the mPEG-COOH chains were grafted by esterification in presence of dicyclohexylcarbodiimide (DCC) [21]. The diblock synthesis (PEG-b-PLA, polymer B in Figure 1) was performed as follow: mPEG-OH 2kD was used as a macro-initiator during the ring-opening polymerization of dilactide in presence of SnOct2 as previously described [20]. Polymer properties obtained from GPC and 1H-NMR are summarized in Table 1.

All chemicals were from Sigma-Aldrich (Oakville, ON Canada) unless otherwise stated in the text. Solvents were from Fisher Scientific (Fisher Canada, ON). Curcumin was obtained from AK scientific (AK Scientific, Union city, CA, USA). SK-N-SH cells which are human neuroblastoma cells, were from ATCC (Manassas, VA, USA), Cell culture media, minimal essential medium Eagle (MEM), fetal bovine serum, penicillin, streptomycin, and sodium pyruvate were obtained from Sigma-Aldrich (Oakville, ON, Canada). LDH and Tox-8 detection kits were from Sigma-Aldrich (Oakville, ON Canada).

6.3.2 NPs fabrication and purification

NP batches were prepared by nanoprecipitation. Briefly, 60 mg of PEGylated polymer were dissolved in 3 ml acetone. For drug-loaded NP batches, curcumin was added to the organic phase at a determined curcumin/polymer ratio (from 0 to 20 % w/w). The organic phase was slowly injected with a syringe pump (Kent Scientific Corp. Torrington, CT, USA)

at a rate of 1mL/min with a 26G needle in 15 mL of PBS 10mM (pH 7.4) placed in a 25 ml beaker. The aqueous phase was kept under constant stirring (530 rpm) with a magnetic agitator during the injection of the organic phase.

NPs were purified by centrifugation on a tabletop centrifuge (Multi RF centrifuge, Thermo Electron Corp. Needham heights MA, USA) to remove eventual large debris, aggregates and precipitated non-encapsulated curcumin (5 min at 5000 rpm). Supernatant was finally dialyzed against PBS during 2 h in a regenerated cellulose membrane bag, with a cut-off of 6-8000 Da (SpectraPor, Spectrum Laboratories, Rancho Dominguez, USA) to remove organic solvent residuals as well as small non-precipitated polymer chains. NPs were stored in a dark container at 4°C or were used immediately after preparation. Residual amount of non-encapsulated curcumin in solution are rapidly degraded in the aqueous phase during NP suspension storage and are thus not contributing to observed biological properties.

6.3.3 NPs characterization

• ***Size measurements.*** The NPs size was measured by Dynamic Light Scattering (DLS) on a Zetasizer Nano-ZS (Malvern Instruments, Worcester, UK). Three measurements of 15 (10 seconds) runs were performed at 25°C and averaged.

• ***Zeta potential measurements.*** NPs suspended in 1 ml of PBS 0.1 X pH 7.4 were placed in a disposable folded capillary cell to measure ζ on a Malvern Zetasizer (Malvern, Worchester, UK) in triplicate.

• ***Loading efficiency (LE) and drug loading (DL).*** LE and DL were assessed by UV/Vis spectrophotometry (MBI Lab equipment, Montréal, CA) using a standard curve of curcumin in dichloromethane (DCM) at λmax=419 nm. Briefly, 1 mL of NPs was lyophilized and precisely weighted, then dissolved in DCM. Dissolved polymers effect on absorbance was found not significant. Curcumin concentration was then measured by UV/Vis. LE and DL were calculated using equations (Eq. 1) and (Eq. 2) respectively:

$$LE = \frac{\text{weight of curcumin in NPs}}{\text{initial weight of curcumin}} \times 100 \ (Eq.\ 1)$$

$$DL = \frac{\text{weight of curcumin in NPs}}{\text{weight of NPs}} \times 100 \ (Eq.\ 2)$$

NP exact weights were adjusted for the presence of PBS salts in samples.

6.3.4 Differential Scanning Calorimetry (DSC)

DSC experiments were performed on blank and loaded NPs. A mass of about 5 mg of freeze-dried (blank or drug-loaded) NP was disposed in crimped aluminum pan. DSC analysis were performed under nitrogen flow from -40oC to 80oC at 10oC min-1, hold for 1 minute and cooled at a rate of 20oC min-1 to -40oC and reheated to 80oC at 10oC min-1. First run was analyzed for NP samples using TA instruments Universal Analysis 2000, version 4.5A (TA Instruments – Waters LLC, USA).

6.3.5 Transmission electronic microscopy (TEM)

● ***Sample preparation for TEM.*** Diluted NP suspension in MilliQ® water at a concentration of about 1 to 2 mg/ml were deposited on a carbon film of 400 square mesh copper grids (Electron Microscopy Sciences, Hatfield, PA USA). The volume of the droplet was about 2 to 4 µl. The droplet was allowed to sit for 5 minutes before excess of liquid was drained-out with filter paper. Grids were allowed to dry in air for 1-2 hours before image acquisition. No staining procedure was introduced.

● ***TEM imaging.*** TEM image acquisition was done in bright field mode on a JEM-2100F, Field Emission electron microscope (Jeol Ltd, Tokyo, Japan) equipped with a sample holder cooled by liquid nitrogen (Gatan inc. Warrendale, Pittsburg, PA, USA). The grids were maintained at -170oC throughout the acquisition with a temperature controller (Smart Set Model 900 Cold Stage controller; Gatan inc. Warrendale, Pittsburg, PA, USA). The grids were

introduced in the microscope column under vacuum. Liquid nitrogen was added to the sample holder and temperature recorded. The sample was exposed to the electron beam only after the temperature had reached -170oC. The acceleration voltage was set at 200 kV. Images were digitally recorded at a low electron dose to prevent damage to the heat-sensitive particles (current densities were between 5 and 15 pA/cm2).

6.3.6 Drug release studies

Release studies were carried out in triplicate using the dialysis bag method at 37°C in an orbital shaker. In brief, 3 mL of NPs suspension were placed in a dialysis bag (Cellulose ester membrane, cut-off 100 kDa, Spectrum Laboratories, Rancho Dominguez, USA) and then, immersed in 30 mL of 10 mM PBS (pH 7.4) supplemented with 50 mM Sodium Dodecyl Sulfate (SDS) to increase curcumin solubility in the release medium and insure sink conditions. Ascorbic acid (ASA) was also added to the medium (25µM) to minimize curcumin oxidation. At each time-point, 3 mL of external media were removed and replaced by fresh solution. The curcumin solution was dosed by UV/Vis spectrophotometry according to a standard curve of curcumin in a 10 mM PBS/SDS/ASA buffer at λmax=422 nm.

6.3.7 Cytotoxicity studies

Cytotoxicity studies were carried out as described previously [22] with some modifications described here. Briefly, SK-N-SH cells were maintained in MEM, supplemented with 10% v/v FBS, 100 U/mL penicillin, 100 g/mL streptomycin, and sodium pyruvate (1mM) in a humidified incubator at 37 °C with 5% CO2. Cells were grown to 80% confluence and then seeded in multi-well cell culture plates.

● ***Cytotoxity assays.*** SK-N-SH cells were plated at a density of 2.0 × 104 cells/well in 96-well plates and incubated for 24 h at 37 °C. Cells were then treated with either free curcumin, blank NP or curcumin-loaded NP in presence or absence of H2O2 (250µM) (n=3). Curcumin solutions are prepared as follow to avoid precipitation: A stock solution of 200 µM is prepared by the solubilisation of 1 mg of curcumin in 0.5 mL of Ethanol and the volume is completed

with 13 mL of PBS. This stock solution was used to prepare solution of free curcumin in all biological tests. Control experiments (not shown in this study) had previously showed that this procedure had not effect on biological results [10]. Preparation of blank or curcumin-loaded NP, characterized for their size, mass concentration and drug loading, were diluted to obtain 0.25 to 1 μM curcumin equivalent concentration in either blank or curcumin-loaded NP samples. Practically, the same concentration of particles was used in experiments involving blank and loaded NPs. This allows for a direct comparison and control of NP effects, to be distinguished from curcumin effects. Cell death and survival were measured 24 h after the treatment using the cytotoxicity detection kit-LDH and the survival detection kit Tox-8 (Resazurin-based) respectively. The kits were used following the manufacturer's instructions. Values obtained from controls, untreated cells, were considered as 100% of proliferation for Resazurin-based assays. For cell mortality assays (LDH-based assays) and ROS level determination (DCF-DA assays), values obtained from controls untreated cells were considered as 0% effect on mortality, while values obtained from control untreated cells exposed to 250μM H2O2 were considered as 100% effect on mortality. Raw results from treated cells were thus normalized based on these controls to allow a direct comparison of the different treatments and account for cell-assays variability from plate to plate.

6.3.8 Effect of Reactive Oxygen Species (ROS) and reactive nitrogen species (RNS).

Effect of NPs on intracellular ROS and RNS as well as protective effect of blank and drug loaded NPs on neuronal cells in presence or absence of 250 μM H2O2 were assessed by following the oxidation of 2',7' –dichlorofluorescin diacetate (DCF-DA) a non-fluorescent, cell permeable dye that, upon hydrolysis by intracellular esterase, reacts with ROS/RNS to produce a highly fluorescent compound, 2', 7' –dichlorofluorescein (DCF), which is trapped inside the cells. Briefly, SK-NSH cells (2 × 104/well) were plated into 96-well plates. After 24 hours, cells were exposed with 10 □M DCF-DA for 20 min and treated with either free curcumin, blank NP or curcumin-loaded NP for 1 h in presence or absence of H2O2. At the end of the treatment, cells were then washed with PBS containing Ca2+/Mg2 and the

fluorescence was determined with the excitation/emission filters at 485/ 535 nm using a Synergy HT multi-detection microplate reader (BioTek Instruments, Inc, Highland Park, Winooski, Vermont USA).

ROS level determination (DCF-DA assays), values obtained from controls untreated cells were considered as basal level (0%), while values obtained from controls untreated cells exposed to 250µM H2O2 were considered as the 100% effect on ROS levels. Raw results from treated cells were thus normalized based on these controls to allow a direct comparison of the different treatments and account for cell-assays variability from plate to plate.

6.3.9 Statistical analyses

Multiple groups comparison of cell-based assays were performed with a one-way Anova on SigmaStats® (Systat Software Inc.) using the Holm-Sidak method. Significance level was set at $p<0.05$.

6.4 Results and discussion

6.4.1 Polymer characteristics

The polymers used in this study, noted as PEG-g-PLA throughout the text, are comb-like polymers composed of a PLA backbone on which PEG chains are grafted. In addition to PEG-g-PLA polymers, PLA polymer bearing no PEG chain (OH-g-PLA) as well as a PEG-b-PLA di-block polymer were included to the study in order to better characterised the effect of PEG content and architecture. The polymers' architectures are presented in Figure 1. The properties of the polymer used in this study are listed in Table 1.

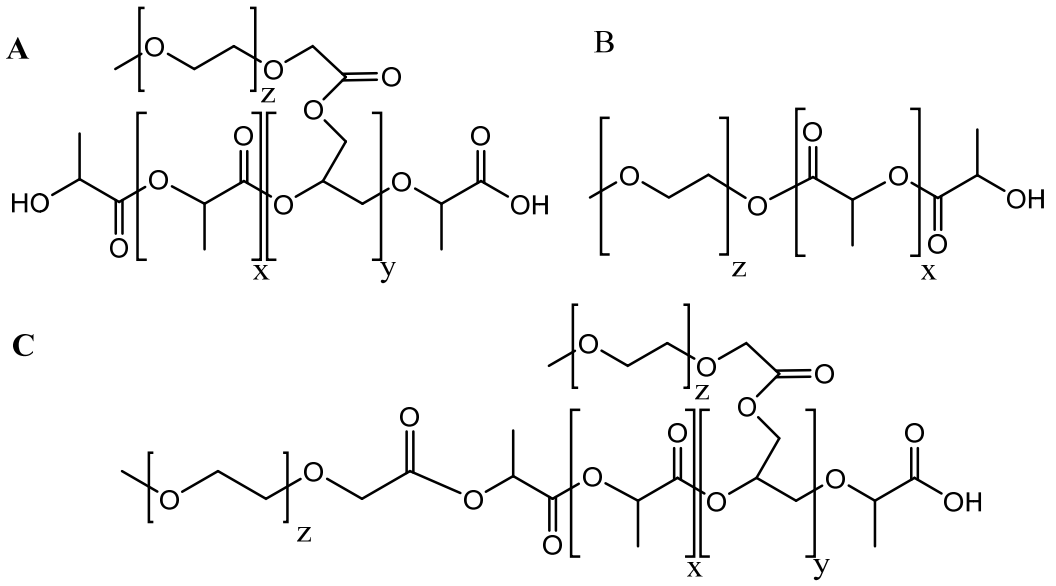

Figure 6.1. Structures of the polymers used in this study. **(A)** PEG-*g*-PLA; **(B)** PEG-PLA di-block polymer, **(C)** PEG-*g*-PLA with a terminal PEG graft. (z= 45; y : 0.5-2.5/100 LA monomers)

PEG chains (Mw=2 000 g/mol) were grafted on a PLA backbone of Mw ≈25 000 g/mol (Table 1). The resulting polymers exhibited a PEG content varying from 8 to 37.9 %w/w (Table 1). The choice of the PLA backbone size was determined by its appropriate short degradation time [23]. Numbers of grafted PEG chains on polymeric chain were determined by 1H-NMR [20].

Table 6.1. Polymer properties (from [20])

Polymer	***Molar Mass M_w***		***%PEG***	***Structure***
	PLA (g/mol)	*PEG (g/mol)*	*(% w/w)*	*See figure 1*
OH-g-PLA	*23 990*	-	*0*	-
PEG-PLA	*23 000*	*2 000*	*6*	*B*
PEG8%-g-PLA	*28 300*	*2 000*	*8*	*A*
PEG12%-g-PLA	*40 300*	*2 000*	*11.6*	*A/C*
PEG15%-g-PLA	*33 890*	*2 000*	*14.9*	*A/C*
PEG20%-g-PLA	*19 820*	*2 000*	*19.9*	*C*
PEG25%-g-PLA	*23 990*	*2 000*	*24.9*	*C*
PEG38%-g-PLA	*28 300*	*2 000*	*37.9*	*C*

6.4.2 NP preparation and characterization

NP made with different curcumin contents (% w/w ratio curcumin/polymer varying from 0 to 20%) in the organic phase were prepared by nanoprecipitation and characterized. Except for NPs prepared with OH-g-PLA, curcumin-loaded NP showed no significant size differences compared to blank NPs (Fig. 2a). This observation is in agreement with Budhian et al. who encapsulated haloperidol in PLA-based nanoparticles and found that NPs mean diameter was independent of the initial haloperidol content [24]. Similar observations were made by Gou et al. in a work involving encapsulation of curcumin in a micellar system [25].

Fig. 2b shows the evolution of the NPs hydrodynamic diameter as a function of PEG content in the polymer (% w/w PEG/PLA). NPs size was found to be constant and independent of PEG content up to 15 % w/w PEG. Above this value, a sharp decrease in size is observed to about 50 nm at 25% w/w PEG/PLA. Afterwards, NPs hydrodynamic diameters increase again slowly, up to 100 nm with increasing PEG content (Fig. 2b). This increase could be due to the higher surface PEG chain density resulting in stretched PEG chains and increase in particle hydrodynamic diameter, as predicted by De Gennes' theory [26]. Similar observations were reported for this polymer library previously for blank NPs [20].

OH-g-PLA NPs (NPs made of polymer before it has been modified by PEG grafting) showed a different behaviour when prepared with a ratio of 15% w/w curcumin/polymer. The colloidal system was instantaneously destabilized, resulting in a drastic NP hydrodynamic diameter increase. It can be hypothesized that, when OH-g-PLA is used, curcumin precipitation occurred much faster than the polymer precipitation and particles formation. As a result, curcumin precipitation drags down polymer chains leading to the complete destabilization of the system. On the other hand, PEG side chains in di-block and comb-like copolymers contribute to the nano-suspension stabilization.

NPs zeta potential was also studied as a function of PEG content in polymer (Fig. 2c). OH-g-PLA NPS exhibited a strongly negative zeta potential of -75 mV providing a strong

electrostatic repulsion in aqueous solution between PLA particles. The presence of PEG chains on PLA backbone decreases drastically zeta potential to a value of -15 mV. However this decrease remained independent of the polymer PEG content. NPs produced with the diblock polymer exhibited a zeta potential slightly more negative compared to NPs obtained with comb-like polymers. The dramatic decrease in zeta potential with increased PEG content has been also reported by Gref et al. [27]. Such phenomenon has been attributed to the displacement of the shearing plane far away from NPs surface by the presence of PEG chains around the NPs, hiding the carboxylic groups present in the PLA core. However, low electrostatic repulsions for PEG-g-PLA NPs are counterbalanced by the increased steric hindrance around PEGylated NPS which guarantees a stable colloidal suspension. The difference between diblock and PEG-g-PLA zeta potentials can be explained by the smaller PEG/PLA ratio used in the diblock copolymer (Table 1) which decreases the PEG density around corresponding NPs. Another explanation can be related to the structural organization of comb polymer preventing PLA terminal COOH to be exposed at the NP surface [20].

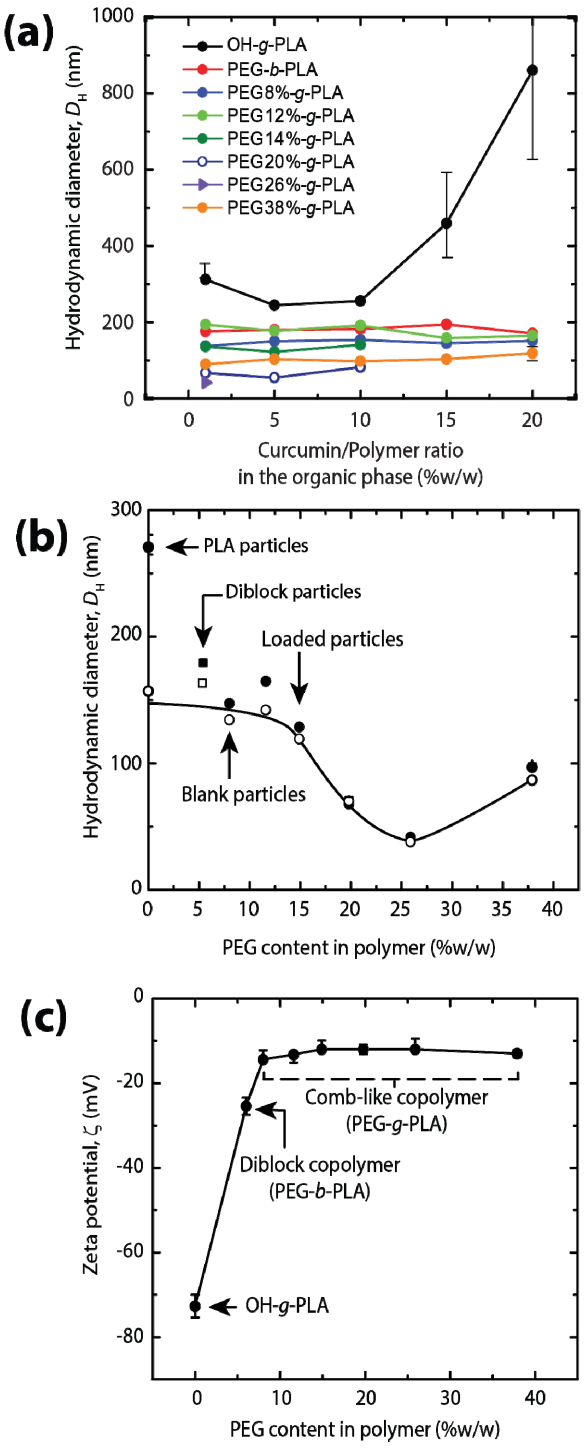

Figure 6.2. Particle hydrodynamic diameter as a function of: **(a)** initial curcumin/polymer content in the organic phase (% mass); or **(b)** PEG content. **(c)** Zeta potential of the NPs as a function of polymer PEG content. In (a) and (b) some error-bars are not showing since they are smaller than the symbol used.

Morphology of blanks and drug-loaded particles was examined by TEM. To prevent damage or deformation of the NPs, TEM grids were maintained at -170oC during image acquisition. No structural differences were noticeable between blank and curcumin-loaded particles (Fig. 3). Between 0 and 12-15 % w/w of PEG, NPs appear to belong to a particulate (solid particle) regime and the size of the hydrophobic core determined the NPs size. Between 0 and 12-15 % w/w of PEG, NPs appear as solid particles. NPs with a 8% PEG content (Figure 3C and D), as well as control NPs prepared from pure PLA or OH-g-PLA, (Figure S2) exhibit a large particle size and a homogeneous core.

Beyond 15% of PEG content, it was hypothesized that nanocarriers switch to a "micellar-like" or "polymer nano-aggregate" structural organization, a kinetically micellar frozen system (Fig 3E,F,G,H) in response to increased PEG content per polymeric chain [20]. All polymer nano-aggregate particles appeared round shaped and non-aggregated.

The changes in particle size previously observed by DLS were confirmed by TEM. Particles with PEG content below 12 % w/w were found to be much larger (>100 nm) than those with higher PEG content (<100m). Interestingly, our results show that the transition from solid NPs to polymer aggregate NPs depends only on the PEG content in the polymer and its architecture but not on the molecule encapsulated in the NPs, since no difference was observed between curcumin-loaded-NP and blank NP. Noteworthy, the morphology of diblock NP appears more spherical and less polydispersed than particles made from comb polymer of similar PEG content. The dramatic change in size and particle morphology from solid polymeric NPs to soft polymeric aggregates is not only related to polymer PEG content but also to polymer architecture as PEG-b-PLA diblock with PEG content about 6% adopt a soft particle morphology as seen in TEM (Fig. 3A and B)).

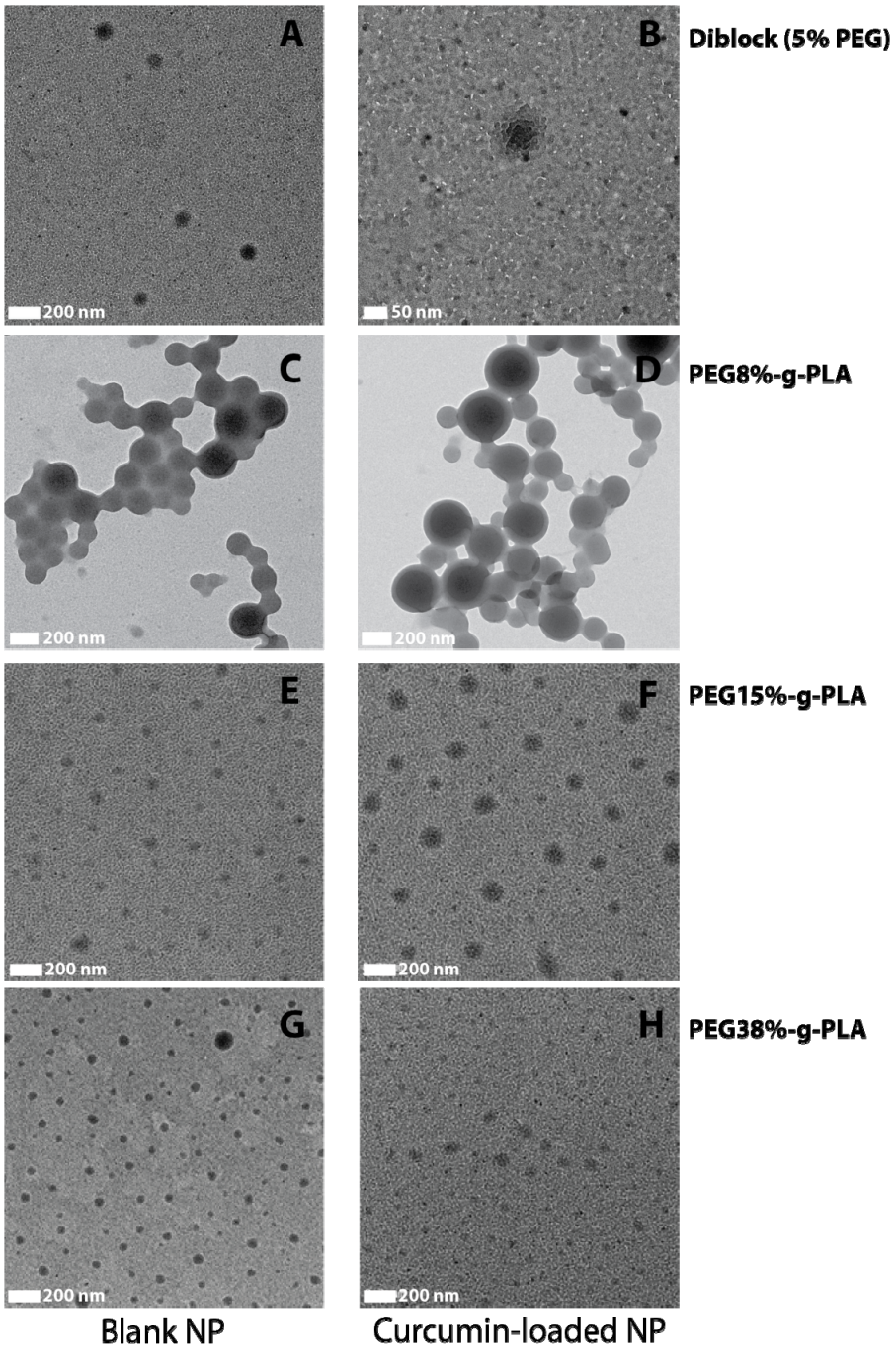

Figure 3. Representative TEM images of the NPs under study. On left panels: blank particles; on the right panel: curcumin-loaded particles. Acquisition at 15 000 X, except (B) acquisition at 25 000 X. (A and B), Diblock PEG-*b*-PLA NPs; (C and D), PEG8%-*g*-PLA NPs; (E and F) PEG15%-*g*-PLA NPs; (E and F) PEG38%-*g*-PLA NPs

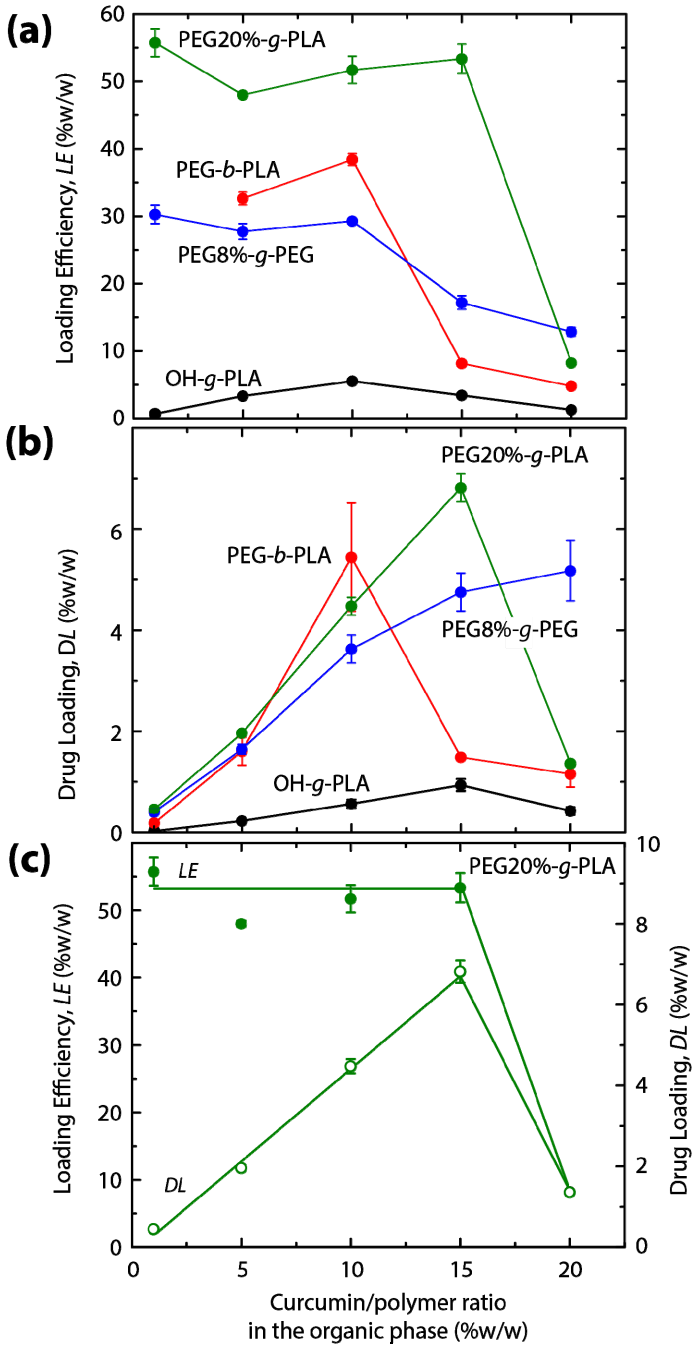

Figure 6.4. Optimization of encapsulation process: **(a)** Loading efficiency (LE) as a function of curcumin/polymer ratio; **(b)** Drug loading (DL) as a function of curcumin/polymer ratio; **(c)** Direct comparison of Loading efficiency and Drug loading (DL) as a function of curcumin/polymer ratio for "polymer nano-aggregate" particle made of PEG20%-*g*-PLA.

6.4.3 Curcumin encapsulation

Systematic quantification of the loading efficiency (LE) and the drug loading (DL) of curcumin in the NPs were conducted to correlate these properties with the architecture and PEG content of the polymers. Fig. 4 shows the evolution of the LE and DL as a function of the initial curcumin/polymer ratio in the organic phase.

LE was found to vary between nearly 0% for OH-g-PLA NPs, 20% for solid particles and up to 50% for the polymer nano-aggregate NPs. For DL, values spread out from 0% for OH-g-PLA to 5% for polymer nano-aggregate NPs. As a result, these NPs exhibiting the highest PEG content were found to have the highest values of LE and DL. As shown in Fig. 4, LE exhibited a plateau before drastically decreasing to values lower than 10 % at 20% w/w curcumin/polymer (Fig. 4a). At the same time, the DL first increased up to a maximum value, which depends on the polymer PEG content, before decreasing (with the exception of PEG8%-g-PLA (Fig. 4b). Budhian et al. reported a similar behaviour for the encapsulation of haloperidol in PLA based-NPs [24, 28]. The authors explained this phenomenon as the result of the drug/polymer interactions. By increasing the curcumin initial content, the encapsulation yield (LE) remains at the maximum efficiency as indicated by the plateau, and the drug loading (DE) increases until it reaches its maximum, which can be considered as the drug maximum solubility in the polymeric matrix (Fig. 4c). Beyond this limit, LE drastically decreases due to drug saturation in the NPs. It follows that curcumin concentration in the aqueous phase increases and reaches rapidly its saturation in solution and precipitates. The non-encapsulated curcumin precipitate drags down polymer chains, destabilizing the system and resulting in a dramatic decrease in DL [29].

The NPs ability to encapsulate curcumin was also correlated to NPs hydrodynamic diameter (Fig. 5). The highest values of LE and DL were obtained for the smallest nanocarriers with a LE of about 50% (Fig. 5a) and a DL of about 5% (Fig. 5b). Both LE and DL decrease with the particle size to reach values close to 0% for NPs produced with OH-g-PLA polymer (i.e. PLA chain with hydroxyl branching points along the polymer backbone). Noteworthy, the size of particle is also directly correlated to PEG content. Although curcumin

is poorly soluble in PEG, NP PEG content could play a role in LE and DL values. For instance, PLGA nanoparticles prepared with PEO-PPG, an amphiphilic molecule known to cover the surface of the NPs, were shown to be more efficient to encapsulate curcumin than "bare" PLGA NPs [30].

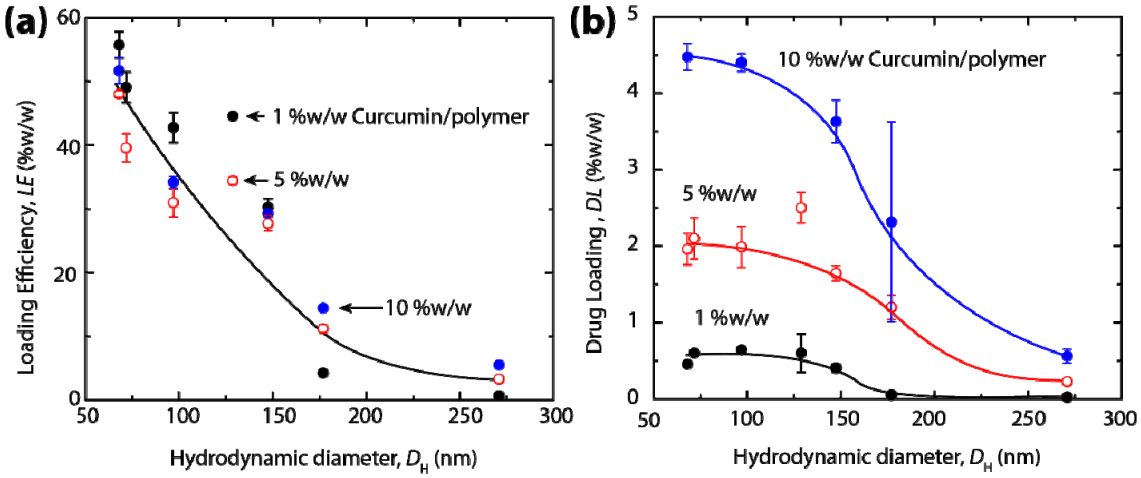

Figure 6.5. Evolution of **(a)** Loading Efficiency (LE) and **(b)** Drug Loading (DL) as a function of the NPs hydrodynamic diameter.

The relationship between polymer architecture, PEG content and encapsulation properties can be summarize as follow: The increase of PEG content is related to an increase in LE. Noteworthy PEG-b-PLA with a 6% PEG content showed a higher LE than PEG8%-g-PLA comb polymer pinpointing the role of polymer architecture. The maximum DL is about 4-6% regardless of the PEG content. For each polymer, the maximum DL is obtained at different drug/polymer ratio as seen in Fig 4b. This may be related to two parameters: 1) solubility of curcumin in polymer, mainly the hydrophobic PLA backbone chains present in variable amount in each polymer; 2) the relative precipitation speed between the polymer chains and curcumin as discussed above, and finally 3) a retention effect of curcumin inside the NP due to the hydrophilic PEG layer.

The encapsulation efficiency depends on drug/polymer interactions [29], the structural organization of the NP and the preparation process of the NP. During the nanoprecipitation process, a key factor is the relative rate of precipitation of the hydrophobic drug and the polymer. If the rates of precipitation of the two species are equal, they will form homogeneous

particles while large differences between rates will force the selective precipitation of each component and disfavor the encapsulation of the drug. The rate of precipitation of the polymer is mainly controlled by its PEG content, being lower at high PEG content.

Regarding the role of the interactions between the drug and the polymer, in our case, the strong affinity of the drug to the PLA backbone of the polymer is due to hydrophobic forces. As shown in our previous study [20], NPs obtained from polymers of high PEG content tend to exhibit more hydrophobic central cores compared to lightly PEGylated NPs. As PEG content increases in the polymer, it becomes more segregated to the surface of the NPs during the fabrication process which allows, to a certain extent, to improve drug solubility in the core of the NPs. On the other hand, the increased density of the PEG layer on the surface of the NP impedes to some extend curcumin release during the encapsulation process during release experiments as observed in our experimental data. These points are further discussed in light of release and diffusion study results (Section 3.4).

6.4.4 Curcumin release and stability studies.

Release studies were carried out using the same initial curcumin content in NPs over 1 week. Because quantity of encapsulated curcumin in pure PLA NP was so small, it was not possible to dose any release with the detection method used (UV absorbance). This formulation was removed from the release studies. Fig. 6a shows representative release profiles of curcumin from NPs suspended in PBS supplemented with SDS and ascorbic acid at 37°C. Acid Ascorbic was used as an anti-oxidant to prevent curcumin degradation [30] and SDS was added to increase the solubility of curcumin in the aqueous media and ensure sink conditions [31]. Release profiles followed trends independently of the PEG content in the NPs (Fig. 5a). During the first 24 h of release, a fast increase of curcumin concentration is observed followed by an exponential decrease over more than 48 h to reach the detection limit of curcumin released. The apparent decrease of curcumin concentration is due to its degradation by oxidation besides the presence of ascorbic acid. Curcumin is known to be unstable in several aqueous media with a degradation of 90% in 30 min in PBS 100mM [4, 32].

In order to quantify curcumin degradation during the release studies, degradation kinetics were quantified in the same media than release studies, at two different concentrations. In these conditions, the degradation kinetics showed a first order degradation rate with a constant kd equal to 0.01h-1 (see Fig. S1) and a degradation of 50% after 3 days at 37°C. With the purpose to obtain more insights on the effect of polymer architecture and PEG content on curcumin release, a simple diffusion-degradation model was fitted to the experimental data (Eq. 3) [33].

$$\frac{Mt}{M\infty} = \exp(-k_d \cdot t) - \frac{6}{\pi^2}\sum_{n=1}^{\infty}\frac{1}{n^2}\cdot\exp\left(-\frac{D\cdot n^2\cdot\pi^2\cdot t}{r^2}\right) \quad \text{(Eq. 3)}$$

where Mt and M are the released mass of curcumin at time t and time infinite respectively, D is the diffusion coefficient of curcumin in the NPs and r is the NP radius (see Table S1 for the list of calculated modelling parameters). The first term in the equation accounts for the degradation of curcumin while the second term models the Fickian diffusion of the drug from spherical particles. [34] We ensured that the assumptions of the diffusion model, namely: 1) Perfect sink conditions of curcumin in release media, 2) Solubility concentration higher than drug concentration within the NP matrix, 3) No swelling, degradation, surface and bulk erosion of the copolymer during the release timeframe, were verified experimentally. As mentioned already, sink conditions were fulfilled thanks to SDS addition which increases curcumin solubility in the release media [31]. TEM pictures were examined and DSC analyses were performed to identify the presence of any crystallized areas in the NPs, which could suggest that curcumin concentration was higher than its solubility in the NP. It was found that the polymeric matrix was homogenous and no fusion peak appeared on the DSC thermograms, suggesting curcumin solubilisation in the polymeric matrix (data not shown). Moreover, encapsulated curcumin has no apparent effect on polymer thermal properties (tg) and thus their organization within the NPs (Fig. S3). Right after the release experiments, absence of polymer degradation and bulk erosion in curcumin-loaded NP material were verified by GPC and DLS size measurements respectively (data not shown) supporting a model for which drug diffusion is the limiting factor of the release. This is not unexpected as it has been reported previously that erosion plays a minor role in drug release from diblock polyesters-PEG NPs. [35]

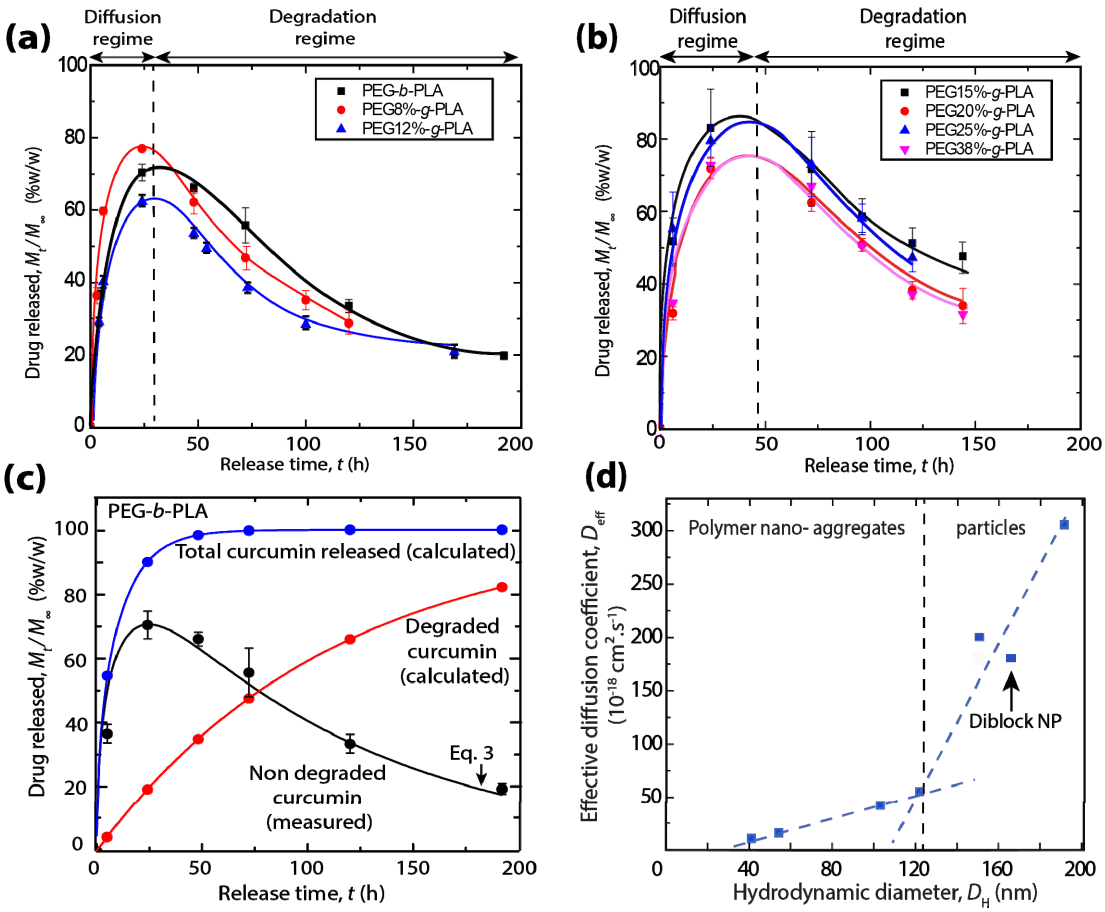

Figure 6.6. Representative release profiles of curcumin at 37°C from **(a)** solid NP and **(b)** "micelle-like" or "polymer nano-aggregate" NPs. **(c)**. Modelling of curcumin release from diblock NPs, showing the evolution with time of the purely diffusive and drug degradation contributions. **(d)**.Dependence of the drug diffusion coefficient *D* obtained using Eq. 3 on NP size.

Equation 3 was used to obtain the diffusion coefficient of curcumin in the NPs. The diffusion coefficient (D) was set as the sole free parameter. It was then possible to estimate the theoretical curcumin release without its degradation (Fig. 6c top curve). Results revealed that the diffusion coefficient in the largest NPs was about 10 times higher than in the smallest NPs (Fig. 6d). One possible explanation in the difference between the diffusion constant of the different particle batches could be linked to the surface density and thickness of PEG outside layer creating a diffusion barrier to the very hydrophobic curcumin molecule in the smaller particles. Peracchia et al. were the first to report a slowing down of the drug release from

polymeric NP having a surface PEG coating. Moreover, they showed that this effect was surface PEG density and PEG chain length dependent [35]. Another explanation could come from the internal structure differences between particles of different size. For instance, porosity may be higher in large particle compared to nanoparticles favouring hydration of the particle core and release of their content [36]. This hypothesis is also in agreement with Budhian et al. who measured a higher diffusion coefficient of haloperidol encapsulated in 1.3 μm PLA/PLGA micro-particles (without PEG chains corona) compared to 450 nm NPs and to 220 nm NPs [24]. On the other hand, diffusion through the polymer matrix can be favoured by low polymer tg or by a molecularly dispersed drug as seen by DSC for all the NPs tested.

The PEG content and polymer architecture play a role not only in the determination of NP structure but on drug encapsulation and release. The drug release profiles (Fig 6a and b) and diffusion constants as calculated during release modelling show two regimes, related in part to the size of the NP (Fig 6d). They are also related to the NP morphologies observed, i.e. solid particles (NP made with comb-polymers with low PEG content) and polymer nano-aggregate particles (NP made of comb-polymers with high PEG content and diblock polymer) (see Fig. S4, plotting Deff against polymer PEG content). Relatively large but "soft" diblock NPs appear in an intermediate position in term of drug diffusion (Fig. 6d), highlighting the role of polymer architecture.

6.4.5 In vitro studies.

6.4.5.1 Cytotoxicity studies

To test the protective properties of the curcumin-loaded NPs against oxidative stress, we performed two separate tests using resazurin test and LDH assay respectively. Resazruin test allows the monitoring of cell proliferation and metabolism, while LDH assay monitors change in cell membrane integrity.

Di-block NP (5% PEG w/w), comb-polymer PEG-g-PLA at 8 and 38% PEG content (%w/w) were tested in cell culture model as representative of solid particle and nano-aggregate NP batches. Resazurin test, a cell proliferation assay confirmed the absence of

adverse effects on cell proliferation and metabolism in the range of tested concentrations for both blank and curcumin-loaded particles (Fig. 7a and b). In the presence of hydrogen peroxide (Fig. 7c), cell survival was reduced by 40% and 20% with blank NPs and Cur-NP, respectively.

These results demonstrate that encapsulated curcumin was efficient to protect cells against hydrogen peroxide oxidative stress. But on the other hand there is only a partial preservation of cell proliferation and metabolism upon addition of curcumin-loaded NP. Moreover, we found no clear dose-response relationship showing an increase of cell proliferation and metabolism upon addition of higher curcumin dose. This result could be put in perspective with the curcumin release kinetic in regard on the condition of the assays performed here, as discussed in the following section.

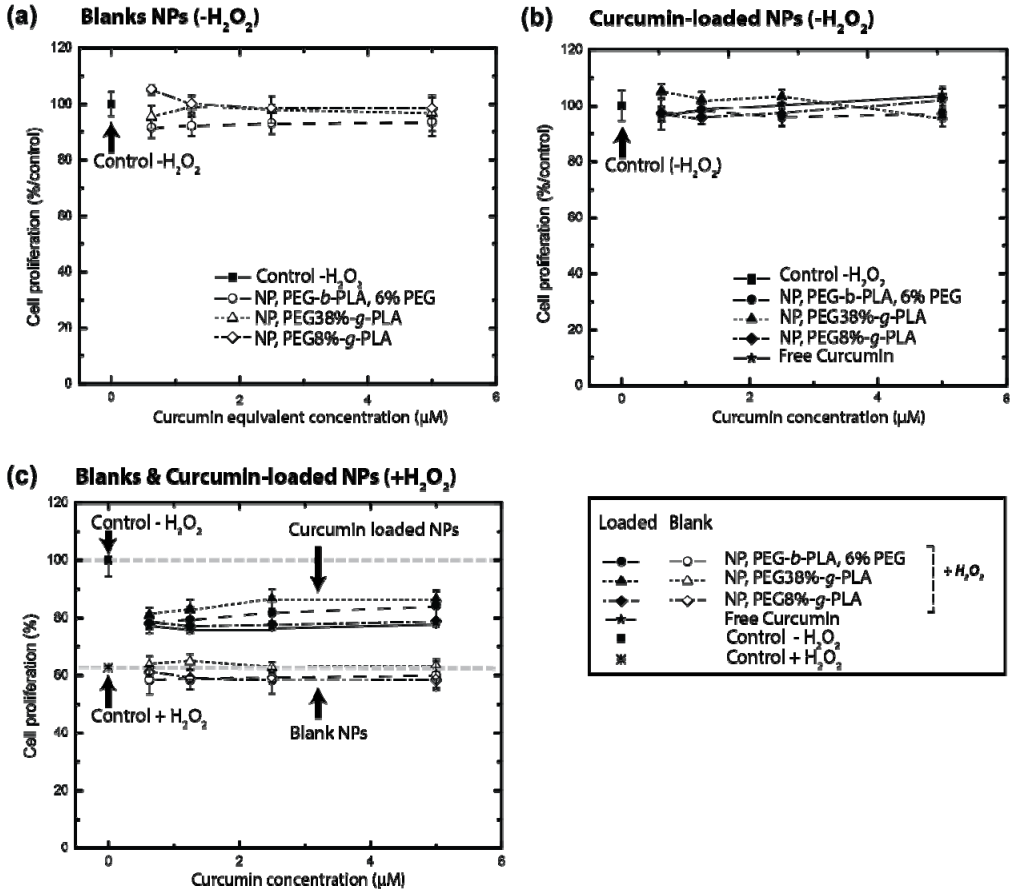

Figure 6.7. Cytotoxicity as assessed by the Rezasurin – cell viability assay of blank NPs (a) and curcumin-loaded NPs (b) on SK-N-SH neuronal cells. Panel (c) shows Rezasurin – cell proliferation assay in presence of H_2O_2 (250μM) in the medium. Particle concentrations were adjusted to curcumin concentrations (or equivalent for blank NP): For blank NP, abscises are expressed in curcumin concentration for comparison purpose. Practically, an equivalent quantity of drug-loaded NP in blank NP are added for each curcumin concentration levels

LDH assays did not reveal any evidence of cytotoxicity for blank (Fig. 8a) and curcumin-loaded NPs (Fig. 8b) of any batches of NPs on neuronal cell line SK-N-SH. These tests demonstrate that, independently of their size, polymer architecture and PEG content, the NPs under study are clearly not cytotoxic to neuronal cells.

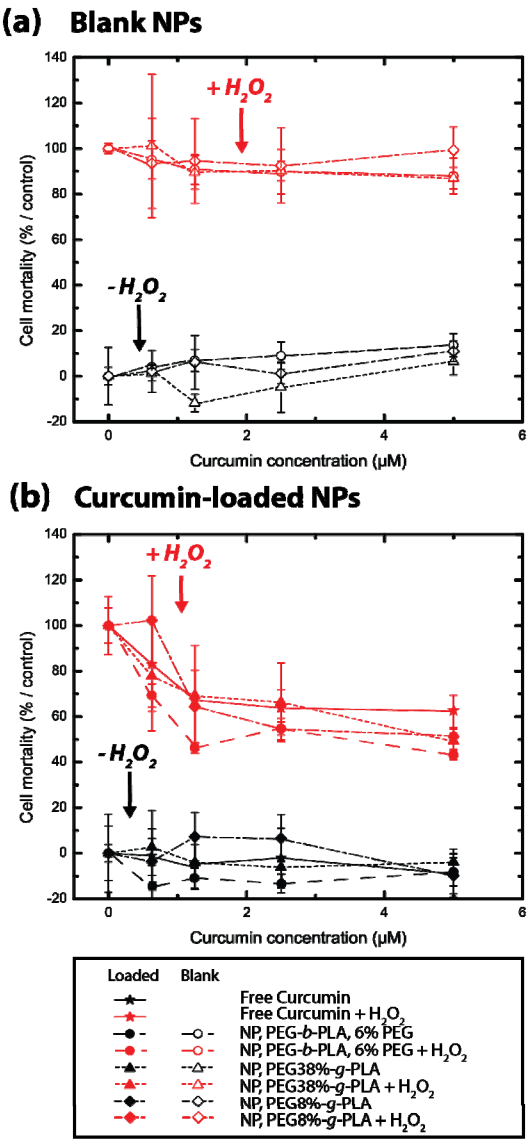

Figure 6.8. Relative LDH release assay (cell mortality assay). **(a)** Controls experiments with blank NP **(b)** Curcumin-loaded NP with (symbol in red) or without (symbol in black) addition of H_2O_2 in the medium. The level of LDH release induced by H_2O_2without treatment has been considered as 100%. For blank NP, abscise is expressed in curcumin concentration for comparison purpose. Practically, an equivalent quantity of drug-loaded NP in blank NP are added for each curcumin concentration levels

In assays involving addition of H2O2, as expected, an increase in cell mortality (measured by LDH released in the medium) is observed in controls experiments (Fig. 8).

Noteworthy, NP toxicity was not exacerbated by induction of oxidative stress upon addition of H2O2 in the medium (Fig. 8a). The addition in the media of the blank NP did not affect the release of LDH in the media (Fig. 8a). This indicates that NP themselves are not able to counteract cell mortality induced by hydrogen peroxide. This is an important control as seemingly non-specific effect of blank NP has been reported and attributed to the properties of NP to carry serum proteins to the cells in culture and induce change in cell proliferation and mortality [37].

On the other hand, curcumin-loaded NP appeared to have a significant effect under the tested conditions (Fig. 8b), particularly for the di-block NP (5% w/w PEG). However the magnitude of the effect is comparable to free curcumin added to the media (no statistical differences between the groups, $p>0.05$)

6.4.5.2 Reactive Oxygen Species production and inhibitions

The direct measurement of intracellular ROS was performed by DCF fluorescence dosage. The control experiments with blank NP show little or no effect on intracellular ROS concentration (Fig. 9a). No statistically significant scavenging effect was observed for blank particles (upper curves in Fig. 9a). On the other hand, curcumin-loaded NPs showed a dose-response decrease on intracellular ROS levels (Fig. 9b). At the highest tested concentrations, di-block loaded NP and polymer nano-aggregate loaded particles were able to restore ROS level to a level comparable to untreated cells, while loaded solid NPs (PEG8%-g-PLA) appear to be less efficient to counteract the elevation of ROS (Fig. 9b). The di-block and nano-aggregate NP were found to be as effective as free curcumin, as no statistically significant difference between free curcumin, curcumin-loaded di-block or polymer nano-aggregate particles were found (Fig. 9b). The difference in effects of each curcumin-loaded NPs batches on ROS levels (Fig. 9b, may arise from the size of the NP, the rate of release, site of release (extra or intracellular release) and the possible interaction with cells.

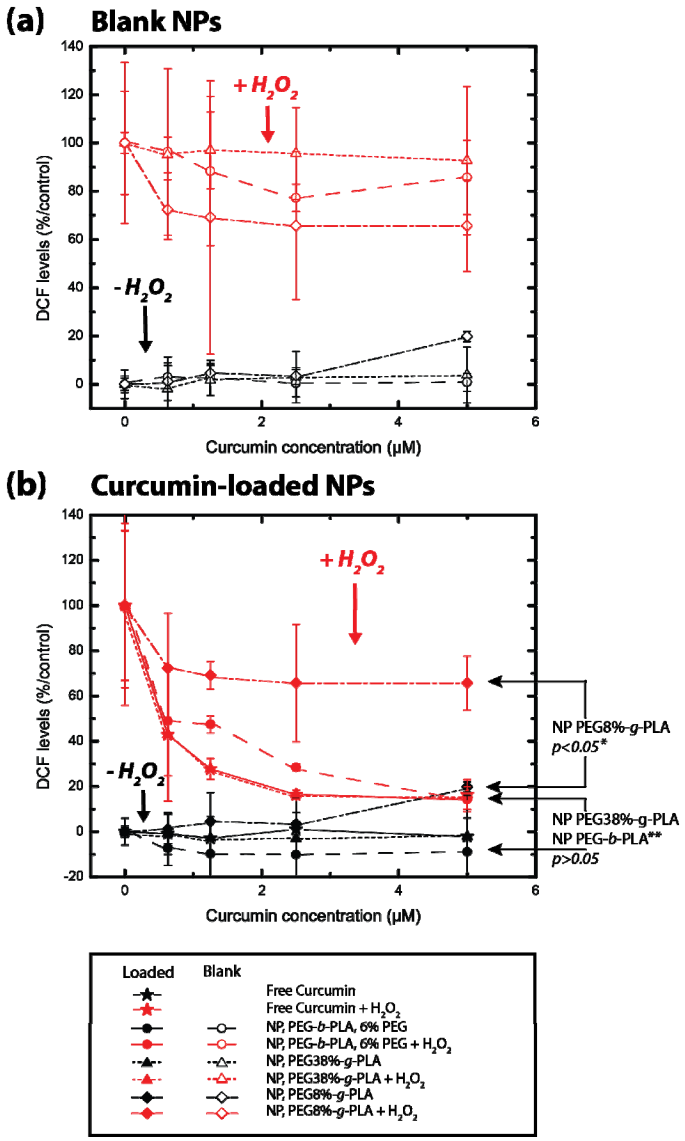

Figure 6.9. Relative intracellular levels of ROS (a) Control experiments with blank NP (blank NP concentration equivalent to concentration of curcumin-loaded NP) without addition of H2O2 (black symbol) or with H2O2 (250μM added to the medium). (red symbol); (b) Treatment experiments: Level of ROS as determined by DCF detection in response to treatment with curcumin-loaded NP without addition of H2O2 (black symbol) or with H2O2 (250μM added to the medium). (red symbol) The level of ROS induced after H2O2 addition without treatment has been considered as 100%

All these results should be correlated to the kinetic of drug release by these NPs. Figure 6a shows a superior release for high PEG content NP compared to low PEG content NP. A faster release of curcumin should translate into greater scavenging effect considering the conditions of these experiments. Within the time frame of the experiment (1 h) the curcumin dose encapsulated into the NP is only partially released (about 25 to 35% of the dose as seen in Fig. 6a and 6b), limiting its scavenging effect. Moreover the released content is exposed to degradation in the medium and the cytosol, decreasing the effective dose at a given time point.

The polymer architecture controls the drug release (as seen in section 3.4 "Curcumin release and stability studies") and modulates exposure of curcumin to ROS (Fig 9). In spite of PEG-b-PLA NPs and PEG38%-g-PLA NPs differences in hydrodynamic diameters and PEG content, they appear as effective to decrease intracellular ROS levels. On the other hand, PEG-b-PLA and PEG8%-g-PLA NPs with similar size and similar PEG content show large difference in scavenging efficacy.

6.4.5.3 Polymeric NP toxicity

Induction of oxidative stress effects by NPs has been reported mostly for silica or metal oxides NPs (inorganic) as well as carbon nanotubes and carbon particulates generated by pollution. The type of stress reported can go from damages to proteins by reactive NPs surface, to the generation of oxygen reactive species or the depletion of the medium from antioxidant molecules [38]. Even if these effects were reported for organic NPs [10, 22, 39], few studies on polymeric NP toxicity address this issue. In the conditions of the test, however, we did not detect any effect of di-block and polymer nano-aggregate NPs, either blank or drug-loaded on the generation of intracellular ROS (Fig. 9b). A minor effect on ROS level is observed for solid NP (NP made from PEG8%-g-PLA) at the higher dose (5µM curcumin or equivalent) as seen on Fig. 9a and 9b. This effect on ROS levels is not correlated with cell mortality as shown in Figure 8a and 8b depicting LDH release in the medium and its origin is unknown at this time.

6.4.5.4 Discussion summary

This work showed the intimate relationship between the polymer architecture, block composition and the biophysical properties of the resulting NPs. We previously identified a transition of physio-chemical properties of NP made of PEG branched PLA around 15% PEG content (w/w) [20]. In this study, drug encapsulation and release properties are found to also follow this trend as shown by encapsulation results (Fig. 4), release profiles (Fig. 6) and notably biological effects (Fig. 9). The increase of PEG content is related to an increase in LE (Fig. 4). On the other side, PEG-b-PLA diblock with a 6% PEG content showed a higher LE than PEG8%-g-PLA comb polymer illustrating the role of architecture. The drug release profiles (Fig. 6a, 6b) and diffusion constants show two regimes, related in part to the size of the NP (Fig. 6d) and the NP morphologies observed, i.e. solid particles (NP made with comb-polymers with PEG content <15%) and polymer nano-aggregates (NP made of comb-polymers with PEG content >15% and diblock polymer). Relatively large but "soft" diblock NPs appear in an intermediate position in term of drug diffusion coefficient (Fig. 6d), highlighting again the role of polymer architecture on the NPs inner structure and fluidity. Finally, polymer architecture controls and modulates exposure of curcumin to ROS and thus antioxidant activity. Diblock polymer and high PEG content comb polymers appeared to be the most efficient to reduce oxidative stress (Fig 9). In this study we have limited our investigation to copolymers of PEG 2kD chains and hydrophobic PLA backbones of almost constant molecular weight. The information we gathered from the comb-like polymers library in comparison to diblock PEG-b-PLA and PLA only suggest that both PEG content and polymer architecture (i.e. the position at which PEG chains are attached to the hydrophobic backbone) play a role in the NP properties. PEG content appears determinant for particle size, while architecture seems determinant for the structural organization of the particle (solid NPs vs nanoaggregates) This aspect was extensively discussed in a previously published work describing the polymer synthesis and characterization of blank NPs [20]. All together these results contribute to shed light on new approaches to design efficient polymer-based drug carriers.

6.5 Conclusion

A library of PEGylated grafted PLA polymers were used in order to establish correlations between physico-chemical properties of the NPs and curcumin encapsulation and release properties of the said particles. A structural transition, described previously for several particle properties, located around 15 % PEG content (% w/w) and suggesting a transition from a solid particle regime to a micelle-like behaviour, was also found for release properties of curcumin. This transition initially identified in term of structural properties, seems related to changes in encapsulation and release properties of loaded curcumin as well.

Release studies and mathematical modelling of curcumin taking into account degradation was designed to fit the experimental data and to estimate the real release. Cell-based assays support the non-toxicity of the particles to neuronal cell lines. Moreover, oxidation scavenging effects of curcumin-loaded NP show the potential benefit of those formulations for oxidative-stress-related CNS diseases. Di-block and micelle like NP were found as effective as free curcumin in the condition of the experiments. However, NP formulation may prove to be superior on long term effect thank to their protective effect on curcumin and slow release properties. This aspect will be address in future studies. PEGylated polymeric particle may also have therapeutic benefit by themselves in AD by their effect on amyloid aggregation [40]. This assumption has to be clarified by further studies in our system. Lastly, another point to be explored is the optimization of the blood brain barrier crossing of different formulation with the view to develop in vivo assays.

ASSOCIATED CONTENT

Supporting Information. TEM images, Curcumin degradation kinetics, table of modelling parameters and DSC results. This material is available free of charge via the Internet at http://pubs.acs.org.

AUTHOR INFORMATION

Corresponding Author

* E-mail : ; Fax : (+1) 514-343-2470; Tel. (+1) 514-343-2102;

Author Contributions

The manuscript was written through contributions of all authors. All authors have given approval to the final version of the manuscript. ‡These authors contributed equally.

Notes. Authors declare no competing financial interest

ACKNOWLEDGMENT

JMR wish to thank the "*Fonds de Recherche du Québec – Nature et Technologie*" (Québec, Canada) and the Faculty of pharmacy of the Université de Montréal for doctoral fellowships. XB acknowledges the support of Canada Research chair program of the government of Canada, PH acknowledges FRQ-NT funding and CR support from "*Chaire de recherche Louise et André Charron sur la maladie d'Alzheimer"* of INRS-Institut Armand-Frappier, Laval, Québec, Canada. Technical assistance of Johanne Habr in encapsulation studies as well as the help of Soudeh F. Tehrani in polymer synthesis are acknowledged. TEM imaging was performed at the Centre de Caractérisation Microscopique des Matériaux (CM^2) of the École Polytechnique (Montréal, QC, Canada) with the help of Jean-Philippe Massé.

REFERENCES

1. Patel, M.M., et al., *Getting into the Brain: Approaches to Enhance Brain Drug Delivery.* CNS Drugs, 2009. **23**(1): p. 35-58 10.2165/0023210-200923010-00003.
2. Rabanel, J.M., et al., *Drug-loaded nanocarriers: passive targeting and crossing of biological barriers.* Current Medicinal Chemistry, 2012. **19**(19): p. 3070-102.
3. Sahni, J.K., et al., *Neurotherapeutic applications of nanoparticles in Alzheimer's disease.* J Control Release, 2011. **152**(2): p. 208-31.
4. Wang, Y.-J., et al., *Stability of curcumin in buffer solutions and characterization of its degradation products.* Journal of Pharmaceutical and Biomedical Analysis, 1997. **15**(12): p. 1867-1876.
5. Mathew, A., et al., *Curcumin loaded-PLGA nanoparticles conjugated with Tet-1 peptide for potential use in Alzheimer's disease.* PLoS One, 2012. **7**(3): p. e32616.
6. Belkacemi, A., et al., *Challenges associated with curcumin therapy in Alzheimer disease.* Expert Reviews in Molecular Medicine, 2011. **13**: p. null-null.

7. Zensi, A., et al., *Albumin nanoparticles targeted with Apo E enter the CNS by transcytosis and are delivered to neurones.* J Control Release, 2009. **137**(1): p. 78-86.
8. Taylor, M., et al., *Effect of curcumin-associated and lipid ligand-functionalized nanoliposomes on aggregation of the Alzheimer's Abeta peptide.* Nanomedicine, 2011. **7**(5): p. 541-50.
9. Gastaldi, L., et al., *Solid lipid nanoparticles as vehicles of drugs to the brain: current state of the art.* Eur J Pharm Biopharm, 2014. **87**(3): p. 433-44.
10. Doggui, S., et al., *Neuronal Uptake and Neuroprotective Effect of Curcumin-Loaded PLGA Nanoparticles on the Human SK-N-SH Cell Line.* Journal of Alzheimer's Disease, 2012. **30**(2): p. 377-392.
11. Mulik, R.S., et al., *ApoE3 Mediated Poly(butyl) Cyanoacrylate Nanoparticles Containing Curcumin: Study of Enhanced Activity of Curcumin against Beta Amyloid Induced Cytotoxicity Using In Vitro Cell Culture Model.* Molecular Pharmaceutics, 2010. **7**(3): p. 815-825.
12. Tsai, Y.-M., et al., *Curcumin and its nano-formulation: The kinetics of tissue distribution and blood–brain barrier penetration.* International Journal of Pharmaceutics, 2011. **416**(1): p. 331-338.
13. Kreuter, J., *Drug delivery to the central nervous system by polymeric nanoparticles: What do we know?* Advanced Drug Delivery Reviews, 2014. **71**(0): p. 2-14.
14. Andrieux, K. and P. Couvreur, *Polyalkylcyanoacrylate nanoparticles for delivery of drugs across the blood–brain barrier.* Wiley Interdisciplinary Reviews: Nanomedicine and Nanobiotechnology, 2009. **1**(5): p. 463-474.
15. Hrkach, J., et al., *Preclinical Development and Clinical Translation of a PSMA-Targeted Docetaxel Nanoparticle with a Differentiated Pharmacological Profile.* Science Translational Medicine, 2012. **4**(128): p. 128ra39.
16. Calvo, P., et al., *Quantification and localization of PEGylated polycyanoacrylate nanoparticles in brain and spinal cord during experimental allergic encephalomyelitis in the rat.* Eur J Neurosci, 2002. **15**(8): p. 1317-26.
17. Wohlfart, S., S. Gelperina, and J. Kreuter, *Transport of drugs across the blood–brain barrier by nanoparticles.* Journal of Controlled Release, 2012. **161**(2): p. 264-273.
18. Hillaireau, H. and P. Couvreur, *Nanocarriers' entry into the cell: relevance to drug delivery.* Cell Mol Life Sci, 2009. **66**(17): p. 2873-96.
19. Rabanel, J.-M., P. Hildgen, and X. Banquy, *Assessment of PEG on polymeric particles surface, a key step in drug carrier translation.* Journal of Controlled Release, 2014. **185**(0): p. 71-87.
20. Rabanel, J.-M., et al., *Effect of Polymer Architecture on the Structural and Biophysical Properties of PEG-PLA Nanoparticles.* ACS Applied Materials and Interfaces, 2015. **7**(19): p. 10374–10385.
21. Neises, B. and W. Steglich, *Simple Method for the Esterification of Carboxylic Acids.* Angewandte Chemie, International Edition in English 1978. **17**(7): p. 522-524.
22. Doggui, S., et al., *Curcumin protects neuronal-like cells against acrolein by restoring Akt and redox signaling pathways.* Molecular Nutrition & Food Research, 2013. **57**(9): p. 1660-1670.
23. Shive, M.S. and J.M. Anderson, *Biodegradation and biocompatibility of PLA and PLGA microspheres.* Adv Drug Deliv Rev, 1997. **28**(1): p. 5-24.

24. Budhian, A., S.J. Siegel, and K.I. Winey, *Haloperidol-loaded PLGA nanoparticles: Systematic study of particle size and drug content.* International Journal of Pharmaceutics, 2007. **336**(2): p. 367-375.
25. Gou, M., et al., *Curcumin-loaded biodegradable polymeric micelles for colon cancer therapy in vitro and in vivo.* Nanoscale, 2011. **3**(4): p. 1558-1567.
26. de Gennes, P.G., *Polymers at an interface; a simplified view.* Advances in Colloid and Interface Science, 1987. **27**(3–4): p. 189-209.
27. Gref, R., G. Miralles, and É. Dellacherie, *Polyoxyethylene-coated nanospheres: effect of coating on zeta potential and phagocytosis.* Polymer International, 1999. **48**(4): p. 251-256.
28. Panyam, J., et al., *Polymer degradation and in vitro release of a model protein from poly(D,L-lactide-co-glycolide) nano- and microparticles.* J Control Release, 2003. **92**(1-2): p. 173-87.
29. Letchford, K., R. Liggins, and H. Burt, *Solubilization of hydrophobic drugs by methoxy poly(ethylene glycol)-block-polycaprolactone diblock copolymer micelles: Theoretical and experimental data and correlations.* Journal of Pharmaceutical Sciences, 2008. **97**(3): p. 1179-1190.
30. Mayol, L., et al., *Curcumin loaded PLGA–poloxamer blend nanoparticles induce cell cycle arrest in mesothelioma cells.* European Journal of Pharmaceutics and Biopharmaceutics, 2015. **93**(0): p. 37-45.
31. Tønnesen, H.H., *Solubility, chemical and photochemical stability of curcumin in surfactant solutions. Studies of curcumin and curcuminoids, XXVIII.* . Pharmazie, 2002. **57**(12): p. 820-4.
32. Oetari, S., et al., *Effects of curcumin on cytochrome P450 and glutathione S-transferase activities in rat liver.* Biochemical Pharmacology, 1996. **51**(1): p. 39-45.
33. Siepmann, J. and F. Siepmann, *Mathematical modeling of drug delivery.* International Journal of Pharmaceutics, 2008. **364**(2): p. 328-343.
34. Arifin, D.Y., L.Y. Lee, and C.-H. Wang, *Mathematical modeling and simulation of drug release from microspheres: Implications to drug delivery systems.* Advanced Drug Delivery Reviews, 2006. **58**(12–13): p. 1274-1325.
35. Peracchia, M.T., et al., *PEG-coated nanospheres from amphiphilic diblock and multiblock copolymers: Investigation of their drug encapsulation and release characteristics.* Journal of Controlled Release, 1997. **46**(3): p. 223-231.
36. Sant, S., V. Nadeau, and P. Hildgen, *Effect of porosity on the release kinetics of propafenone-loaded PEG-g-PLA nanoparticles.* J Control Release, 2005. **107**(2): p. 203-14.
37. Hussien, R., et al., *Unique growth pattern of human mammary epithelial cells induced by polymeric nanoparticles.* Physiological Reports, 2013. **1**(4): p. n/a-n/a.
38. Møller, P., et al., *Role of oxidative damage in toxicity of particulates.* Free Radical Research, 2010. **44**(1): p. 1-46.
39. Aranda, A., et al., *Dichloro-dihydro-fluorescein diacetate (DCFH-DA) assay: A quantitative method for oxidative stress assessment of nanoparticle-treated cells.* Toxicology in Vitro, 2013. **27**(2): p. 954-963.
40. Brambilla, D., et al., *PEGylated nanoparticles bind to and alter amyloid-beta peptide conformation: toward engineering of functional nanomedicines for Alzheimer's disease.* ACS Nano, 2012. **6**(7): p. 5897-908.

7 Discussion générale

La première partie de cette discussion portera sur les synthèses et les caractérisations des polymères synthétisés pour cette étude (Chapitre 4 et 5). Dans une seconde partie, nous nous attacherons à discuter les déterminants possibles de la morphologie et les propriétés de surface des particules obtenues en fonctions de l'architecture des polymères synthétisés. Les expériences étudiant les propriétés de surface (adsorption de protéine, microcalorimétrie) seront aussi discutées en regard des propriétés des polymères (Chapitre 4). Enfin, les effets de l'architecture sur l'encapsulation et la libération d'un principe actif hydrophobe seront analysés (Chapitre 6). Les limites et les questions encore en suspens soulevées par ces travaux seront mises en évidence.

Comme il est mentionné dans l'introduction, la majorité des travaux concernant les systèmes de livraison polymériques de médicament, portent sur des copolymères en blocs linéaires. Quelques études plus récentes ont mis en évidence l'intérêt d'architectures alternatives, telles que les copolymères en blocs en étoiles ou les copolymères branchés, dits « en peigne » ou « en brosse ». Quelques études se sont intéressées à des polymères « peigne » constitués d'une chaîne principale hydrophile sur laquelle des groupements hydrophobes variés sont greffés pour essentiellement des applications de modification de surface. La situation inverse, c'est-à-dire une chaîne principale hydrophobe avec des chaînes pendantes hydrophiles, neutres ou de type polyélectrolytes a également été très étudié [1]. L'utilisation de ce type de polymère pour des applications en nanoformulation est cependant peu fréquente et notre groupe est un des rares laboratoires à avoir étudié ce type de structure pour la préparation de NPs à usage thérapeutique [2-4].

7.1 Synthèse de copolymères « en peigne »

Les approches de synthèses de copolymères polyesters branchés (« en peigne ») que nous avons proposées et mises en œuvre sont des évolutions de l'approche développée précédemment dans le laboratoire du Pr Patrice Hildgen [4]. Cette méthode reposait sur une synthèse en trois étapes soient, 1) la copolymérisation par ouverture de cycle (ROP) du

dilactide avec l'allyle glycidyl éther, 2) la modification par oxydation de la fonction allyle pendante en fonction carboxylique et enfin 3) le greffage de méthoxy-PEG (mPEG-OH) par l'intermédiaire de la fonction hydroxyle [4]. Deux limitations avaient été identifiées dans cette stratégie, soient, le nombre d'étapes de synthèse d'une part et d'autre part l'incidence des conditions de synthèses sur l'intégrité de la chaîne de polyesters.

7.1.1 Insertion de groupes pendants par l'utilisation du benzyle glycidyl éther

Au point de vue du contrôle des conditions de synthèse, le problème le plus important était d'éliminer les étapes d'oxydation de la fonction allyle (Figure 1.4). Pour cela nous avons choisi d'introduire dans la chaîne des fonctions pendantes directement disponibles pour des réactions de greffage ou modifiables dans des conditions qui ne soient pas dommageables pour les liaisons esters de la chaîne principale. La première modification a donc été d'introduire un nouvel époxy substitué, le benzyle glycidyl éther (2-[(benzyloxy)méthyl]oxirane) pour obtenir un polyester-co-éther avec des groupes latéraux benzyloxy. Le groupe benzyloxy est facilement retiré par hydrogénation catalytique pour faire place à un groupement hydroxyle, qui peut être utilisés pour des réactions d'estérification. L'avantage principal de cette approche est de s'affranchir des étapes d'oxydation qui se traduisaient par une diminution des masses molaires des chaînes de PLA. La déprotection des fonctions hydroxyles est une réaction douce qui ne conduit pas à des variations des masses molaires (Table 4.1). Dans une dernière étape les chaînes de méthoxy-PEG-COOH (mPEG-COOH,) sont greffées sur les groupes hydroxyles disponibles (Scheme 4.1). De façon générale cette approche permet un meilleur contrôle du produit final.

La taille de la chaîne principale

La problématique avec l'utilisation du PLA comme matériel de base est son caractère hydrophobe et sa dégradation très lente [5]. Ceci a des conséquences sur la vitesse et le contrôle de la libération des molécules actives. Les tailles de chaîne visées ont été choisies pour avoir une dégradation assez rapide afin d'obtenir une libération des molécules actives

dans une fenêtre de temps compatible avec l'efficacité du traitement. Cependant il faut noter qu'en fait ces deux processus ne sont pas forcément reliés. En effet, comme il a été constaté dans le Chapitre 6, la libération de la curcumine s'est révélée complète alors même que les poids moléculaires des polymères formant les NPs n'avaient pas significativement changés. Le contrôle de la taille s'est effectué par le contrôle du ratio de catalyseur ($SnOct_2$)/monomère [6]. La stratégie de synthèse initiale n'était pas compatible avec l'utilisation de chaînes de petites tailles (15-25 kD) à cause des phénomènes de dégradation liés à l'oxydation nécessaire de la fonction allyle. Le contrôle de la taille des chaînes polyesters-co-éthers se complique du fait que le ratio des deux monomères, glycidyl éther et dilactide dans le milieu réactionnel a lui aussi une influence sur les poids moléculaires obtenus. Une décroissance de la taille des chaînes est observée avec l'augmentation de la quantité du monomère glycidyl éther (Figure 7.1). Cette décroissance suit une apparente fonction exponentielle. Elle a été aussi observée par d'autres pour des copolymérisations similaires [7, 8].

Les niveaux d'insertion du second monomère glycidyle éther.

On observe également que l'efficacité d'insertion des chaînes pendantes diminue avec l'augmentation du ratio initial du monomère glycidyl éther / acide lactique. On aurait pu s'attendre à ce que le glycidyl éther ayant un cycle à 3 atomes qui est plus tendu, soit plus réactif qu'une lactone ayant un cycle à 6 atomes et donc soit efficacement inséré dans la chaîne en train de grandir.

L'insertion des monomères glycidyl éther dans la chaîne durant la polymérisation par ouverture de cycle se ferait par un mécanisme impliquant deux centres métalliques (deux molécules du catalyseur $SnOct_2$) et impliquerait un transfert de chaîne et l'interruption de l'élongation d'une des deux chaînes (*Jean-Richard Bullet et coll.*, manuscrit en préparation). Cette hypothèse est basée sur l'observation d'une diminution de la taille des chaînes avec l'augmentation du ratio initial glycidyl éther/acide lactique, alors que le taux de conversion du dilactide reste à peu près constant, quel que soit ce ratio.

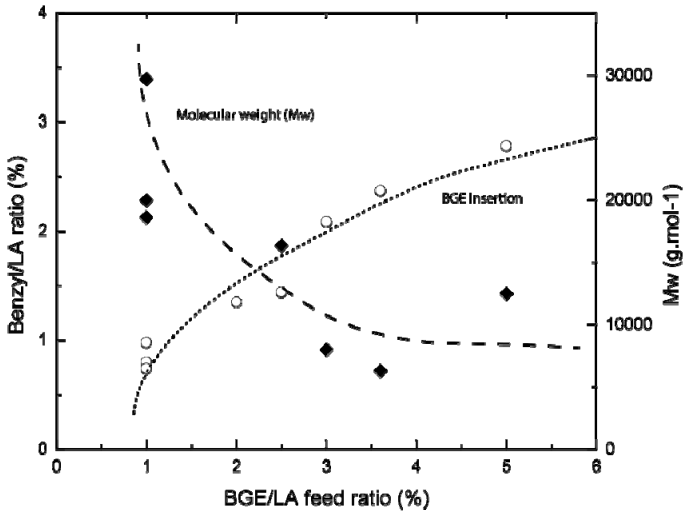

Figure 7.1. Niveau d'insertion du BGE (en % molaire du monomère acide lactique) et poids moléculaire du copolymère en fonction de la quantité initiale de BGE dans le milieu réactionnel.

L'indice de dispersion de taille

La dispersité de tailles des polymères obtenus est relativement élevée (>1,2) par rapport à d'autres types de synthèses de polymère plus contrôlées (<1,1). Ceci peut être également dû à l'étape de copolymérisation et son mécanisme réactionnel discuté plus haut. Cette dispersité peut avoir un effet sur la taille et les propriétés des particules formées. Cet effet peut être amplifié à la suite du greffage du PEG. En effet, les plus petites chaînes polyesters seront plus affectées dans leur poids, leurs propriétés de solubilité et leur caractère amphiphile que les chaînes plus importantes. Cette remarque est surtout valide pour les étapes de greffage susceptibles de se produire non seulement sur les fonctions latérales (« pendantes »), mais aussi sur les terminaisons des chaînes principales.

7.1.1.1 Greffage du PEG par acylation

La première stratégie de greffage utilisée a été de préparer des mPEG-COOH par oxydation et de procéder par acylation (Chapitre 4, Scheme 4.1). Cette procédure bien que simple s'est avérée assez peu efficace, pour obtenir des taux de greffage élevés, probablement en raison de la difficulté à sécher adéquatement les différents éléments. Cette méthode ne nous

a pas permis d'obtenir des copolymères avec un contenu en PEG au-delà de 15 % en poids, avec des rendements de greffage de l'ordre de 25 à 30% par rapport aux sites de greffage disponibles. Une analyse rétrospective de nos protocoles a aussi mis en évidence la présence de stabilisants, tels que des alcools, dans les solvants chlorés utilisés dans les réactions, qui pouvaient interférer dans l'efficacité du greffage.

7.1.1.2 Greffage par couplage DCC/DMAP

Une seconde approche de greffage sur les hydroxyles disponibles sur la chaîne de OH-*g*-PLA a été de tester les couplages par l'intermédiaire du dicyclohéxylcarbodiimide (DCC) [9]. Cette approche s'est révélée beaucoup plus satisfaisante au point de vue de l'efficacité de greffage (>90%). Les taux de greffage (nombre de chaînes de PEG par chaîne) se sont retrouvés plus élevés. Outre les groupes hydroxyles terminaux des groupes pendants latéraux (alcools primaires), il apparaît dans notre analyse que l'alcool secondaire à l'extrémité de la chaîne de PLA a aussi été modifié par la réaction de couplage. Ceci est conforme au mécanisme d'estérification des acides activés par le DCC avec les alcools primaires et secondaires [9].

7.1.2 Insertion de groupes pendants pour le greffage par chimie clic

Cette dernière approche de synthèse de copolymères en peigne repose sur la copolymérisation du dilactide avec le glycidyl propargyle éther en vue d'obtenir un polyester-co-éther avec des groupes pendants latéraux possédant un groupement alcyne terminal. L'alcyne terminal de la chaîne latérale est par la suite mis à profit pour greffer par cycloaddition catalysée par le cuivre (CACC) un Méthoxy-PEG-azide (mPEG-N_3).

L'avantage de cette approche par rapport à la précédente est la diminution du nombre d'étapes de synthèse. Une autre différence importante est l'impossibilité de greffage de chaînes de PEG sur les extrémités des chaînes de PLA. Le fait d'avoir des chaînes de PEG greffées uniquement latéralement a des conséquences directes sur l'architecture des copolymères et donc l'organisation des particules. Cet aspect est discuté dans la section 7.2 en regard des résultats obtenus avec les autres architectures.

Tout comme pour l'insertion lors de la copolymérisation du BGE, on peut faire les mêmes constatations quant à la dépendance de l'efficacité d'insertion du GPE par rapport au ratio initial (GPE/AL). De façon similaire on constate également une diminution du poids moléculaire des chaînes de PLA obtenues lorsque ce ratio augmente [8].

7.2 Types de particules et structure interne

La synthèse d'une libraire de polymères branchés avec des contenus en PEG variant de 0 à 50% (poids/poids) a permis la fabrication des lots de particules avec des caractéristiques variables. De nombreux systèmes ont été conçus pour préparer des nanotransporteurs polymériques et pour l'encapsulation d'une grande variété de molécules actives. L'originalité de notre étude est d'avoir étudié de façon systématique une série ***continue*** de copolymères. Cette série est ***continue*** du fait qu'elle est constituée d'un élément central à peu près constant (la chaîne principale hydrophobe) substitué par des chaînes de PEG et ayant un contenu en PEG variant de 0 à 45 % (poids/poids). Ceci est obtenu par un nombre variable de blocs hydrophiles de même taille sur les différents lots de polymères préparés (Chapitre 4) ou par un nombre variable de blocs hydrophiles ayant des tailles différentes (Chapitre 5). Cette étude systématique a permis de mettre en évidence la possibilité de fabriquer des particules ayant des caractéristiques morphologiques (Chapitre 4 et 5), d'encapsulation et de libération de molécules actives, variables (Chapitre 6). Elle nous a permis de montrer quelques propriétés spécifiques à l'architecture choisie en comparaison avec des copolymères dibloc et les copolymères de OH-*g*-PLA ou alcyne-*g*-PLA (polyesters-co-éther avec groupes latéraux hydroxyles ou alcynes, mais sans chaînes de PEG greffées), qui sont les matériaux de référence.

7.2.1 Méthodes de préparation des nanoparticules

Pour la majorité de ces travaux, nous avons retenu la méthode de préparation par nanoprécipitation avec des paramètres contrôlés afin d'isoler les facteurs de variations dus aux polymères seuls. Du fait de la présence de blocs hydrophobes et hydrophiles, les copolymères utilisés sont des macromolécules amphiphiles dont les propriétés dépendent de la taille des

chaînes de PEG (blocs hydrophiles), de la taille de la chaîne principale (bloc hydrophobe), du contenu total en PEG et finalement de l'architecture (les points de branchements des PEG).

Le choix de cette méthode a été guidé par sa simplicité de mise en œuvre, la possibilité d'adapter facilement la taille de lot et par la possibilité de faire varier plusieurs paramètres facilement. Le choix a aussi été guidé par la possibilité de s'affranchir de l'utilisation de surfactants ou autres stabilisants stériques qui auraient pu s'absorber sur la surface des particules et sont très difficiles à éliminer [3]. Cette absence est indispensable pour les analyses de surface (mesure de charge de surface, RMN et XPS en particulier). C'est aussi un aspect important afin que la taille et la morphologie des particules obtenues soient directement reliées aux propriétés des copolymères utilisés. Entre autres, nous avons écarté la méthode par émulsion/évaporation de solvant en raison de l'utilisation de PVA qui persiste en quantité non négligeable malgré les lavages intensifs [3, 10].

Des étapes de purification par dialyse sont néanmoins nécessaires pour éliminer l'acétone, le PEG résiduel non lié ainsi que les plus petites chaînes de polymères. Ce dernier point est appuyé par l'augmentation observée des M_n et M_w entre le copolymère brut et le copolymère provenant de lots de nanoparticules dialysées et lyophilisées.

Par ailleurs des essais avec les procédés de « nanoprécipitation flash » et de « microfluidique » ont été réalisés sur les polymères obtenus par chimie clic et leur efficacité ont été comparées (Chapitre 5). Dans la mesure du possible, nous nous sommes efforcés de comparer les méthodes en utilisant des paramètres les plus proches possible (concentrations de polymères, vitesse de mélange, ratio de phase). Un tableau comparatif des trois méthodes basé sur les informations trouvées dans la littérature et les résultats obtenus ici (Chapitre 5) résume les avantages et limitations de chaque méthode (Table 7.1). De façon surprenante, tel que mentionné plus haut (Chapitre 5), les distributions de taille, obtenue par DLS, sont apparues plus homogènes par le procédé de nanoprécipitation classique qu'en nanoprécipitation flash et microfluidique (dans cet ordre). La raison n'est pas comprise pour le moment, il pourrait s'agir d'un résultat spécifique à ce type de copolymère en peigne, car c'est plutôt l'effet inverse qui a été rapporté jusqu'à maintenant pour les particules lipidiques ou les particules faites de polymères diblocs [11, 12]. Avec nos matériaux, l'avantage de ces méthodes est probablement

plus dans la diminution des tailles des particules et une meilleure robustesse interopérateur ou interlaboratoire que dans l'obtention de lots plus homogènes.

Table 7.1. Comparaison des méthodes de préparation des NPs

Méthodes	Mise en oeuvre	Avantage	Inconvénients
Nanoprécipitation classique	Simple injection Dispersion rapide sous agitation	Rapidité Peu de matériel	Difficulté pour mettre à l'échelle Contrôle des conditions du mélange Reproductibilité
Nanoprécipitation « flash »	Chambre de mélange avec une géométrie bien définie Collision des deux phases	Mise à l'échelle facile Contrôle des paramètres	
Microfluidique	Microcanaux gravés dans des puces de Poly(diméthylsiloxane) Mélangeur chaotique	Possibilité de faire des lots très petits Fabrication rapide de bibliothèques de particules Contrôle (taille et PD) et reproductibilité Mise à l'échelle ("chips" ou microplaquettes en parallèle)	Concentration en polymère peut être limitée Polydispersité élevée Coût des puces Compatibilité des solvants avec les matériaux

7.2.2 Méthodes analyses structures internes

7.2.2.1 La Cryo-MET

Les principales évidences concertant les différences structurales et morphologiques nous ont été données par les expériences en cryo-MET. La technique de cryo-MET est une technique de microscopie électronique à transmission sur des échantillons de particules, déposés sur une grille et refroidis par l'azote liquide. Cette technique doit être distinguée de la

cryo-MET dans laquelle l'échantillon est vitrifié dans un milieu liquide et imagé dans son milieu de suspension congelé [13]. La technique que nous avons employée est plus simple à mettre en œuvre pour des échantillons très sensibles à la chaleur, cependant les informations fournies ne sont pas de la même nature. En effet, les morphologies observées sont celles de particules immobilisées et séchées sur le support de carbone ce qui peut provoquer des déformations importantes. Ceci est particulièrement vrai pour des systèmes qui s'organisent en fonction de leur milieu, tel que des micelles ou des agrégats. L'image peut ne pas refléter l'aspect de la particule en suspension, son état natif hydratée. Par ailleurs, malgré le faible contraste fourni par les nanoparticules polymériques, nous avons pu obtenir des images sans colorations positives ou négatives ou agents de contraste qui contribuent à des artefacts. Ceci est intéressant du point de vue de l'étude morphologique, la plupart des images MET de NPs rapportées dans la littérature ont été réalisées par exemple en présence de sels de métaux lourds.

7.2.2.2 Nanoparticule, micelle et agrégats

La série de polymères possède une continuité de contenu en PEG de 0 à 45%, mais les caractéristiques morphologiques des NP présentent un changement brusque, une discontinuité, vers 15% PEG. Cette discontinuité morphologique est visible pour la première bibliothèque de copolymère et reflète celle déjà observée en DLS pour les tailles (Chapitre 4 et 6). On observe une transition des particules solides vers des agrégats de type « pseudo-micellaires ». Les agrégats sphériques produits par les copolymères blocs (le plus souvent des structures diblocs) ont été nommés « micelles polymériques» par analogie avec les micelles résultant de l'association de petites molécules de surfactant [14]. Ils ont été nommés particules de type pseudo-micellaire (« micelle-like ») ou micelle-gelée («frozen-micelle ») du fait également de leur analogie structurale de type « cœur-couronne » avec les micelles de surfactants [15]. Elles ont également été nommées « crew-cut micelle » par opposition à des « hairy micelles » [16-18], étant caractérisées par un bloc hydrophile plus petit que le bloc hydrophobe constituant le cœur de la particule.

Cependant ces objets ne peuvent pas, à l'instar des micelles, être considérés comme des structures dynamiques. En effet, les échanges de chaînes entre les agrégats sont très lents

au point qu'en certains cas les chaînes polymériques peuvent être considérées comme « cinétiquement piégées » [19]. Ceci peut s'expliquer principalement par l'insolubilité dans l'eau du bloc hydrophobe du copolymère. La pénalité entropique associée à l'extraction de la chaîne de la particule, la traversée de la couronne hydrophile et la création d'une interface avec l'eau est si considérable que les échanges d'unimères (les molécules de copolymère faisant partie de la structure particulaire « pseudo-micellaire ») ne sont pas mesurables en pratique [20]. De fait, il a été proposé de réserver le nom de micelle aux seuls systèmes dynamiques, tandis que le vocable « nanoparticules » recouvrirait tous les autres types de particules, matricielle solide, agrégat, etc. [21].

Cependant les résultats obtenus dans l'article de recherche 1 (Chapitre 4), montrent qu'une distinction doit être faite entre les structures des nanoparticules obtenues, en fonction de la quantité de blocs hydrophiles présente dans le copolymère. L'observation en MET de particules « molles » (structure aplatie, contours moins définis) lorsque les ratios de PEG dépassent 15% (poids/poids) montre l'existence de structures clairement distinctes des particules solides obtenues avec des ratios de PEG plus faibles (Chapitre 4, Figure 4.2). Nous avons opté donc pour une appellation neutre d'agrégats polymères (« polymer nano-aggregate ») [22].

La transition d'un type de structure à l'autre est très sensible à une faible variation de contenu en PEG aux alentours de la concentration critique. Cette transition est plus brutale que pour les diblocs de chimie similaire pour lesquels on observe une décroissance exponentielle de la taille des particules quand la fraction hydrophobe du dibloc diminue [23]. Cette transition peut être attribuée à l'effet de la structure du polymère en peigne (vs en bloc linéaire) présentant plus de contraintes stériques pour l'arrangement des chaînes. Le passage d'un type de structure à l'autre se traduit aussi dans des modifications des capacités d'encapsulation et de libération d'un actif modèle hydrophobe, la curcumine, cet aspect est discuté plus loin (section 7.5).

Les variations de morphologies des agrégats micellaires en fonction de la taille relative des différents blocs ont été largement étudiées par Adi Eisenberg *et coll.* notamment sur les PAA-PS copolymères [18]. Si l'asymétrie des blocs et ses effets sur la taille et la morphologie

des particules ont été étudiés; peu d'études se sont penchées sur l'effet du contenu en PEG, de copolymère avec une architecture alternative aux polymères linéaires constitué d'un nombre variable de blocs hydrophiles de taille identique.

7.2.2.3 Arrangement des chaînes

L'arrangement spatial que prennent les chaînes et les branches d'un polymère pendant le processus de fabrication et dans le milieu de dispersion a été très peu étudié, surtout lorsque l'objet considéré est de taille nanométrique. Il est le plus souvent considéré comme une simple transposition des phénomènes que l'on retrouve dans un film de polymère. Cependant on constate que malgré une absence d'organisation régulière, les NPs possèdent des propriétés reproductibles et qui leur sont propres [24]. Ceci implique l'existence d'une organisation supramoléculaire des blocs polymères. Par analogie avec les micelles, un type d'organisation possible est la séparation cœur hydrophobe/couronne hydrophile. Ce modèle est à nuancer, pour deux raisons. L'une est la problématique de l'échelle de taille entre les chaînes de polymères et les tailles de particules. Si la taille des particules est beaucoup plus grande que les chaînes de polymères en extension maximale, il n'est pas possible d'envisager que tous les blocs hydrophiles se retrouvent confinés dans la couronne externe de la particule. L'autre raison est donnée par un autre résultat important qui est la répartition des chaînes de PEG dans les particules entre la fraction localisée en surface et celle encore piégée à l'intérieur, telle que démontrée par les analyses de RMN ^{1}H quantitatives.

Répartition du PEG dans la structure de la particule

Nos résultats montrent que les pourcentages de PEG piégé à l'intérieur de la particule (non observable en RMN) varient autour de 25% du PEG total, pour des particules préparées avec des polymères ayant des contenus en PEG de 15% et plus en poids. Ceci a été aussi décrit pour des diblocs de type PEG-*b*-PLA en utilisant d'autres techniques [23, 25].

Ces taux sont moindres pour les particules solides préparées avec des polymères en peigne avec des taux de PEG 8-15%. On peut présumer qu'en fonction de la taille, la surface, l'architecture du PEG, il y a un maximum de chaînes de PEG qui peuvent être insérées en surface. Tout ajout se traduit par soit une augmentation de la quantité de PEG à l'intérieur de

la particule soit par une diminution de taille des particules (pour augmenter la surface totale disponible).

La polydispersité des tailles varie avec le type de particule obtenue. Celle-ci est moindre dans le cas des particules présumées « solides » (0,1 et moins). Elle est par contre plus élevée dans le cas des particules de types « micellaire » (0,1 à 0,3). Cette dispersion de taille peut potentiellement être reliée à la dispersion des tailles des polymères : les polymères les plus PEGylés (avec les fractions massiques de PEG les plus importantes) sont également les polymères dont les PDI sont les plus élevés (Chapitre 4, 5). Elle doit certainement jouer un rôle dans la structuration des NTP, mais cet aspect n'est pas aisément accessible à l'analyse.

7.2.2.4 Rôle du type de greffage

Un résultat intéressant est l'influence du type de greffage sur la morphologie des NPs obtenues. Tel que décrit dans la Figure 4.2(a) (Chapitre 4), les NPs préparées à partir de copolymères obtenus par acylation ont des diamètres plus élevés et plus stables sur une plus grande plage de contenu en PEG que les NPs préparées à partir de copolymères obtenus par couplage DCC/DMAP. L'évolution de ces dernières se rapproche de la situation décrite par Riley *et coll.* pour les diblocs [23]. Nous faisons l'hypothèse que ceux-ci, compte tenu des taux de PEG observés, ont vu l'alcool secondaire terminal de leur chaîne de PLA estérifié par un mPEG-COOH, leur conférant une architecture se rapprochant des diblocs.

Un cas limite est celui de deux lots de polymères avec des contenus massiques en PEG équivalent (9% environ) qui résultent dans des particules de tailles et de morphologie très différentes (Figure 7.2). La taille de la chaîne PLA est légèrement différente, mais du même ordre de grandeur et ne peut expliquer à elle seule cette différence. Cette observation renforce l'hypothèse que les greffages en bout de chaîne jouent un rôle pour modifier le comportement du copolymère en solution et lors de son assemblage pour le rapprocher de celle des diblocs.

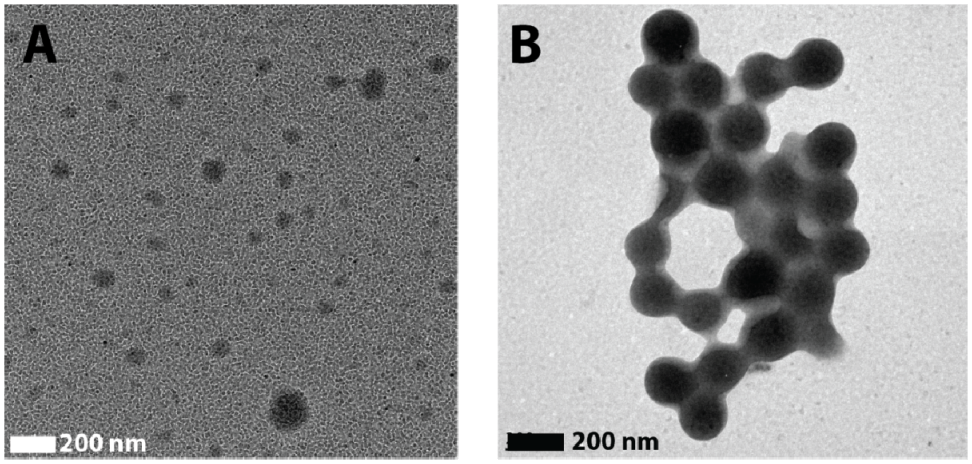

Figure 7.2. Comparaison de deux lots de nanoparticules produits avec des lots de polymères ayant des contenus en PEG (% poids/poids) identiques, mais obtenus par des méthodes de greffage différentes (A) Greffage par la réaction DCC/DMAP, (B) Greffage par Acylation.

Les copolymères obtenus par greffage par chimie clic ne peuvent avoir de chaîne de PEG que latérales, et de fait on constate que les particules formées sont plutôt du type solide telles qu'observée en MET, avec un diamètre particulaire qui varie peu sur une large gamme de contenu en PEG (Chapitre 5). La structure et les propriétés physicochimiques ont été évaluées dans les deux cas afin de vérifier l'impact du procédé de fabrication sur la structure, l'hypothèse de travail étant que la nature du solvant, la vitesse de transfert vers la phase externe ont un effet sur l'organisation des chaînes. La seule différence notable entre les différents procédés est celle de la taille.

7.2.2.5 Rôle des méthodes de préparation

Au point de vue de la préparation des NPs, du fait que le bloc hydrophobe du copolymère n'est pas soluble dans l'eau, les phénomènes d'autoassemblage en milieu aqueux (méthode de préparation par dialyse ou film) ne peuvent se produire, les particules sont plutôt fabriquées par nanoprécipitation. L'assemblage doit se produire dans un milieu hétérogène caractérisé par le retrait du solvant organique qui « gèle » les chaînes de copolymère et la structure sous forme d'une NP. Ces particules ne sont pas à l'équilibre thermodynamique [21].

La préparation des particules par différentes méthodes, nanoprécipitation, nanoprécipitation « flash » et microfluidique (Chapitre 5) montre que les différences restent principalement au niveau de la taille. Cet effet est relié à la rapidité du mélange des deux phases. En effet lorsque le débit augmente dans une méthode on observe une relation inverse avec la taille des particules, qui a tendance à diminuer. Ceci est valide pour les différentes méthodes. Par ailleurs, l'organisation interne et de surface ne semble pas grandement affectée par la méthode de préparation des NPs, notamment les densités de PEG en surface. Les diminutions de taille qui induisent des augmentations de surface dans la nanosuspension sont compensées par des effets sur l'organisation des chaînes de polymères.

7.2.3 Micellisation de copolymères bloc non-linéaires.

De façon générale, la taille et le nombre de chaînes dans une particule micellaire sont dépendants de la taille du bloc hydrophobe, plus que de la taille du bloc hydrophile. De façon générale, l'augmentation de la taille du bloc hydrophobe diminue la CMC, tandis que l' augmentation de la taille du bloc hydrophile conduit à la diminution du nombre d'agrégations et donc à la taille. Or dans notre système le premier est relativement constant, alors que le second varie grandement (de 0 à 50% en poids de polymère constitué de PEG). Cependant, une interprétation des changements de taille basée sur la longueur des blocs hydrophobes et hydrophiles n'est probablement pas valide du fait de la complexité de l'architecture des polymères. Dans notre cas, la longueur des chaînes hydrophiles est constante (PEG 2kD) c'est plutôt leur nombre par bloc hydrophobe qui varie.

Peu d'études se sont intéressées à l'organisation des chaînes de copolymère bloc non linéaire dans une particule. Une série d'études sur des polymères en étoiles (« miktoarm star polymer ») nous donne cependant quelques indications sur les effets de l'architecture sur le processus de micellisation. De façon générale, les particules produites à partir de copolymères bloc non linéaires, (Figure 7.3A), montrent une décroissance du nombre d'agrégation et de taille lorsque comparées aux particules préparées avec un dibloc linéaire équivalent en poids moléculaire [26, 27]. Certaines des variations de structures étudiées par ces auteurs (Figure 7.3A) ont des ressemblances avec nos propres polymères (Figure 7.3B).

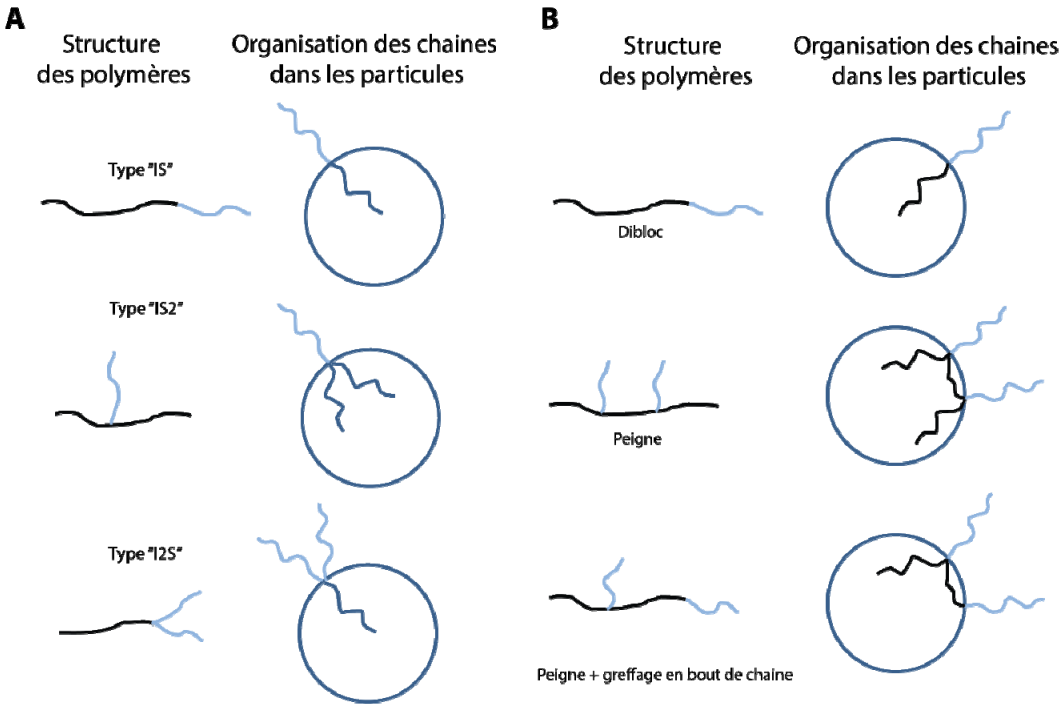

Figure 7.3. (A) Micellisation de polymères étoilés tel que décrit par [27]; (B) Arrangements hypothétiques des copolymères décrits dans cette étude en fonction de leur architecture (dibloc, strictement « en peigne » ou encore « en peigne », mais additionné d'un greffage en bout de chaîne).

Les positions des points d'ancrage des blocs qui forment la couronne externe de la particule ont une influence sur l'aire occupée (« footprint ») par cette chaîne à la surface du cœur de la particule. Cette aire est supérieure dans le cas de structure de type IS2 à celle de diblocs linéaires (IS) équivalent (Figure 7.3A). Ceci peut s'expliquer par les contraintes sur la chaîne polymérique formant le cœur de la particule, pour adopter cette disposition. Ceci peut avoir des conséquences en termes de densité de surface des chaînes polymériques constituant la couronne de la particule, mais aussi en termes de taille de la particule. On peut aussi supposer que cela peut influencer le nombre de chaînes nécessaire pour obtenir une particule stable (Nombre d'agrégations), donc d'influer sur la taille de la particule.

7.2.4 Microscopie en Faisceau d'Ions Focalisé / Microscopie Électronique à Balayage (FIB-SEM).

Les observations en microscopie bimode (faisceau d'ions et faisceau électronique) ont également nourri la réflexion sur l'organisation structurale des NPs. Cette technique encore inédite dans l'analyse de la structure interne des NP à usage pharmaceutique permet moyennant une destruction partielle de la particule par un faisceau d'ions de Gallium (voir en annexe un schéma de l'appareil), un accès à la structure interne de la particule par microscopie électronique à balayage [28]. Une brève description de la méthodologie est disponible en annexe avec les résultats discutés ici (données non encore publiées).

Les images les plus intéressantes ont été obtenues avec des particules de 300 à 500 nm (exemple en Figure 7.4 et en Annexe 5) sur des particules fabriquées à partir de copolymères avec un contenu modéré en PEG (5, 9 et 11% poids/poids) et traitées au préalable par une fine couche de platine *in situ*. Dans les essais préliminaires, nous avons été limités sur deux fronts. D'abord, la taille des particules inférieures à 300 nm les rend difficiles à capturer sur image, car elles sont facilement déplacées par le faisceau ionique et du fait de leur moindre résistance au traitement thermique. Nous n'avons pas obtenu d'images exploitables de particules dibloc, un polymère avec environ 6% de PEG. Les particules préparées avec ce copolymère apparaissaient complètement aplaties en MEB.

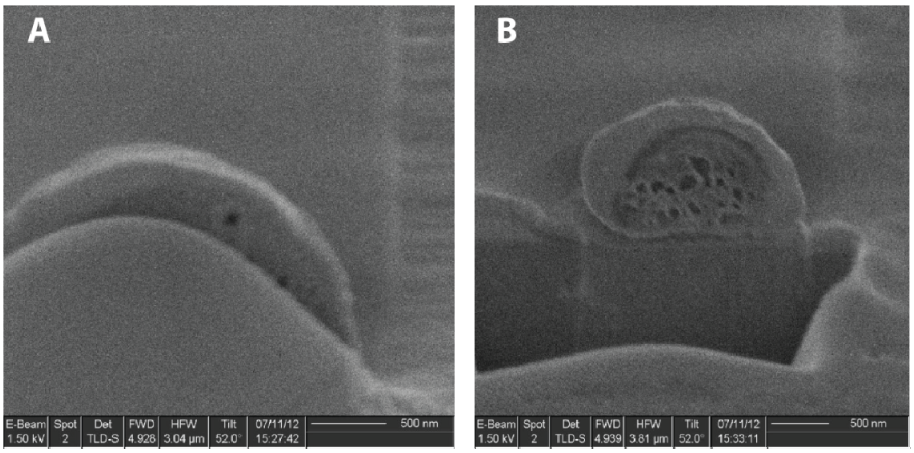

Figure 7.4. Exemple de découpe de nanoparticules (500 nm-1µm). (A) et (B) Vues de côté (angle de 51°) en microscopie électronique à balayage. (Images réalisées au Laboratoire de Microfabrication, École Polytechnique, Montréal avec l'aide de Mme MH Bernier).

Les observations préliminaires montrent des variations de densité électroniques de la tranche de la particule indiquant des variations de composition chimique. Ceci confirme une certaine organisation des copolymères. Les particules plus petites apparaissent plus homogènes (Figure A5.5) bien que possédant elles aussi des cavités. Les particules de 1 à 5 µm ont d'autres caractéristiques telles que des domaines zones sphériques de densités électroniques qui différent du reste de la particule (Figure A5.6).

Les particules examinées étaient dans le domaine des particules « solides ». Cette technique n'apparaît pas adéquate pour des objets de type « agrégats de polymères » du fait de leur faible rigidité. Par exemple, il n'a pas été possible d'examiner la structure interne des particules de type dibloc PEG-PLA, très sensibles au faisceau électronique. Les résultats semblent confirmer l'existence d'une organisation générale cœur-couronne. De plus dans le cœur de la particule on observe des vésicules et des domaines de densité électronique différente. Tout ceci est valide pour des particules de taille de quelques centaines de nanomètres. Cela reste à confirmer pour des tailles plus petites, car la structure interne peut aussi dépendre de la taille.

7.3 Propriétés des surfaces

7.3.1 Analyse de surface : densité de surface du PEG

Malgré les nombreuses études, une utilisation quasi universelle en nanotechnologie (y compris pour des produits commerciaux), en deux décennies d'utilisation il n'y a pas de consensus sur la densité, la conformation et épaisseur de la couche de PEG nécessaire pour obtenir un effet furtif optimal et un ciblage efficace. De plus on constate un manque généralisé de méthodes fiables pour caractériser directement les surfaces et quantifier de manière précise le PEG en surface [29].

La problématique de l'analyse de la densité de greffage de PEG en surface de nanoparticules peut être résumée de la façon suivante (Figure 7.5).

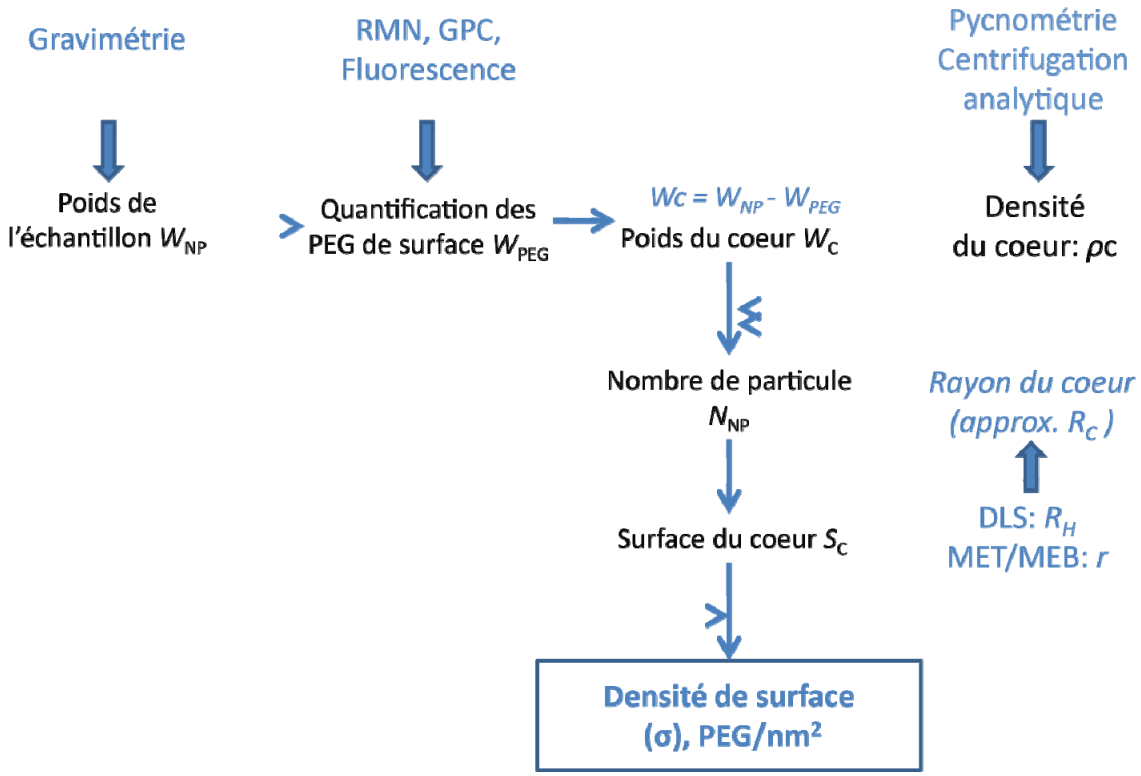

Figure 7.5. Étapes et données nécessaires à la détermination de la densité de PEG en surface

Les modèles de calcul ont été développés et se retrouvent d'une part dans la section « Supporting information » de l'article de revue [29] (voir Annexe 1) et dans le Chapitre 4 [22]. Sans revenir de façon détaillée sur la discussion des différentes problématiques de détermination de ces densités de surface, nous voudrions souligner ici quelques points clés.

Le premier est l'obtention de la taille du cœur de la particule (R_C). Au premier abord la détermination de la taille d'un objet semble la propriété la plus facile à mesurer. Cependant, à un niveau analytique sa mesure est extrêmement difficile à obtenir de façon exacte à l'échelle nanométrique.

La mesure de taille est obtenue de façon routinière par DLS qui donne un diamètre hydrodynamique. Les analyses de tailles sont complétées habituellement par des analyses MEB, MET ou AFM [30]. Il y a une différence importante entre les deux méthodes : dans un cas on mesure le rayon hydrodynamique, la particule hydratée dans un milieu liquide, dans l'autre cas on observe une particule déshydratée dans le vide et parfois (MEB) recouverte

d'une couche métallique. La mesure du rayon hydrodynamique par DLS est basée sur une répartition en intensité, qui donne un biais en faveur d'une taille moyenne plus élevée que la réalité de l'échantillon, les particules les plus grosses diffusant plus la lumière que les plus petites [31]. Cette différence est faible si l'indice de polydispersité est faible, mais existe dans tous les cas.

Ces techniques sont relativement adaptées à la mesure du rayon de la particule. Mais pour déterminer une densité de surface, on se doit de mesurer le diamètre du cœur de la particule, la surface à partir de laquelle les chaînes de PEG se détachent de la particule. Celui-ci sera plus accessible par microscopie électronique, la couche de PEG étant très peu dense aux électrons et n'est habituellement pas détectable. Cependant cela nécessite le traitement d'un nombre important d'images avant d'obtenir des résultats statistiquement valides.

Les autres problématiques sont reliées à la détermination exacte de la masse d'une particule, la détermination de sa densité et les moyens de quantifier le nombre de particules en solution.

Calcul de l'aire occupée par une chaîne de PEG

Le calcul de l'aire occupée par une chaîne de PEG est le calcul de la densité de surface. Ce calcul dépend d'une bonne estimation de la surface de la particule. Ici le rayon de courbure de la particule joue un rôle dans ces calculs.

(A) Si la hauteur L de la couche de PEG en surface n'est pas négligeable en regard du diamètre hydrodynamique de la particule, on a le rayon du cœur R_C différent de R_H et le volume occupé par la chaîne de PEG ressemblera à un cône tronqué (Figure 7.6). L'aire occupée au niveau du cœur de la particule sera différente de l'aire occupée au niveau du rayon hydrodynamique de la particule. Si la méthode de mesure repose sur R_H on sous-estimera la densité de PEG (la densité est inverse de l'aire occupée par chaîne) en surface du cœur de la particule.

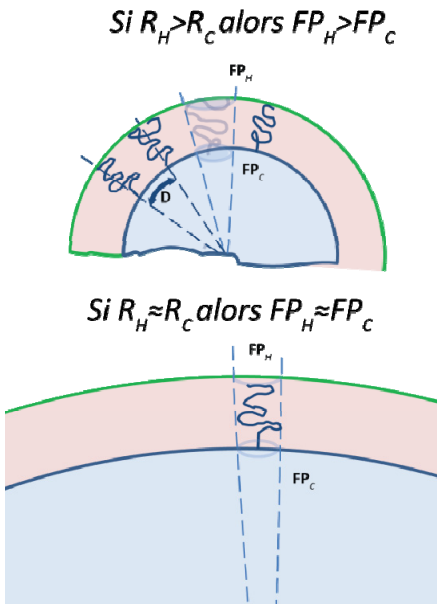

Figure 7.6. Empreinte (« Footprint ») d'une chaîne de PEG, calculée depuis le rayon hydrodynamique (FP_H) ou le rayon du cœur de la particule (FP_C).

Pour illustrer cette problématique, voici un bref exemple numérique. Si on considère que la densité de PEG est telle que cette couche représente 5 nm d'épaisseur. Pour une particule d'un R_H de 50 nm (si on fait l'approximation que R_H est donné par la mesure DLS), cela veut dire que le R_C est de 45 nm. La différence de surface pour une particule ($Surface\ sphère = 4\pi r^2$) :

Surface hydrodynamique, S_H avec R_H =50 nm, S_H=31415 nm^2

Surface du cœur, S_C avec R_C =45 nm, S_C=25446 nm^2

Si la densité de surface calculée sur R_H est de 1 PEG/nm^2, en fait la densité au niveau de l'attachement de la chaîne à la surface du cœur de la particule est de 1,25 PEG/nm^2

(B) Si la hauteur L de la couche de PEG est négligeable par rapport à la valeur de R_H , lors l'aire occupée par une chaîne de PEG au niveau du cœur sera équivalente à l'aire occupée au niveau du rayon hydrodynamique. Les densités calculées seront entachées de peu d'erreurs.

Estimation des densités de surface (si la valeur de R_C n'est pas disponible)

Dans notre approche du problème, nous avons grandement simplifié le système à analyser, réduit à un copolymère, sans utilisation de surfactants et de molécules actives encapsulées. Les calculs de densités de surface des chaînes de PEG dans le régime particulaire solide sont assez directs. Ceci pour une raison principale : on a accès assez facilement à la taille du cœur de la particule, la surface à partir de laquelle les chaînes de PEG sont attachées.

Les choses deviennent plus complexes dans le cas des particules dans le régime « agrégat polymérique ». Si l'on applique les mêmes calculs, on retrouve des densités de PEG en surface qui diminuent drastiquement alors que la quantité de PEG totale dans les NPs augmente et que la taille des particules diminue. Le principal problème auquel on est confronté en fait dans ce régime c'est d'avoir accès à la surface, le vrai rayon du cœur de la particule (R_C). Dans le Chapitre 4, nous avons donc opté pour une approche plus théorique basée sur les travaux de A.. Halperin [32] afin d'estimer les densités de surface à partir de nos résultats expérimentaux. A Halperin a développé une théorie capable de prédire les dimensions (R_H, R_C) de micelles préparées à partir de polymères dibloc, connaissant les caractéristiques des copolymères et de la taille du bloc hydrophile. Dans notre estimation, le copolymère peigne est assimilé à un copolymère dibloc, soit 1) comme un polymère « segmenté » alors que chaque chaîne de PEG (2kD) est associée au nombre moyen de résidus d'acide lactique par chaîne de PEG; soit 2) comme un copolymère « complètement dibloc » alors que toutes les chaînes de PEG sont combinées pour être considérées comme un seul bloc hydrophile. Les deux situations sont des situations extrêmes qui ne reflètent pas la réalité du copolymère, mais donc les calculs doivent nous donner un intervalle de densité de surface.

Le rayon hydrodynamique (R_H) et le rayon du coeur (R_C) ont donc été respectivement calculés des équations 7.1 et 7.2, en utilisant N_B, le nombre de monomères d'acide lactique dans le bloc hydrophobe, N_A le nombre de monomères de PEG et a, la taille du monomère [32]:

$$R_H = N_B^{4/5} * N_A^{3/5} * a \qquad \text{(Éq. 7.1)}$$

$$R_C = N_B^{3/5} * a \qquad \text{(Éq. 7.2)}$$

La densité de surface Γ (PEG/nm^2) peut alors être calculée de :

$$\Gamma = \frac{1}{3}\left(\frac{R_h^3}{R_0^3}\right) * \%PEG_{surf} * \%PEG_{total} * \rho_{pol} * \frac{6.022\ 10^{23}}{M_{w\,PEG}} \qquad \text{(Éq. 7.3)}$$

Dans laquelle $\%PEG_{surf}$ est le pourcentage du PEG total présent à la surface de la NP; $\%PEG_{total}$ est le contenu en PEG dans le polymère (% w/w); ρ_{pol} est la densité massique du polymère et M_{wPEG}, le poids moléculaire de la chaîne de PEG. Comme l'équation 7.3 le montre, il y a un rôle prépondérant pour la taille de la NP au détriment du contenu en PEG. Cependant la taille de la NP dépend de la quantité de PEG. Lors de la transition autour de 15%, avec le passage d'un régime de particule solide à un régime d'agrégat de polymère alors que l'observe une augmentation de quelques % PEG cela induit un changement drastique des tailles et des densités de surface.

7.3.2 Quantification par XPS

La technique de XPS est à la base une technique semi-quantitative. Le signal détecté (surface des pics) est proportionnel à la masse de l'élément chimique évalué (carbone, oxygène, azote pour les substances organiques), ce qui permet d'évaluer la composition chimique des premiers nanomètres sous la surface d'un solide. Une supposition très importante pour pouvoir faire des calculs est que la composition chimique ne varie pas avec la profondeur, que le volume analysé est homogène. On n'a pas le choix de faire cette présomption, mais il faut être conscient que dans le cas de matériaux structurés tels que des nanoparticules avec des interfaces cela ne reflète peut être pas la réalité même sur des épaisseurs aussi minces que 5 à 10 nm (zone analysée lorsqu'on analyse le carbone ou l'oxygène). On peut donc obtenir des surfaces de pic identiques pour des cas de répartition chimique dans la masse très différents [33]. Ceci est une des principales limites de la technique de XPS en mode quantitatif.

À noter que les informations semi-quantitatives nous sont données sur les atomes, tels que le carbone. Par la suite un facteur de correction doit être introduit pour déterminer la composition d'un mélange de substance (telle que PLA et PEG ici), pour tenir compte que la contribution du carbone à la masse de chaque substance est différente.

Les mesures XPS sont réalisées dans le vide poussé, donc sur des matériaux secs. La couche de PEG en surface se retrouve dans une organisation possiblement effondrée, dépendant sans doute de la densité de surface. L'effet du séchage sur l'organisation de la couche de PEG et sur sa quantification n'est pas connu.

7.4 Interactions surface et milieux biologiques

Afin d'obtenir des indications préliminaires sur le comportement de nos particules dans des milieux biologiques, nous avons étudié leur stabilité en fonction de la force ionique du milieu ainsi que l'absorption de protéines par l'enregistrement d'isothermes d'absorption et la microcalorimétrie sur des protéines modèles.

Le but de ces tests était de tenter de faire un lieu entre l'architecture des copolymères, l'effet de cette architecture sur la structure de la surface des NPs et les propriétés de surface qui ont une incidence sur le devenir de celles-ci en milieu biologique. Par exemple, il a été montré récemment que des chaînes de PEG en forme de dendrons avaient un effet positif sur la stabilité des particules et contribuait à diminuer l'absorption de protéines [34].

7.4.1 Stabilité des suspensions

Les surfaces des particules formées de polymères de types polyester sont normalement chargées négativement. Ceci prévient leur agrégation lorsqu'elles sont suspendues dans l'eau. Cependant l'augmentation de la force ionique, fait normalement écran aux charges de surfaces et diminue les forces de répulsion électrostatique, conduisant habituellement à de l'agrégation et ou à la floculation sous l'influence des forces attractives de van der Walls. Des surfaces possédant des chaînes polymériques neutres agissant comme "répulseur" stérique peuvent compenser pour ces effets, dans la mesure où leurs densités de surface et leurs longueurs sont suffisantes. Le but final est d'obtenir des nanosupsensions stables, à des forces ioniques habituellement retrouvées en milieu biologique isotonique (équivalent de 150 mM NaCl environ).

Comme démontré dans le Chapitre 4, les particules voient leur stabilité dans une solution saline de NaCl augmenter avec le contenu en PEG dans le polymère. Ceci nous donne une façon de classer les formulations les unes par rapport aux autres. Cela nous permet aussi

d'évaluer le rôle du contenu en PEG et l'architecture des copolymères sur la stabilité des nanosuspensions. Par contre, ces expériences ont une portée prédictive limitée du fait que la réalité des milieux biologiques est plus complexe. Dans un milieu biologique, on retrouvera des ions sodium et chlore, mais également d'autres sels, incluant des cations divalents qui peuvent avoir des effets sur nos particules chargées négativement. De plus dans les milieux biologiques se retrouvent des lipides, des protéines. Ces dernières peuvent avoir différents effets donc celui de promouvoir l'agrégation et l'assemblage des NPs entre elles.

7.4.2 Isothermes d'absorption de protéines

Une façon d'évaluer l'efficacité de la couronne hydrophile de PEG à la surface des NPs à prévenir l'opsonisation est de suivre l'absorption de protéines en fonction de la quantité de protéines dans le milieu, donc réaliser un isotherme d'adsorption.

Dans la pratique, il n'est pas aisé de faire des études sur des milieux biologiques complexes, car de nombreuses protéines coexistent (>3000 dans le plasma) et interagissent entre elles en ayant des cinétiques et des énergies d'absorption variables. Pour notre étude, nous avons testé deux protéines modèles : l'albumine, car c'est la protéine la plus abondante dans le plasma et le lysozyme, une protéine chargée positivement à pH physiologique. Dans la procédure suivie, nous avons réalisé une mesure indirecte de l'adsorption en mesurant la concentration résiduelle de protéines après exposition de la solution protéique aux NPs.

Les données expérimentales sont habituellement interprétées (détermination de la saturation et des cinétiques) en utilisant l'équation de l'isotherme de Langmuir. Cependant, il est bien établi que ce modèle suppose que les protéines s'adsorbent de façon réversible, qu'il existe un seul type de site (une seule affinité) et qu'il n'y a pas d'effet répulsif ou coopératif entre les protéines (irréaliste lorsqu'on s'approche de la situation présentant une monocouche).

Les résultats de ces analyses se trouvent dans le Chapitre 4. Les résultats d'adsorption de l'albumine bovine montrent que cette protéine est très adsorbée sur les surfaces. Ceci n'est pas surprenant, car *in vivo*, bien que très abondante l'albumine n'a pas la plus grande affinité pour les surface polymériques. D'autre part, l'albumine est chargée négativement à pH physiologique, tout comme nos particules, ce qui pourrait indiquer un rôle pour des répulsions

électrostatiques. Les polymères présentant des surfaces hydrophobes sont prompts à être opsonisés par interactions hydrophobes.

L'adsorption du lysozyme, une protéine chargée positivement, est comme prévu bien plus importante que pour l'albumine. On observe que les surfaces les plus PEGylées retiennent moins de lysozyme. On n'arrive pas à la saturation, à l'obtention d'un plateau d'adsorption. Cependant dans l'intervalle de concentration (et du temps d'incubation testé) on n'atteint pas une couverture proche de la monocouche théorique de protéine en surface. Il est à noter que les résultats pour les NPs faites de PLA et celle de PEG-*g*-PLA avec un contenu de PEG de 8% (poids) sont proches, mais que dans les deux cas les potentiels Zêta sont encore largement négatifs. Ce n'est pas le cas des NPs faites de PEG-*g*-PLA avec 28% de contenu en PEG, dont le potentiel zêta est proche de 0.

7.4.3 Microcalorimérie (ITC)

La « titration calorimétrique isotherme » (ITC) est une méthode d'analyse très puissante des interactions intermoléculaires, permettant de s'affranchir de système de marquage fluorescent ou radioactif. L'ITC mesure les échanges de chaleur associés aux interactions moléculaires à température constante. L'ITC permet de déterminer les changements d'enthalpie (ΔH), l'affinité de liaison (constante d'association (Ka)) et la stœchiométrie (n) dus à l'interaction. Les changements dans l'entropie (ΔS) et énergie libre de Gibbs (ΔG) peuvent être déterminés en utilisant l'équation 7.4:

$$\Delta G = -RT \ln Ka = \Delta H - T\Delta S \qquad \text{(Éq. 7.4)}$$

Ces différents paramètres sont liés au mécanisme de liaison entre les protéines et les surfaces que ce soient les interactions électrostatiques, les liaisons hydrogènes, les interactions hydrophobes.

Cependant, cette technique n'est pas facile à mettre au point pour mettre en évidence les interactions de protéines avec la surface de NPs. En particulier, nous avons pu montrer que cette méthode est très sensible à la présence d'acétone résiduelle ou de PEG libre en solution, résidus de la préparation des NPs par nanoprécipitation. Une purification poussée des

échantillons de NPs par dialyse ou lavages combinés avec la filtration tangentielle est essentielle.

Pour obtenir des signaux significatifs, il faut atteindre des niveaux de concentration importants de particules (10 mg/ml pour les nanoparticules de PLA de 100 nm environ). En effet, il est nécessaire d'atteindre des surfaces de liaisons très importantes, car les chaleurs résultantes des interactions des protéines avec les surfaces sont très faibles [35]. Ceci se fait au détriment de la qualité du signal, alors que ces concentrations de particules génèrent beaucoup de bruit.

D'un autre côté, nous sommes limités du côté des concentrations de protéines alors que l'albumine bovine forme des agrégats au-delà de 3 mg/ml, ce qui produit des signaux thermiques non spécifiques à l'adsorption. C'est une limitation en termes d'intensité de signal, d'atteinte ou non de la saturation des surfaces. Mais c'est aussi une limitation dans la représentativité des informations obtenues, car ce sont des concentrations très inférieures à ce que l'on retrouve dans les milieux biologiques.

Nous avons essayé de mesurer et d'identifier par cette méthode les interactions de l'albumine bovine et du lysozyme avec la surface des NPs. Si le lysozyme a permis d'obtenir des chaleurs d'adsorption, l'albumine n'a pas généré de signaux thermiques mesurables ce qui est cohérent avec les résultats des isothermes d'adsorption.

On voit que la transition de taille et de morphologie observée pour les particules fabriquées avec des contenus en PEG supérieur à 15% se traduit également par des effets sur les propriétés d'interactions de surface. Ceci doit être relié à la densité de PEG en surface, tant il est vrai que, si celle-ci est insuffisante, elle peut permettre des interactions directes entre la surface hydrophobe du cœur de la particule et les protéines [36, 37].

Dans des travaux futurs d'autres protéines devront être évaluées, car si l'on retrouve l'albumine à la surface des nanotransporteurs de médicament du fait qu'elle est la protéine la plus abondance dans le sérum, ce n'est pas la protéine qui a le plus d'affinité pour les surfaces des NPs [38]. La protéine C3b du système du complément (système immunitaire inné) ou les IgG sont plus directement responsables de la reconnaissance par les macrophages [39] et devront être étudiées pour évaluer la furtivité de nos NPs.

7.5 Encapsulation de molécule active

7.5.1 L'efficacité d'encapsulation

Les conséquences sur l'encapsulation et la libération de molécule active de l'architecture non linéaire, du nombre de chaînes et du contenu variable en PEG sont des points d'importance primordiale dans la perspective du développement pharmaceutique de ces polymères. L'étude menée sur une molécule active, la curcumine ((1E,6E)-1,7-Bis(4-hydroxy-3-methoxyphenyl)-1,6-heptadiene-3,5-dione), nous a démontré le rôle du contenu en PEG sur l'efficacité d'encapsulation d'une molécule très peu soluble dans l'eau. La curcumine possède des propriétés physicochimiques qui en font une molécule particulièrement difficile à formuler avec un LogP apparent de 3.2 et trois pKa entre 9 et 10 environ. Lors de l'encapsulation, la curcumine interagit essentiellement avec la partie hydrophobe du copolymère soit la chaîne de PLA. Cette affinité a été quantifiée pour le poly(caprolactone) par l'intermédiaire du paramètre de Flory-Huggins χ_{SP} qui exprime la capacité expérimentale de solubilisation d'une petite molécule carbonée [40].

Hypothétiquement, le PEG aurait un rôle de barrière hydrophile pour s'opposer à la sortie de la curcumine hydrophobe lors de la formation de particule. Ceci expliquerait les faibles taux d'encapsulation dans les particules de PLA ou OH-*g*-PLA, ne possédant pas de couronne hydrophile. La situation est plus cependant plus complexe. Les ratios curcumine/polymère sont fixés sur le poids en polymère, incluant la fraction constituée de PEG. Lorsque le pourcentage de PEG augmente, la quantité de PLA diminue pour un même poids de polymère. Si l'efficacité de chargement de la curcumine dépend en partie de son affinité pour le PLA, on pourrait s'attendre à une efficacité d'encapsulation et à des taux d'encapsulation qui diminuent avec l'augmentation du contenu en PEG. En regard de ces constations il faut noter que les NPs "dibloc" avec un contenu de 6% en PEG démontrent une efficacité d'encapsulation (EE) plus grande que des NPs préparées avec un copolymère en peigne avec 8% de PEG. Ceci met en évidence le rôle de l'architecture du polymère se superposant à l'effet du contenu en PEG.

La question de la localisation précise de la curcumine dans la particule en fonction de l'architecture du polymère n'est pas élucidée, non plus que le rôle de la fraction de PEG (environ 25%) située à l'intérieur de la particule sur l'efficacité d'encapsulation.

7.5.2 La libération

La libération de la curcumine s'est révélée complète alors même que les poids moléculaires des polymères formant les NPs n'avaient pas significativement changé (Chapitre 6). Les phénomènes d'érosion souvent invoqués dans la libération de molécule d'une matrice polymère ne sont pas ici déterminants. Les phénomènes de diffusion se sont révélés comme les facteurs limitants de la libération de la curcumine.

Les constantes de diffusion calculées en utilisant un modèle mathématique prenant en compte sa diffusion et sa dégradation nous montrent deux régimes de diffusion vers l'extérieur de la particule. Ces deux régimes semblent reliés à la taille des particules et au type de morphologie des particules tel qu'observé en MET. Cette dernière dépend également du contenu en PEG du polymère. Les particules faites de « dibloc » sont des particules de taille similaires aux particules solides, avec des contenus en PEG similaire aux particules solides (6% poids/poids), mais avec une morphologie de particule « molles ». En termes de diffusion, elles apparaissent dans une position intermédiaire entre les particules "solides" et les particules de type "micellaire" ou de type "agrégats". Ce qui semble indiquer un rôle pour l'architecture du polymère. L'effet de l'architecture du copolymère sur la diffusion pourrait se jouer dans les niveaux de porosité des particules et dans l'architecture de cette porosité (forme et connexions des pores) [41].

La diffusion à travers la matrice polymérique peut être favorisée par des *Tg* peu élevés (inférieur à la température du milieu) ou par l'état physique de la curcumine, ici dissoute et dispersée dans la matrice (« moléculairement dispersée ») selon les résultats de CDB. La porosité de la particule et l'entrée d'eau dans la particule sont peu susceptibles de jouer un rôle, compte tenu des constantes de diffusion dans les milieux confinés comme les pores et par la faible solubilité de la curcumine dans l'eau [41].

Des résultats préliminaires nous indiquent que la curcumine est non dégradée lorsqu'elle est encapsulée et qu'elle peut être conservée plusieurs jours, voire plusieurs semaines sous cette forme sans perte significative de dose. Alors qu'en solution neutre ou basique la curcumine est oxydée complètement en quelques heures ou moins, notamment si elle est exposée à la lumière [42].

7.5.3 Ciblage intracellulaires et ciblage tissulaire

Un des intérêts de l'encapsulation est la protection du principe actif jusqu'à ce qu'il atteigne la zone à traiter et qu'il soit libéré. En ce qui concerne l'action antioxydante de la curcumine, c'est une action intracellulaire, on a donc avantage à cibler l'internalisation de la particule pour qu'elle libère son contenu dans le cytoplasme. Également de nombreuses études ont montré que la curcumine pouvait cibler les mécanismes impliqués dans la maladie d'Alzheimer, comme la cascade amyloïde-béta, la phosphorylation de la protéine Tau et le stress oxydant [43]. Par ailleurs dans le cadre du développement d'une plateforme pour la livraison au cerveau pour le traitement de maladie ayant une composante oxydative, telle que la maladie d'Alzheimer, les particules doivent pouvoir traverser la barrière hématoencéphalique (BHE). Ceci est particulièrement important pour le développement pharmaceutique de la curcumine, alors que sa solubilité est faible et que sa perméabilité vis-à-vis de la BHE est limitée. La BHE est particulièrement efficace pour protéger le cerveau des substances étrangères, grâce à sa structure comportant des jonctions serrées et des pompes d'efflux. Néanmoins, il a été démontré que les cellules vasculaires de la BHE étaient capables de transporter vers le parenchyme, des particules lipidiques endogènes comme les LDL. Ceci est médié par des récepteurs membranaires des lipoprotéines situées en surface de ces particules [44].

Les particules polymériques de type PLGA et PLA, poly(caprolactone) and poly(butyl cyanoacrylate) ont été proposées et ont démontrées une certaine efficacité à traverser la BHE [45, 46]. En particulier, il a été démontré que plusieurs molécules se retrouvent à des doses plus élevées au niveau du système nerveux central (SNC) lorsqu'elles sont administrées sous forme encapsulées plutôt que sous forme libre [46]. À noter que la plupart de ces systèmes particulaires possèdent une couche de PEG en surface. C'est un aspect que nous n'avons pas

eu le temps d'explorer et la possibilité que des différences de pénétration de BHE existent, en fonction du contenu en PEG et de l'architecture du polymère, est très intrigante. Mais la Figure 7.7 le montre: le passage d'un composé encapsulé dans une NP, du flot sanguin à la cellule neuronale ciblée est un processus complexe, qui implique de nombreux phénomènes de transport et de nombreux obstacles [47] [48].

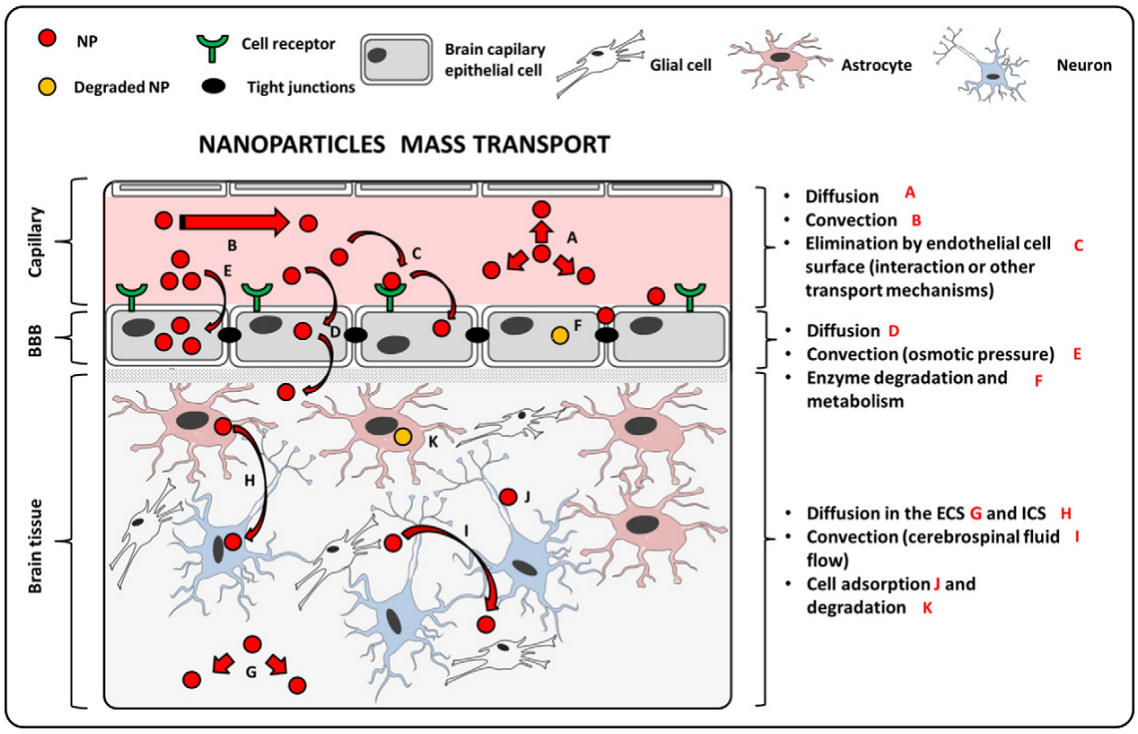

Figure 7.7. Schéma illustrant la complexité des phénomènes de transport de nanoparticules au niveau de la BHE et du SNC (d'après M.A. Lauzon *et coll.* [47]). ECS : espace extracellulaire; ICS : espace intracellulaire, NP : Nanoparticules; BBB : Barrière hématoencéphalique.

Les résultats d'études cellulaires que nous avons menées avec la collaboration de l'équipe du Pr Charles Ramassamy, nous ont montré l'efficacité de la curcumine encapsulée sur une lignée neuronale *in vitro* à diminuer les doses intracellulaires de ROS et RNS suite à stress oxydatif induit (Chapitre 6). Plusieurs études ont montré que les cellules neuronales avaient la capacité d'internaliser des NPs chargées en médicament [49, 50]. Dans notre étude, l'efficacité est égale pour des doses équivalentes de curcumine libre et de curcumine encapsulée. Sachant que la curcumine libérée durant le temps de l'essai n'est qu'une fraction

de la dose encapsulée totale, nous pouvons en conclure que cette stratégie est plus efficace. Nous n'avons pas de preuve directe de l'internalisation des particules, mais ce résultat pourrait le suggérer. En effet si les NPs libéraient la curcumine à l'extérieur de la cellule, la dose libérée étant beaucoup plus faible que la dose introduite sous forme libre, on devrait obtenir des efficacités moindres. Les études se poursuivent pour éclairer ce point.

8 Conclusion & Perspectives

L'hypothèse centrale de recherche à l'origine de ces travaux était que la structure des polymères définissait les structures internes et de surface des NTP et ultimement les propriétés physico-chimiques des particules. Secondairement, ce travail portait sur l'utilité des polymères polyesters branchés sur la préparation de NP à usage pharmaceutique. Les différents objectifs de recherche afin de tester cette hypothèse ont été réalisés, soient : 1) la conception, synthèse et caractérisation d'une libraire de copolymères branchés avec différentes architectures; 2) la préparation de particules par nanoprécipitation et leur caractérisation structurale et finalement 3) l'étude de leurs propriétés de stabilité, d'interactions avec les protéines et d'encapsulation avec une molécule active modèle.

Dans ces travaux, nous avons expérimentalement montré la dépendance entre l'architecture et le contenu en PEG sur la taille, la morphologie et l'organisation des NPs obtenues. Nous avons pu ainsi identifier qu'un changement du contenu en PEG induisant des transitions en termes de structures, de tailles et de propriétés d'encapsulation et de libération d'actif pour la première bibliothèque de copolymères. Cette transition qui par sa forme semble caractéristique des polymères PEGylées en peigne dépend de la taille du bloc hydrophobe et de la présence de chaîne de PEG en bout de chaîne principale. Les NPs ont montré leur efficacité pour l'encapsulation d'un actif modèle (la curcumine) améliorant sa stabilité en milieu biologique et sa solubilité. Tel que mentionné dans la section Hypothèse (2.1), notre approche basée sur des polymères fonctionnels préformés composés de produits déjà utilisés en clinique a le potentiel de faciliter le développement et la translation vers la clinique.

Ce travail a permis de développer au sein du laboratoire de nouvelles techniques de caractérisation de surface, d'en proposer des améliorations et d'en identifier des limites. Il s'agit d'une part de la quantification des densités de PEG en surface par RMN et d'une nouvelle méthode de quantification à partir des données XPS. Et d'autre part, il s'agit de la caractérisation des propriétés de surface par microcalorimétrie ITC.

Les travaux futurs faisant suite à ces études pourraient comporter deux volets. Un premier aspect est l'étude plus fondamentale de l'organisation des copolymères en peigne présentés sous forme de particule ou d'agrégat de type micellaire. Pour cela, plusieurs approches pourraient être suivies. Une première approche, qui est amorcé dans le laboratoire est de tendre à obtenir des polymères plus réguliers. En effet, les chaînes obtenues jusqu'à présent sont des copolymères aléatoires de dilactide et de glycidyl éther, la répartition des chaînes pendantes de PEG est également aléatoire. On ignore si des copolymères statistiques se comportent comme des copolymères plus organisés. Il y a ici actuellement une limite à l'interprétation des résultats obtenus. Une approche de synthèse permettant de mieux contrôler les distances entre les points de branchement avec, par exemple, l'utilisation de lactones fonctionnalisées permettrait de faire plus finement le lien entre les propriétés structurales des NPs et l'architecture des polymères. Une seconde approche pour améliorer la compréhension de l'organisation des chaînes de polymères en peigne serait de développer la modélisation moléculaire, en se basant sur les modèles développés pour les micelles et les polymères bloc linéaires.

Le second volet est l'utilisation des informations obtenues pour développer des formulations testables en cliniques. Un aspect à explorer pour montrer l'intérêt de notre approche serait de relier les caractérisations structurales et physico-chimiques des NPs de notre bibliothèque à des comportements *in vivo*, tels que la persistance dans la circulation sanguine, la biodistribution, le passage des barrières endothéliales (telle que la barrière hématoencéphalique). Ce sont des aspects qui permettraient de faire avancer les nouvelles approches de livraison de médicament et qui pourraient résulter dans des traitements alternatifs ou complémentaires pour le traitement de maladies graves.

Une analyse de la littérature montre que les systèmes simples avec peu de composants semblent être la voie pour les nanoformulations. Les systèmes plus complexes incluant les systèmes de ciblage sophistiqués n'ont pas augmenté significativement les efficacités en phases cliniques [51]. Un système simple c'est important pour des raisons de mise en œuvre, de fabrication, de contrôle qualité et de profil de toxicité, mais aussi tout aussi important en sciences pharmaceutiques pour des raisons d'approbation réglementaire. En contraste avec une

grande partie de ce qui publié dans le domaine des nanotechnologies pharmaceutiques nous sommes donc efforcés d'explorer des systèmes polymériques simples avec un minimum de composants, tous déjà approuvés individuellement pour usage interne en gardant en tête que ces systèmes doivent être sans aucun effet toxique sur une grande gamme de doses. Nous sommes attachés aussi à mieux caractériser les transporteurs et de contribuer à des tests plus standardisés pour des fins de contrôle qualité, mais aussi pour être capables dans le futur de comparer des performances de différentes nanoformulations.

Montréal le 30 avril 2015

Références (Chapitre 7 et Conclusion)

1. Ge, Z. and S. Liu, *Supramolecular Self-Assembly of Nonlinear Amphiphilic and Double Hydrophilic Block Copolymers in Aqueous Solutions.* Macromolecular Rapid Communications, 2009. **30**(18): p. 1523-1532.
2. Essa, S., J.M. Rabanel, and P. Hildgen, *Characterization of rhodamine loaded PEG-g-PLA nanoparticles (NPs): Effect of poly(ethylene glycol) grafting density.* International Journal of Pharmaceutics, 2011. **411**(1-2): p. 178-187.
3. Sant, S., S. Poulin, and P. Hildgen, *Effect of polymer architecture on surface properties, plasma protein adsorption, and cellular interactions of pegylated nanoparticles.* Journal of Biomedical Materials Research, Part A, 2008. **87A**(4): p. 885-895.
4. Nadeau, V., et al., *Synthesis of new versatile functionalized polyesters for biomedical applications.* Polymer, 2005. **46**(25): p. 11263-11272.
5. Göpferich, A., *Mechanisms of polymer degradation and erosion.* Biomaterials, 1996. **17**(2): p. 103-114.
6. Dechy-Cabaret, O., B. Martin-Vaca, and D. Bourissou, *Controlled Ring-Opening Polymerization of Lactide and Glycolide.* Chemical Reviews, 2004. **104**(12): p. 6147-6176.
7. Wurth, J.J. and V.P. Shastri, *Synthesis and characterization of functionalized poly(ε-caprolactone).* Journal of Polymer Science Part A: Polymer Chemistry, 2013. **51**(16): p. 3375-3382.
8. Teske, N.S., J. Voigt, and V.P. Shastri, *Clickable Degradable Aliphatic Polyesters via Copolymerization with Alkyne Epoxy Esters: Synthesis and Postfunctionalization with Organic Dyes.* Journal of the American Chemical Society, 2014. **136**(29): p. 10527-10533.
9. Neises, B. and W. Steglich, *Simple Method for the Esterification of Carboxylic Acids.* Angewandte Chemie, International Edition in English 1978. **17**(7): p. 522-524.
10. Rizkalla, N., et al., *Effect of various formulation parameters on the properties of polymeric nanoparticles prepared by multiple emulsion method.* J Microencapsul, 2006. **23**(1): p. 39-57.
11. Belliveau, N.M., et al., *Microfluidic Synthesis of Highly Potent Limit-size Lipid Nanoparticles for In Vivo Delivery of siRNA.* Mol Ther Nucleic Acids, 2012. **1**: p. e37.
12. Karnik, R., et al., *Microfluidic Platform for Controlled Synthesis of Polymeric Nanoparticles.* Nano Letters, 2008. **8**(9): p. 2906-2912.
13. Cui, H., et al., *Elucidating the assembled structure of amphiphiles in solution via cryogenic transmission electron microscopy.* Soft Matter, 2007. **3**(8): p. 945-955.
14. Gaucher, G., et al., *Block copolymer micelles: preparation, characterization and application in drug delivery.* Journal of Controlled Release, 2005. **109**(1-3): p. 169-188.
15. Riley, T., et al., *Colloidal stability and drug incorporation aspects of micellar-like PLA–PEG nanoparticles.* Colloids and Surfaces B: Biointerfaces, 1999. **16**(1–4): p. 147-159.

16. Zhang, L. and A. Eisenberg, *Multiple Morphologies and Characteristics of "Crew-Cut" Micelle-like Aggregates of Polystyrene-b-poly(acrylic acid) Diblock Copolymers in Aqueous Solutions.* Journal of the American Chemical Society, 1996. **118**(13): p. 3168-3181.
17. Allen, C., D. Maysinger, and A. Eisenberg, *Nano-engineering block copolymer aggregates for drug delivery.* Colloids and Surfaces B: Biointerfaces, 1999. **16**(1–4): p. 3-27.
18. Mai, Y. and A. Eisenberg, *Self-assembly of block copolymers.* Chemical Society Reviews, 2012. **41**(18): p. 5969-5985.
19. Letchford, K. and H. Burt, *A review of the formation and classification of amphiphilic block copolymer nanoparticulate structures: micelles, nanospheres, nanocapsules and polymersomes.* European Journal of Pharmaceutics and Biopharmaceutics, 2007. **65**(3): p. 259-269.
20. Nicolai, T., O. Colombani, and C. Chassenieux, *Dynamic polymeric micelles versus frozen nanoparticles formed by block copolymers.* Soft Matter, 2010. **6**(14): p. 3111-3118.
21. Johnson, B.K. and R.K. Prud'homme, *Mechanism for Rapid Self-Assembly of Block Copolymer Nanoparticles.* Physical Review Letters, 2003. **91**(11): p. 118302.
22. Rabanel, J.-M., et al., *Effect of Polymer Architecture on the Structural and Biophysical Properties of PEG-PLA Nanoparticles.* ACS Applied Materials and Interfaces, 2015. **7**(19): p. 10374–10385.
23. Riley, T., et al., *Physicochemical Evaluation of Nanoparticles Assembled from Poly(lactic acid)−Poly(ethylene glycol) (PLA−PEG) Block Copolymers as Drug Delivery Vehicles.* Langmuir, 2001. **17**(11): p. 3168-3174.
24. Sant, S., V. Nadeau, and P. Hildgen, *Effect of porosity on the release kinetics of propafenone-loaded PEG-g-PLA nanoparticles.* J Control Release, 2005. **107**(2): p. 203-14.
25. Yang, B., et al., *Small Angle Neutron Scattering Studies on the Internal Structure of Poly(lactide-co-glycolide)-block-poly(ethylene glycol) Nanoparticles as Drug Delivery Vehicles.* Biomacromolecules, 2014.
26. Riess, G., *Micellization of block copolymers.* Progress in Polymer Science, 2003. **28**(7): p. 1107-1170.
27. Pispas, S., et al., *Effect of Architecture on the Micellization Properties of Block Copolymers: A2B Miktoarm Stars vs AB Diblocks.* Macromolecules, 2000. **33**(5): p. 1741-1746.
28. Volkert, C.A. and A.M. Minor, *Focused Ion Beam Microscopy and Micromachining.* MRS Bulletin, 2007. **32**: p. 389-399.
29. Rabanel, J.-M., P. Hildgen, and X. Banquy, *Assessment of PEG on polymeric particles surface, a key step in drug carrier translation.* Journal of Controlled Release, 2014. **185**(0): p. 71-87.
30. Gaumet, M., et al., *Nanoparticles for drug delivery: the need for precision in reporting particle size parameters.* Eur J Pharm Biopharm, 2008. **69**(1): p. 1-9.
31. Hackey, V.A. and J.D. Clogston, *Measuring the size of nanoparticles in aqueous media using batch-mode dynamic light scattering*. 2010, NIST-NCL Joint Assay Protocol, PCC-1, version 1.1.

32. Halperin, A., *Polymeric micelles: a star model.* Macromolecules, 1987. **20**(11): p. 2943-2946.
33. Baer, D.R. and M.H. Engelhard, *XPS analysis of nanostructured materials and biological surfaces.* Journal of Electron Spectroscopy and related Phenomena, 2010. **178–179**(0): p. 415-432.
34. Gillich, T., et al., *PEG-Stabilized Core–Shell Nanoparticles: Impact of Linear versus Dendritic Polymer Shell Architecture on Colloidal Properties and the Reversibility of Temperature-Induced Aggregation.* ACS Nano, 2012. **7**(1): p. 316-329.
35. Lee, V.A., et al., *Microcalorimetry of the adsorption of lysozyme onto polymeric substrates.* Journal of Colloid and Interface Science, 2005. **288**(1): p. 6-13.
36. Vonarbourg, A., et al., *Parameters influencing the stealthiness of colloidal drug delivery systems.* Biomaterials, 2006. **27**(24): p. 4356-73.
37. Bosker, W.T.E., et al., *BSA adsorption on bimodal PEO brushes.* Journal of Colloid and Interface Science, 2005. **286**(2): p. 496-503.
38. Shehata, T., et al., *Prolongation of residence time of liposome by surface-modification with mixture of hydrophilic polymers.* Int J Pharm, 2008. **359**(1-2): p. 272-9.
39. Mosqueira, V.C.F., et al., *Relationship between complement activation, cellular uptake and surface physicochemical aspects of novel PEG-modified nanocapsules.* Biomaterials, 2001. **22**(22): p. 2967-2979.
40. Letchford, K., R. Liggins, and H. Burt, *Solubilization of hydrophobic drugs by methoxy poly(ethylene glycol)-block-polycaprolactone diblock copolymer micelles: Theoretical and experimental data and correlations.* Journal of Pharmaceutical Sciences, 2008. **97**(3): p. 1179-1190.
41. Lemaire, V., J. Belair, and P. Hildgen, *Structural modeling of drug release from biodegradable porous matrices based on a combined diffusion/erosion process.* Int J Pharm, 2003. **258**(1-2): p. 95-107.
42. Wang, Y.-J., et al., *Stability of curcumin in buffer solutions and characterization of its degradation products.* Journal of Pharmaceutical and Biomedical Analysis, 1997. **15**(12): p. 1867-1876.
43. Belkacemi, A., et al., *Challenges associated with curcumin therapy in Alzheimer disease.* Expert Reviews in Molecular Medicine, 2011. **13**: p. null-null.
44. Kreuter, J., et al., *Apolipoprotein-mediated transport of nanoparticle-bound drugs across the blood-brain barrier.* J Drug Target, 2002. **10**(4): p. 317-25.
45. Sahni, J.K., et al., *Neurotherapeutic applications of nanoparticles in Alzheimer's disease.* J Control Release, 2011. **152**(2): p. 208-31.
46. Gagliardi, M., G. Bardi, and A. Bifone, *Polymeric nanocarriers for controlled and enhanced delivery of therapeutic agents to the CNS.* Ther Deliv, 2012. **3**(7): p. 875-87.
47. Lauzon, M.-A., et al., *Nanoparticle-mediated growth factor delivery systems: A new way to treat Alzheimer's disease.* Journal of Controlled Release, 2015. **206**(0): p. 187-205.
48. Rabanel, J.M., et al., *Drug-loaded nanocarriers: passive targeting and crossing of biological barriers.* Current Medicinal Chemistry, 2012. **19**(19): p. 3070-102.
49. Mathew, A., et al., *Curcumin loaded-PLGA nanoparticles conjugated with Tet-1 peptide for potential use in Alzheimer's disease.* PLoS One, 2012. **7**(3): p. e32616.

50. Doggui, S., et al., *Neuronal Uptake and Neuroprotective Effect of Curcumin-Loaded PLGA Nanoparticles on the Human SK-N-SH Cell Line.* Journal of Alzheimer's Disease, 2012. **30**(2): p. 377-392.
51. Kwon, I.K., et al., *Analysis on the current status of targeted drug delivery to tumors.* Journal of Controlled Release, 2012. **164**(2): p. 108-114.

9 Annexes

Annexe 1. Article de revue « Supporting Information »

J-M. Rabanel, P. Hildgen, X. Banquy, JCR, *Vol. 185 pp71-87 (2014)*

List of abbreviations, symbols and units

Symbol	Parameter	Units
ρ	Volumetric density	g/cm^3
ρ_c	Volumetric density of the NP core	g/cm^3
ρ_{NP}	Particle volumetric density	g/cm^3
ρ_{sh}	PEG layer volumetric density	g/cm^3
Γ	Weight coverage-density	g/m^2
σ	Chain coverage-density	PEG/nm^2
M_{PEG}	Molecular weight of PEG	g/mole
W_{PEG}	Total weight of surface PEG chains in the sample	g
N_{PEG}	Number of PEG chain in a sample	
W_S	Weight of the sample	
W_C	Total weight of the particle core in the sample	g
W_{SH}	Weight of a NP shell	g
W_{NP}	Weight of a single particle	g
$\mathcal{N}$	Avogadro number	
N_{NP}	Total number of particles in a sample	
V	Total volume of particles in a sample	cm^3 or nm^3
V_C	Total volume of the NP core in the sample	cm^3 or nm^3
V_{NP}	Volume of a particle	cm^3 or nm^3
V_{sh}	Volume of the shell layer	cm^3 or nm^3
S	Total NP surface in a sample	m^2
S_{NP}	Surface of one nanoparticle	nm^2
S_C	Total surface of the particle core in a sample	nm^2
d	Particle diameter	nm or µm
r	Particle radius (dry state)	nm or µm
R_H	Particle hydrodynamic radius	nm or µm
R_C	Particle core radius	nm
a	Monomer size (0.35 nm)	
N	Number of monomer in PEG chain	
L	Thickness of the PEG layer	nm
D	PEG inter-chain distance	nm
FP	PEG footprint (projected area)	nm^2
A_{PEG}	Area available to PEG chains (mushroom regime)	nm^2

S1. Calculation methods of PEG coverage-density

S1.1. PEG layer coverage and chain conformation

PEG chains terminally-attached to a non-adsorbing surface at a solid/liquid interface can adopt different conformations in a good solvent [1, 2] as represented in Fig. S1. Two important parameters define the conformation of a terminally attached PEG chain:

- The surface chain coverage-density (σ), reported as number of PEG chain per nm^2, or the mean distance (D) between anchored PEG chains on the surface ($D = 2\sqrt{\frac{FP}{\pi}}$);
- The thickness of the PEG layer (L) which depends on the PEG chain molecular weight M_w, and Γ.

For a given chain length, the conformation of the PEG chain goes from mushroom at $D>R_F$ to brush as $R_F<D<2R_F$, to dense brush $D< R_F$; R_F being the Flory radius defined by the relation [2]:

$$R_F = a\, N^{\frac{3}{5}} \qquad \textbf{(S1-1)}$$

where a is the PEG monomer size (3.5 Å) and N the number of monomers in a PEG chain.

In the mushroom regime and in a good solvent, PEG chains adopt a random coil conformation normal to the surface. The mean volume occupied by the PEG chains is a hemisphere of radius R_F (zone of PEG mobility, Fig. S1-A). Therefore the footprint FP (or projected area) occupied by a single chain is $FP = \pi\, R_F^2$ and the unperturbed height of the PEG layer is approximately R_F (Fig. 2-A).

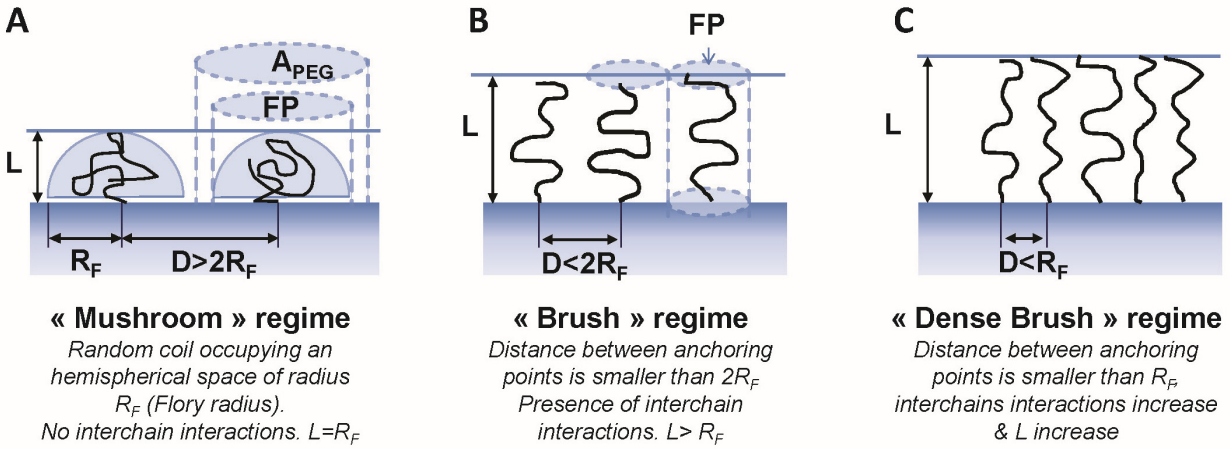

Figure S1. Evolution of PEG chains conformation as a function of the surface grafting density R_F*:* Flory radius; L: layer thickness (in mushroom regime $L=R_F$); *D:* distance between anchoring points; FP: PEG chain footprint, A_{PEG}: Area available to each PEG chain. In the brush regime $FP=A_{PEG}$, in the mushroom regime $A_{PEG}>FP$

In the brush regime, the unperturbed layer thickness is given by:

$$L_o = a\,N\,\left(\frac{a}{D}\right)^{\frac{2}{3}} \qquad \textbf{(S1-2)}$$

where L represents the height of the brush thickness, D is the distance between PEG chain attachment to the surface [2].

In the special case where the polymer chains are interacting with the surface (adsorbing surface), chains are no longer repelled from the surface and will adopt a "pancake" conformation (Fig. 1-C). PEG loop conformation (Fig. 1-C) had also been reported to confer steric repulsion to particle surface [3, 4]. PEG layer organization in this conformation has not been thoroughly studied although certain experimental evidences show that they behave as "effective brush" of half the molecular weight of the loop segment and twice the grafting density [3].

Table S1. Calculated PEG layer characteristics at mushroom/brush transition

Molecular weight	Degree of polymerization	Flory radius[a]	Chain footprint or projected area[b]	Chain coverage density[c]	Grafting Point Distance[d]	Unperturbed brush height[e] (at D=1 nm)
Mw	***DP***	***RF***	***FP***	***σ***	***D***	***L***
g. mol^{-1}		*nm*	*nm^2*	*PEG/nm^2*	*nm*	*nm*
750	17	1.9	11.3	0.089	3.8	2,96
1 000	23	2.3	16.6	0.060	4.6	4,00
2 000	44	3.4	36.3	0.022	6.8	7,65
5 000	114	6.0	98.5	0.007	12.0	19,83
10 000	230	9.7	295	0.0034	19.4	40,00
20 000	450	14.4	651	0.0015	28.8	78,26

Notes. *Mw = molecular weight; DP=degree of polymerization;* ***a****: calculated from equation 1-1 assuming a=35Å;* ***b****: chain projected area in mushroom conformation calculated as $\pi R_F{}^2$;* ***c****: coverage-density σ at the boundary between mushroom and brush regime, calculated from equation $\sigma = \frac{1}{A}$;* ***d****: D, Distance between anchoring point;* ***e****: unperturbed layer height based on scaling theory (equation 2-2) considering D = 1 nm*

Table S1 presents calculations of the key parameters describing PEG conformation. The reported values were calculated at the transition between the mushroom and the brush regime. Additionally the unperturbed brush height, L, was calculated for a distance, D, between PEG chains of 1 nm. For example, the Flory radius of a PEG chain of N=44 is about 3.4 nm in a good solvent such as water at room temperature. It means that one PEG chain in the mushroom regime occupies a surface of 36.3 nm^2, has a layer thickness of about R_F (see figure S1-A) and the coverage-density at the transition between the mushroom and brush regimes is Γ=0,022 PEG/nm^2.

In order to prevent protein adsorption on a planar surface, theoretical analysis predicts that the distance (*D*) between PEG chains should be in the range of 1 nm [2, 5-7]. The radius of curvature may play a role in antifouling efficacy of spherical particle, due to its effect on PEG chains packing however, its effect on PEG layer excluded volume is not completely elucidated [6].

S1.2. General equations

The objectives of this section are to provide general calculation methods to estimate the coverage-density of PEG chains on spherical particles as well as to detail the basic assumptions and the sources of errors involved in each of them. The analytical techniques described in the manuscript are, for most of them, used to quantify PEG by mass, moles or number of PEG chains relative to the total sample mass (mg or g of particle). Once the quantity of PEG is known, in order to estimate the coverage-density, PEG quantity has to be normalized by the surface area of the particle sample analyzed. These calculations require the knowledge of three critical parameters, namely the particle size, the volumetric density of the particles and the sample weight.

Different approaches have been used to estimate PEG surface density, but all of them use the same experimental variables: 1) the surface PEG to particles mass ratio; 2) the total mass of the sample analyzed; 3) the size of the particles, and 4) the density of the particle.

The PEG surface coverage-density σ (PEG/nm^2) is written as:

$$\sigma = \frac{N_{PEG}}{S} \qquad \textbf{(S2-1)}$$

where N_{PEG}, is the total number of PEG chains present at the surface of the *sample* and S is the *total* surface area of the core particles present in the *sample*. S is written as:

$$S = \left\lfloor \left(\frac{W_C}{V_C\,\rho_C}\right) S_C \right\rfloor \qquad \textbf{(S2-2)}$$

Using equation S2-2 we can rewrite equation S2-1, where W_C, is the total mass of particle cores in the sample, V_C is the average volume of one core particle, ρ_C, is the mass density of the particle core and S_C, is the mean surface area of one particle core:

$$\sigma = N_{\mathrm{PEG}} \Big/ \left\lfloor \left(\frac{W_C}{V_C\,\rho_C}\right) S_C \right\rfloor \qquad \textbf{(S2-3)}$$

The total number of PEG chains in the sample is obtained from the analytic quantification data (weight of PEG found on the sample surface):

$$N_{\mathrm{PEG}} = \frac{W_{\mathrm{PEG}}}{M_{\mathrm{PEG}}}\,\mathcal{N} \qquad \textbf{(S2-4)}$$

where W_{PEG}, is the mass of surface-bound PEG present in the *sample*, M_{PEG} is the molecular weight, of a PEG chain, and $\mathcal{N}$ is the Avogadro number.

Using equation S2-4, one can rewrite Eq. S2-1 in terms of experimentally accessible quantities for spherical particle:

$$\sigma = \frac{\rho_{\mathrm{C}}\, R_{\mathrm{C}}\, \mathcal{N}\, W_{\mathrm{PEG}}}{3\, M_{\mathrm{PEG}}\, W_{\mathrm{C}}} \qquad \textbf{(S2-5)}$$

Analogous equations have been proposed previously in different studies, noteworthy in [8-12]. In most pharmaceutical papers, coverage-density is noted σ. The different parameters discussed can be visualized in Fig. S1 and S2.

This equation can be adapted to particle geometry other than spherical. Indeed with the increased interest in the role of particle shape on biological response and fate of particle in the body [13, 14] and the development of fabrication techniques such as lithography, there is a need to assess quantitatively PEG coverage-density on non-spherical particles too. PEG coverage of non-spherical NP has been reported for gold nanorod [15], Print® particles [11] and micellar system. One example of PEG coverage-density calculation on rod-like micelle surface has been recently reported [16]. The assessment of the geometric dimensions of a population of non-spherical particle may rely essentially on imaging techniques such as TEM [15] and AFM [11]. The expression of S_C for different type of geometry (rod, disc, ellipse of different lengths ratio, oblate particle, etc.) will require usually more than one dimension (contrary to spherical NP which can be defined with only their radius) increasing the source of error on the final calculations.

A general expression of the uncertainty of PEG surface coverage-density for spherical particle can be derived from Eq. S2-5:

$$\frac{\Delta\,\sigma}{\sigma} = \sqrt{\left(\frac{\Delta W_{\mathrm{PEG}}}{W_{\mathrm{PEG}}}\right)^2 + \left(\frac{\Delta W_{\mathrm{C}}}{W_{\mathrm{C}}}\right)^2 + \left(\frac{\Delta R_{\mathrm{C}}}{R_{\mathrm{C}}}\right)^2 + \left(\frac{\Delta \rho_{\mathrm{C}}}{\rho_{\mathrm{C}}}\right)^2} \qquad \textbf{(S2.6)}$$

As can be seen in Eq. S2-6, the four parameters (weigh of sample, weight of PEG, particle density and radius) are contributing equally to the uncertainty on the coverage-density. In what

follows we will provide an estimate of each contributions depending on the quantification method used and the assumptions made.

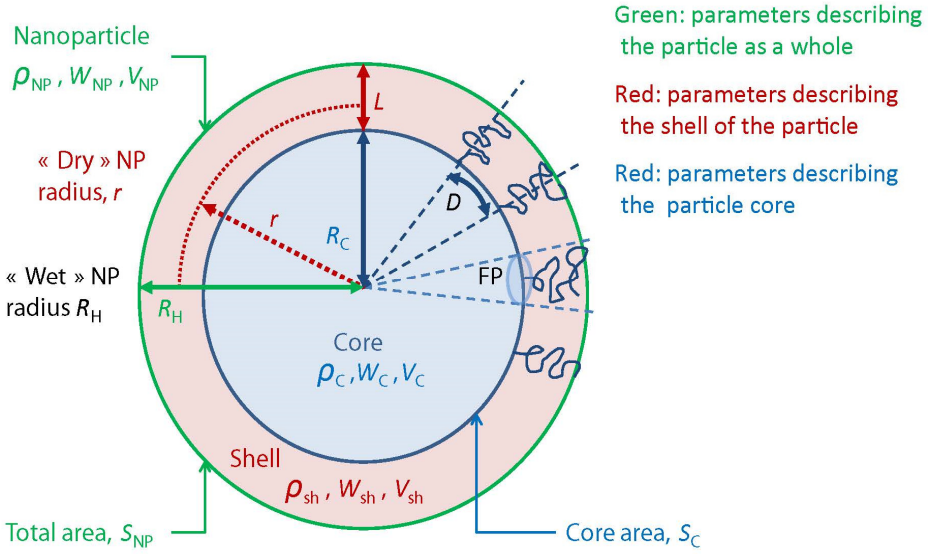

Figure S2. Physical dimensions of a PEGylated particle

S1.3. Error analysis

Error on surface PEG weight (W_{PEG}) in the sample

Error and uncertainties on W_{PEG} depend directly on the analytical method used and may vary from procedure to procedure and yield of purification if applicable.

For instance, in quantitative NMR, PEG quantification procedure may introduce four main sources of errors: the weighting of particle sample, the error in the calibration curve, the error on the data acquisition and on the peaks integration. On the other hand, in the differential method, i.e. the measurement of non-reacted PEG to estimate grafted PEG, the total error will result from two separate analytical measures: the error on the quantification of initial PEG amounts and the error on the measurement of residual PEG.

Error on the particle core weight (W_C) in the sample

The determination of the total particle core weight in the sample is not an easy task. For simplicity, most reports assume that $W_C = W_S - W_{PEG} \sim W_S$, W_S being the total sample weight. Measurement of W_S is usually performed by methods such as freeze-drying and weighting and thermogravimetry (TGA). The experimental error associated to such measurement is small as long as the total mass of the sample is large enough to be accurately measured, the number of repeats is large enough (minimum of three) and the conditions of sample preparation are well controlled

(e.g. complete drying conditions before weighting). Under well-established routine conditions, error can be as small as 1-2 %.

Therefore the major sources of error contributing to error on PEG coverage-density comes from the approximation $W_C = W_S$ which introduces an error on the number of particle in the sample (Equation S2-2) and leads to an overestimate of the particle surface.

A more accurate estimate of W_C can be obtained by taking into account the contribution of W_{PEG}. As we previously saw, W_{PEG} can be measured by techniques such as qNMR or XPS. It is important to keep in mind that W_{PEG} represents the mass of PEG at the surface of the NP and therefore does not represent the total PEG amount in the sample. As a consequence, the volumetric density of the core of the particle has to be estimated taking into account the presence of PEG in the core.

Error on the mean radius of the particle core (R_C)

The most used methods to estimate particle mean radius and to calculate their surface are DLS or TEM/ SEM and AFM. An important point to keep in mind when using these techniques is the physical meaning of each parameter each method provides. For instance, DLS measures the hydrodynamic radius of a NP (R_H), which includes the hydrophilic PEG corona and a hydrodynamic layer of fluid (beyond PEG distal end, closely bound ions, water moving along with the particle), as seen in Fig. 3.

Size determination by AFM is preferably performed in the dry state [17]. TEM or SEM are also "dry" techniques able to provide a value for the radius value, *r,* which is expected to be closer to R_C than R_H (Fig. S1). TEM measures the projected area of the NP and is more appropriate to provide the most accurate value of the core size, if enough particles are analysed [18]. This technique is more laborious as image processing is needed to yield statistically significant mean values. Moreover particle shrinkage is not uncommon due to intense drying under vacuum and heat generated by the electron beam. Cryo-TEM may be an option for sensitive particles [19].

Does the approximation of R_C=R_H contributes significantly to the error in coverage-density? The answer will indeed vary with particle size and PEG chain length. For particles of several hundred of nanometer up to 1 or 2 µm (limit of DLS), the addition of the PEG layer size and its associated hydrodynamic layer will be negligible compared to the particle radius (less than 1 %). In other words the approximation is valid if $R_C >>> L$. On the other hand, with NP of 100-200 nm in size, the contribution of the PEG layer is more significant and ranges between 2 to 10%. For

particle less than (around) 40 nm, the effect of using hydrodynamic radius over core radius is even more pronounced as the PEG layer thickness become similar to the particle core radius ($R_C \sim L$).

For example, Xu *et al.* determined the surface coverage-density of PLGA-PEG diblock particles by quantitative NMR (qNMR), using the particle diameter from DLS [12]. Cu *et al.* measured PLGA particle diameters using SEM over DLS due to strong aggregation of the NPs. The authors characterized over 500 NPs in order to obtain statistically significant measurement of the mean diameter, associated volume and surface [20]. In a study using commercially available PS-COOH NP, Nance *et al.* grafted PEG-NH_2 chains on the NP surface and later evaluated the grafting density of the shell by qNMR. The PEG quantity was reported normalized by the surface area calculated from the mean diameter obtained by DLS [21].

As an alternative, the specific surface area (in m^2/g of particle) can be obtained directly and without diameter information by gas adsorption giving the BET surface area [22, 23]. The value obtained could be substituted in equation S2-2. This method is valid for smooth sphere but may overestimate surface area if particle are made of nano-porous material whose pores are much smaller than the PEG chain size.

Error on particle core volumetric density, ρ_C

The other parameter needed to convert the PEG quantity determination into PEG coverage-density is the particle core volumetric density (ρ_C). Vauthier *et al.* used isopycnic centrifugation of particle in a linear gradient of sucrose to determine NP volumetric densities [24]. Alternatively the volumetric density of polymeric material constituting the particle can be used for, or as a substitute to the particle density. In certain cases, this information can be found in reference tables or on supplier data sheets. However for newly synthesized polymers, the technique of choice for volumetric density determination is helium pycnometry. This technique provides an accurate measurement of the density due to the small size of the helium molecule and its ability to penetrate into most of the pores and inter-chain spaces [25]. On the downsides, helium picnometry requires significant amounts of polymer (generally one to several grams) and it is unclear if polymer volumetric-density will perfectly match particle volumetric-density. From our experience, we have found very good correlation between density of poly(lactic) polymers measured by Helium pycnometry and the reported densities of NP made with the same type of polymer (unpublished data). If the particle batches are large enough, it could be possible to measure the "true density" of the particles by this method [26]. In spite of the availability of the technique, this parameter is seldom measured and assumptions are the norm.

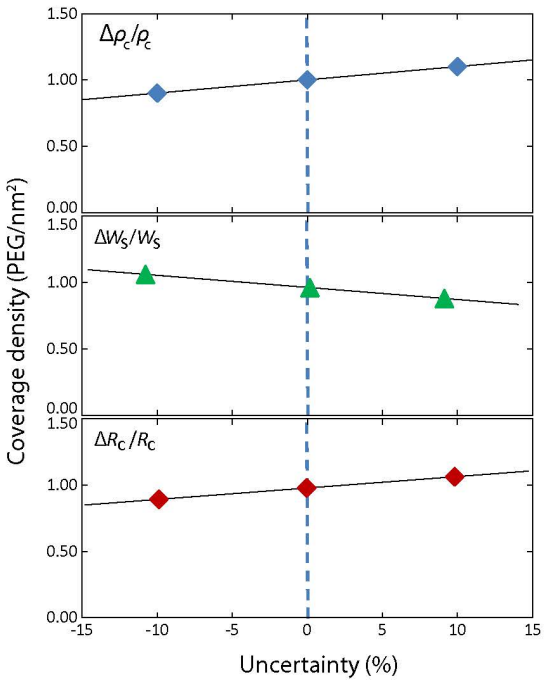

Figure S3. Influence of different types of uncertainties on the final PEG coverage-density quantification. Constant Parameters: W_S=10 mg; R_C=100 nm; ρ_C=1.2 g/cm^3

Volumetric-density of organic particles is usually comprised between 1.1 g/cm^3 and 1.35 g/cm^3. Moreover, according to equation S2-5, variations of 10% in density at constant mean diameter and constant PEG quantity, result in a variation of 10% in coverage-density values (Fig. S2). Volumetric density uncertainties affect the value of the coverage-density via its effect on the number of particles in the sample and thus the sample total surface area.

S2. Miscellaneous measurement methods

One method consists in obtaining the thickness of the PEG layer through the measurement of the viscosity of the NP suspension [27]. The polymer layer on the surface of the NP increases the hydrodynamic diameter of the NP and therefore the viscosity of the particle suspension. The ratio of the intrinsic viscosity of the NP suspension with an adsorbed layer over the intrinsic viscosity of the bare particles is equal to the ratio of volume fraction for polymer-covered particle over the volume fraction of bare NP [28, 29]. This technique usually requires large quantities of particle suspension to achieve measurable viscosity differences and is best suited for hard particles rather than soft particle.

Viscosity measurements showed that the apparent viscosity of a suspension of NP with a PEG layer in the mushroom conformation is higher than NP with a PEG layer with brush regime [30, 31].

Analytical Ultracentrifugation (AUC) has been used to measure changes in sedimentation coefficient of gold (Au) NP before and following addition of PEG, allowing the determination of the coverage-density of the polymer shell. Concordant results for this method with TGA and TOC results were reported for Au PEGylated NP [32]. The applicability of AUC to determine PEG coverage-density of purely organic particles has still to be demonstrated, as the difference between core volumetric density (ρ_C) and shell volumetric density (ρ_{SH}) is not as great as with metallic or inorganic NP [33]. Yet the recent developments of AUC, allowing the determination of size, shape and density of polymeric NP [34, 35] have positioned this technique as a very promising NP analytical tool [36].

Electrospray differential mobility (ES-DMS) analysis separates aerosol (dry) particles on the basis of their surface-to-charge ratio. In the case of Au particles this approach was able to correlate amounts of PEG absorbed on the particle surface and separation [37]. Here again, adaptability to purely organic particles remains to be demonstrated.

Scattering techniques can also provide structural information on a PEG layer. Small angle X-rays scattering (or SAXS) has been used to provide a direct measurement of the conformation and the thickness of a PEG layer on uni and multilamellar liposome [38]. SAXS structural information are deduced from an electron density profile of the bilayer. Its applicability to other type of NP is still unknown.

Small angle neutron scattering (SANS) is based on the diffraction of a neutrons beam by the atoms constituting the particle. Hydrogen and Deuterium have very different scattering angles which gives access to information at the nanoscale level such as density profile and layer thickness. SANS requires deuterated solvent or polymer in order to obtain a contrast between the different layers of the NP. With a deuterated particle core for example, only the coated layer is contributing to the scattered signal. This technique has been firstly used to investigate PS polymer brushes grafted on a flat substrate for the determination of the volume fraction profile of the polymer [39]. Riley *et al.* elucidated the conformation of PEG chains on PLA-PEG particles using the technique of contrast-matched interface using a deuterated PLA in the copolymer and a deuterium oxide enriched suspension media [40]. The authors used a core-shell model to fit the obtained scattering data to calculate different structural parameters such as NP size, PEG layer thickness, PEG footprint on the particle core, etc. Ramzi *et al.* conducted similar experiments with

block polymer of pHPMAmDL-*b*-PEG forming a core shell structure, but using a somewhat different model to calculate the structural parameters [41]. SANS can also be used to simply measure the size of the nanoparticle core. The results obtained by SANS can be compared to hydrodynamic radius obtained by DLS. This approach was proposed to define the thickness of a diffuse layer of polysaccharides on poly(cyanoacrylate)-Dextran NPs [42].

SANS is a model dependant technique, requiring few fittings parameters. SANS experiments based on contrast variation, provide information not only on structural parameters such as the layer thickness, core size, etc., but also on the aggregation number (number of chains in the particle) and chain density simultaneously. PEG coverage-density is determined indirectly and deduced based on the measured structural parameters. However, it is not a routine analysis technique, as it requires specialized equipment, experienced personnel for data collection and interpretation.

REFERENCES (SUPPORTING INFORMATION)

1. Alexander, S., *Adsorption of chain molecules with a polar head a scaling description.* J. Phys. France, 1977. **38**(8): p. 983-987.
2. Degennes, P.G., *Conformation of polymers attached to an interface.* Macromolecules, 1980. **13**(5): p. 1069-1075.
3. Peracchia, M.T., et al., *Complement consumption by poly(ethylene glycol) in different conformations chemically coupled to poly(isobutyl 2-cyanoacrylate) nanoparticles.* Life Sciences, 1997. **61**(7): p. 749-761.
4. Lacasse, F.X., P. Hildgen, and J.N. McMullen, *Surface and morphology of spray-dried pegylated PLA microspheres.* International Journal of Pharmaceutics, 1998. **174**(1–2): p. 101-109.
5. Jeon, S.I., et al., *Protein surface interactions in the presence of polyethylene oxide.1.Simplified theory.* Journal of Colloid and Interface Science, 1991. **142**(1): p. 149-158.
6. Vonarbourg, A., et al., *Parameters influencing the stealthiness of colloidal drug delivery systems.* Biomaterials, 2006. **27**(24): p. 4356-73.
7. Marsh, D., R. Bartucci, and L. Sportelli, *Lipid membranes with grafted polymers: physicochemical aspects.* Biochimica et Biophysica Acta - Biomembranes, 2003. **1615**(1-2): p. 33-59.
8. Bazile, D., et al., *Stealth Me.PEG-PLA nanoparticles avoid uptake by the mononuclear phagocytes system.* J Pharm Sci, 1995. **84**(4): p. 493-8.
9. Vittaz, M., et al., *Effect of PEO surface density on long-circulating PLA-PEO nanoparticles which are very low complement activators.* Biomaterials, 1996. **17**(16): p. 1575-1581.
10. Gref, R., et al., *'Stealth' corona-core nanoparticles surface modified by polyethylene glycol (PEG): influences of the corona (PEG chain length and surface density) and of the core composition on phagocytic uptake and plasma protein adsorption.* Colloids Surf B Biointerfaces, 2000. **18**(3-4): p. 301-313.

11. Perry, J.L., et al., *PEGylated PRINT Nanoparticles: The Impact of PEG Density on Protein Binding, Macrophage Association, Biodistribution, and Pharmacokinetics.* Nano Letters, 2012. **12**(10): p. 5304-5310.
12. Xu, Q., et al., *Scalable method to produce biodegradable nanoparticles that rapidly penetrate human mucus.* Journal of Controlled Release, 2013. **170**(2): p. 279-286.
13. Tao, L., et al., *Shape-specific polymeric nanomedicine: emerging opportunities and challenges.* Exp. Biol. Med., 2011. **236**(1): p. 20-29.
14. Decuzzi, P., et al., *Intravascular Delivery of Particulate Systems: Does Geometry Really Matter?* Pharmaceutical Research, 2009. **26**(1): p. 235-243.
15. Xia, X., et al., *Quantifying the Coverage Density of Poly(ethylene glycol) Chains on the Surface of Gold Nanostructures.* ACS Nano, 2011. **6**(1): p. 512-522.
16. Tockary, T.A., et al., *Tethered PEG Crowdedness Determining Shape and Blood Circulation Profile of Polyplex Micelle Gene Carriers.* Macromolecules, 2013. **46**(16): p. 6585-6592.
17. Grobelny, J., et al., *Size measurement of nanoparticles using atomic force microscopy*. 2009, NIST-NCL Joint Assay Protcol, PCC-6, version 1.1.
18. Bonevich, J.E. and W.K. Haller, *Measuring the size of nanoparticles using transmission electron microscopy (TEM)*. 2010, NSIT-NCL Joint Assay Protocol, PCC-7, version 1.1.
19. Leung, A.K.K., et al., *Lipid Nanoparticles Containing siRNA Synthesized by Microfluidic Mixing Exhibit an Electron-Dense Nanostructured Core.* The Journal of Physical Chemistry C, 2012. **116**(34): p. 18440-18450.
20. Cu, Y. and W.M. Saltzman, *Controlled Surface Modification with Poly(ethylene)glycol Enhances Diffusion of PLGA Nanoparticles in Human Cervical Mucus.* Molecular Pharmaceutics, 2008. **6**(1): p. 173-181.
21. Nance, E.A., et al., *A Dense Poly(Ethylene Glycol) Coating Improves Penetration of Large Polymeric Nanoparticles Within Brain Tissue.* Science Translational Medicine, 2012. **4**(149): p. 149ra119.
22. Lowell, S., et al., *Characterization of Porous Solids and Powders: Surface Area, Pore Size and Density*. 2004, Dordrecht: Kluwer Acadamic Publishers.
23. Sant, S., M. Thommes, and P. Hildgen, *Microporous structure and drug release kinetics of polymeric nanoparticles.* Langmuir, 2008. **24**(1): p. 280-287.
24. Vauthier, C., C. Schmidt, and P. Couvreur, *Measurement of the Density of Polymeric Nanoparticulate Drug Carriers by Isopycnic Centrifugation.* Journal of Nanoparticle Research, 1999. **1**(3): p. 411-418.
25. Viana, M., et al., *About pycnometric density measurements.* Talanta, 2002. **57**(3): p. 583-593.
26. Sinha, B., B. Mukherjee, and G. Pattnaik, *Poly-lactide-co-glycolide nanoparticles containing voriconazole for pulmonary delivery: in vitro and in vivo study.* Nanomedicine: Nanotechnology, Biology and Medicine, 2013. **9**(1): p. 94-104.
27. G. J. Fleer, et al., *Polymers at interfaces* 1993, London: Chapman and Hall.
28. van den Boomgaard, T., et al., *The influence of temperature on the adsorption and adsorbed layer thickness of various molecular weight fractions of poly(vinyl alcohol) on polystyrene latex particles.* Journal of Colloid and Interface Science, 1978. **66**(1): p. 68-76.
29. Doroszkowski, A. and R. Lambourne, *A viscometric technique for determining the layer thickness of polymer adsorbed on titanium dioxide.* Journal of Colloid and Interface Science, 1968. **26**(2): p. 214-221.
30. Al-Hanbali, O., et al., *Concentration Dependent Structural Ordering of Poloxamine 908 on Polystyrene Nanoparticles and Their Modulatory Role on Complement Consumption.* Journal of Nanoscience and Nanotechnology, 2006. **6**(9-1): p. 3126-3133.

31. Hamad, I., et al., *Distinct Polymer Architecture Mediates Switching of Complement Activation Pathways at the Nanosphere−Serum Interface: Implications for Stealth Nanoparticle Engineering.* ACS Nano, 2010. **4**(11): p. 6629-6638.
32. Benoit, D.N., et al., *Measuring the Grafting Density of Nanoparticles in Solution by Analytical Ultracentrifugation and Total Organic Carbon Analysis.* Analytical Chemistry, 2012. **84**(21): p. 9238-9245.
33. Krpetić, Ž., et al., *High-Resolution Sizing of Monolayer-Protected Gold Clusters by Differential Centrifugal Sedimentation.* ACS Nano, 2013. **7**(10): p. 8881-8890.
34. Bootz, A., et al., *Comparison of scanning electron microscopy, dynamic light scattering and analytical ultracentrifugation for the sizing of poly(butyl cyanoacrylate) nanoparticles.* European Journal of Pharmaceutics and Biopharmaceutics, 2004. **57**(2): p. 369-375.
35. Anderson, W., et al., *A comparative study of submicron particle sizing platforms: Accuracy, precision and resolution analysis of polydisperse particle size distributions.* Journal of Colloid and Interface Science, 2013. **405**(0): p. 322-330.
36. Planken, K.L. and H. Colfen, *Analytical ultracentrifugation of colloids.* Nanoscale, 2010. **2**(10): p. 1849-1869.
37. Tsai, D.-H., et al., *Competitive Adsorption of Thiolated Polyethylene Glycol and Mercaptopropionic Acid on Gold Nanoparticles Measured by Physical Characterization Methods.* Langmuir, 2010. **26**(12): p. 10325-10333.
38. Varga, Z., et al., *Characterization of the PEG layer of sterically stabilized liposomes: a SAXS study.* Chemistry and Physics of Lipids, 2012. **165**(4): p. 387-392.
39. Auroy, P., Y. Mir, and L. Auvray, *Local structure and density profile of polymer brushes.* Physical Review Letters, 1992. **69**(1): p. 93-95.
40. Riley, T., et al., *Core−Shell Structure of PLA−PEG Nanoparticles Used for Drug Delivery.* Langmuir, 2003. **19**(20): p. 8428-8435.
41. Ramzi, A., et al., *Core−Shell Structure of Degradable, Thermosensitive Polymeric Micelles Studied by Small-Angle Neutron Scattering.* The Journal of Physical Chemistry B, 2008. **112**(3): p. 784-792.
42. Vauthier, C., et al., *Protein adsorption and complement activation for di-block copolymer nanoparticles.* Biomaterials, 2011. **32**(6): p. 1646-1656.

Annexe 2. Article 1 (Chapitre 4) « Supporting Information »

Effect of Polymer Architecture on the Structural and Biophysical Properties of PEG-PLA Nanoparticles

*Jean-Michel Rabanel[1,2], Jimmy Faivre[2], Soudeh F. Tehrani[1], Augustine Lalloz[1,2], Patrice Hildgen[1 *], Xavier Banquy[2 *]*

[1] Laboratoire de Nanotechnologie Pharmaceutique,

[2] Canada Research Chair on Bioinspired Materials and interfaces

Faculté de pharmacie, Université de Montréal,

C.P. 6128, Succursale Centre-ville, Montréal, Québec, H3C 3J7, Canada

***** *Corresponding author*s

S.1. Polymer characterizations

S.1.1. ^{1}H NMR

The initial step of polymer synthesis involves copolymerization of dilactide with benzyl glycidyl ether. After characterization by GPC and NMR, the polymers are treated by catalytic hydrogenation to remove benzyl group and unveil hydroxyl groups that will be used for PEG grafting in the final step.

The successive reactions steps were followed by ^{1}H NMR. Insertion of benzyl pendant groups in the polymer backbone is evidenced by signal (1) and (2) respectively attributed to the aromatic ring and the CH_2 group of the benzyl group while the epoxy proton signals are abolished (Figure S1). In spectra A, integration of the signal (1) at 7.25 ppm (5H, Benzyl) yield a benzyl content in the polymer of 0.78 % relative to lactic monomer. Consistently, the signal (2) attributed to CH_2 in vicinity with the aromatic ring (2H, methine) give a content of 0.76 % relative to lactic monomer. The removal of benzyl groups by catalytic hydrogenation is shown by the disappearance of signal (1) and (2) in spectra B. Finally grafting (by acyl chloride reaction path) of Methoxy-PEG is shown by signal (5) and (6) respectively attributed to CH_2-CH_2-O PEG repetition unit and O-CH_3 terminal

group. Lactic monomer is represented by signal (3) and (4) respectively attributed to methine proton on the asymmetric carbon and the methyl group. The PEG content relative to lactic monomer, is given by the ratio of peak (6) (PEG CH_3-O, 3 protons) over peak (3) (Lactic acid CH, 1 proton). In the example shown in Figure S1, the PEG content is 0.48 grafted PEG chain for 100 lactic monomers. Moreover the PEG weight content (PEG % w/w) can be calculated:

$$PEG\ (\%\, w/w) = \frac{y \times M_{PEG}}{72 \times 100} \qquad \textbf{(S-1)}$$

with y being the number of PEG chain for 100 lactic acid residues, 72, the molecular weight of the lactic acid monomer in the chain.

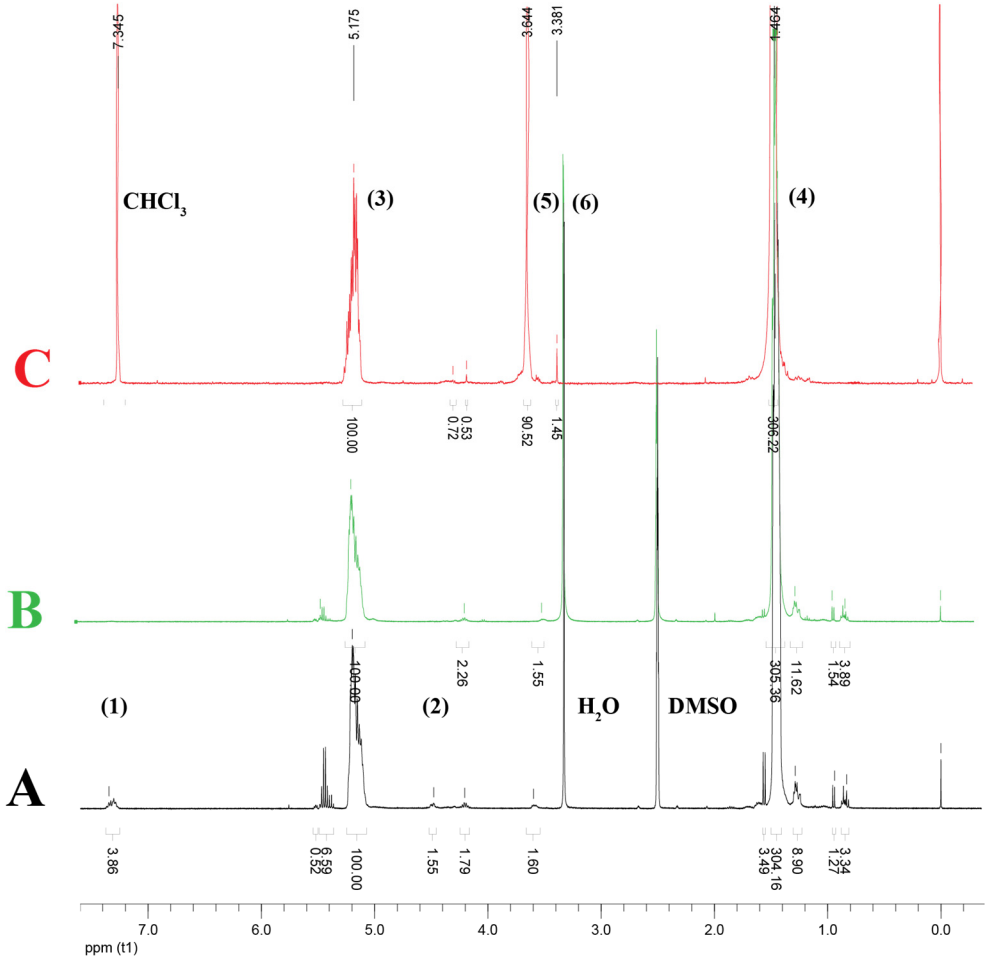

Figure S1 (A) NMR spectra of Bz-*g*-PLA, (B) HO-*g*-PLA and (C) PEG-*g*-PLA. Signal attributions are presented in Figure S-2.

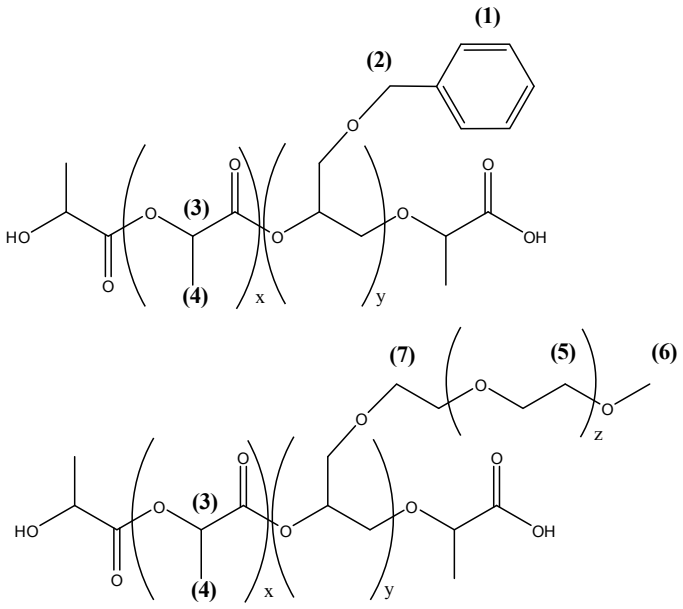

Figure S2 ^{1}H-NMR signals attribution for a Bz-*g*-PLA copolymer and PEG-*g*-PLA polymer

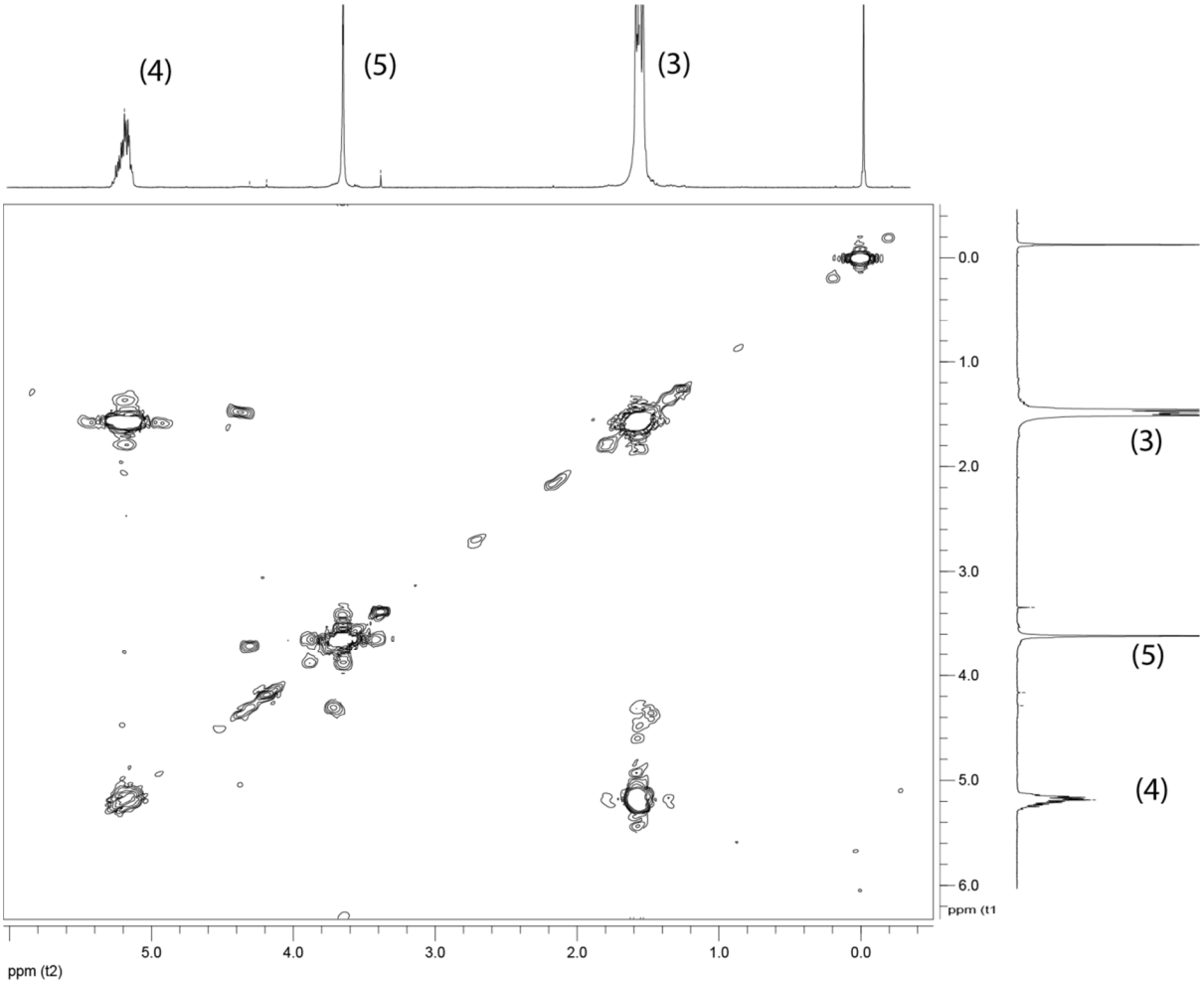

Figure S3 Representative Cosy NMR spectra of PEG-*g*-PLA prepared by the acyl-chloride pathway. For proton signal attribution see Figure S-2. Characteristic coupling peaks are displayed in the spectra in the 4.1-4.4 ppm region between lactic monomer, PEG and grafting moieties.

In table S-1, are presented the characterization of the copolymer backbone. The calculations for the number of available hydroxyl groups for each batch are also included. These calculations are based on the number of benzyl group prior catalytic hydrogenation, the M_n of each polymer and of PEG used in this study (M_w 2000). In all case, after catalytic hydrogenation, the benzyl group peaks were below detection limit by NMR and the reactions were considered as complete. The total numbers of hydroxyl groups are calculated by chains and as percentage of lactic acid monomer.

Table S1 Examples of PLA backbones polymers synthesis and characterization from polymerization of Bz-*g*-PLA to catalytic hydrogenation and preparation of HO-*g*-PLA

BGE/LA	Benzyl/LA	GPC after			GPC after catalytic			pendant	terminal	total OH	total OH
feed ratio	ratio	polymerization			hydrogenation			OH	OH		
	RMN	*Mn*	*Mw*	*Pd*	*Mn*	*Mw*	*Pd*	*per chain*	*per chain*	*per chain*	*% LA*
%	*%*	*g/mol*	*g/mol*		*g/mol*	*g/mol*					
0,5	**0,42**	14720	24240	1,64	24330	33890	1,39	***0,86***	***1***	1,86	0,91
1	**0,55**	15700	22700	1,145	31000	45800	1,48	***2,15***	***1***	3,15	1,45
1,00	**0,75**	15030	23170	1,54	18580	28360	1,52	***1,93***	***1***	2,93	1,40
1,50	**1,08**	18480	31660	1,71	14180	23990	1,69	***2,77***	***1***	3,77	1,47
2,00	**0,77**	17190	28070	1,63	16720	25190	1,50	***1,82***	***1***	2,82	1,18
2,00	**1,14**	23880	36800	1,54	25250	37385	1,48	***3,78***	***1***	4,78	1,44

S.1.2. Acyl chloride PEG coupling reaction

The alternative grafting procedure by DCC coupling is presented in Scheme S-1.

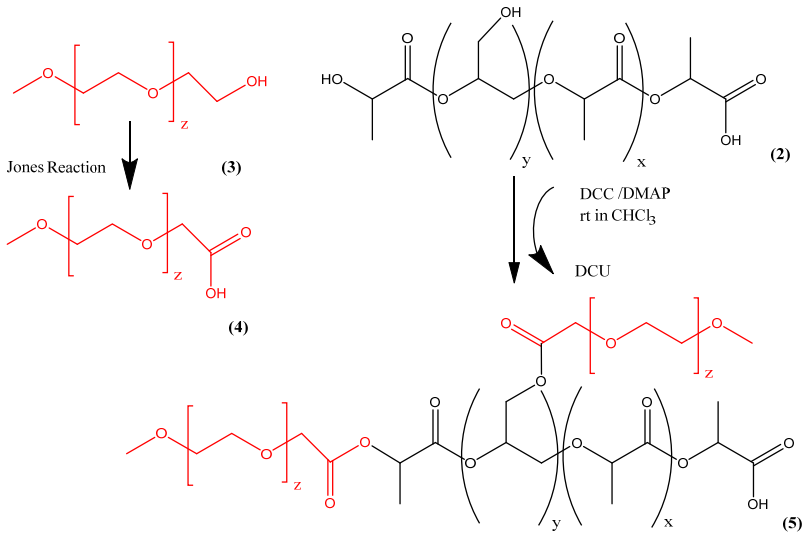

Scheme S1 PEG grafting on HO-*g*-PLA with DCC coupling reaction illustrating the grafting sites for PEG chains.

S.1.3. Infrared spectra

In figure S-4 are presented some representative FTIR spectra of the synthetized polymers acquired in ATR mode (see Material and methods). Peaks lists are presented in Material and Methods.

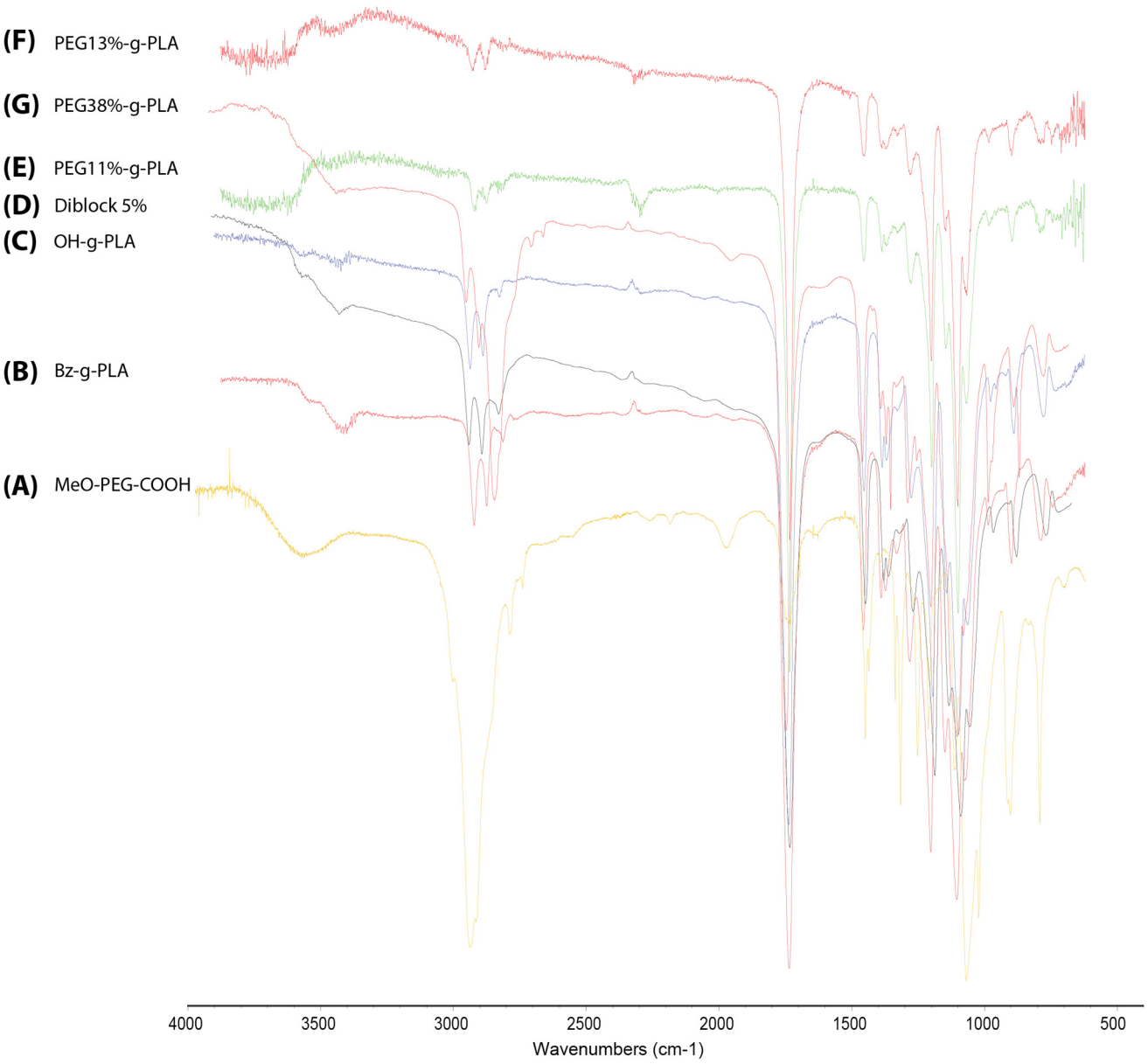

Figure S4. FTIR of the polymers: (A) MeOPEG-COOH, (B) Benzyl-*g*-PLA, (C) OH-*g*-PLA (D) Diblock (5% PEG % w/w) and (E) PEG-*g*-PLA with a PEG content of 11% (w/w) (F) PEG-*g*-PLA with a PEG content of 13% (w/w) (G) PEG-*g*-PLA with a PEG content of 38%. Peaks list for representative polymers can be found in the Material and method section.

S.1.4 Pycnometry, polymer density

Helium pycnometry gave a density of around the true density of the polymers used and for instance, density was found to be around 1.25 $g.cm^{-3}$ for all the PEGylated polymers tested (molecular weight 20,000 to 35,000 and % w/w PEG content of 5 to 35%). This value was retained for future calculations. We took this average value to calculate individual NP weight, number of polymer chain in each NP (for a given M_n) , and thus, number of PEG chain (based on equations presented in section S-3) present in the NPs of different radius. NP microporosity volume correction factor, as determined by gas adsorption [1] was included in the calculations but play a minor role in these determinations.

S.2. Methoxy-PEG oxidation

Methoxy-PEG 2kD oxidation to Methoxy-PEG-carboxy was followed by NMR. As seen on Figure S-5, CH_2 in the vicinity of the carboxyl group is displaced to 4.2 ppm upon hydroxyl oxidation. The integration relative to the Methoxy protons (3H at 3.45 pp) gives a global yield of oxidation of 95%.

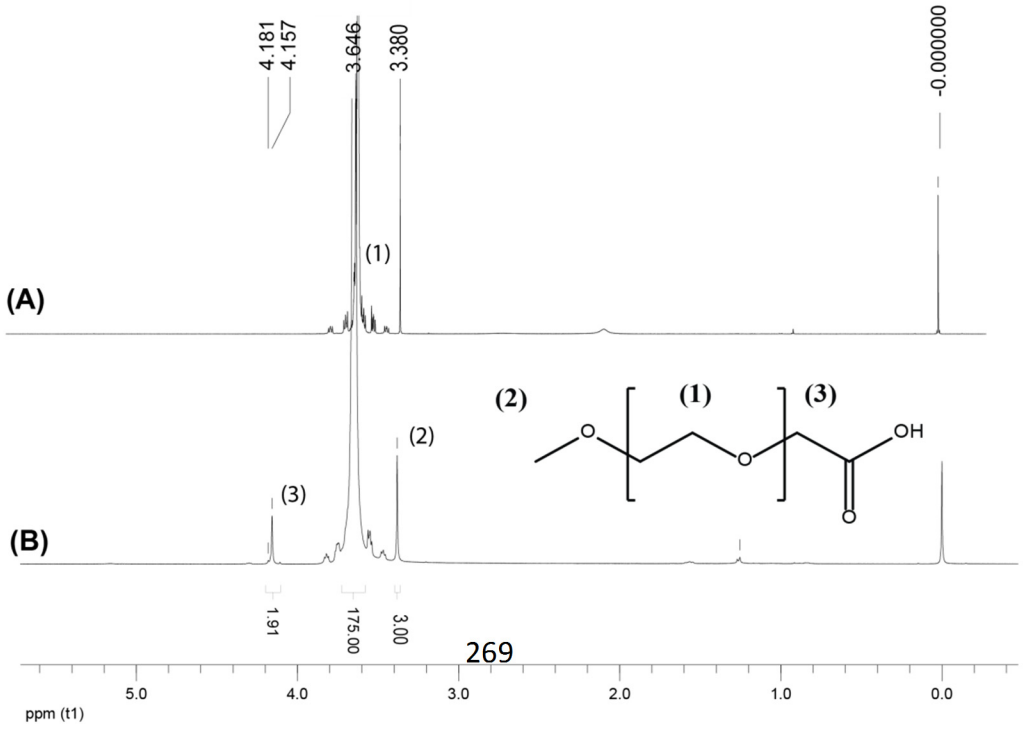

Figure S5 ^{1}H-NMR spectra of MeO-PEG before (A) and after (B) Jones oxidation.

S.3. Theoretical calculations.

The calculations below were used in polymer characterization.

S.3.1 Number of PEG chain per polymer chain

PEG-*g*-PLA is a random-branched polymer with a structure shown in Figure. S-2. *x* is the number of lactic moieties in the chain; *y* the number of grafted moieties and *p* is defined as the molar faction of *y* (value obtained by ^{1}H NMR) and it is expressed by equation (S3-1) :

$$p = \frac{y}{x+y} \qquad \textbf{(S3-1)}$$

The molecular weight of polymer chain (m_p) is the sum of all lactic units and grafted branches and it is expressed by equation (S3-2), with 72 being the molecular weight of a lactic acid monomer; m_g: molecular weight of a grafted moiety (as seen in Figure S-2) :

$$m_p = 72\,x + m_g\,y \qquad \textbf{(S3-2)}$$

Extracting *x* from (**S3-1**), yield

$$x = \left(\frac{1-p}{p}\right) y \qquad \textbf{(S3-3)}$$

Substituting x in (S3-2) and expressing y, the number of grafted chains per polymer chain:

$$y = \frac{m_p\,p}{72(1-p) + p\,m_g} \qquad \textbf{(S3-4)}$$

p is calculated from NMR spectrum (equation S3-1, value between 0 and 1); m_p is measured by GPC; m_g is the M_n of PEG chain considering that the grafting connecting group (glycidyl ether) has a minor impact on M_n of pendant groups (PEG).

S.3.2. Polymer PEG content (% w/w)

Finally percentage of PEG in the copolymer expressed in weight/weight (% w/w) content is

calculated as follow (similar to equation S1-1):

$$PEG\ (\%\ w/w) = \frac{y \times M_g}{M_p} \times 100 \qquad \textbf{(S3-5)}$$

Noteworthy, some approximations are inherent to these calculations. First of all, M_n of random branched polymer is determined by GPC using linear PS standard as references. Copolymer of PLA and PEG may have a different behavior in eluent resulting in uncertainty over M_n. If the calculations are based on mean (M_n), but all these polymers have a significant PDI, number of PEG chains may differ and consequently polymers may differ in properties. Noteworthy, the equation is valid whether the grafting occurred only on pendant groups or if it also occurred on the OH terminal group of the PLA chains.

S.4. Polymer viscosity data

One of the determinants of particle properties produced by nanoprecipitation is polymer content in the organic phase and its effect on the phase viscosity. As shown in Figure S-6, the addition of PEG chains on otherwise constant hydrophobic PLA backbones (here around 25 kD) decrease the viscosity of the acetone organic phase. Beside PEG stabilization of newly formed nanoparticles, this could also affects, size and yield of NP production. [2]

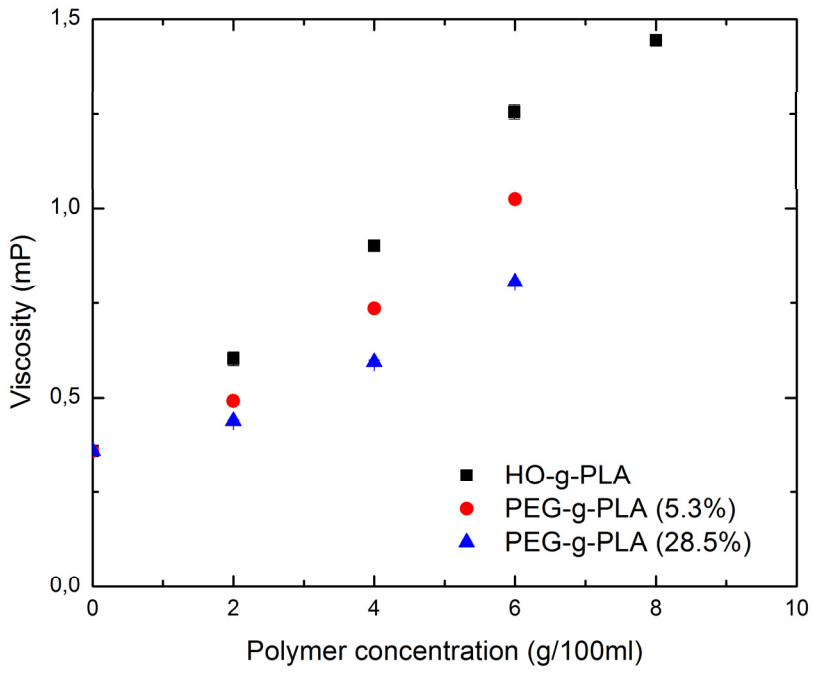

Figure S6 Viscosity of PLA-PEG solutions in function of concentration

S.5. X-rays photon spectroscopy (XPS)

S.5.1 XPS Survey data

Measurements of NPs in the dry state, allowed the quantification of chemical bonds and thus chemical entities, such as PEG or preparation additives on the outmost portion (5-10 nm) of the particles surface. Quantification of relative presence of PEG based on survey (elemental) analysis is difficult as both PEG and PLA segments of the copolymer have close carbon and oxygen composition. Moreover, carbon contamination by environmental exposure of the samples during transfer complicates the analysis. The survey scans results giving element composition in relative % are available in Table S-2. The data are expressed as a percentage of total elements present. No relationships were found between these data and NP PEG content.

Table S2 Elemental composition of NP surface, XPS survey analysis (total element=100%).

	Polymers			**Nanoparticles**					
	PEG	Diblock	HO-g-PLA	NP-PLA	NP-Diblock	NP-PEG-g-PLA	NP-PEG-g-PLA	NP-PEG-g-PLA	NP-PEG-g-PLA
PEG content w/w (%)	0	5	0	0	5	5.6	8.3	11.1	16.5
	% element	% element	% element	% element	% element	% element	% element	% element	% element
C1s (%)	64.4	60.5	58.6	58.3	63.8	59.8	60.6	62.2	61.8
O1s (%)	35	39.5	41.4	40.3	35.5	39.8	38.9	36	36.8
Others (%)	0.7	0	0	0.7	0.7	0.3	0.5	1.9	1.5

	Nanoparticles					
	PEG-b-PLA *		PEG-g-PLA *		PEG-g-PLA *	
PEG content w/w (%)	5		8.9		13.3	
	% element	*SD*	% element	*SD*	% element	*SD*
C1s (%)	61.4	*1.5*	61.8	*2.1*	59.7	*1.9*
O1s (%)	38.5	*1.4*	37.8	*2.1*	39.6	*1.4*
Others (%)	0.1	*0.2*	0.42	*0.4*	0.5	*0.1*

* measures n=3

S.5.2 XPS High resolution data

Table S3 High resolution data, chemical composition of NP surface

		Polymer	**Nanoparticles**												
		PEG	PLA	PEG-b-PLA	PEG-g-PLA	PEG-g-PLA	PEG-g-PLA	PEG-g-PLA	PEG-g-PLA	PEG-g-PLA	PEG-g-PLA	PEG-g-PLA	PEG-g-PLA	PEG-g-PLA	PEG-b-PLA	PEG-b-PLA
	PEG content w/w (%)	0	0	5	5.6	8.3	11.1	16.5	11.1	8.9	8.9	8.9	13.3	13.3	5	5
Identification	Binding energy (eV)		*Relative Atomic percentage (each element on 100%)*													
C-C (Cont.)	285	7.9														
C-C (PLA)	285		35.6	37.6	28.7	27	24.1	22.6	33.7	39.7	33.05	36.7	31.45	33.65	32.3	34.75
C-O (PEG)	285.9-286.6	**85.7**		**11.4**	**19.6**	**24.4**	**32.5**	**36.6**	**21.4**	**21.7**	**27**	**21.9**	**31.35**	**19.9**	**27.15**	**25.7**
C-O (PLA)	287.0-287.2		34	26.2	27.3	25.7	22.9	21.5	23.9	23.9	25.15	20	19.35	25.25	29.7	28
C=O	288	6.4														
O-C*=O (PLA)	289.0-289.2		30.4	24.6	24.4	22.9	20.5	19.2	21	14.7	14.8	21.4	17.8	21.2	10.85	11.6
O=C (PLA)	531.2-532.5	10.1	51.8	49.1	43.6	45.5	38.8	36.2								
O-C (PEG)	533	89.9		**5.1**	**15.8**	**12.1**	**25**	**30.1**								
O*-C=O (PLA)	533.5-533.9		48.2	45.8	40.6	42.4	36.2	33.7								
Particle size (dist. by number)			117.4	59.9	110.2	96.5	107.7	103.3	87.5	149.1	100.95	83.1	131.05	109.6	71.05	50.95
Polydispersity index			0.079	0.136	0.068	0.093	0.104	0.078	0.076	0.113	0.09	0.096	0.069	0.0675	0.2515	0.105
Nanoprecipitation conditions (polymer conc, mg/ml)			20	20	20	20	20	20	20	33	20	12.5	33	20	33	20
Repeats (n)											n=2		n=2	n=2	n=2	n=2

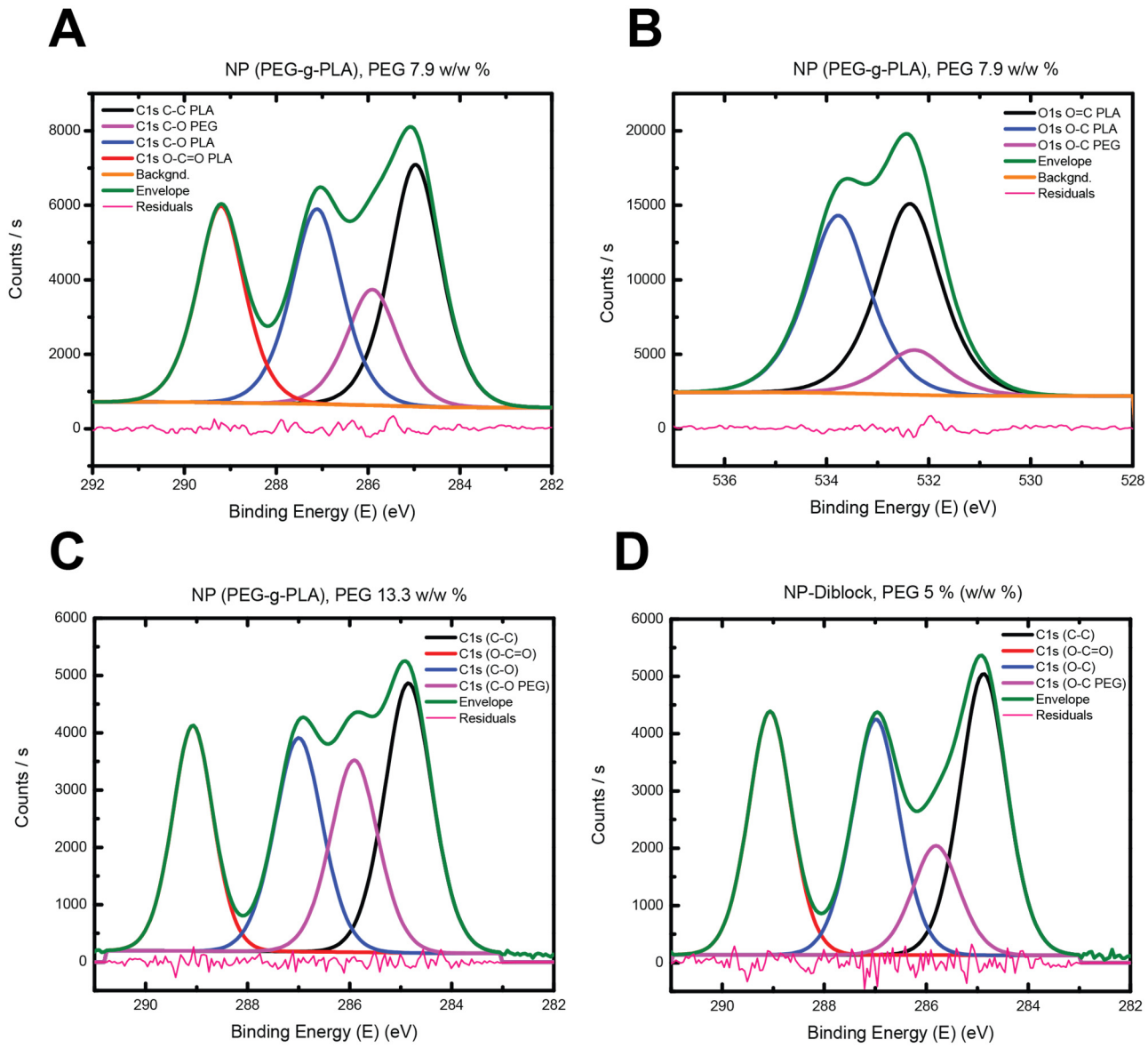

Figure S7 Examples of high resolution data with deconvoluted C1s (A) and O1s peaks (B) for PEG-g-PLA NP with a 7,9 % PEG content. (C) PEG-g-PLA NP with a 13.3 % PEG content and (D) for PEG-b-PLA diblock NP (5% PEG content).

PEG amounts on the NP surface were thus estimated on the basis of high resolution spectra allowing calculation of relative contribution of different chemical bonds. Ether bond are specific to PEG, although it can be found in the copolymer as a result of copolymerization

of glycidyl ether with dilactide, albeit at a very low percentage that could be neglected (see Scheme 1 and Scheme S-1). It gives a specific signal that could be distinguished from PLA signals. [3] The depth of upper layer accessible to analysis depends on several factors: nature of the element (C, O), angle of emission, nature of the material (density), etc. For the type of polymer studied and the emission angle used (0^o), we estimate the maximum depth of analysis (99% of the signal observed) for carbon to be 9.6 nm; and 7.8 nm for Oxygen. [4]

S.5.3 Calculation of PEG surface density estimates by XPS

PEG surface content was evaluated from high resolution XPS spectra (representative examples are shown in Figure S-7). As mentioned earlier, XPS is collecting information from the 10 nm outer layer of nanoparticles for C1s. The percentages given by XPS result are expressed in weight percentage of polymer (Table S-3). As only two components are present on the NP surface (PLA and PEG), is thus possible to give an estimation of the number of PEG chain in the 10 nm outer layer of the particle and deduced a surface density, ***if we assume that all the PEG chains detected are localized exclusively at the interface***.

a. Volume and weight of the XPS analyzed area

$$V_{OL} = \frac{4\pi r^3}{3} - \frac{4\pi(r-10)^3}{3} \qquad \textbf{(S5-1)}$$

V_{OL} is the volume of the 10 nm outer layer (nm^3) with r the mean radius (nm) of the nanoparticle batch as determined by DLS or TEM.

$$W_{OL} = \left(\frac{V_{OL}}{10^{21}}\right) \times \sigma_{POL} \qquad \textbf{(S5-2)}$$

W_{OL} is the weight of this outer layer (in g) with σ_{POL} the density of the polymer (g cm^{-3}), values given by pycnometry on raw polymers.

These calculations are estimate as several sources of uncertainty could be evoked: radius of particle is determined by DLS (error on measure), density could slightly vary if PEG content in copolymer increase (pure PEG have a density around 1.1 $g.cm^{-3}$, while PEG-g-PLAs have densities around 1.25 $g.cm^{-3}$), M_n of branched copolymers is determined as a normal distribution of molecular weight by GPC compared to linear PS standards, which could also introduced bias in M_n results.

b. XPS results

Calculations are based on C1s signal deconvolution (Figure S-7). Area percentages carbon bonds are proportional to mass of carbon in each polymer species in the NP outer layer, defined as the layer of the nanoparticle accessible to XPS analysis. Ether bonds are almost exclusively found in the PEG (negligible amount in copolymer, and they are not detected prior PEG grafting on OH-*g*-PLA) and are representative of PEG carbon content. In the nanoparticle, we have a material composition that can be described as a binary polymer blend of PLA and PEG (as no other species are present) and :

Fraction of PLA = (1 - Fraction of PEG)

$\%W_{PEG}$, weigh percentage of PEG in the outer layer according to XPS data will be calculated from:

$$\%\,W_{PEG} = \frac{Area_{Carbon\,(PEG)} \times 1.83}{\left[Area_{Carbon\,(PEG)} \times 1.83\right] + \left[Area_{Carbon\,(PLA)} \times 2\right]} \qquad \textbf{(S5-3)}$$

Or more precisely:

$$\%W_{PEG} = \frac{Area_{O-C(PEG)} \times 1.83}{\left[Area_{O-C(PEG)} \times 1.83\right] + \left[\left(Area_{C-C(PLA)} + Area_{O-C=O(PLA)} + Area_{C-O(PLA)}\right) \times 2\right]}$$

The ratio added to each peak contribution to convert specific carbon content to specific polymer content are calculated from the carbon contribution to each polymer total weight:

1.83 is given by $\frac{Total\ Mass\ of\ PEG}{Total\ Mass\ of\ carbon} = \frac{Mass\ of\ PEG\ monomer}{Mass\ of\ carbon} = \frac{44}{24} = 1.83$

2.00 is given by $\frac{Total\ Mass\ of\ PLA}{Total\ Mass\ of\ carbon} = \frac{Mass\ of\ PLA\ monomer}{Mass\ of\ carbon} = \frac{72}{36} = 2$

Thus , W_{PEG}, weigh of PEG (g) in the outer layer can be calculated with σ_{OL} density of the polymer in the outer layer (we used σ_{POL}determined by pycnometry in our calculations):

$$W_{PEG} = \%W_{PEG} \times W_{OL} = \%W_{PEG} \times \left(\frac{V_{OL}}{10^{21}}\right) \times \sigma_{OL} \qquad \textbf{(S5-4)}$$

Number of PEG chain according to XPS in the outer layer:

$$N_{PEG} = \frac{W_{PEG}}{M_{n(PEG)}} \times \mathcal{N} \qquad \textbf{(S5-5)}$$

with M_n as the molecular weight by number of PEG (g. Mole^{-1}) and $\mathcal{N}$ the Avogadro number (6.022 10^{23}).

Finally, PEG density on the surface (D_{PEG}), will be given by (S5-6); assuming all PEG detected in the outer layer are on the surface only and the surface:

$$D_{PEG} = \frac{N_{PEG}}{4\pi r^2}\ (PEG/nm^2) \qquad \text{(S5-6)}$$

Similar calculations can be carried out with O1s results and they give concordant results with C1s (data not shown).

S.6. PEG surface density calculation based on NMR results

S.6.1 NMR quantification spectra

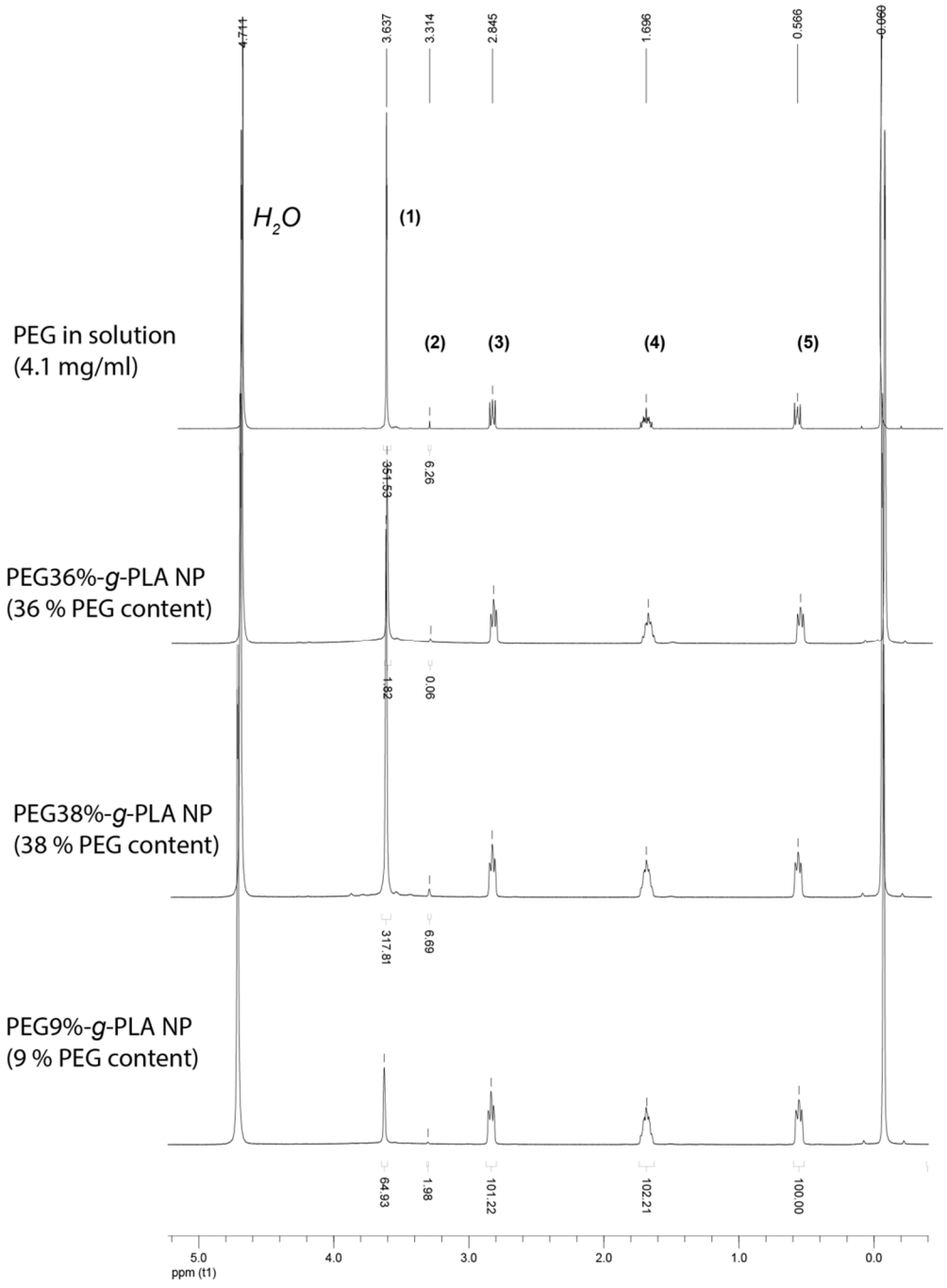

Figure S8 NMR results of NP suspensions diluted in Deuterium oxide.
Internal standard peaks (3), (4) and (5) of the 3-(trimethylsilyl)-1-propanesulfonic acid, sodium salt (DSS) – (CH_3) serve as reference standard (each methyl group peak were arbitrarily set at 100), while Methoxy-PEG peaks (1) and (2) serve for quantification.

S.6.2 Calculations of PEG surface density based on NMR results

Calculations were based on the NP diameter (radius from the distribution in number) obtained by DLS, mass concentration of particles in the assay measured by gravimetry, the average mass of a single particle: assuming a mono-disperse population of NP centered on average mean size and a density of 1,253 g/cm3 (see *Picnometry*). The values calculated are the area per PEG (nm^2), the number of PEG per surface unit and the percentage % of total PEG found on the surface.

a. Total PEG in polymer or NP samples

The total PEG content in weight percentage (PEG % w/w) could be calculated from:

$$F_{PEG} = \frac{y \times M_{PEG}}{M_{POL}} \qquad \textbf{(S6-1)}$$

with F_{PEG} the weight fraction of PEG in a polymer, y the number of grafted chains, M_{PEG} the molecular weight of PEG chains and M_{POL} the molecular weight of the PEGylated polymer.

The total weight of PEG in the sample is thus:

$$TW_{PEG} = W_s \times F_{PEG} \qquad \textbf{(S6-2)}$$

with W_s, weigh of nanoparticle (weight of sample) in mg in the tube.

In NMR experiment, polymer or lyophilized NP are dissolved in $CDCl_3$. As seen in Figure S1, spectrum (C) the ratio between PEG signals (CH2-CH2-O, δ at 3.6 ppm or CH3-O-, δ at 3.3 ppm) and lactic acid monomer CH signal (CH, δ at 5.2 ppm), give the number of PEG chains (*y*).

b. PEG percentage on the surface

When concentrated particle suspensions are resuspended in D_2O (or when particles are prepared by nanoprecipitation with D_2O as an aqueous external phase), PEG detected by NMR is the surface PEG. The surface PEG weight in the sample (SW_{PEG} in mg) can be calculated from free PEG standard solution in D_2O using the same internal standard. In our case we used the water soluble 3-(trimethylsilyl)-1-propanesulfonic acid, sodium salt (DSS) at a concentration of 1% (w/w).

The PEG percentage of total PEG segregated at the NP surface can be calculated from:

$$\%S_{PEG} = \frac{SW_{PEG}}{TW_{PEG}} \times 100 \qquad \textbf{(S6-3)}$$

c. PEG density on the surface (PEG/nm^2)

In order to calculate PEG surface density from NMR data, we need the following information: 1) the surface PEG to particles mass ratio (given by the analytical method); 2) the total mass of the sample analyzed (given by gravimetry); 3) the diameter of the particles (given by DLS, TEM, etc.), and 4) the volumetric density of the particle (given by pycnometry

from polymer volumetric density data). Details about the equations can be found in the supporting information section of the review by Rabanel *et al.*. [5] The PEG surface coverage-density σ (PEG/nm^2) is written as:

$$\sigma = \frac{N_{PEG}}{S} \qquad \textbf{(S6-4)}$$

where N_{PEG}, is the total number of PEG chains present at the surface of the *sample* and S is the *total* surface area of the core particles present in the *sample*. S is written as:

$$S = \left|\left(\frac{W_C}{V_C\,\rho_C}\right) S_C\right| \qquad \textbf{(S6-5)}$$

Using the equation above we can rewrite equation S6-4, where W_C, is the total mass of particle cores in the sample, V_C is the average volume of one core particle, ρ_C, is the mass density of the particle core and S_C, is the mean surface area of one particle core:

$$\sigma = N_{\mathrm{PEG}} / \left|\left(\frac{W_C}{V_C\,\rho_C}\right) S_C\right| \qquad \textbf{(S6-6)}$$

The total number of PEG chains in the sample is obtained from the analytic quantification data (weight of PEG found on the sample surface):

$$N_{\mathrm{PEG}} = \frac{W_{\mathrm{PEG}}}{M_{\mathrm{PEG}}}\,\mathcal{N} \qquad \textbf{(S6-7)}$$

where W_{PEG}, is the mass of surface-bound PEG present in the *sample*, M_{PEG} is the molecular weight, of a PEG chain, and $\mathcal{N}$ is the Avogadro number. Using equation S6-7, one can rewrite Eq. S6-4 in terms of experimentally accessible quantities for spherical particle:

$$\sigma = \frac{\rho_C\,R_C\,\mathcal{N}\,W_{\mathrm{PEG}}}{3\,M_{\mathrm{PEG}}\,W_C} \qquad \textbf{(S6-8)}$$

Discussion on PEG density

The factors likely playing a role in NP PEG surface density (outside PEG content in %w/w and the number of PEG chain) are the M_w of the hydrophobic part of the copolymer; the PEG chain foot print preventing high density related to M_w of PEG chain. When distances between PEG chain attachment points are smaller than R_f, PEG chains start to overlap and tend to form "brush", and PEG layer thicken. When surface density increase, PEG chain repulsion may result in free energy penalty leading to a maximum PEG chain surface density. Indeed it can be speculated that hydrated PEG chains can sterically repulse themselves creating an energetic barrier to PEG layer densification above a critical density at the time of NP formation. Formation of dense polymer brushes extending well into the bulk liquid is limited in liposome by steric interactions. PEG chains reciprocal lateral repulsions opposed to anchoring stability (provides by the cohesion of the phospholipids bilayer) are making them unstable above a PEG content threshold. [6-7] In contrast, one can expect to be able to reach higher density for polymeric NP as PEG chains are anchored to a stable core. However, in polymeric NP, the PEG density could be also limited by steric constraints either from the architecture of the polymer used or by steric hindrances at the surface. One other important constraint is the polymer entanglements (topological constraints) during solvent removal from the droplet trapping PEG inside the NP core, decreasing the availability of PEG at the surface. This effect increases with the size of the NP.

S.7. Differential Scanning Calorimetry of polymers and NPs

Table S4 Tg of polymers and freeze-dried NP

Samples	PEG content	Tg	Tg interval	M_w
	% w/w	°C	°C	

Polymers before PEG grafting				
Bz-*g*-PLA	0	31,9	28.1-34.9	28100
OH-*g*-PLA	0	39,7	36.1-42.3	25300
PLA	0	50,8	47.1-51.8	46 400
Polymers after PEG grafting				
PEG-b-PLA (diblock)	5	28,6	20.6-31.2	23 800
PEG-*g*-PLA	9	28,5	21.8-34.1	36 560
PEG-g-PLA	9	25.7	22.4-28.3	29 890
PEG-*g*-PLA	11	24,3	15.4-31.8	35 200
PEG-*g*-PLA	20	19,5	12.3-22.3	28 950
PEG-*g*-PLA	25	-4,3	-15.8-9.3	33 080
Nanoparticles (1st run)				
Solid particle	0	14.7	13.3-16.5	19 500
	9	11,9	9.3-14.4	21 530
	11	12.3	10.7-14.7	35 200
	13,3	11.7	9.8-13.7	34 490
	16,5	12.5	10.7-13.6	35 800
Micelle-like NP	15	11,9	11.1-13.1	38 150
	19,8	12.5	10.9-13.8	33 080
	35,7	13.0	11.1-14.8	33 600
	37,9	13.2	11.5-15.1	31 420

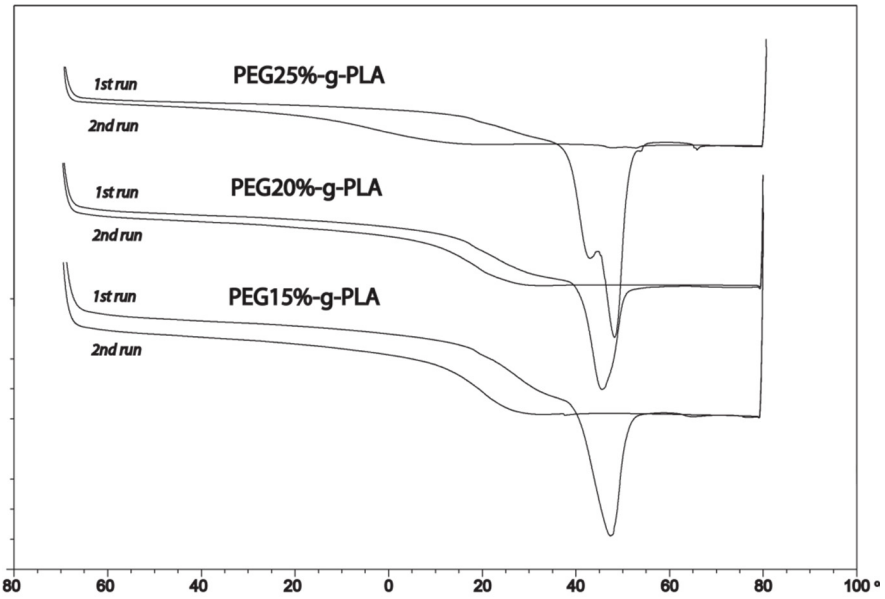

Figure S9 DSC thermograms of polymers used in this study (first and second runs). Polymer with high PEG percentage (>15% w/w)

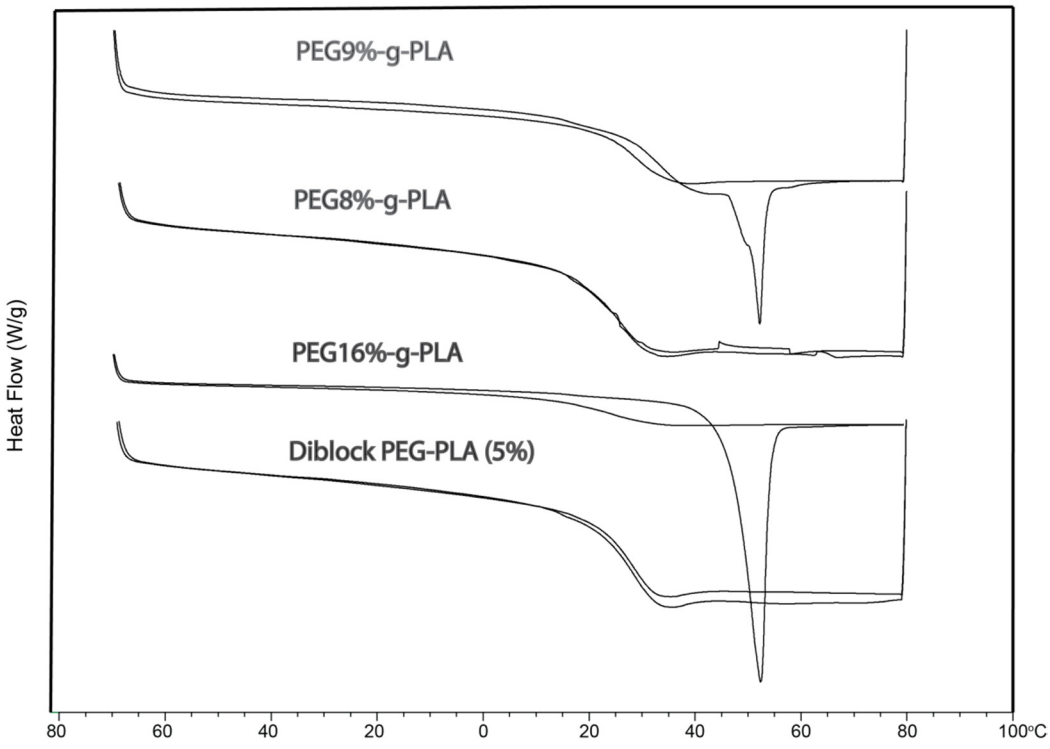

Figure S10 DSC thermograms of polymers used in this study (first and second runs). Polymer with low PEG percentage content (<10% w/w)

S.8. TEM observation: apparent core-shell.

As discussed in the main text, the apparent core-shell structure observed is likely due to the contact between the particle and the carbon film of the TEM grid as demonstrated in the cartoon below (Figure S-12). If the darker central area was due to a core component, its position will not be changed upon tilting of the sample grids. The fact is that upon sample tilt (+15 and +30° angle), the darker area shift from the center to its edges support the hypothesis. The surface of contact is dependent over the geometry of the particle, its general softness or the deformability of the outer layer of the particle upon drying. It was not possible to draw conclusions about a possible relationship between the PEG content w/w% (and thus possible softness of particle) and relative size of the contact zone.

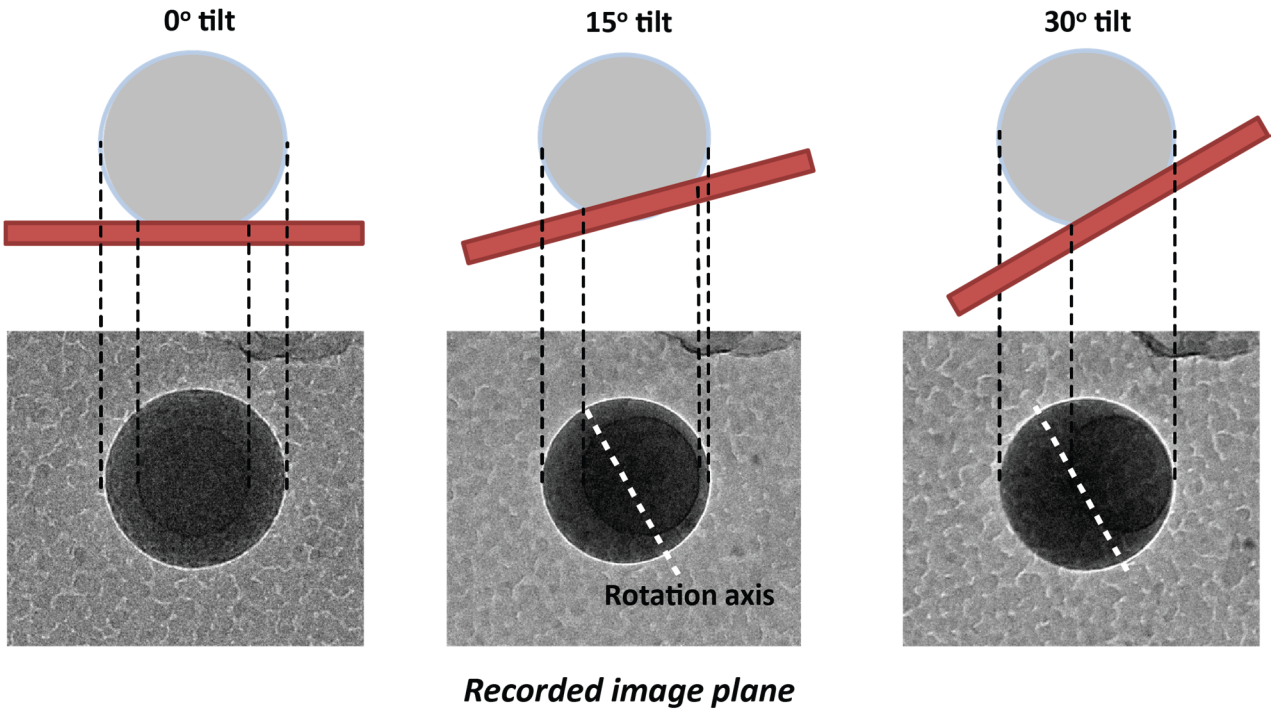

Figure S11 TEM of polymeric NP: illustration of the apparent core-shell structure

S.9. Proteins absorption studies

The absorption isotherms and data analysis were based on the following BSA and LYS parameters displayed in Table S-4.

Table S5 Properties of the proteins used in the protein adsorption studies

	M_w	**IP**	**Dimensions**	**Volume**	**Surface 1**	**Surface 2**
	KDa		*nm*	*nm^3*	*nm^2*	*nm^2*
BSA	68	4.7	9 x 5 x 5	237.5	45	25
Lysozyme	14.3	11.35	4.2 x 3 x 3	37.8	12.6	9

* M_w: molecular weight, IP: isoelectric point

S.10. Particles preparation and concentration.

Prior ITC experiments and NMR quantification, particles batches were concentrated. Solid particles were concentrated with a cross-flow filtration column, while micelle-like particles were concentrated by reverse osmosis as described in Material and methods. The results displayed in Table S-5, show the evolution of size and polydispersity following the concentration procedure. The most PEGylated polymeric NP, and smaller NP, were concentrated by reverse osmosis while less PEGylated (below 14 % PEG w/w) were concentrated by cross-flow filtration. The trend with the reverse osmosis concentration method shows an increase of PDI while size (Mean in number and z-average) stay stable. With the

cross-flow filtration method, we observed a stability of size and PDI upon concentration of the NP suspension.

Table S6 Size and PDI measurements of NP batches before and after concentration, either by cross-flow filtration (solid particle) or inverse osmosis (micelle-like particle).

Concentration method		Before concentration			After concentration		
	NP batches	D_N *	D_Z *	PDI	D_N	D_Z	PDI
	polymer	*nm*	*nm*		*nm*	*nm*	
Cross-flow filtration	PLA	159.1	194.3	0.08	160.2	215,4	0.090
	PEG-b-PLA	132.1	160.6	0.061	135.6	178.3	0.112
	PEG8%-g-PLA	141.1	176.7	0,082	142.9	171.7	0.063
	PEG11%-g-PLA	134.8	172.2	0.087	141.2	169.9	0.081
Inverse osmosis	PEG15%-g-PLA	68.9	139.8	0.18	94.5	262.0	0.376
	PEG20%-g-PLA	31.7	107.3	0.233	28.9	69.2	0.249
	PEG36%-g-PLA	16.9	37.1	0.253	13.6	36.0	0.345
	PEG38%-g-PLA	55.6	107.4	0.158	62.8	109.2	0.147

** D_N number averaged mean diameter; D_Z: z-averaged mean diameter*

S.11 Colloidal stability and protein binding

Table S7 BSA Protein binding study before and after ITC experiments, NP size measures by DLS and Zeta potential measured on a Zetasizer, Malvern®.

NP batches	Type		Size		Zeta pot.	
			Mean	PDI	Mean	SD
			nm		*mV*	*±mV*
NP Peg-g-PLA	**Comb**	Pre-ITC	120,9	0,079	-52,7	±10,8
9%		Post-ITC	123,1	0,099	-26,6	±16,6
NP Peg-g-PLA	**Comb**	Pre-ITC	109,0	0,080	-38,9	±10,5
11%		Post-ITC	110,2	0,088	-24,5	±8,38
NP Peg-g-PLA	**Comb**	Pre-ITC	126,3	0,068	-45,0	±11,8
4,50%		Post-ITC	128,0	0,067	-23,8	±11,7
Diblock	**Diblock**	Pre-ITC	135,7	0,147	-9,7	±7,25
5 %w/w PEG		Post-ITC	135,3	0,173	-8,4	±7,43

The NP size is not affected by incubation with BSA in all cases. The decrease of Zeta potential supports interaction of BSA (PI: 4.7-4.9) with NP surface. No changes were observed for diblock NP.

REFERENCES

1. Sant, S.; Thommes, M.; Hildgen, P., Microporous structure and drug release kinetics of polymeric nanoparticles. *Langmuir* **2008,** *24* (1), 280-287.
2. Legrand, P.; Lesieur, S.; Bochot, A.; Gref, R.; Raatjes, W.; Barratt, G.; Vauthier, C., Influence of polymer behaviour in organic solution on the production of polylactide nanoparticles by nanoprecipitation. *Int. J. Pharm.* **2007,** *344* (1-2), 33-43.
3. Beamson, G.; Briggs, D., *High resolution XPS of organic polymers The Scienta ESCA300 Database.* John Wiley & Sons Ltd.,: West Sussex, England, **1992**.
4. Tanuma, S.; Powell, C. J.; Penn, D. R., Calculations of electron inelastic mean free paths. V. Data for 14 organic compounds over the 50–2000 eV range. *Surf. Interface Anal.* **1994,** *21* (3), 165-176.
5. Rabanel, J.-M.; Hildgen, P.; Banquy, X., Assessment of PEG on polymeric particles surface, a key step in drug carrier translation. *J. Control. Release* **2014,** *185* (0), 71-87.
6. Bedu-Addo, F.; Tang, P.; Xu, Y.; Huang, L., Effects of Polyethyleneglycol Chain Length and Phospholipid Acyl Chain Composition on the Interaction of Polyethyleneglycol-phospholipid Conjugates with Phospholipid: Implications in Liposomal Drug Delivery. *Pharm. Res.* **1996,** *13* (5), 710-717.
7. Allen, C.; Dos Santos, N.; Gallagher, R.; Chiu, G. N. C.; Shu, Y.; Li, W. M.; Johnstone, S. A.; Janoff, A. S.; Mayer, L. D.; Webb, M. S.; Bally, M. B., Controlling the Physical Behavior and Biological Performance of Liposome Formulations Through Use of Surface Grafted Poly(ethylene Glycol). *Biosci. Rep.* **2002,** *22* (2), 225-250.

Annexe 3. Article 2 (Chapitre 5) « Supporting Information »

Effect of Formulation Parameters and Polymer Architecture on the Surface Properties of Nanoparticles Prepared from Clickable Comb-like Copolymers

Jean-Michel Rabanel[1, 2], Patrice Hildgen[1], Xavier Banquy[2,§]

[1] Laboratoire de Nanotechnologie Pharmaceutique,

[2] Canada Research Chair on Bioinspired Materials and Interfaces

Faculté de Pharmacie, Université de Montréal,

C.P. 6128, Succursale Centre-ville, Montréal, Québec, H3C 3J7, Canada

[§] Corresponding author

1. Methoxy-PEG-azide (mPEG-N_3) characterizations

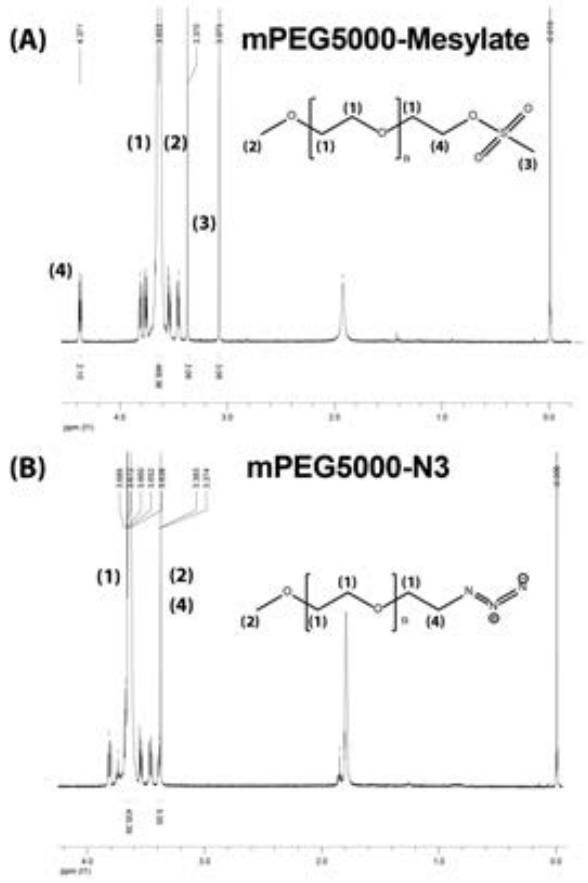

Figure S5.1. ^{1}H NMR spectra of mPEG-Mesylate and mPEG-N_3.

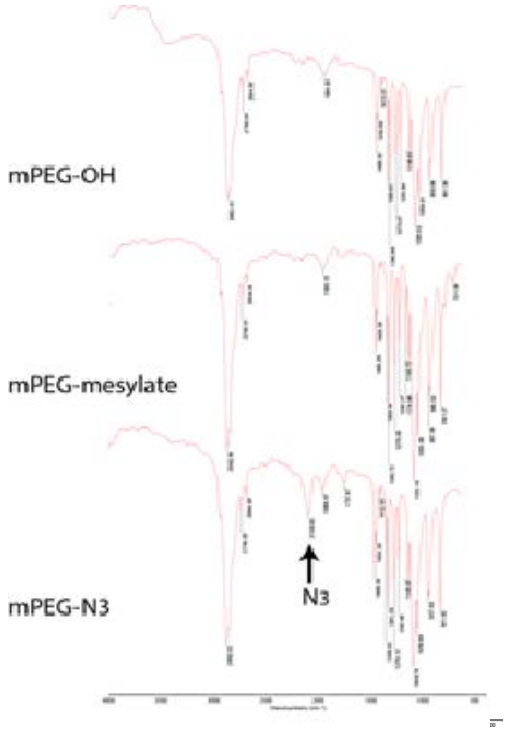

Figure S5.2. FTIR specta of mPEG, mPEG-Mesylate and mPEG-N_3 with the characteristic 2100 cm-1 band (azide)

2. PEGylated polymer characterizations

a. ^{1}H NMR

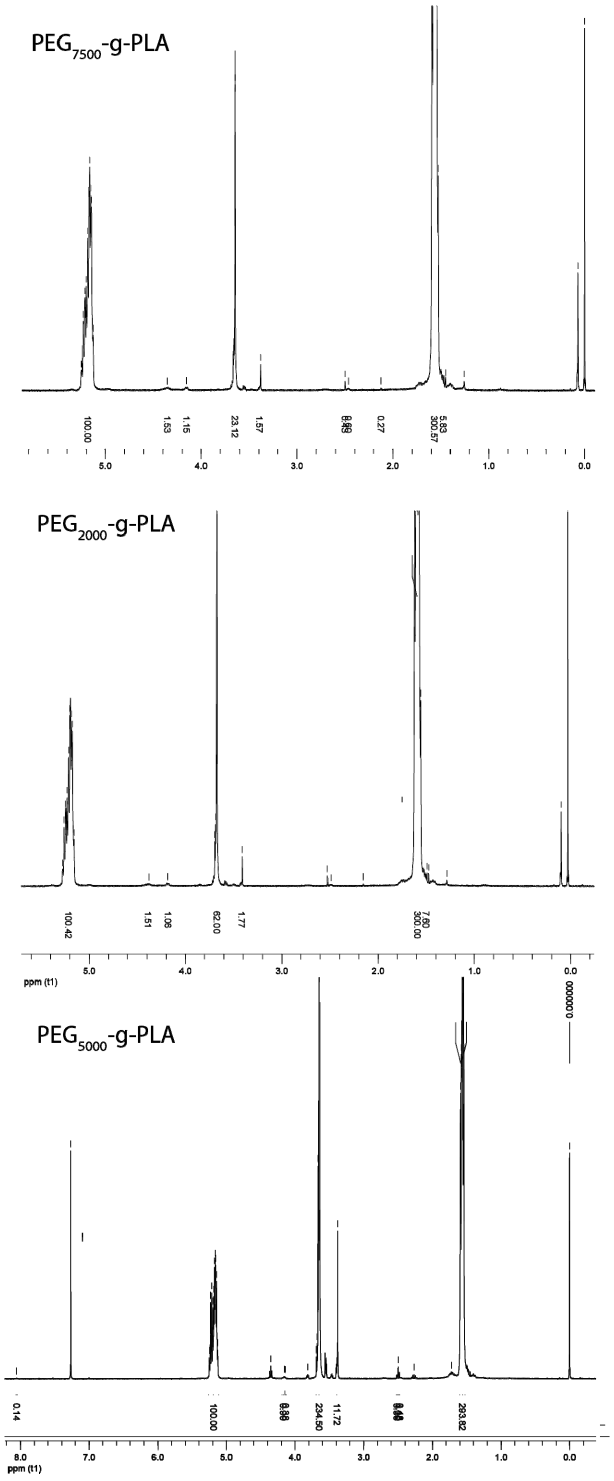

Figure S3. NMR spectra of PEG-g-PLA obtained by click chemistry

3. XPS data

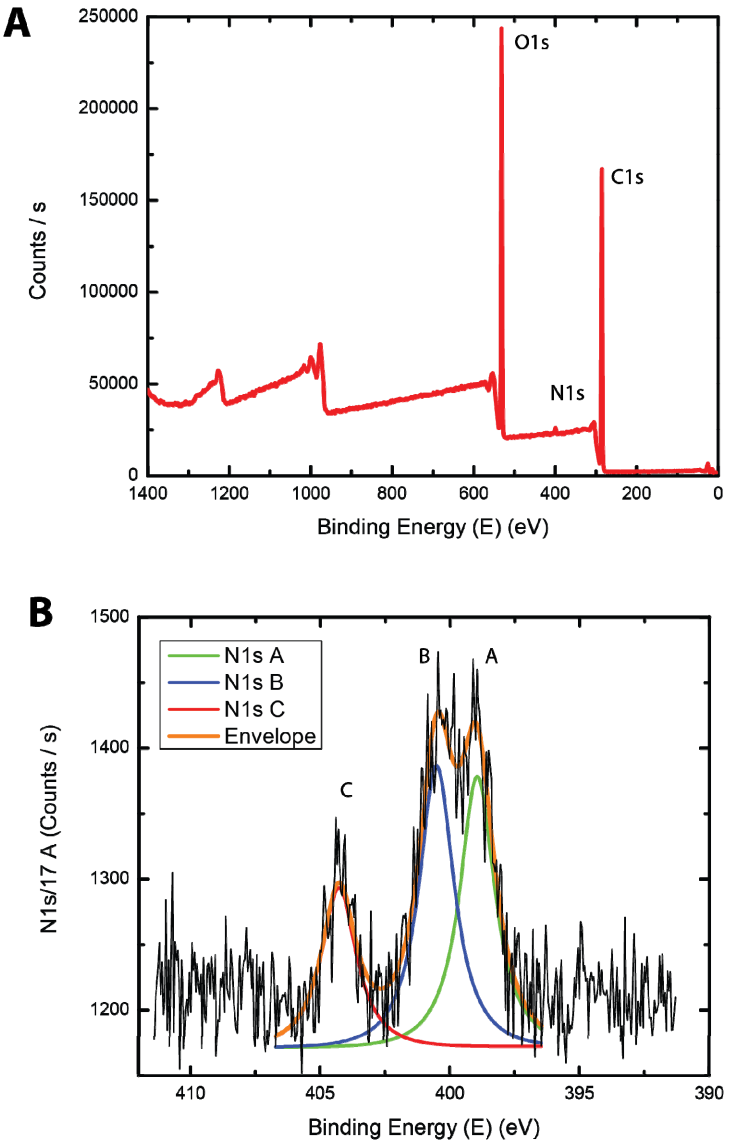

Figure S5.4. XPS survey (A) and high resolution N1s peak (B) of mPEG-N_3 (5kD). Panel B show the characteristic XPS profile of N1s resolved as a 3 peaks entity representing the azide group.

4. Stability of NP size upon concentration

Particles prepared by nanoprecipitation (20 mg/mL PEG-g-PLA in acetone)

Table S.1 Effect of NP concentration by tangential filtration on diameter

		BEFORE CONCENTRATION			AFTER CONCENTRATION		
PEG length	**PEG content**	**Z-Average**	**Number Mean**	**PdI**	**Z-Average**	**Number Mean**	**PdI**
Mw	*% (w/w)*	*d.nm*	*d.nm*		*d.nm*	*d.nm*	
750	3,4	184	151,6	0,081	195,8	157	0,176
2000	33	156,7	123,1	0,078	157,9	119,8	0,085
5000	51	164,9	129,2	0,093	167,7	114,6	0,169
750	3,4	159,7	136,6	0,064	236,7	135,8	0,288
2000	8,7	162,2	139,2	0,048	179	112,6	0,193
5000	32,8	151,8	126,1	0,039	168,6	112,9	0,179
750	0,4	147,1	98,81	0,162	161,9	112,1	0,252
2000	4	161,6	120,6	0,097	171,1	134,4	0,194
5000	10,6	145,9	109,6	0,084	179,2	118,5	0,269

Annexe 4. Article 3, (Chapitre 6) « Supplementary Information »

Effect of Polymer Architecture on Curcumin Encapsulation and Release from Pegylated Polymer Nanoparticles: Toward a CSN Drug Delivery Nano-platform

*Jean-Michel Rabanel[1,2], Jimmy Faivre[1], Ghislain Djokeng Paka[3], Charles Ramassany[3], Patrice Hildgen[2], Xavier Banquy,[1, *]*

[1] Canada Research Chair on Bio-inspired materials
Faculté de Pharmacie, Université de Montréal,
C.P. 6128, Succursale Centre-ville, Montréal, Québec, H3C 3J7, Canada

[2] Laboratoire de Nanotechnologie Pharmaceutique,
Faculté de Pharmacie, Université de Montréal,
C.P. 6128, Succursale Centre-ville, Montréal, Québec, H3C 3J7, Canada

[3] Chaire de recherche Louise et André Charron sur la maladie d'Alzheimer
INRS-Institut Armand-Frappier, 531, Boulevard des Prairies
Laval, Québec H7V 1B7, Canada

[*] Corresponding authors

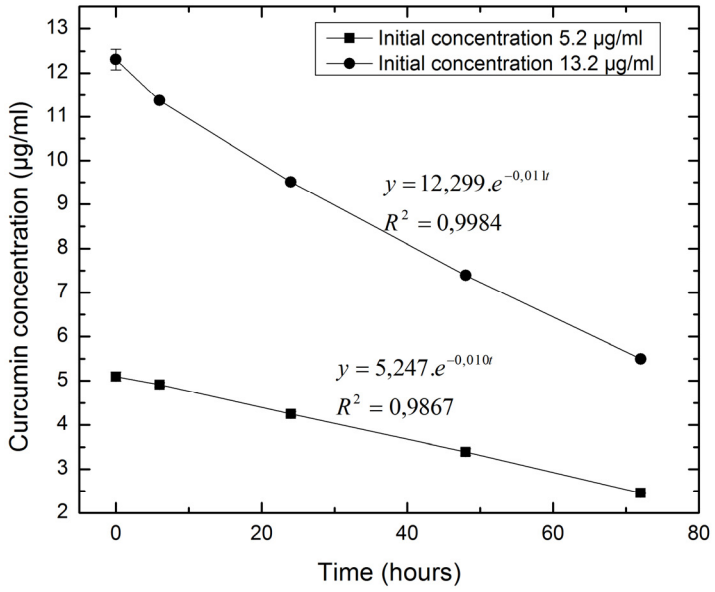

Figure S1. Kinetics of free curcumin degradation in PBS, SDS and ascorbic acid (respectively at 10mM, 50mM and 25µM) at 37°C

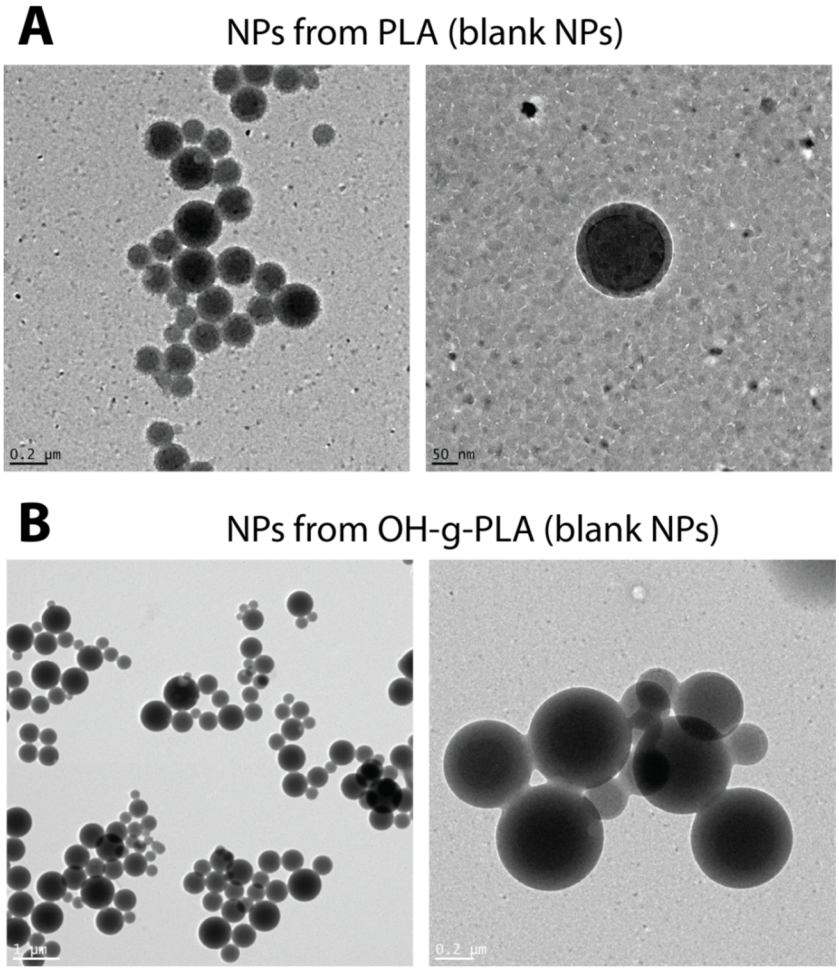

Figure S2. Cryo-TEM images of (A) NPs made from PLA (17 kD) and (B) from OH-*g*-PLA (see table 1 for structural information). Cryo-TEM image acquisition conditions are described in Material and Methods and are identical to the conditions used to generate images of PEGylated NPs displayed in Figure 3.

Table S1. Calculated modelling parameters for different NP batches

Polymer	***Fitted Parameters***		
	K_d (h^{-1})	D ($\times 10^{-18}\ m^2.h^{-1}$)	D ($\times 10^{-18}\ cm^2.s^{-1}$)
PEG-PLA (6%)	*0.009*	*63*	*175*
PEG-8%g-PLA	*0.01*	*75*	*208.3*
PEG-12%g-PLA	*0.01*	*110*	*305.6*
PEG-15%g-PLA	*0.008*	*18*	*50*
PEG-20%g-PLA	*0.008*	*3,5*	*9.7*
PEG-26%g-PLA	*0.01*	*6*	*16.7*
PEG-38%g-PLA	*0.011*	*10*	*27.8*

Table S2. Curcumin physical properties

(source: PubChem http://pubchem.ncbi.nlm.nih.gov/)

Parameters	***Values***	***Units***
M_w	368.38	$g.mol^{-1}$
Melting point	183	^oC
Pka	7.8; 8.5; 9.0	
Water solubility	3.12	$mg.l^{-1}$
PBS 10 mM, 7.4 solubility *	$2.99\ 10^{-8}$	$mol.l^{-1}$
Log P	3.47	

* *from reference* [1]

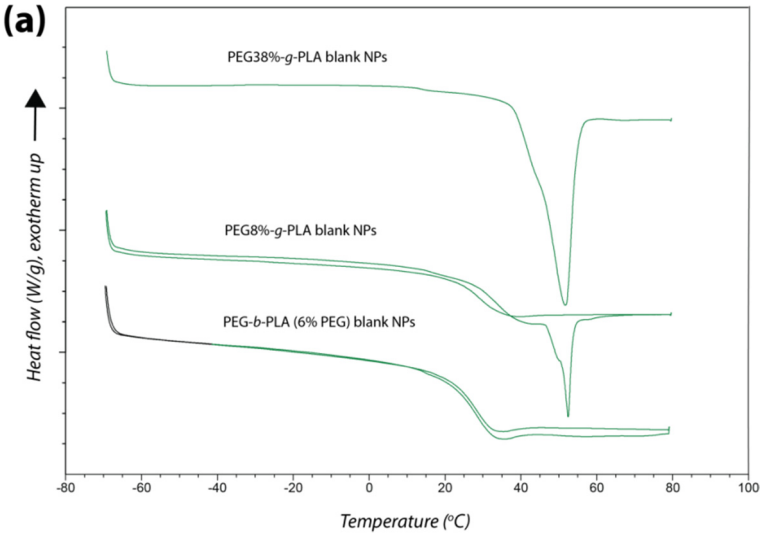

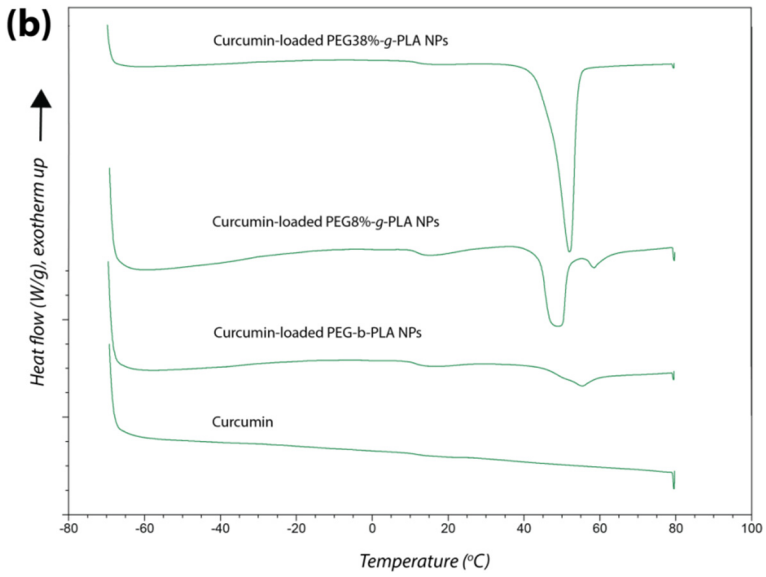

Figure S3. DSC thermograms, of blank (a) and curcumin-loaded NPs (b), showing effect of curcumin encapsulation on polymer thermal properties.

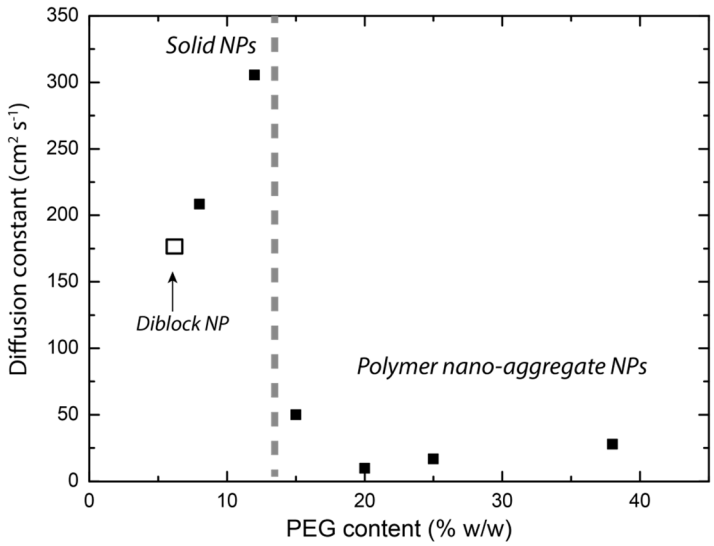

Figure S4. Curcumin diffusion constant as a function of polymer PEG content (% w/w).

REFERENCE

1. Letchford, K.; Liggins, R.; Burt, H., Solubilization of hydrophobic drugs by methoxy poly(ethylene glycol)-block-polycaprolactone diblock copolymer micelles: Theoretical and experimental data and correlations. *J. Pharm. Sci.* 2008, 97, (3), 1179-1190.

Annexe 5. Faisceau d'ion focalisé – Microscopie électronique à balayage.

Matériel et méthodes

La technique de FIB-SEM repose sur des microscopes bimodes (ion-électron). Le faisceau d'ions permet le machinage des surfaces grâce à un faisceau de Gallium qui pulvérise dont on peut déterminer le trajet et la profondeur. Un schéma sommaire de l'appareil est présenté en Figure A5.1. Un exemple séquentiel de traitement d'un échantillon est illustré en Figure A5.2.

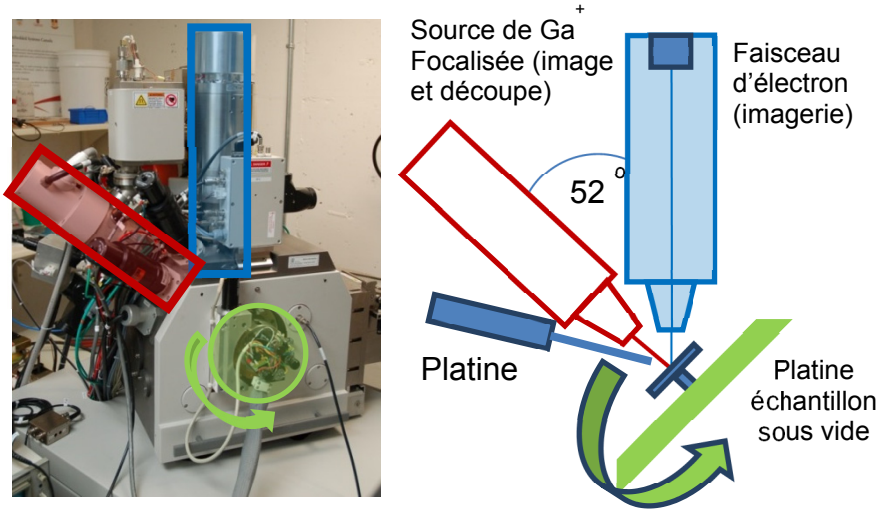

Figure A5.1. FIB/SEM Dual beam microscope (FEI Strata DB 235)

Les échantillons ont été préparés tels que décrit dans la Figure A5.2. La plupart des images ont été acquises pour des NPs déposées sous forme de suspension liquide sur une pièce de silicone montrée sur un support. L'appareil utilisé est un microscope bimodal, FIB/SEM Dual beam microscope, FEI Strata DB 235 (FEI, Japon) équipé d'une source de Gallium (Ga+) et d'une source d'électrons installées à un angle de 52º. L'appareil est également équipé d'une tige de Platine permettant le dépôt métallique sur des zones de l'échantillon. Lorsque le dépôt de platine a été utilisé, celui a été déposé en premier en utilisant le faisceau d'électron, puis la couche a été épaissie en utilisant un

faisceau de 10 pA pour ne pas déformer les sphères. Les coupes ont été effectuées avec la source ionique de Gallium à une puissance de 50 à 100 pA en utilisant le logiciel pour définir la zone et la profondeur de pulvérisation.

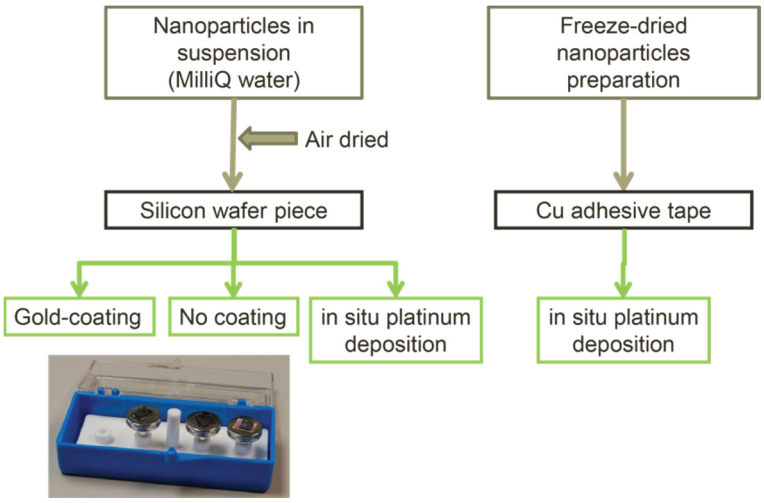

Figure A5.2. Méthodes de préparation des échantillons.

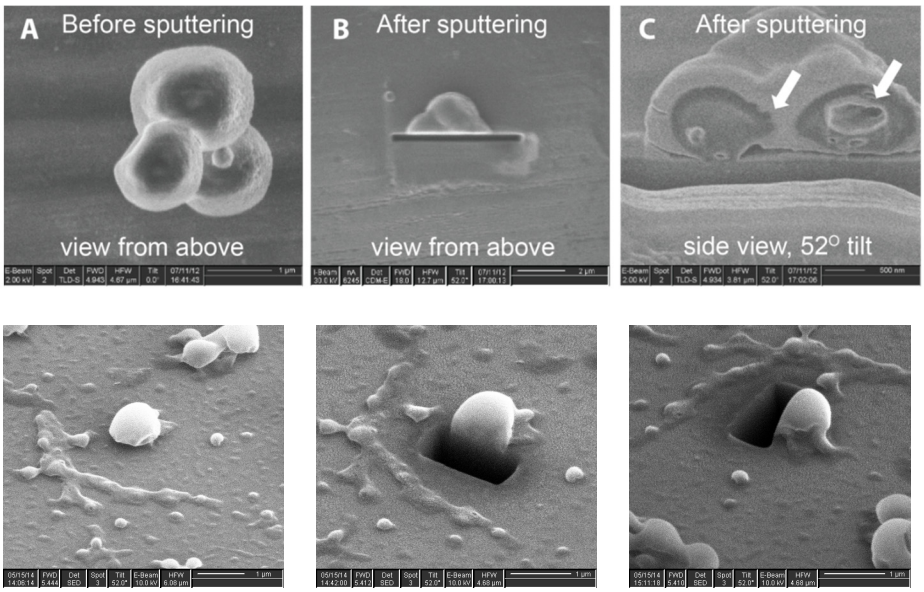

Figure A5.3 Processus de pulvérisation et observation en microscopie électronique. En haut observation en microscopie ionique (A et B), électronique (C) après dépôt de platine. En bas, images en MEB : découpe d'une particule après couverture d'or.

En Figure A5.3, la même particule est imagée à différents angles pour illustrer le machinage. On distingue bien sur les images le fit que le faisceau de Gallium a creusé le

support de silicone en même temps qu'il pulvérisait une tranche de la particule. Les particules apparaissent un peu fondues à cause du dépôt d'or, le traitement préalable à l'imagerie.

Résultats

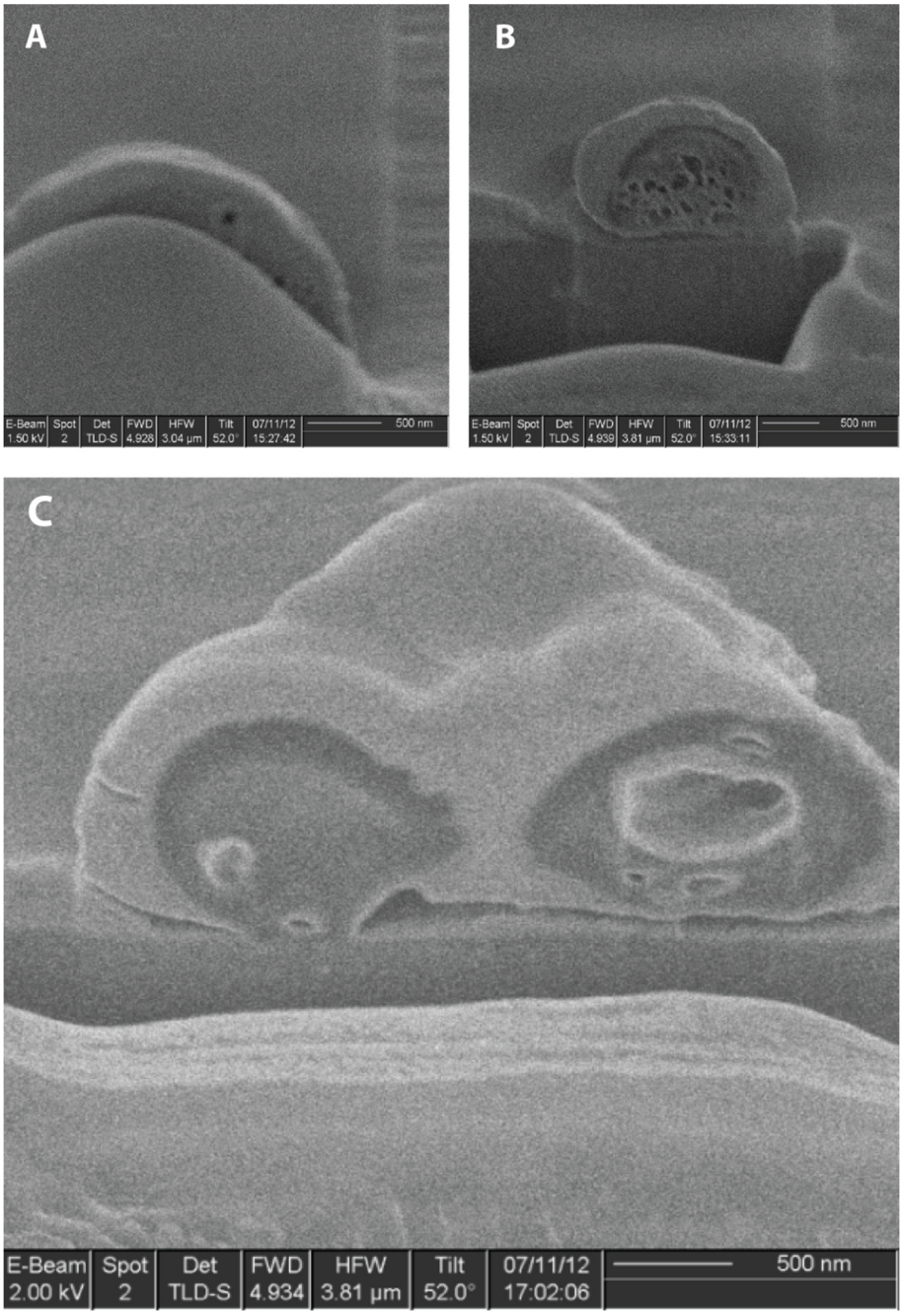

Figure A.5.4. Particules de PEG-g-PLA lyophilisées, déposées sur un ruban de cuivre et visualisées après recouvrement d'une couche de platine et découpe par le faisceau de Gallium.

On distingue une zone moins dense autour de la particule et autour des cavités que l'on retrouve dans le cœur de la particule (Figure A.5.3 (B) et (C)). D'après les autres résultats d'analyse (XPS et RMN) on peut présumer qu'il s'agit d'une zone enrichie en PEG. Les cavités ne semblent pas être seulement un artefact d'observation, par exemple résultant du chauffage dus à la pulvérisation d'une partie de la particule ou de l'imagerie par le faisceau d'électron.

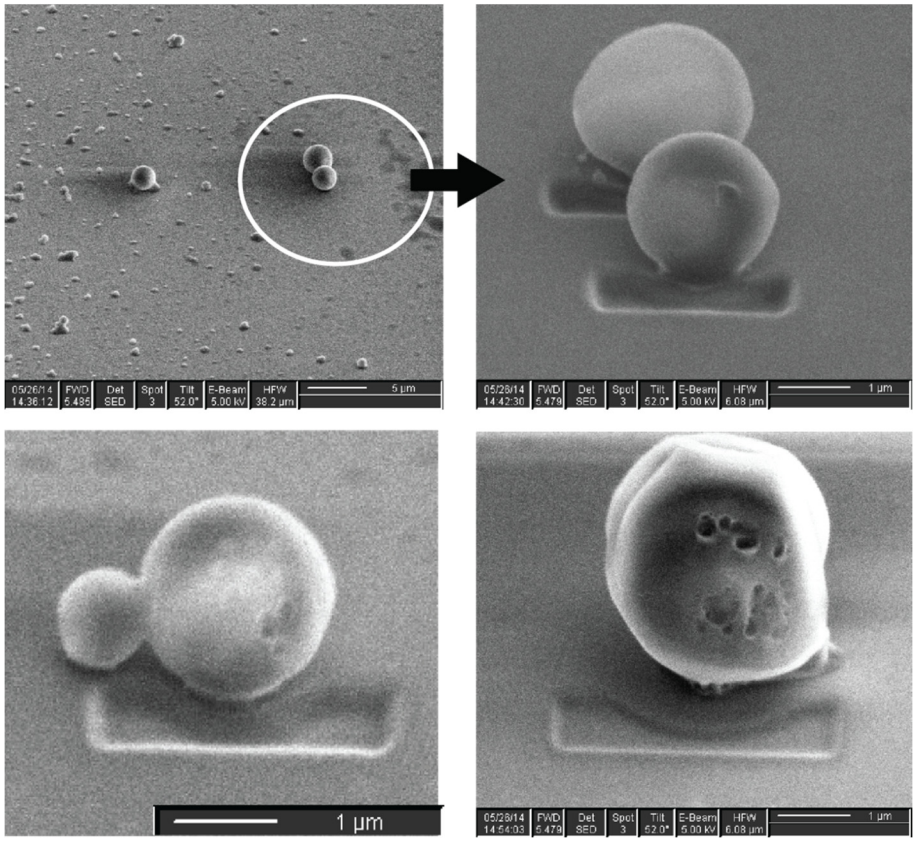

Figure A.5.5. Particules (500 nm à 1 µm) de PEG-g-PLA déposées sur un support en silicium sans traitement métallique.

Dans les particules en Figure A.5.5., on distingue des cavités ainsi que certaines inhomogénéités dans les densités qui reflètent peut-être l'organisations interne des copolymères.

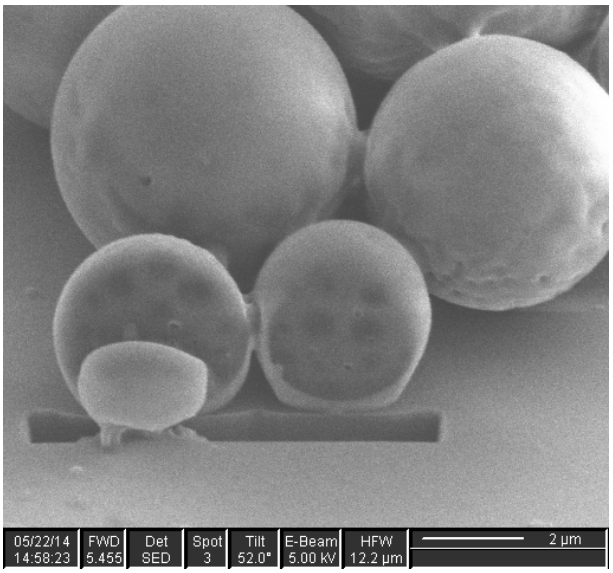

Figure A.5.6. Microparticules (PEG-g-PLA, 9% PEG). Vue de côté en MEB.

On distingue dans le bas de l'image la trace de la découpe dans le support de silicium par le faisceau de Gallium. La surface des particules est légèrement fondue (en haut), se masque en partie une certaines rugosité visible vers le bas de la particule. La tranche des deux microparticules en avant nous montre des zones de densités électronique différentes : proches de la surface (claires, peu denses) et à l'intérieur sous forme de domaine sphérique (plus foncées plus denses).

Annexe 6. Liste des articles publiés et soumis; affiches et présentations orales durant la durée du doctorat.

En préparation

(--) Jean-Michel Rabanel, Patrice Hildgen, Xavier Banquy "Effect of Formulation Parameters and Polymer Architecture on the Surface Properties of Nanoparticles Prepared from Clickable Comb-like Copolymers" En preparation

Soumis/Accepté

(--) Jean-Michel Rabanel, Jimmy Faivre, Ghislain Djiokeng Paka, Charles Ramassamy, Patrice Hildgen, Xavier Banquy « Effect of polymer architecture on Curcumin encapsulation and release from pegylated polymer nanoparticles: toward a drug delivery nano-platform to the CNS » European Journal of Pharmaceutics and Biopharmaceutics, (Soumis avril 2015, Accepté le 7 septembre 2015)

Publiés

(16) Jean-Michel Rabanel, Jimmy Faivre, Soudeh F. Tehrani, Augustine Lalloz, Patrice Hildgen, Xavier Banquy « Effect of polymer architecture on the structural and biophysical properties of PEG-PLA nanoparticles » ACS Appl. Mater. Interfaces 2015, 7, 10374–10385.

(15) Igor Elkin, **Jean-Michel Rabanel**, Valery Aoun, Patrice Hildgen "Synthesis and Evaluation of Symmetrically PEG-Decorated Triglycerides of Fatty Acid as Drug-Encapsulating Agents" Macromolecular Chemistry and Physics, DOI: 10.1002/macp.201400486 - Vol. 216 (4), pages 427-438, (February 2015)

(14) Jean-Michel Rabanel, Patrice Hildgen, Xavier Banquy "Assessment of PEG on Polymeric Particles Surface, a Key Step in Drug Carrier Translation" Journal of Controlled Release, Vol. 185, p71-87 (2014)

(13) Jean-Michel Rabanel, Valery Aoun, Igor Elkin, Mohamed Mokhtar & Patrice Hildgen "Drug-loaded nanocarriers: passive targeting and crossing of biological barriers" Current Medicinal Chemistry, Vol. 19 (19), p 3070-3102, (2012)

(12) Sherief Essa, **Jean Michel Rabanel**, Patrice Hildgen "Characterization of rhodamine loaded PEG-g-PLA nanoparticles (NPs): Effect of poly(ethylene glycol) grafting density" International Journal of Pharmaceutics, Vol. 411(1-2) p178-187 (2011)

Affiche et présentation en congrès.

Affiches

(19) "The NanoAssemblr™ Platform: Microfluidics-Based Manufacture of Dibloc PEG-Polylactic Acid Nanoparticles", A Lalloz, G. Heuck, **JM Rabanel**, Xavier Banquy, 2015 AAPS Annual Meeting and Exposition, October 25-29, 2015 Orlando, Fla.

(18) "Curcumin-loaded Nanoparticles made of Brush-like PEG-PLA Copolymers as a Potential Drug Delivery System for Neurodegenerative Diseases" Jimmy Faivre, **Jean-Michel Rabanel**, Ghislain Paka Djiokeng, Charles Ramassany, Patrice Hildgen, Xavier Banquy, Journée Phare 2014, Orford, Qc, November 13-14, 2014

(17) "Quantification of PEG surface coverage-density on polymeric nanoparticle and its effect on physico-chemical properties" **Jean-Michel Rabanel**, Shaker Al-sharif, Patrice Hildgen, Xavier Banquy, Controlled Release Society Annual Meeting, Chicago, Ill 12-16 juillet 2014 *Extended abstract & poster.*

(16) "Relationship between PEG surface coverage-density and the physico-chemical properties of polymeric nanoparticles" **Jean-Michel Rabanel**, Patrice Hildgen, Xavier Banquy, Canadian Society of Pharmaceuticals Sciences (CSPS), Congrès annuel, Montréal, Canada 10-13 juin 2014 *Résumé publié dans "J. Pharm. Pharmaceut. Sci. (2014)".*

(15) « Effect of polymer architecture on hydrophobic drugs encapsulation and release from polymeric nanoparticles » Jimmy Faivre, **Jean-Michel Rabanel**, Patrice Hildgen, Xavier Banquy, Canadian Society of Pharmaceuticals Sciences (CSPS), Congrès annuel, Montréal, Canada 10-13 juin 2014 *Résumé publié dans "J. Pharm. Pharmaceut. Sci. (2014)".*

(14) "Caractérisation de la couche externe de nano-transporteurs de médicament" **Jean-Michel Rabanel** & Patrice Hildgen, Journée de la recherche, Faculté de Pharmacie, Université de Montréal, 5 décembre 2013

(13) "Contribution à la compréhension de la structure de la couche externe de nano-transporteurs de médicament" **Jean-Michel Rabanel** & Patrice Hildgen, Journée CECSP, Faculté de Pharmacie, Université de Montréal, 6 mars 2013

(12) "Impact of Polymer Physico-chemical Properties on PEG-grafted-PLA Nanoparticles Structure" (extended abstract) **J.M. Rabanel**, V. Aoun & P. Hildgen, 39th Controlled Release Society annual meeting, 15–18 juillet, 2012, Québec, Canada

(11) "Synthesis of PEG grafted polyester polymers to improve targeted delivery of nanocarriers" **Jean-Michel Rabanel** & Patrice Hildgen, Canadian Society of Pharmaceuticals Sciences (CSPS), Congrés annuel, Toronto, Canada 12-15 juin 2012 *Résumé publié dans "J. Pharm. Pharmaceut. Sci. Vol 15, No 4 (2012)".*

Présentation orale

(5) "Effect of polymer architecture and PEG content on micro-structuration of polymeric nanoparticles" **Jean-Michel Rabanel**, Patrice Hildgen, Xavier Banquy, Canadian Biomaterials Society Annual Meeting, 4-7 juin 2014, Halifax, NS, Canada

(4) « Relation entre la densité de surface de Poly(éthylène glycol) et les propriétés de nanoparticules polymériques » **Jean-Michel Rabanel**, Patrice Hildgen, Xavier Banquy, 7ème Journée Scientifique du GRUM, Université de Montréal, 2 mai 2014

(3) « Caractérisations par XPS de la couche hydrophile externe de nanovecteurs de médicament » **Jean-Michel Rabanel**, Patrice Hildgen, Xavier Banquy
Journée scientifique de l'AFAM, Morin-Heights, octobre 2013